INFRARED SPECTRA AND NORMAL COORDINATE ANALYSIS OF SOME SILYL AND GERMYL COMPOUNDS

by

Donald C.J. Skea

A thesis presented for the degree of
Doctor of Philosophy

University of Edinburgh
1980

To my Mother and Father,
and Helen

CONTENTS i

The work described in this thesis is the original work of the author except where specific reference is made to other sources. It has not been submitted, in whole or in part, for any degree at any other University.

ACKNOWLEDGEMENTS

I would like to thank Dr A. Morrison of Aberdeen University for running the high resolution gas phase infrared spectra of SiH_3CN. I would also like to thank Dr I. Sadler, Mr J. Millar and Dr A. Boyd for obtaining the nuclear magnetic resonance spectra of the silyl pseudohalides.

Thanks are due to Professor E.A.V. Ebsworth for reading the first draft of this thesis and for a number of helpful discussions in the course of the work.

Above all, I must thank my supervisor, Dr S. Cradock, for his advice and encouragement at all times, and for giving me the benefit of his experience and knowledge of infrared spectroscopy and normal coordinate analysis.

Thanks are due to the Science Research Council for a maintenance grant.

ABSTRACT

The molecules SiH_3NCO, SiH_3NCSe, GeH_3NCO, GeH_3NCS, SiH_3CN and $SiH_2(NCO)_2$ have been studied in the mid and far infrared. Most have also been studied with isotopically substituted atoms; a large number of the infrared spectra were recorded with samples in matrix isolation. The data obtained from the mid and far infrared spectra were used in a normal coordinate analysis of each molecule, with the exception of GeH_3NCS.

Chapter 1 gives an introduction to infrared spectroscopy and its use in conjunction with matrix isolation. The following chapter outlines aspects of relevant theory. The techniques of sample handling and matrix isolation, instruments used and preparations are described in Chapter 3.

The results chapters, 4-7, each deal with a molecule or pair of molecules. In each chapter a brief introduction outlines previous work in the infrared, microwave and in electron diffraction. There is a description of the mid infrared spectrum in an argon or nitrogen matrix together with the assignment of the observed bands. Far infrared spectra of gas phase samples are described and their meaning discussed. Finally the results of a normal coordinate analysis are given with a number of calculated interatomic amplitudes of vibration and distance correction parameters.

Additional results are from the infrared spectra of SiH_3NCO in CO_2 and allene matrices, the high resolution mid infrared gas phase spectrum of SiH_3CN and the mid infrared gas phase band contours of $SiH_2(NCO)_2$.

Chapter 8 gives the results of nuclear magnetic resonance spectra of the $-SiH_3$ compounds. Isotopically substituted species with ^{15}N and ^{13}C serve to provide a large number of additional chemical shifts and coupling constants. Chapter 9 gives some general conclusions, with suggestions for future work.

CHAPTER 1 - INTRODUCTION

1.1 General

The results contained in this work have been largely obtained by use of the technique called infrared spectroscopy. Infrared spectroscopy is, as are all forms of spectroscopy, concerned with the measurement of a physical property of matter, enabling deductions to be made about the sample by application of theory. In the case of infrared spectroscopy, the absorption of infrared radiation as a function of wavelength is measured by an infrared spectrophotometer.

An infrared spectrum consists, most commonly, of a trace on a sheet of paper on which the abscissa measures the wavenumber of the radiation and the ordinate gives the intensity. The wavenumber is in units of cm^{-1} - the number of wavelengths per cm, and the intensity gives a measure of the amount of energy absorbed by the sample. The intensity is usually given in % transmittance; given by the formula $100\ P/P_o$. P_o is the input energy to the sample and P is the output energy. For quantitative calculations on intensities it is often easier to express the absorbed energy in units of absorbance = $\log \frac{P_o}{P}$.

Qualitatively, infrared spectroscopy can be used to 'fingerprint' samples since the absorption bands observed in the spectrum are characteristic of the molecule producing them. This is an excellent way of identifying

samples and checking purity. Quantitatively, infrared spectroscopy can yield information about molecular structures, rotational moments of inertia and, particularly relevant to this work, normal modes of vibration. The term normal mode refers to the mode of movement of the atoms in a molecule which results in the absorption of infrared radiation at a particular wavenumber. This is the link between infrared spectroscopy and the analysis of normal coordinates (modes).

Infrared radiation is, of course, only part of the electromagnetic spectrum. The boundary to shorter wavelength is with the visible part of the spectrum, while that to longer wavelength is with the microwaves. Boundaries between these and other regions of the electromagnetic spectrum are not clear-cut, but the range of the infrared is generally considered to be 200 - 2μm wavelength.

Resonant interaction of matter with any form of radiation occurs when the energy of the radiation matches an energy level transition in the sample. In the case of infrared radiation, absorption occurs when the changing electric dipole of a sample molecule as it vibrates interacts with the oscillating electric field. Such vibrations which result in a changing molecular electric dipole moment are said to be infrared active.

In this work the vast majority of infrared spectra have been run using the technique of matrix isolation.

This technique traps the sample molecules under study in a rigid matrix cage, consisting of a vast excess of inert molecules, thereby isolating them from each other. The technique was developed primarily for study of highly reactive species which could thus be isolated from each other and studied at leisure. However, it is also extremely useful in studying stable molecules.

If the sample molecules are trapped in a rigid cage there is no rotation possible. Study of molecules by infrared spectroscopy in a matrix therefore gives infrared absorption bands free of any rotational fine structure and which are, consequently, very sharp. This means that accurate determinations of vibrational frequency and isotopic shifts can be made. In an analysis of normal coordinates this is exactly what is required.

The great advantage of matrix isolation spectra over gas phase spectra is that very close absorption bands (in energy) can be observed separately due to their sharpness. This is true for bands as close as 1 cm^{-1} or even less. For the same reason small isotopic shifts can be determined accurately and easily without the burden of a rotational analysis of a band, necessary in the gas phase. Isotopic substitution is an extremely important means of assigning infrared bands to particular vibrations, since it gives information about the principal moving atoms in a normal mode. Naturally occurring mixtures of isotopes are also

useful in matrix isolated spectra since isotopic splitting patterns are easily picked out. This is not so in gas phase spectra where large numbers of isotopes only serve to confuse the spectrum.

The choice of matrix materials is governed by their chemical inactivity and lack of infrared spectrum. Both criteria are satisfied by nitrogen and the rare gases. In order to create a rigid cage with these gases we require an extremely low temperature infrared window - of the order of 10 K. This is achieved by using a low temperature cryogenic refrigerator (for a full description of experimental details see later). The vast majority of experiments described in this work used nitrogen or argon matrix gases, although a few others were used.

1.2 Aims

On beginning a piece of research it is important that the aims of the research are well-defined. The aims of this work were defined as follows:

(i) to study the matrix isolated infrared spectra of samples and determine the frequencies of vibration;

(ii) to use the spectra of isotopically labelled species to help assign the observed frequencies to particular vibrations;

(iii) to analyse frequency and isotopic data to give

normal coordinates; and

(iv) if possible, to extract any structural information available from the matrix isolated spectra.

In general, these aims have remained of primary importance during the work. However, it has inevitably proved necessary to undertake work in other areas; for example, gas phase spectra in the far infrared and computer programming. A full account of this work is also given.

1.3 Area of Study

As the title indicates, the molecules studied contained the silyl ($-SiH_3$) and germyl ($-GeH_3$) groups. More specifically they were the silyl and germyl pseudo-halides. The word pseudohalide defines a group of atoms which shows characteristics similar to the halogens. That is, a group of atoms which is monovalent, anionic in solution and which undergoes chemical reactions similar to the halogens. The examples of such groups dealt with in this work are NCO^-, NCS^-, $NCSe^-$ and CN^-. The molecules dealt with, then, were silyl isocyanate, SiH_3NCO; silyl isoselenocyanate, SiH_3NCSe; germyl isocyanate, GeH_3NCO; germyl isothiocyanate, GeH_3NCS; silyl cyanide, SiH_3CN and silyl bis-isocyanate, $SiH_2(NCO)_2$.

These species are very volatile and can be handled well in a vacuum line system. Vacuum line techniques were used extensively in the course of this work. Using a

vacuum system also means that the species which are reactive in air (particularly the silyls) can be kept isolated.

As one would expect, some of the above compounds are more volatile than others. The volatilities range from the highest, SiH_3NCO, which has a vapour pressure at 0^oC of 363 mmHg to the lowest, GeH_3NCS, with a vapour pressure of 3 mmHg at room temperature. For molecules such as GeH_3NCS the low vapour pressure makes vacuum line handling less easy but, nevertheless, still desirable.

Another point in favour of using vacuum line techniques is that samples are easily stored at liquid nitrogen temperatures. This is particularly important since many of the above species are unstable at room temperature. Possibly the most unstable of the group is SiH_3NCSe which decomposes when left at room temperature for long periods to give selenium deposits. However, it can be stored in a pure state for long periods at liquid nitrogen temperatures.

The above named species display a number of properties of interest to an infrared spectroscopist. The number of atoms present in each molecule provides a sufficient challenge in identifying all of the frequencies of vibration, and isotopic shifts. Each molecule also possesses a very low frequency bending vibration which can be observed only in the far infrared.

The structures of the molecules are also interesting - the infrared spectrum confirms that the NCO, NCSe and NCS groups are bonded to silicon through the nitrogen atom. In the case of the CN group the bonding is through the carbon atom. Other structural considerations are concerned with the linearity, or otherwise, of the heavy atom chain in the ground vibrational state. Matrix isolation provides some information about this aspect.

Comparisons between these related compounds also prove extremely interesting; also comparisons with the corresponding methyl and methylated compounds. A general comparison of the carbon, silicon and germanium compounds indicates that the carbon and germanium species behave somewhat similarly in terms of structure, while the silicon compounds are slightly different. For example, CH_3NCO and GeH_3NCO have bent heavy atom chains while SiH_3NCO has a linear chain (all in the gas phase). This has been ascribed to the p-d π-bonding of the nitrogen lone pair to silicon which does not occur in the methyl case, and which may occur to a lesser extent in the germyl case. All of these molecules have low frequency bending vibrations - CH_3NCO at 200 cm^{-1} [1], GeH_3NCO at 53 cm^{-1} (this work) and SiH_3NCO at 64 cm^{-1} (this work). The closely related compound $(CH_3)_3SiNCO$ has been shown to have a linear heavy atom chain by microwave spectroscopy[2] and has a low frequency bending vibration at 37 cm^{-1} [3].

The related compounds containing the NCS group have similar properties. CH_3NCS has a bent heavy atom chain[1] while SiH_3NCS is linear (see later). GeH_3NCS appears to be a borderline case in this respect (see later). Again, low frequency bending vibrations are: CH_3NCS, 180 cm^{-1} [1], SiH_3NCS, 65 cm^{-1} [4] and GeH_3NCS, 49 cm^{-1} (this work).

The most closely related compounds to SiH_3CN are, again, the carbon and germanium equivalents. These compounds all have linear heavy atom chains. Here, the carbon compound is the only one to have the iso form as well as the normal form, i.e. CH_3NC as well as CH_3CN. They have both been studied in the infrared[5] and microwave regions[6,7]. It has been claimed that the related compound $(CH_3)_3SiCN$ exists in small proportion as $(CH_3)_3SiNC$[8], although the evidence is far from conclusive. There is, however, no iso form of SiH_3CN.

CHAPTER 2 - THEORY

2.1 Introduction

This chapter outlines the theoretical basis for infrared spectroscopy, together with specific aspects of theory used later in this work. The specific topics to be dealt with include the use of group theory and symmetry, normal coordinate analysis and gas phase infrared band shapes and analysis.

2.2 Theory of Infrared Spectroscopy[9,10]

Infrared spectroscopy has as its basis the ideas of quantum mechanics. The first postulate of quantum mechanics is that the state of a system is described by a function Ψ - the wavefunction. Ψ is a function of such quantities as distance or time which define the system. The wavefunction contains all the information about the system, and physical observables can be evaluated by performing the appropriate operation on the wavefunction. Different observables can be calculated by the use of different mathematical operators. This introduces the idea of the eigenvalue equation:

$$\hat{H}\Psi = E\Psi$$

$\hat{H}$ is the mathematical operator which gives the value of the observable, E, after operating on Ψ. The observable quantity, E, may be a position, momentum or energy

depending on the form of $\hat{H}$.

In the case of a molecule the wavefunction, Ψ, describes the state of the whole system - that is, nuclear, electronic and spin states. In order to deal with the nuclear motions (vibrations and rotations) it is necessary to separate as far as possible the various contributions to Ψ. To a good approximation, the electronic motions can be treated assuming fixed nuclear positions. This is known as the Born-Oppenheimer approximation[44]. Thus we have the approximation $\Psi = \psi_n\psi_e$ where ψ_n is the nuclear wavefunction and ψ_e is the electronic wavefunction.

It is possible to further separate the nuclear wavefunction ψ_n into the vibrational wavefunction ψ_v, and the rotational wavefunction ψ_r, i.e. $\psi_n = \psi_v\psi_r$.

In some cases it is not possible to write the overall wavefunction in such a way due to interaction terms between the different types of coordinates.

We can now write down a wave equation which deals solely with the vibration of the nuclei in a molecule:

$$\hat{H}_v\psi_v = E_v\psi_v$$

Here, $\hat{H}_v$ is the energy operator and E_v is the energy eigenvalue.

The form of $\hat{H}_v$ will depend on the system of coordinates used in the calculation. The most convenient coordinates to use are normal coordinates, since each

normal coordinate is associated with one single mode of vibration of the molecule. By using normal coordinates, the vibrational wave equation separates into a number of individual equations - one for each mode of vibration.

Solving $\hat{H}_v\psi_v = E_v\psi_v$ for each vibration gives a set of discrete solutions for E_v. This means that each vibration of a molecule can possess only certain discrete energies satisfied by the above equation. Each energy state is labelled by a quantum number, v_i, where i is the particular vibration in question. This quantum number can possess values v_i = 0, 1, 2, 3, ...

It is only now that the connection with infrared spectroscopy is apparent. Radiation in the infrared region has the correct energy to cause transitions between the discrete energy levels labelled v_i. Thus the origin of the absorption bands in an infrared spectrum is the change in quantum state of the vibrations of the sample molecules. There are absorption bands at different energies corresponding to different vibrations of the sample molecules.

The main absorption bands in an infrared spectrum are generally due to the $v_i = 0 \rightarrow v_i = 1$ (fundamental) transitions. There are a number of reasons for this. Firstly the proportion of molecules in a state other than $v_i = 0$ at room temperature is very small as dictated by the Boltzmann distribution. Secondly, the rules governing

the changes in quantum state for a vibration dictate that only $\Delta v_i = 1$ is possible. This rule is derived from quantum mechanics assuming that all vibrations are harmonic, i.e. the restoring force on the atoms in a molecule undergoing a vibration is linearly dependent on their displacement from equilibrium.

In some cases levels other than $v_i = 0$ can be populated if the vibration is of low energy. We then observe the absorption of energy in the infrared spectrum corresponding to the transitions $v_i = 1 \rightarrow v_i = 2$, $v_i = 2 \rightarrow v_i = 3$ etc. Furthermore the idea of harmonic molecular vibration is only approximately true, thus allowing transitions of the form $\Delta v_i = 2$, $\Delta v_i = 3$ etc. to occur. However, the probability of such transitions decreases rapidly as Δv_i increases in magnitude, for approximately harmonic vibrations. Absorptions in the infrared spectrum due to such transitions are therefore weak. The $v_i = 0 \rightarrow v_i = 2$ transition of a vibration is called the 'first overtone'.

Thus we see that quantum mechanics is the basis of infrared spectroscopy which in turn introduces the idea of the normal coordinate. The data obtained from an infrared spectrum can be used to provide information about the normal coordinates of a molecule which describe the modes of vibration.

2.3 Normal Coordinate Analysis[10,11,12]

Quantum mechanics has led to an understanding of the process of absorption of infrared radiation by molecules. The data obtained from an infrared spectrum are energy values corresponding to the vibrational transitions of a molecule. Such energy values are usually measured in units of wavenumber, cm^{-1} (the number of wavelengths of the incident radiation per cm). The cm^{-1} value can be related to the energy of the transition by the equation:

$$E = hc\bar{\nu}$$

where $\bar{\nu}$ is the wavenumber, h is Planck's constant and c is the speed of light.

The wavenumber value can also be regarded as a 'frequency' - the resonant frequency of the vibration undergoing the quantum transition. More specifically, the 'frequency' of the $v_i = 0 \rightarrow v_i = 1$ transition of a vibration is assumed to be the 'harmonic' frequency of the vibration. Since molecular vibrations are rarely perfectly harmonic this is an approximation, although corrections for anharmonicity can be made. Such frequency values for each vibration of a molecule can thus be used in a semi-classical normal coordinate analysis.

In performing a normal coordinate analysis we begin with the frequency values obtained from an infrared spectrum, and a known or assumed molecular structure. The problem then is to calculate the force constants

governing the molecular vibrations in terms of a set of coordinates which are most physically reasonable. The coordinates which are of most use physically are the 'internal coordinates'.

There are a number of different types of internal coordinate which define different types of vibration. They are:

(i) bond stretching, (ii) angle bending (angle $\neq 180^{\circ}$), (iii) linear angle bending, (iv) out-of-plane bending, and (v) torsion.

The internal coordinates are best described in terms of a set of cartesian displacement coordinates, $\underline{x}$. $\underline{x}$ is a column vector of the cartesian displacements, three coordinates for each atom in the molecule. Assuming infinitesimal amplitudes of vibration, the vector, $\underline{x}$, can be related to the set of internal coordinates, $\underline{r}$, by the linear transformation:

$$\underline{r} = \underline{B}\,\underline{x}$$

($\underline{B}$ is not in general a square matrix)

It is possible to write down expressions for the kinetic energy, T, and the potential energy, V, in matrix form:

$T = \frac{1}{2}\,\tilde{\dot{\underline{x}}}\,\underline{M}\,\dot{\underline{x}}$, $V = \frac{1}{2}\,\tilde{\underline{x}}\,\underline{f}\,\underline{x}$ in terms of cartesian displacements. $\underline{M}$ is a diagonal matrix containing the atomic masses, $\underline{f}$ is the force constant matrix in cartesian

coordinates.

Transferring to internal coordinates:

$$T = \tfrac{1}{2}\, \tilde{\dot{r}}\, G^{-1}\, \dot{r} = \tfrac{1}{2}\, \tilde{\dot{r}}\, K\, \dot{r}$$

$$V = \tfrac{1}{2}\, \tilde{r}\, F\, r$$

where $K = G^{-1} = (B\, M^{-1}\, \tilde{B})^{-1}$, F is the force constant matrix in internal coordinates, $G^{-1}(=K)$ is the kinetic energy matrix in internal coordinates.

The application of Lagrange's equation $\frac{d}{dt}\frac{dT}{d\dot{r}_i} + \frac{dV}{dr_i} = 0$ for each value of i yields the equation:

$$F\, r + K\, \ddot{r} = 0$$

Introduce a further transformation which relates the internal coordinates to the normal coordinates, Q.

$$r = L\, Q$$

Expanding this equation for one internal coordinate:

$$r_i = \sum_k L_{ik} Q_k$$

The normal coordinates are now assumed to be harmonic with Q_k of the form $Q_k = A_k \cos(2\pi\nu_k t + \delta)$. This yields the equation:

$$\ddot{r}_i = -\sum_k \lambda_k L_{ik} Q_k \quad \therefore \quad \ddot{r} = -\lambda\, L\, Q, \quad [r = L\, Q,\ \lambda_k = 4\pi^2\nu_k^2]$$

Substituting into $F\, r + K\, \ddot{r} = 0$ we obtain:

$$\underline{F}\,\underline{L}\,\underline{Q} - \underline{K}\,\underline{\lambda}\,\underline{L}\,\underline{Q} = 0 \therefore \underline{F}\,\underline{L} - \underline{K}\,\underline{\lambda}\,\underline{L} = 0$$

$$\therefore \underline{G}\,\underline{F}\,\underline{L} = \underline{L}\,\underline{\lambda} \text{ since } \underline{K}^{-1} = \underline{G} \text{ and } \underline{\lambda} \text{ is diagonal.}$$

This latest equation is the most general form of the problem for analysis of normal coordinates. $\underline{G}$ is known from the molecular structure, $\underline{\lambda}$ is known from the vibrational frequencies.

The solution to the above equation is greatly simplified by the use of symmetry and group theory. A molecule is assigned a 'point group' which describes its symmetry. The group consists of a number of symmetry operations which, when carried out on the molecule, leave it indistinguishable from the original. Each symmetry operation has an associated transformation matrix (called the 'representative') which depends on the coordinate basis (cartesian, internal, symmetry). The form of the representative will also change when the coordinate axes are changed; however, the trace (or character) of the representative is constant with choice of axes. The set of characters for all of the symmetry operations is called a representation of the group. Any representation of a group can be expressed in terms of a combination of 'irreducible representations' of which there are a fixed number for each group. The number of irreducible representations can be derived from a reducible representation from,

$$n_j = \frac{1}{h} \sum_i \chi_j(i) \chi_\gamma(i)$$

where n_j is the number of irreducible representations j, h is the number of symmetry operations in the group, $\chi_j(i)$ is the character of the irreducible representation j for symmetry operation i, $\chi_\gamma(i)$ is the character of the reducible representation γ for symmetry operation i. This equation leads to the assignment of vibrational modes to symmetry classes (names for irreducible representations). For example, H_2O has point group C_{2v}, vibrations have symmetry class $2A_1 + B_2$.

In solving $\underline{G}\ \underline{F}\ \underline{L} = \underline{L}\ \underline{\lambda}$, the problem is greatly simplified by transforming the basis from internal to symmetry coordinates. The transformation is carried out by a unitary matrix such that:

$\underline{s} = \underline{U}\ \underline{r}$, $s_i = \sum_j U_{ij} r_j$ where s_i is the symmetry coordinate. Symmetry coordinates can be generated by the following equation:

$$s_i = \frac{1}{h} \sum_R \chi_i(\underline{R}) \underline{R}\ r_1$$

where $\underline{R}$ is the representative of a symmetry operation of the group, $\chi_i(R)$ is the character of the representative R (symmetry class i), r_1 is any internal coordinate (the 'generator'). Using different generators, a set of symmetry coordinates is built up.

Transforming to symmetry coordinates has transformed

the $\underline{G}$ and $\underline{F}$ matrices thus:

$$\underline{G} \rightarrow \underline{U}\ \underline{G}\ \tilde{\underline{U}}$$
$$\underline{F} \rightarrow \underline{U}\ \underline{F}\ \tilde{\underline{U}}$$

By suitable ordering of symmetry coordinates, $\underline{G}$ and $\underline{F}$ are now block diagonal in structure - all terms connecting coordinates of different symmetry class are zero. The transformation $\underline{s} = \underline{U}\ \underline{r}$ also means that the $\underline{L}$ matrix now relates the normal coordinates to the symmetry coordinates:

$$\underline{s} = \underline{L}\ \underline{Q}$$

The block diagonal structure of the $\underline{G}$ and $\underline{F}$ matrices allows the separate solution of normal coordinates in different symmetry classes.

In mathematical terms, the solution of the equation $\underline{G}\ \underline{F}\ \underline{L} = \underline{L}\ \underline{\lambda}$ involves the assumption of a trial $\underline{F}$ matrix which is then refined to fit best the observed frequencies of vibration (and any other experimental data, e.g. coriolis constants). Let the trial matrix be $\underline{F_o}$,

$$\therefore \underline{G}\ \underline{F_o}\ \underline{L_o} = \underline{L_o}\ \underline{\lambda_o}$$

$\underline{F_o}$ is not the true $\underline{F}$ matrix so the eigenvalues $\underline{\lambda_o}$ will be different from the experimental ones. It is possible to apply a correction to $\underline{F_o}$ which will improve the fit with the experimental frequencies according to

$$\underline{J}\,\Delta\underline{F} = \Delta\underline{\lambda}$$

where $\Delta\underline{F}$ is the matrix of corrections to $\underline{F}_o$, $\Delta\underline{\lambda}$ is $\underline{\lambda}_{obs} - \underline{\lambda}_{calc}$ and $\underline{J}$ is the Jacobian matrix of $\underline{\lambda}$ with respect to $\underline{F}$. The elements of $\underline{J}$ are calculated numerically in the programme used in this work.

It is possible at this stage to introduce a weighting matrix which governs the contribution to $\underline{J}$ from the different observed frequencies. $\underline{\lambda}$ will usually consist of a set of frequencies, and isotopic shifts which further constrain the solution.

The above procedure is correct only to first order so a number of corrections to $\underline{F}_o$ must be carried out. At each stage the equation $\underline{G}\,\underline{F}\,\underline{L} = \underline{L}\,\underline{\lambda}$ is reduced to symmetric form since $\underline{G}\,\underline{F}$ is not symmetric. Once $\Delta\underline{\lambda}$ is reduced to an acceptable value the iterative procedure can be stopped, thus yielding $\underline{F}$.

The equation to be solved is very often underdetermined since for n vibrations there is an n x n matrix to be fixed, with $\frac{1}{2}n(n+1)$ independent elements. Hence, the data from isotopically labelled species and coriolis coupling constants are very valuable in constraining the solution.

In practical terms, the solution of $\underline{G}\,\underline{F}\,\underline{L} = \underline{L}\,\underline{\lambda}$ was carried out by digital computer at Edinburgh, using the normal coordinate programme GAMP. This programme allows easy input of all molecular structure data and frequencies

either directly from a teletype or by reading a character file. The particular problem under study is only defined once since all the relevant information is immediately stored on input.

The programme deals with each symmetry species in turn and stores the latest solution for future refinement. A considerable level of interaction with the user is allowed for; different commands can be given after each cycle of refinement. It is possible at each stage to refine different $\underline{F}$ matrix elements, to fix 'by hand' named elements or to change the weights for each frequency or isotopic shift.

There are also facilities to allow the user to see the potential energy distribution (see later) or the Jacobian matrix, or even to reassign the observed frequencies. The user is thus allowed maximum flexibility in the attempts to reach an acceptable solution.

In performing a refinement one is faced with the problem of deciding which off-diagonal $\underline{F}$ matrix elements, if any, are required to be non-zero. This is by no means easy since an under-determined problem will have an infinite number of solutions. There are, however, a number of good indicators one can use to help.

Firstly, coordinates which are spatially very close in the molecule are likely to be coupled; also those which are close in energy. Other required off-diagonal elements

may be indicated by the potential energy distribution and by patterns in the observed and calculated frequencies and isotopic shifts. Once the non-zero off-diagonal elements of the $\underline{F}$ matrix are identified it is best to allow as many $\underline{F}$ matrix elements as possible to refine simultaneously. A number of such iterations will eventually lead to the best least squares fit for the frequencies and isotopic shifts.

The final solution of the normal coordinate analysis gives the $\underline{F}$ matrix and the important related matrix, $\underline{L}$, the eigenvectors. Further application of relevant theory leads to the calculation of a number of important and physically observable parameters.

2.4 Further Calculations using $\underline{F}$ and $\underline{L}$[10,12,13]

As mentioned previously, it is of interest to obtain an output of the 'potential energy' distribution both during and after the $\underline{F}$ matrix refinement. The potential energy distribution gives information on the contribution of each force constant, F_{ij}, to the normal coordinate.

It is possible to show that the fractional contribution of off-diagonal and diagonal elements of the $\underline{F}$ matrix to the potential energy are $2L_{ji}L_{ki}F_{jk}/\lambda_i$ and $L_{ji}^2F_{jj}/\lambda_i$ respectively. In practice the contributions of the diagonal elements are most useful.

A normal coordinate solution allows the calculation

of a number of quantities useful in the study of a molecule by electron diffraction. Electron diffraction structures are averaged over all of the vibrations of the molecule at the temperature of the experiment. From such a study one can obtain experimental interatomic amplitudes of vibration, which can be compared to the theoretical amplitudes calculated by normal coordinate analysis.

The theory involved in such calculations is based on quantum mechanics. We use the infrared spectral data in normal coordinate analysis in a classical manner - as classical frequencies of vibration. Now we revert to quantum mechanical theory to calculate the amplitudes of vibration.

At a given temperature the observed distances and amplitudes of vibration are a statistical mechanical mean of the Maxwell-Boltzmann distribution. Theoretically this can be expressed for the mean square amplitude of a normal coordinate, $\langle Q_i^2 \rangle$ as:

$$\langle Q_i^2 \rangle = \frac{h}{8\pi^2 c\omega_i} \coth \frac{hc\omega_i}{2kT}$$

where h is Planck's constant, c is the speed of light, ω_i is the frequency of the normal coordinate, k is Boltzmann's constant and T is the temperature. Thus, the above formula accounts for the distribution of vibrational states at temperature, T, for the normal mode

of vibration, Q_i. The orthogonality of normal coordinates also means that $\langle Q_k Q_i \rangle = 0$ for $k \neq i$.

In matrix form we can therefore construct a diagonal matrix, $\underline{\delta}$, of the mean square amplitudes of the normal coordinates $\underline{\delta} = \langle \underline{Q}\ \underline{Q}^* \rangle$ ($\underline{Q}^*$ is the complex conjugate of $\underline{Q}$). The coordinate transformation $\underline{S} = \underline{L}\ \underline{Q}$ leads to the mean square amplitude matrix of symmetry coordinates, $\underline{\Sigma}$:

$$\underline{\Sigma} = \langle \underline{S}\ \underline{S}^* \rangle = \underline{L} \langle \underline{Q}\ \underline{Q}^* \rangle \tilde{\underline{L}} = \underline{L}\ \underline{\delta}\ \tilde{\underline{L}}.$$

The observed quantities in electron diffraction are interatomic root mean square amplitudes of vibration. In order to calculate these from $\underline{\delta}$ we must first calculate the mean square interatomic cartesian amplitudes, using a transformation operator on the matrix $\tilde{\underline{L}}^{-1}\ \underline{\delta}\ \underline{L}^{-1}$. The operator itself is derived from the $\underline{B}$ matrix and the inverse masses of the two atoms in question. A set of mean square interatomic cartesian amplitudes is calculated for each atom pair in the molecule for each symmetry species. The amplitudes for each atom pair are summed over all symmetry species at the end of the calculation.

A simple coordinate transformation places the z direction of a local set of axes along each atom pair from which $\langle \Delta z^2 \rangle$ (mean square parallel amplitude) and $\langle \Delta x^2 \rangle$, $\langle \Delta y^2 \rangle$ (mean square perpendicular amplitudes) are calculated.

The output from the normal coordinate analysis programme

(see later chapters) gives a table of a number of interatomic distances and amplitudes.

(i) r_a - the distances r_a are the interatomic distances as calculated from the input structural parameters. All of the structural parameters used for the molecules studied were taken from electron diffraction studies (r_a structures) $r_a = \langle r^{-1} \rangle^{-1}$. r_a values do not give geometrically consistent structures due to a number of dynamic effects. The use of r_a values in a normal coordinate analysis is therefore an approximation. This, however, does not affect the calculated amplitudes.

(ii) U - root mean square interatomic parallel amplitude, $\langle \Delta z^2 \rangle^{\frac{1}{2}}$.

(iii) P - root mean square interatomic perpendicular amplitude, $\{\frac{\langle \Delta x^2 \rangle + \langle \Delta y^2 \rangle}{2}\}^{\frac{1}{2}}$.

(iv) L - parallel amplitude correction $\frac{U^2}{r_e}$. r_e is the equilibrium value of interatomic distance. $r_e \approx r_a$ is used as a good approximation.

(v) K - perpendicular amplitude correction $\frac{\langle \Delta r^2 \rangle + \langle \Delta y^2 \rangle}{2r_e}$. Again $r_e \approx r_a$.

(vi) r_g - average value of interatomic distance, $\langle r \rangle$ (for a particular temperature). $r_g = r_a + L$.

(vii) RALPHA (r_α) - distance between the mean positions of atoms at a particular temperature,

$r_\alpha = r_g - K = r_a + L - K.$

The relationship between r_a and r_g is derived from theoretical considerations concerned with an anharmonic vibration defined by a Morse function. The correction to give r_α is an approximation from a binomial expansion which relates the instantaneous distances of atoms to r_e.

$$r_{inst} = (\Delta x^2 + \Delta y^2 + (r_e + \Delta z)^2)^{\frac{1}{2}}$$

$$\approx r_e + \Delta z + (\Delta x^2 + \Delta y^2)/2r_e$$

r_g is the vibrational average $r_e + \langle \Delta z \rangle + \dfrac{\langle \Delta x^2 \rangle + \langle \Delta y^2 \rangle}{2r_e}$

where $r_\alpha = r_e + \langle \Delta z \rangle$. $\therefore r_\alpha = r_g - K.$

It is possible, then, to compare experimental amplitudes of vibration (from electron diffraction) with those obtained theoretically by normal coordinate analysis. A number of quantities calculated by normal coordinate analysis can also lead to the derivation of other physically important parameters, e.g. r_g. Furthermore, comparison of observed and calculated shrinkage effects is possible.

A shrinkage effect is most easily understood when dealing with a linear chain of atoms in a molecule. As a result of the modes of vibration perpendicular to the chain axis, the vibrationally averaged observed distance, d(1,3),

of atoms 1 and 3 in a chain is smaller than the sum of the distances d(1,2) plus d(2,3). This arises because the vibrational average position of the atoms is not a linear configuration.

The electron diffraction observed shrinkage, δ, of a chain of three atoms is equal to $r_a(1,2) + r_a(2,3) - r_a(1,3)$. The calculated value from a normal coordinate analysis is found as follows:

$$\delta = r_a(1,2) + r_a(2,3) - r_a(1,3)$$

$$= r_\alpha(1,2) - L(1,2) + K(1,2) + r_\alpha(2,3) - L(2,3)$$

$$+ K(2,3) - r_\alpha(1,3) + L(1,3) - K(1,3)$$

$$\rightarrow \quad \delta = K(1,2) + K(2,3) - K(1,3) - L(1,2) - L(2,3) + L(1,3).$$

Since $r_\alpha(1,2) + r_\alpha(2,3) - r_\alpha(1,3) = 0$.

2.5 Coriolis Coupling Constants[10,12,14]

Coriolis coupling constants can be calculated from the results of a normal coordinate analysis. An addition to the programme was made in order to carry out the necessary computation (see Appendix).

A coriolis coupling constant is a measure of the interaction of different vibrations through the rotation of a molecule. In a rotating frame of reference the coriolis forces caused by a particular vibration may excite another vibration of the molecule. Coupling of the

vibrations in this way leads to vibrational angular momentum about the axis of rotation. The magnitude of the angular momentum is the coriolis coupling constant, ζ, (in units of $\frac{\hbar}{2\pi}$).

Such constants are only physically meaningful for molecules with a rotational axis of symmetry, and only in a few cases are experimental coriolis constants obtainable. Where they are obtainable, these constants provide another constraint on the $\underline{F}$ matrix solution. In most cases, although a normal coordinate programme can calculate the coupling constants between any two vibrations in a molecule, only a very few can be observed experimentally. This is because significant effects on a vibrational spectrum are only seen if the two coupled vibrations are close in energy. Thus the effect of coriolis interaction can be seen clearly in the infrared bands of molecules with degenerate vibrations, e.g. symmetric tops.

The theory of calculation of coriolis constants is as follows. In the expression of kinetic energy of a vibrating/rotating molecule the terms corresponding to the interaction of vibration and rotation are of the form:

$$T = \tfrac{1}{2}(\Omega_x\omega_x + \Omega_y\omega_y + \Omega_z\omega_z)$$

where $\omega_{x,y,z}$ are the components of angular velocity in the rotating system of axes. The Ω's are given by

$$\Omega_\alpha = \underline{\tilde{Q}}\ \underline{\zeta}^\alpha\ \underline{\dot{Q}}$$

which is in matrix form with a normal coordinate basis. This defines the $\underline{\zeta}$ matrix of coriolis coupling constants. It can be shown that the matrices $\underline{\zeta}^{\alpha}$ (α = x,y,z) are given by the equation:

$$\underline{\zeta}^{\alpha} = \underline{L}^{-1}\ \underline{B}\ \underline{I}_{\mu}{}^{\alpha}\ \tilde{\underline{B}}\ \tilde{\underline{L}}^{-1}$$

where $\underline{L}$ is the matrix of normal coordinate eigenvectors, $\underline{B}$ is the transformation matrix as in $\underline{s} = \underline{B}\ \underline{x}$ and $\underline{I}_{\mu}{}^{\alpha}$ is a block diagonal matrix of inverse atomic masses, μ, with different form for each direction x, y, z. For a molecule with n atoms there are n diagonal blocks of the form:

$$\underline{I}_{\mu}{}^{x} = \begin{bmatrix} 0 & 0 & 0 \\ 0 & 0 & \mu_n \\ 0 & -\mu_n & 0 \end{bmatrix} \quad \underline{I}_{\mu}{}^{y} = \begin{bmatrix} 0 & 0 & -\mu_n \\ 0 & 0 & 0 \\ \mu_n & 0 & 0 \end{bmatrix} \quad \underline{I}_{\mu}{}^{z} = \begin{bmatrix} 0 & \mu_n & 0 \\ -\mu_n & 0 & 0 \\ 0 & 0 & 0 \end{bmatrix}$$

2.6 Gas Phase Infrared Band Shapes[15]

In the gas phase, molecules may not only change their vibrational state on absorbing radiation but also change their rotational state. This results in rotational structures on the infrared absorption bands. Different types of vibrational transitions have different allowed rotational transitions giving rise to different band shapes. In order to understand infrared band shapes we must look at the theoretical results obtained from vibration/rotation quantum mechanics.

The specific aspects of theory dealt with here are concerned with the band shapes and analysis of parallel (vibrational dipole change along top axis) and perpendicular (dipole change perpendicular to top axis) bands of symmetric tops. A symmetric top molecule has two of its moments of inertia equal in magnitude.

2.6.1 Parallel bands

A parallel band results from a transition between two non-degenerate vibrational levels with dipole change along the top axis. The allowed rotation transitions are:

$\Delta K = 0,\ \Delta J = 0, \pm 1 \qquad K \neq 0$

$\Delta K = 0,\ \Delta J = \pm 1 \qquad K = 0$

For a particular value of K we have a sub-band with P, Q and R branches since $\Delta J = 0, \pm 1$ ($K = 0$ sub-band does not have a Q branch). The whole parallel band is a superposition of many sub-bands - one for each value of K. The origin of each sub-band ($J = 0$) is given by:

$$\nu_o^{sub} = \nu_o + \{(A'_v - A''_v) - (B'_v - B''_v)\}K^2$$

where ν_o is the overall band origin. If the coefficient of K^2 is small, i.e. if $A' \approx A''$ and $B' \approx B''$ then all of the sub-bands will approximately coincide, giving a strong central Q branch with P and R branch lines spaced approximately 2B apart. If $A' - B'$ and $A'' - B''$ show a

large difference in magnitude, the sub-bands will no longer coincide. It should be noted that $J \geqslant K$, so as K increases there is an increasing number of missing lines in the sub-bands.

The analysis of a parallel band of a symmetric top uses the method of combination of differences. This, however, is only applicable if the band is of simple form i.e. all the K sub-bands approximately coincide. The formulae for the J lines of a band with P, Q and R branches are:

$$R(J) = \nu_o + 2B' + (3B' - B'')J + (B' - B'')J^2$$
$$P(J) = \nu_o - (B' + B'')J + (B' - B'')J^2$$
$$Q(J) = \nu_o + (B' - B'')J + (B' - B'')J^2$$

negelecting centrifugal distortion.

It follows that:

$$R(J) - P(J) = 4B'(J + \tfrac{1}{2})$$
$$R(J-1) - P(J+1) = 4B''(J + \tfrac{1}{2})$$

Thus by plotting R(J) - P(J) against J we obtain a line of slope 4B'. Plotting R(J-1) - P(J+1) against J gives a line of slope 4B".

It also follows that $R(J-1) + P(J) = 2\nu_o + 2(B' - B'')J^2$. A plot of R(J-1) + P(J) against J^2 will give a line of slope $2(B' - B'')$ with intercept $2\nu_o$.

It should be noted that systematic errors are present

when using the method on symmetric top parallel bands. Firstly, the K sub-bands may not exactly coincide; secondly, the missing J lines in the individual K sub-bands may affect the measured positions of the P and R branch lines.

2.6.2 Perpendicular bands

In a symmetric top a perpendicular band results from a transition between a non-degenerate and a degenerate level. A fundamental band is the case where the lower state is non-degenerate and the upper state is degenerate. The direction of the dipole change in such a transition is perpendicular to the top axis.

The allowed rotational transitions are:

$$\Delta K = \pm 1, \quad \Delta J = 0, \pm 1.$$

As in the case of a parallel band, a perpendicular band has a number of sub-bands, one associated with each value of K. However, here the sub-bands do not nearly coincide although the formulae governing the J structure of the sub-bands is the same as the parallel band. The sub-band origins in this case are given by the formula:

$$\nu_o^{sub} = \nu_o + \{A_v'(1 - 2\zeta_i) - B_v'\} \pm 2\{A_v'(1 - \zeta_i) - B_v'\}K + \{(A_v' - B_v') - (A_v'' - B_v'')\}K^2$$

This gives a series of almost equidistant sub-bands where

the sharp Q branches form the most prominent features. The inclusion of the ζ value for the upper state means that a method such as combination of differences will not separate the rotational constants for the upper and lower states.

In principle it is possible to obtain B' and B" from a perpendicular band by analysis of the J structure of a single K sub-band by combination of differences. However, the J structure is often not resolved - in cases where the P and R branch lines are resolved the overlapping of neighbouring sub-bands makes assignment impossible. The analysis of a perpendicular band is usually confined to the Q branch series.

A least squares fit of the Q branch positions to the above polynomial in K yields the parameters:

(i) $\nu_o + \{A'_v(1 - 2\zeta_i) - B'_v\}$

(ii) $2\{A'_v(1 - \zeta_i) - B'_v\}$

(iii) $\{(A'_v - B'_v) - (A''_v - B''_v)\}$

Unfortunately solution of the above equations cannot yield unique values for all the unknowns. However, study of the overtone of a vibration together with rotational constants from, for example, microwave studies can give enough additional information to fix the A's and B's, ν_o and ζ_i.

CHAPTER 3 - EXPERIMENTAL TECHNIQUES

3.1 Introduction

This chapter contains descriptions of the various experimental techniques used in the course of this work. The first part describes the methods of sample handling and associated methods of identification. There follows a description of the technique of matrix isolation used to run the infrared spectra, together with a list of the instruments used. A discussion is inserted at this stage on the consequences of using matrix isolation in infrared spectroscopy. The final section deals with the preparation and purification of samples.

3.2 Vacuum Techniques

The use of vacuum techniques for handling samples is now so widespread that only a brief description will be given here.

The advantage of using a vacuum line in handling samples is that they can be moved quantitatively. Thus, vapour pressures, molecular weights and volumes can easily be determined. The types of compounds which lend themselves most easily to vacuum line handling are those which have a significant vapour pressure at room temperature (>5 mmHg) but a very small vapour pressure (<0.1 mmHg) at liquid nitrogen temperature (-196^{o}C). There are many

cases where the use of a vacuum line is essential; for example, when the compounds dealt with are reactive to air or water.

The pumping system used was a mercury diffusion pump backed by a rotary oil pump. This easily gave pressures down to about 10^{-4} mmHg. The pumping section was connected through a muck trap (at -196°C) to a cyclic pyrex glass system. This closed line consisted of a number of sections, each with its own purpose.

On each side of the vacuum line was a trap section used for storage of samples or for trap-to-trap vacuum distillation during purification. The next section, on each side, consisted of a number of ground glass 'take-off' points each with its own glass tap. This facilitated removal or addition of samples to the line. The two sides of the line were closed by a spiral section with a glass spiral gauge for measuring pressure. This was most often used as a null instrument for pressure measurement by introduction of air pressure to the other side of the spiral gauge through the 'back section'. Also on the spiral section was a take-off point suitable for an infrared cell, and a narrow glass finger for vapour pressure measurements.

The sections of the line were connected by cone and socket ground glass joints sealed with Apiezon 'L' grease. Apiezon 'N' grease was used for the ground glass taps.

A vacuum line facilitates a number of special techniques. Gas phase infrared spectra are easily obtained using an attached cell with KBr or CsI end plates. Vapour pressures are obtained by freezing the sample into the spiral section 'cold finger' and reading the pressure gauge at a set temperature. Molecular weights can be determined for samples with high vapour pressures using an attached bulb of known volume - molecular weight bulb. A known volume, pressure and weight of gas sample yields a molecular weight. It is also possible to perform analyses of samples by measuring gas volumes evolved in a particular reaction.

In sample preparations, a vacuum line offers a method of obtaining special conditions. For example, exchange reactions using powder columns can be carried out externally under vacuum simply through a vacuum-tight link to the main system. Also, various inert atrospheres (e.g. nitrogen) can be created at any pressure by attaching an external cylinder.

3.3 Matrix Isolation[16]

Most of the infrared spectra studied in this work were run on sample molecules which were matrix isolated. This technique was developed mainly for study of reactive species which, when trapped in a chemically inert rigid matrix cage, could be studied at leisure. However, matrix isolation is also a useful technique for

studying the infrared spectra of stable species, since the sample molecules are not free to rotate. This leads to very sharp infrared absorption bands which have no rotational fine structure. If a large excess of matrix material is used the sample molecules do not interact with each other, although they do interact to some extent with the matrix cage.

It is an advantage in infrared spectroscopy to have a matrix material which is not only inert but also free of any infrared absorption bands. This suggests either nitrogen or the rare gases. In order to make a rigid cage from such gases we need temperatures of less than one third of the melting point of the solid - about 25 K for nitrogen, 29 K for argon. In order to create the conditions necessary for matrix isolation and infrared spectroscopy, a specialised piece of equipment is required.

The matrix isolation equipment used consisted of a CsI window attached to an Air Products CS-202 micro-refrigerator. The cold window was mounted between two copper plates, with indium gaskets to allow for thermal expansion and contraction. The window assembly was attached to the very cold station (2nd stage) of the refrigerator, and was surrounded by a radiation shield which was cooled by the cold station (1st stage). At the top of the refrigerator were the necessary He gas and electrical connections to the compressor and control

box.

In order to maintain the low temperature required, the whole assembly was suspended in a metal jacket which could be evacuated. A high vacuum surrounding the cold window was necessary to prevent heat gain by conduction from the surrounds, and also to prevent condensation of air. The cold tip could be rotated using 'O' ring seals with the outer jacket, to allow spray-on of the sample from one side and passage of the infrared radiation at 90^{o}. The outer vacuum jacket had two CsI windows to allow the passage of radiation.

A high vacuum was maintained inside the jacket through a port connected to an oil diffusion pump backed by a two-stage rotary pump. The vacuum was typically in the region of 10^{-6} mmHg under working conditions.

It was possible to control the temperature of the cold window by passing a current through some heating coils. The temperature of the window was recorded on an electric thermometer display which was connected to a thermocouple. Typically, the system worked at a temperature of 5-10 K without external heating.

The spray-on port was connected to a vacuum line where the sample/matrix mixtures were prepared. Samples were introduced to the vacuum line, through a ground glass joint, from an ampule. 6 mmHg pressure of sample was measured into a 30 ml bulb and then allowed to

expand into a 1000 ml bulb. This gave about 0.2 mmHg pressure in the 1000 ml bulb. 200 mmHg of matrix gas (N_2 or Ar) was then introduced to give a sample/matrix ratio of about 1:1000. All spectra were run with this ratio unless otherwise stated.

Matrix mixtures were sprayed on to the cold window using the pulsed deposition technique. About 30 ml of matrix mixture were applied quickly to the window using an isolated volume of the vacuum line. Up to 30 seconds were allowed between each pulse while the refrigerator cooled again to the lowest temperature and any non-condensed gas was removed by the pumps. Typically, 25 such pulses were applied, each with average initial pressure in the line of about 160 mmHg. Thus the amount of sample/matrix applied was about 6 mmoles, 6×10^{-3} mmoles being sample. This is roughly equivalent to 2 mmHg pressure of sample in a 10 cm gas cell.

The pulsed deposition technique is an easy way of applying large quantities of matrix to the cold window very quickly. It is only, however, applicable to large, stable, non-reactive species since they are less affected by diffusion on deposition. An advantage of this technique is that local annealing of the matrix takes place as each pulse is applied, giving 'clearer' matrices and sharp infrared lines.

The process of deposition to the cold window is

non-equilibrium - the sample molecules may occupy a number of unstable sites. For the molecules studied in this work the sites occupied in the matrix will be multiple substitutions of matrix molecules - multiple substitutional sites. It follows that for such substitutions there are a number of types of 'cage' for the sample molecules. These cages may distort the molecule in different ways. It is likely also that the matrix lattice is distorted around the sample molecules.

It is possible to reach the most stable arrangement of sites by annealing the matrix. As mentioned earlier, a matrix can only be considered rigid below 30% of its melting temperature. Between 30% and 50% of T_m the matrix molecules became mobile enough to rearrange to stable configurations without allowing diffusion of the sample molecules. This process was carried out often in running the infrared spectra of samples. Warming to between 0.3 T_m and 0.5 T_m occasionally resulted in aggregates of sample molecules forming, especially if the intermolecular forces were large. This, however, is not expected to be a significant effect until the temperature reaches 0.5 T_m. Any formation of aggregates manifested itself in the infrared spectrum as extra absorption bands.

The interaction of sample molecules with the matrix molecules is expected to be small for the matrix gases used. There must, however, be some interaction since

observed infrared frequencies are seen to shift in matrices with respect to the gas phase frequencies, and also with respect to each other for different matrices.

A simple theory of interactions of matrix molecules with sample molecules can predict the shift of an observed infrared frequency with respect to the gas phase frequency for attractive and repulsive potentials. The matrix cage is assumed to be spherically symmetric about the sample molecule. A repulsive interaction between cage and sample perturbs the vibrational potential in such a way as to increase the effective force constant and thus increase the vibrational frequency. An attractive potential serves to decrease the vibrational frequency with respect to the gas phase. It is usually the case that for the same molecule some modes of vibration will be shifted up in frequency and some will be shifted down.

In practice, there are a number of other effects observed in the infrared spectra of matrix isolated molecules. The symmetry of a molecule may be perturbed from the gas phase symmetry on matrix isolation. This may result in relaxation of certain selection rules and lifting of degeneracy. It should be noted that, even for no lowering of symmetry, degenerate modes of vibration may be split in energy due to the non-isotropic nature of the matrix, with different interactions with the vibrational components. One may, thus, observe a number

of closely spaced bands in the infrared spectrum in place of only one expected.

The presence of samples in different matrix sites will also lead to the appearance of multiplets in place of a single band. Aggregates of sample molecules will give extra bands in a spectrum. Both of the above effects can be identified by annealing the matrix and running samples with different matrix ratios.

3.4 Instruments

Most of the sample purity checks were run on a Perkin-Elmer 577 grating infrared spectrophotometer in the gas phase. Any necessary gas phase band expansions were also run on this machine.

The matrix isolated infrared spectra were run on a Perkin-Elmer 225 grating spectrophotometer, the necessary equipment having been mounted in the sample beam. The sample area was sealed with polythene film so that the instrument purger could be used. The slit programme used gave a resolution of about 1 cm^{-1} over the range 4000-200 cm^{-1}. High resolution gas phase spectra were run on a Nicolet 7000 instrument at Aberdeen University.

Far infrared spectra were run using a Beckman RIIC IR 720 Fourier transform spectrometer. Interferograms were stored firstly in a memory as data points, and transformed by a wave analyser attached to the instrument.

This gave a general survey spectrum. For higher resolution spectra, better results were obtained by recording the interferograms on punched tape which could be read into the Edinburgh computing system. The transformation was then carried out using a Fast Fourier transform programme.

The spectra obtained were often a little noisy so a computer programme was written to average the transformed spectra of a number of runs (see Appendix). The output from the computation was either on a line printer or a graph plotter.

Gas phase samples run in the far infrared were introduced to a 150 cm glass cell inserted between source and detector. Such an arrangement provided a large path length, although large amounts of sample were often required. The sample cell had high density polythene windows at each end. In the few matrix isolated far infrared spectra run, the cold window was made of silicon.

Nuclear magnetic resonance spectra were run on three different instruments:

(i)	Bruker WH 360 (Fourier Transform)	^{1}H	360.13 MHz)	^{2}H internal lock
		^{13}C	90.558 MHz)	
		^{29}Si	71.546 MHz)	
		^{77}Se	68.682 MHz)	
		^{15}N	36.498 MHz)	

(ii)	Varian XL-100 (Fourier Transform)	^{1}H	100.06 MHz)	^{2}H internal lock except for ^{2}H which used ^{19}F external lock.
		^{2}H	15.36 MHz)	
		^{13}C	25.16 MHz)	
(iii)	Varian H.A. 100 (Continuous Wave)	^{1}H	100 MHz	^{1}H (TMS) lock plus decoupling experiments with Schlumberger frequency generator.

3.5 Preparations

The following are the preparations carried out in the course of this work. Most are standard preparations - in such cases a reference is given to the original work. Any modifications to the original are detailed.

3.5.1 Silyl isocyanate was prepared by one of two methods.

(i) the reaction of silyl bromide with silver isocyanate.

$$SiH_3Br + AgNCO \rightarrow SiH_3NCO + AgBr$$

This is a modification of the first preparation[17] where silyl iodide was used in place of silyl bromide. Deuterated silyl isocyanate was prepared using SiD_3Br.

(ii) The reaction of isocyanic acid with trisilylamine[18].

$$N(SiH_3)_3 + 4HNCO \rightarrow 3SiH_3NCO + NH_4NCO$$

Deuterated silyl isocyanate was prepared using $N(SiD_3)_3$.

3.5.2 Silyl bromide was prepared by a modification to the method of Fritz and Kummer[19].

50 mmoles phenyl silane and 100 mmoles HBr were co-condensed in a 250 ml ampule fitted with a Sovirel tap. The ampule was immersed in a -78°C bath overnight; fractionation was carried out as normal. Deuterated silyl bromide was prepared from SiD_3Ph.

$$PhSiH_3 + HBr \xrightarrow{-70^{\circ}C} SiH_3Br + PhH.$$

3.5.3 Phenyl silane was prepared by reduction of trichlorophenylsilane by lithium aluminium hydride[19].

$$4PhSiCl_3 + 3LiAlH_4 \rightarrow 4PhSiH_3 + 3LiCl + 3AlCl_3.$$

Deuterated phenyl silane was prepared using $LiAlD_4$.

3.5.4 Silver isocyanate was prepared from potassium cyanide by oxidation with potassium permanganate with cupric hydroxide catalyst[20] to give KNCO and then precipitation with silver nitrate.

$$KCN \xrightarrow[Cu(OH)_2]{KMnO_4} KNCO \xrightarrow{AgNO_3} AgNCO.$$

Isotopically enriched AgNCO was prepared using the appropriate enriched KCN.

3.5.5 Trisilyl amine was prepared by the vapour phase reaction of ammonia and silyl chloride[21].

$$SiH_3Cl + 4NH_3 \rightarrow N(SiH_3)_3 + 3NH_4Cl.$$

3.5.6 Silyl chloride was prepared by passing a stream of silyl bromide through an excess of $HgCl_2$[22].

$$2SiH_3Br + HgCl_2 \rightarrow 2SiH_3Cl + HgBr_2.$$

Deuterated silyl chloride was prepared from deuterated silyl bromide.

3.5.7 Silyl isoselenocyanate was prepared by a modification of the technique of Ebsworth and Mays[23]. Silyl bromide was condensed into an ampule containing dry silver isoselenocyanate and allowed to warm to room temperature. The products were fractionated as normal.

$$SiH_3Br + AgNCSe \rightarrow SiH_3NCSe + AgBr.$$

Deuterated silyl isoselenocyanate was prepared from deuterated silyl bromide, ^{15}N and ^{13}C enriched samples were prepared from the corresponding enriched silver salt.

3.5.8 Silver isoselenocyanate was prepared by a modification to a large scale preparation[24]. The preparation was attempted on a small scale to enable ^{15}N and ^{13}C enriched species to be made.

About 0.2 g KCN was placed in a small ceramic crucible together with a stoichiometric amount of commercially available grey Se. The crucible and contents were heated in a sand bath with continuous stirring until melting occurred at about 125°C. The melt was held at this temperature for a few minutes and stirred thoroughly.

Stirring continued during cooling until solidification. The K^+NCSe^- formed was dissolved in acetone and filtered using a sintered glass funnel. The acetone was blown off using a dry air flow and distilled water added. A measured amount of $AgNO_3$ in distilled water was added which precipitated AgNCSe. This was filtered, washed and dried. The yield of AgNCSe based on the amount of KCN was 93%.

The above proved by far the best way of preparing AgNCSe. A similar preparation using red Se gave no melt even at high temperatures - the Se began to oxidise in air.

Reactions of KCN with Se in liquid NH_3 solution proved only partly successful. NH_3 was frozen down into an ampule containing KCN and Se. The NH_3 (~15 ml) was

allowed to liquify at -78°C. After agitation of the contents, the Se lost its colour and a white precipitate formed. The NH_3 was removed and the remaining contents treated with acetone. Any KNCSe dissolved was then reacted to give AgNCSe as above. The average yield in such reactions was about 15% AgNCSe based on the original amount of KCN.

3.5.9 Germyl isocyanate was prepared by the reaction of germyl bromide with silver cyanate[25].

$$GeH_3Br + AgNCO \rightarrow GeH_3NCO + AgBr.$$

Deuterated germyl isocyanate was prepared from deuterated germyl bromide; ^{15}N and ^{13}C substituted species were prepared from the appropriate silver salt.

3.5.10 Germyl bromide was prepared by reacting germyl chloride with hydrogen bromide[26].

$$GeH_3Cl + HBr \rightarrow GeH_3Br + HCl.$$

3.5.11 Germyl chloride was prepared by chlorination of germane using stannic chloride[27].

$$GeH_4 + SnCl_4 \rightarrow GeH_3Cl + HCl + SnCl_2.$$

3.5.12 Germane was prepared by reduction of a basic solution of germanium dioxide with KBH_4 in acetic acid[28].

$$GeO_2 + KOH + KBH_4 \xrightarrow[\text{acetic acid}]{\text{glacial}} GeH_4 \text{ etc.}$$

3.5.13 Germyl isothiocyanate was prepared by the reaction of germyl bromide with silver thiocyanate[25].

$$GeH_3Br + AgNCS \rightarrow GeH_3NCS + AgBr.$$

3.5.14 Silver thiocyanate was prepared by precipitation by adding an aqueous solution of potassium thiocyanate to an aqueous solution of silver nitrate.

$$AgNO_{3(aq)} + KNCS_{(aq)} \rightarrow AgNCS\downarrow + KNO_{3(aq)}.$$

3.5.15 Silyl cyanide was prepared by a modification to the reaction of Emeleus, Maddock and Reid[29]. Silyl bromide was reacted with silver cyanide.

$$SiH_3Br + AgCN \rightarrow SiH_3CN + AgBr.$$

Deuterated silyl cyanide was prepared from deuterated silyl bromide; isotopically substituted silyl cyanides were prepared from the appropriate silver salt.

3.5.16 Silyl bis-isocyanate and silyl tris-isocyanate were isolated as decomposition products of silyl isocyanate. Ten mmoles of silyl isocyanate were placed in a 15 ml ampule and sealed with a Sovirel tap. The contents were kept at 30°C for 12 hrs. The gas phase infrared spectrum showed that silane had been produced.

Fractionation at -78°C passes the SiH_4 and SiH_3NCO. A less volatile fraction stopped. The gas phase infrared

spectrum indicated a mixture of $SiH_2(NCO)_2$ and $SiH(NCO)_3$. The separation of $SiH_2(NCO)_2$ and $SiH(NCO)_3$ proved difficult, probably due to easy formation of solutions. Repeated and careful fractionation at $-46^{o}C$ gave fairly pure samples of each compound.

CHAPTER 4 - SILYL ISOCYANATE, SiH_3NCO

4.1 Introduction

Since silyl isocyanate was first prepared[17] it has been studied many times using a variety of techniques. The infrared spectrum reported on its initial preparation showed gas phase bands characteristic of a symmetric top. It also served to confirm that the molecule did indeed exist in the iso form, due to the infrared band positions. The most striking evidence in the infrared spectrum for a symmetric top structure was the strong-weak-weak-strong intensity alternation of the Q branches on the perpendicular bands. The spectrum of silyl isocyanate was therefore assigned on the basis of the point group C_{3v} which gives five A_1 and five E modes of vibration.

The assignment of the fundamental bands in the infrared spectrum[30] proved straightforward in terms of a symmetric top model, although some irregularities in detail become apparent in the Q branch series of the perpendicular bands. These suggested that if the molecule was not a symmetric top then it was nearly so.

All of the fundamental bands were observed except that for ν_{10} which is associated with the skeletal band at nitrogen, and which has a very low frequency. The first information obtained on the low frequency

vibration was from microwave studies[31] in which rotational transitions are directly observed. Analysis of the microwave results revealed that the molecule is basically a symmetric top although, as was suggested before, with certain anomalies in behaviour.

The first of these is in the number of absorption lines observed in the rotational spectrum - far more than expected. These were assigned to molecules which were in vibrationally excited states, and it was concluded from the complexity of the spectrum that the proportion of excited state molecules was very high. It was then obvious that ν_{10} was of such low frequency as to be populated significantly in the high quantum states. Other anomalies appeared in the form of irregular changes in rotational constant, B, with different states of ν_{10}, and abnormally high values of the centrifugal distortion constant D_{JK}. These were thought to arise as a result of the high degree of anharmonicity of the low frequency vibration. Estimates of the frequency of ν_{10} were 50 cm^{-1} or less.

More recent microwave studies[32] have sought to obtain more detailed rotational spectra and to explain the anomalies in behaviour of silyl isocyanate quantitatively. Detailed analysis of many J+1 ← J transitions have led to the refinement of a potential function for ν_{10} which reproduces the observed

variations in B and D_{JK}. The form of potential used was $V = Aq^4 + Bq^2$ where A and B are constants and q is a dimensionless coordinate defining the amplitude of ν_{10}. By calculating the eigenenergies for a given potential it was possible to derive the B values in state v,l from $B_{v,l} = B_o - \alpha\langle q^2\rangle - \beta\langle q^4\rangle$. The potential was varied until the best fit with experiment was achieved.

The best potential turned out to be $V = -308\theta^2 + 1043\theta^4$ cm^{-1} where θ (radians) is the deviation from linearity at nitrogen. A cross section through the two dimensional potential shows a double minimum at $\pm 22^o$ and a maximum at $\theta = 0$ of 22.7 cm^{-1}. The ground state of ν_{10} was calculated to be very close to the maximum at $\theta = 0$. The form of the potential is a quartic with a negative quadratic term producing the central maximum. Although this reproduces the microwave data extremely well, a more physically reasonable quadratic well with a central maximum has also been shown to reproduce the data and has indeed proved necessary to explain subsequent observations[33,34].

The structure of silyl isocyanate has been determined in the gas phase by electron diffraction[33]. Again emphasis was put on the effect of the low frequency bending vibration on the experimental results. The molecular geometric structure parameters were surprising since a bent chain at nitrogen was found, despite the

spectroscopic evidence for a symmetric top structure. Here, one must remember that electron diffraction structures are averaged over all vibrations populated at the temperature of the experiment. It is not impossible, then, that the molecule may appear bent at room temperature due to the high population of the higher states of the low frequency bend.

Calculations on the Si...O peak in the electron diffraction probability density distribution led to a theoretical potential function for the low frequency bend. By theoretically fitting the Si...O peak shape a potential $V = -300\theta^2 + 1090\theta^4$ was derived; this has a double minimum at $\pm 21^{\circ}$ with a maximum at $\theta = 0$ of 20 cm^{-1}. It should be noted, however, that similar results were obtained using a quadratic well with a Lorenztzian type central maximum.

A normal coordinate analysis was carried out[35] using existing spectroscopic data for the species SiH_3NCO and SiD_3NCO. The output from such an analysis gives mean amplitudes of vibration and predicted shrinkages. The shrinkages proved to be extremely sensitive to assumed values of ν_{10}. Varying ν_{10} to give a good match with experimental shrinkages gave a best value for the frequency of 69 cm^{-1}.

Normal coordinate analysis assumes that all vibrations are harmonic and this, as we have seen, is

not the case for the low frequency vibration of silyl isocyanate. However, predictions of this sort have often proved to be extremely helpful.

Attempts have been made to observe more directly the low frequency bending mode of SiH_3NCO by far infrared spectroscopy and Raman spectroscopy[36]. Here the whole infrared spectrum was run in the vapour and solid phases and the Raman spectrum was run in all three phases. The assignment of the bands in the mid infrared was essentially the same as before[9]. However, the Raman spectrum in the range 90-150 cm^{-1} showed a series of Q branches assigned to the double quantum transitions of ν_{10}, the bending mode at nitrogen. Q branches have also been observed in Raman spectra of other small molecules at low frequency, notably $(SiH_3)_2O$[37].

The assignment of the Q branches to particular transitions led to the refinement of a potential function for the low frequency bend - $V = 0.856\ q^4 - 12.5\ q^2$. (q is a dimensionless coordinate). Again, the method used a variation procedure using harmonic oscillator wavefunctions to give eigenvalues for different potentials until the best fit with experiment was achieved. No conclusive observations were made in the Raman spectrum below 90 cm^{-1} or in the infrared below 200 cm^{-1} due to impurities such as HNCO and $(SiH_3)_2O$.

Thus the 'fundamental' band corresponding to the low frequency skeletal bend of SiH_3NCO was not observed.

4.2 Related Studies

The most closely related work has been carried out on silyl isothiocyanate, SiH_3NCS, and, in this work, silyl isoselenocyanate, SiH_3NCSe.

Silyl isothiocyanate has presented fewer problems both experimentally and theoretically than silyl isocyanate since it was first prepared[38]. Its preparation has proved less difficult, and obtaining pure samples considerably easier. It has been shown to be much more 'well behaved' in microwave[39,40], infrared[4,41,42] and Raman studies[4].

Initial microwave studies[39] established that the SiNCS chain was linear with much more 'normal' values for rotational constants such as D_{JK}. There were, however, rotational lines due to molecules in excited states of a low frequency vibration similar to that in SiH_3NCO. More recent microwave studies[40] have observed the variation of the rotation constant, B, with quantum state of the low frequency vibration, and concluded that this vibration is close to harmonic.

The first infrared spectra observed[41] gave a vibrational assignment for the species SiH_3NCS and SiD_3NCS. This was entirely consistent with a symmetric

top (C_{3v}) model for the molecule. Some of the perpendicular band Q branches were analysed to give coriolis coupling constants. The Q branches showed the strong-weak-weak-strong alternation in intensity expected for a symmetric top.

In SiH_3NCO the low frequency bending mode has not been directly observed before the present work. However, for SiH_3NCS a low frequency absorption in the infrared and scattering in the Raman has been observed[4]. For the species SiH_3NCS bands were observed at 66 cm^{-1} and 131 cm^{-1}. The first is due to the group of transitions $\Delta v = 1$, $\Delta l = \pm 1$ and the second to the group $\Delta v = 2$, $\Delta l = 0, 2$. The lack of complex structure in this spectrum (as compared to the Raman spectrum of SiH_3NCO) between 90 and 150 cm^{-1} is taken as evidence for a fairly harmonic vibration. That is, there is no significant broadening of the bands caused by a hot band series of different transition energies.

Harmonic force field calculations using spectroscopic data from two isotopic species[35] and matrix isolated data for four isotopic species[42] have also been carried out. Here, calculated parameters from the force field analysis (such as coriolis couplings, mean square amplitudes and shrinkages) were compared with the experimentally observed values[33,40]. These studies contained extensive discussion on the successes and

failures of the harmonic force field approximation.

It is clear that, although much is known about SiH_3NCO, there are areas in which further study would be useful. Firstly, improved force field solutions could be achieved by running infrared spectra of additional isotopically labelled species. Furthermore, the use of matrix isolation may lead to qualitative structural information. Secondly, direct observation of the infrared spectrum of a pure sample in the range 200 - 10 cm^{-1} (so far not obtained) would serve to confirm or refute the observations in the Raman spectrum (between 150 cm^{-1} and 90 cm^{-1}).

Silyl isocyanate was first studied in an argon matrix and then in a nitrogen matrix. The frequencies obtained from the infrared spectra of four isotopic species were used to perform a force field analysis. Further experiments in CO_2 and allene matrices were attempted in order to obtain structural information. In the far infrared, spectra were run in matrix isolation and in the gas phase - the gas phase spectra yielded better results.

Experimental Results

4.3 Silyl Isocyanate in an Argon Matrix

Table 4.1 contains frequency data for SiH_3NCO in an argon matrix. Assuming the point group C_{3v} we expect

Table 4.1

Observed frequencies (cm^{-1}) and assignments for SiH_3NCO, argon matrix (1:1000)

2320.8	v.s.	)	
		)	ν_1, NCO asymmetric stretch
2316.7	s	)	
2235.0	m.s.	)	
		)	
2226.3	s	)	ν_2, ν_6, SiH stretches
		)	
2223.0	m.s.	)	
1471.2	w		ν_3, NCO symmetric stretch
959.7	s	)	
		)	
955.9	s	)	ν_4, ν_7, SiH deformations
		)	
951.0	s	)	
723.5	m.s.	)	
		)	ν_8, SiH_3 rock
712.5	m.s.	)	
611.8(br)	m		ν_9, NCO bend
591.0	s		ν_5, SiN stretch

[v = very, s - strong, m = medium, w = weak, br = broad, sh = shoulder].

to observe 5A and 5E vibrations, i.e. 10 absorption bands in all. The spectrum was run in the mid infrared with a low frequency limit of 200 cm^{-1}, so the lowest frequency band was not observed. This leaves 9 expected fundamental bands in the mid infrared. After annealing the sample no significant changes in the spectrum were observed.

The frequencies in Table 4.1 are each assigned to an approximate description of the associated mode of vibration. They show that all of the degenerate modes (and one of the non-degenerate modes) result in more than one infrared absorption. It is not unusual to observe a slight splitting (<5 cm^{-1}) of degenerate modes in matrix spectra due to the non-isotropic matrix cage interacting differently with the components. However, the splitting is unusually large to be put down to this effect in the case of the SiH_3 rocking mode, which is generally accepted as a good indicator of symmetry both in matrix and gas phase spectra. The splitting may indicate a reduction in symmetry of the molecules from C_{3v}. The splitting in the non-degenerate band, ν_1, is more difficult to explain - it may be caused by inter-molecular association between sample molecules. None of the observed splittings can be due to multiple site effects since the spectrum does not change on annealing the sample.

One unusual feature of the spectrum is the broad band at 611.8 cm^{-1} (matrix isolated samples usually give sharp bands). This is another matrix effect which is difficult to explain, although it has certainly a lot to do with the interaction of the matrix with the sample molecules. Good evidence for differing matrix-sample interactions can be seen on changing to a nitrogen matrix.

4.4 Silyl Isocyanate in a Nitrogen Matrix

On running spectra in a nitrogen matrix slightly sharper bands were observed in the infrared spectrum (see Figures 4.1 and 4.2). Since the spectrum in a nitrogen matrix proved satisfactory from this point of view and also from the point of view of interpretation, the spectra of four isotopic species were run. The observed frequencies and assignment of approximate modes of vibration are given in Table 4.2. The assignment has been based on the molecular point group of C_{3v} despite large 'degenerate' splittings.

The absorption associated with ν_3, the NCO symmetric stretch, appears in all spectra, except the deuterated species, as a weak doublet. The doubling of the band is caused by the Fermi resonance of ν_3 with $2\nu_8$. This will be discussed later. As indicated in Table 4.2 weak bands were observed to low frequency of ν_5 and assigned to the same mode of the naturally

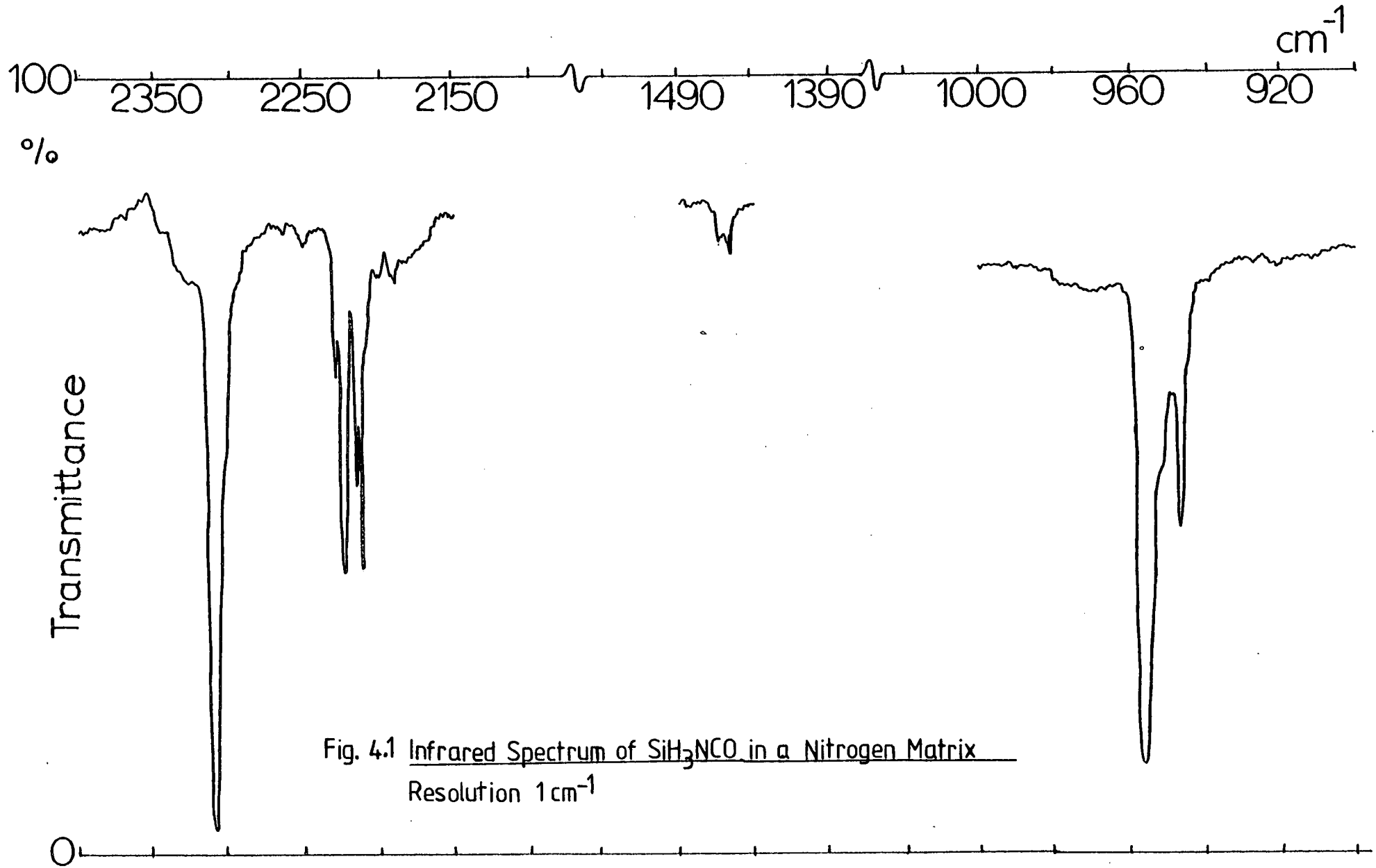

Fig. 4.1 Infrared Spectrum of SiH_3NCO in a Nitrogen Matrix
Resolution 1 cm^{-1}

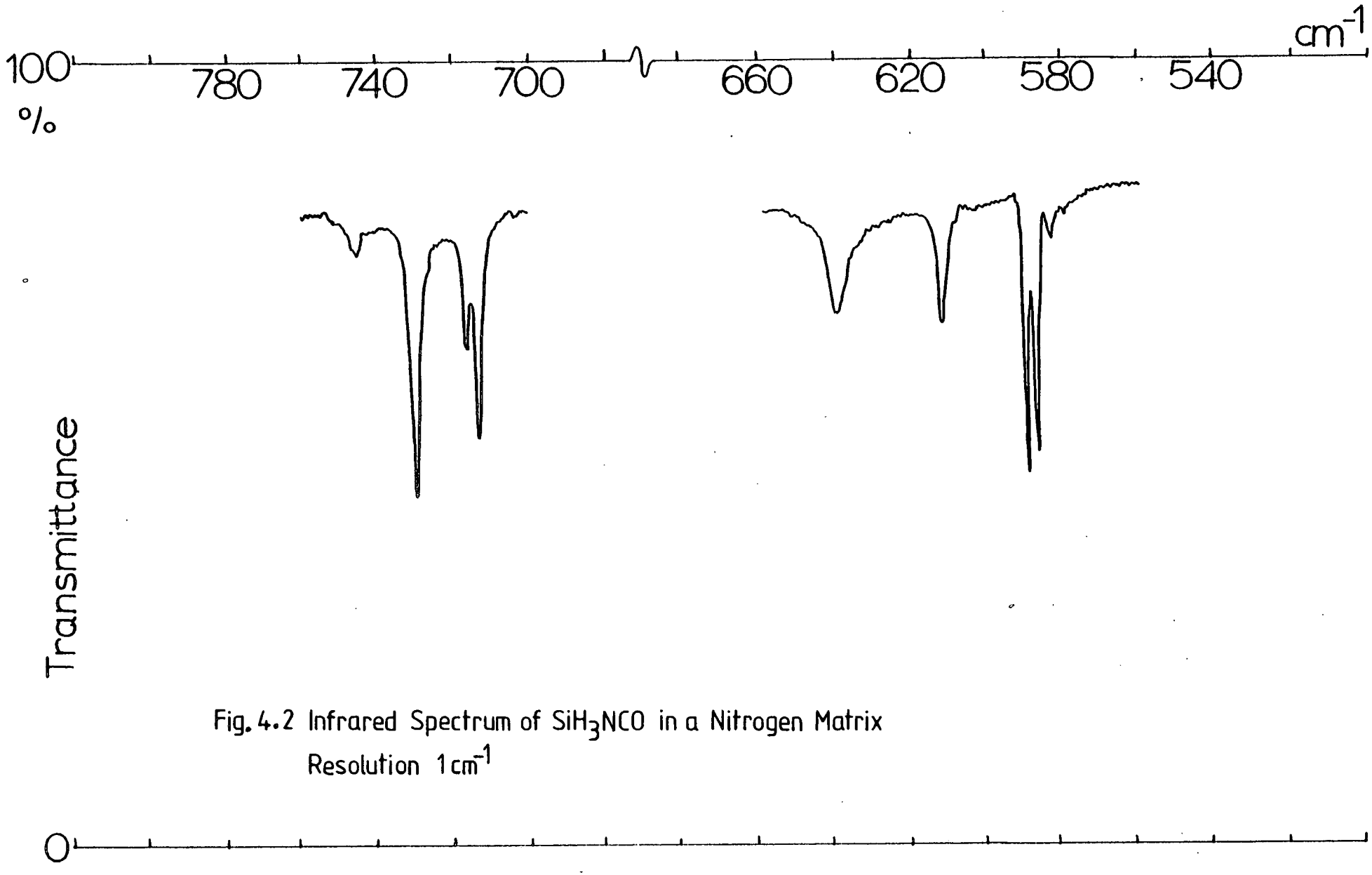

Fig. 4.2 Infrared Spectrum of SiH_3NCO in a Nitrogen Matrix
Resolution 1 cm^{-1}

Table 4.2

Observed frequencies (cm^{-1}) and assignment for SiH_3NCO, N_2 matrix

SiH_3NCO	$SiH_3{}^{15}NCO$	$SiH_3N{}^{13}CO$	SiD_3NCO		
2308.3	2297.5	2252.2	2306.0	v.s., ν_1,	NCO asymmetric stretch
2224	2224	2223.2	1593.5	s., ν_2,	SiH symmetric stretch
2212	2212	2211	1624.5 1622.5	s. ν_6,	SiH asymmetric stretch
1463.5	1433	1462	1460.2	w.) ν_3,	NCO symmetric stretch
1456.5	1423(sh)	1455		w.)	
955.5	955.6	955.6	714.7	v.s., ν_4,	SiH symmetric deformation
946.1	946.2	946.2	685.9	s., ν_7,	SiH asymmetric deformation
730.1	728.7	729.8	544.5	s.) ν_8,	SiH_3 rock
713.4	712.3	713.1	536.1	s.)	
640.3	636.5	630.7	635.0	m.s.) ν_9,	NCO bend
612.5	610.8	595.2	614.0	m.s.)	
590.2	589.8	579.4	579.9	s.) ν_5,	SiN stretch
587.5	587.0			s.)	
583.7	583.7	590.2	575.5	v.w., ν_5,	(4.7% ^{29}Si)
580.1	580.4	587.5	-	v.w., ν_5	(3.1% ^{30}Si)

abundant molecules containing ^{29}Si and ^{30}Si. Isotopic shifts for a diatomic SiN at a similar stretching frequency were calculated to be about 5 cm^{-1}, the same order as the shifts observed here.

The nitrogen matrix spectra show very clearly the reduction in symmetry of SiH_3NCO from C_{3v}. Again the 'degenerate' modes are split in energy by considerable amounts - 15 cm^{-1} for the SiH_3 rock and 25 cm^{-1} for the two bands associated with the two NCO bends. These two bands have appeared in place of the very broad band observed in a similar position in the spectrum in an argon matrix.

Thus SiH_3NCO is a molecule which is apparently a symmetric top in the gas phase but which does not behave as such in a low temperature matrix. This apparent anomaly can be resolved in terms of the low frequency skeletal (SiNC) bending potential which has energy transitions in the far infrared.

4.5 Far Infrared Spectrum of Silyl Isocyanate

Initially attempts were made to run far infrared spectra with matrix isolated samples. The results were inconclusive in that only two absorption bands were observed (in an argon matrix) at 34 cm^{-1} and 45 cm^{-1}. These remained even when the sample molecules were changed to, for example, CH_3NCO. They could not,

therefore, be assigned to vibration of the sample molecule. Extremely large quantities of sample/matrix mixture were used without success. No absorption bands at all were observed in nitrogen matrices.

Attention was turned to running spectra in the gas phase in the far infrared. The far infrared gas phase spectrum of SiH_3NCO is shown in Figure 4.3. The spectrum was run in a 150 cm cell at a pressure of 70 mmHg (resolution 1.2 cm^{-1}).

The spectrum shows two broad bands, one centred at 64 cm^{-1}, the other centred at 134 cm^{-1}. In the mid infrared we are used to observing only the $v = 0 \rightarrow v = 1$ transitions (fundamental transitions) but in the far infrared spectrum very many hot bands contribute to the intensity. For a vibration of such low energy there is significant population of states up to about v = 15. This can be determined very easily using the Boltzmann distribution. The energy levels for this vibration (SiNC bend) are given two quantum numbers. This is true of any degenerate vibration. The first quantum number, already mentioned, is v, the vibrational quantum number; the second is l, the angular momentum quantum number.

In this far infrared spectrum the lower band consists mostly of the intensity from the $\Delta v = 1$, $\Delta l = \pm 1$ transitions and the upper band mostly of the intensity from the $\Delta v = 2$, $\Delta l = 0,2$ transitions. This would seem a

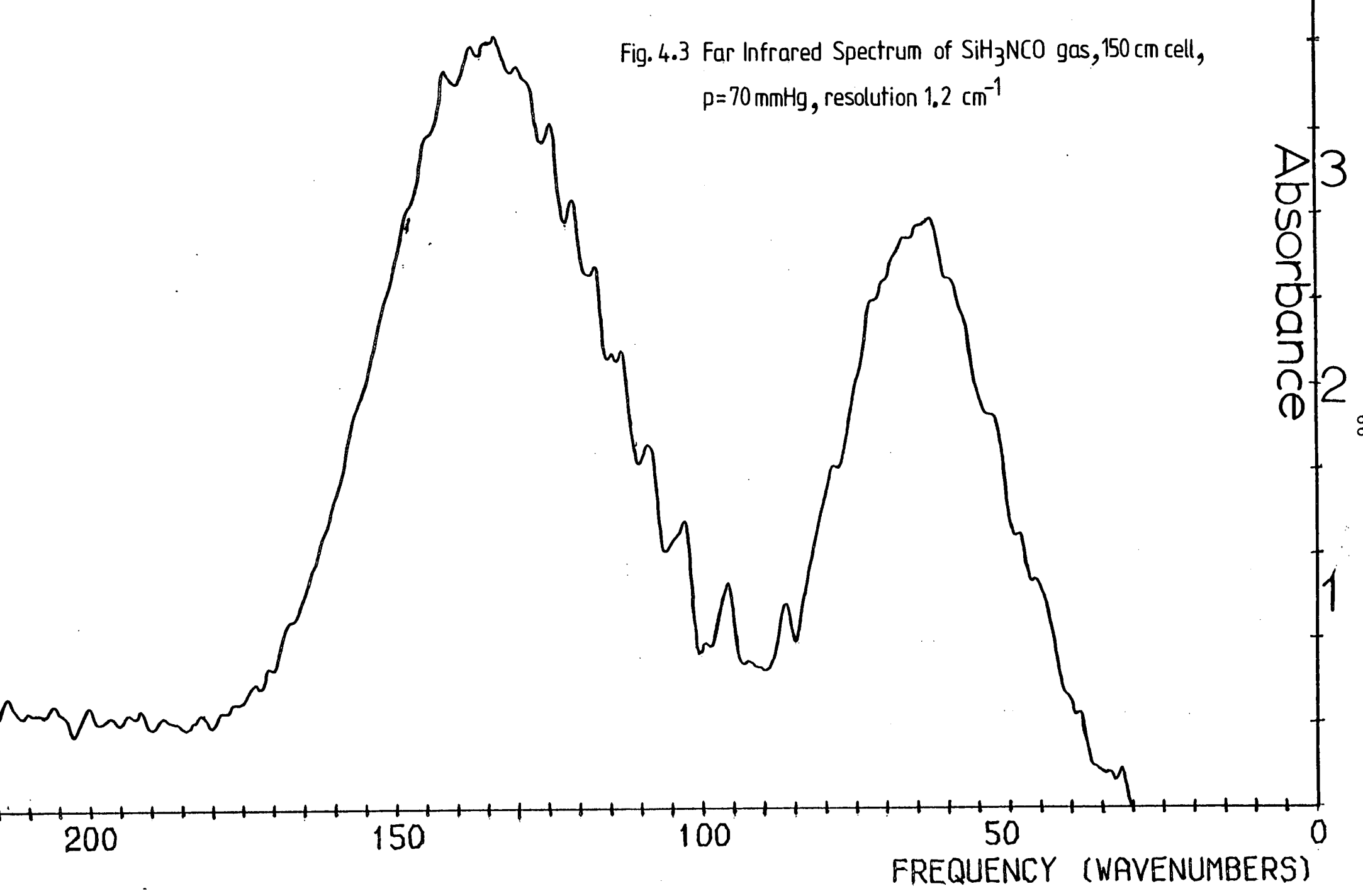

Fig. 4.3 Far Infrared Spectrum of SiH_3NCO gas, 150 cm cell, p = 70 mmHg, resolution 1.2 cm^{-1}

reasonable deduction since the frequency of one band is almost exactly twice that of the other. The two bands are comparable in intensity - unusual for a 'fundamental' and 'overtone'. The appearance of an overtone for any vibration implies that the potential governing the vibration is anharmonic. This would appear to be the case in this instance - in agreement with previous calculation on the low frequency bending potential of silyl isocyanate.

It is expected that the individual transitions $\Delta v = +1$, $\Delta l = \pm 1$ and $\Delta v = 2$, $\Delta l = 0,2$ would be observed in the infrared as a series of discrete bands considering the already proven anharmonicity. This is indeed the case to a significant degree in the region 80-120 cm^{-1} and to a lesser degree in the lower frequency band. The lower frequency band is shown in Figure 4.4 in a spectrum run at 0.66 cm^{-1} resolution. Most of the structure on this band is real as can be seen by comparison with Figure 4.3.

It was considered necessary to check very carefully the purity of the SiH_3NCO after the far infrared experiments in order to be sure that all the features on the spectrum were real and due to the compound under study. The sample was checked by mid infrared spectra (no bands due to common impurities $(SiH_3)_2O$ and HNCO), vapour pressure - 364 mmHg at 0^oC^{30} and molecular weight -

Fig.4.4 Far Infrared Spectrum of SiH_3NCO gas, 150 cm cell, p = 70 mmHg, resolution 0·66 cm^{-1}

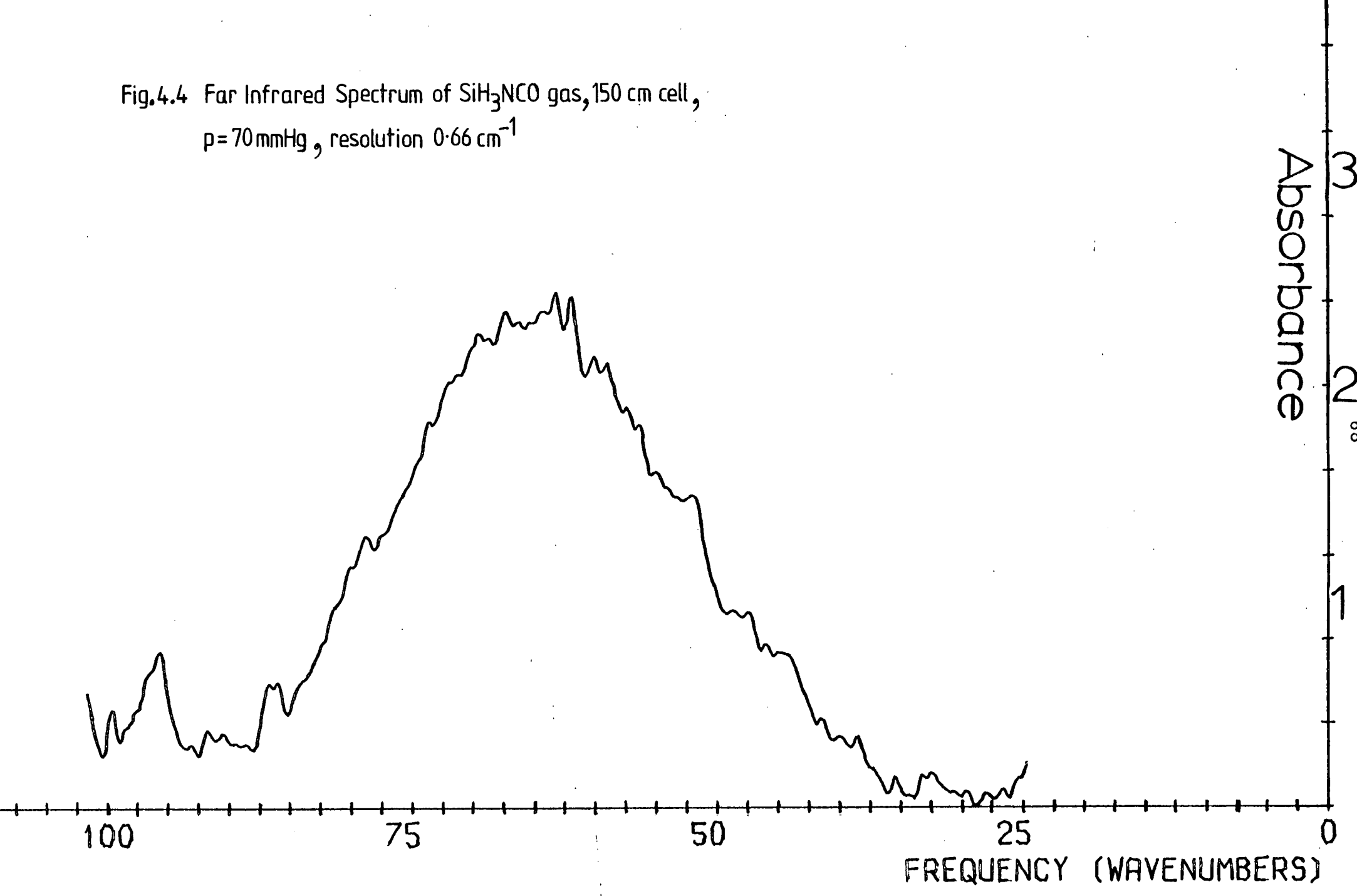

73.98 $gmol^{-1}$ (calculated 73.13 $gmol^{-1}$). It is obvious from the far infrared spectrum itself that there are no bands due to HNCO which has very strong rotational absorptions at 88.26 cm^{-1} ($^{R}Q_1$), 142.20 cm^{-1} ($^{R}Q_2$) and 191.78 cm^{-1} ($^{R}Q_3$)[43].

A set of Q branches might be expected for the lower frequency band (perpendicular band) and there are discrete observed features. The upper band is a parallel band and the prominent features observed in the low frequency shoulder are not Q branches (which are relatively weak) but headed P branches. These occur when there is a large change in rotational constant, B, between the upper and lower vibrational state.

The frequency positions of the P heads, once assigned, proved useful in defining a potential for the low frequency bend. Here the potential parameters could be further constrained by the direct observation of the band centred at 64 cm^{-1}. In order to carry out this analysis a computer programme was developed which calculated eigenenergies for a given two-dimensional potential (see Appendix I).

Having developed the computer programme it was possible to calculate energy levels for a given potential and to simulate the infrared band shape theoretically from the derived band origins. An assignment of the fine structure in the far infrared bands was thus made. The

derived potential was a quadratic with a central maximum given by a Lorentzian function. It reproduced the spectrum in the infrared well, and also reproduced previously obtained microwave data[32]. (For a detailed account of the far infrared band simulation and potential see reference 34).

4.6 Far Infrared Spectrum of SiD_3NCO (Figures 4.5 & 4.6)

The main features of this spectrum are similar to those found for the normal isotopic species - two broad bands are observed. However, the band centres are shifted to 129 cm^{-1} and 62 cm^{-1}. The fine structure features apparent in the spectrum of SiH_3NCO are less prominent and are shifted. Things are made more difficult since the spectra are a little noisy.

It is not easy to correlate one set of fine structure with the other since the P head positions are dependent on many factors. The band origins themselves will be shifted due to the change in reduced mass for the SiNC bend. The position of the P head with respect to the band origin will also change since the change in B value, and the B values themselves, will not be the same as the normal isotopic species values.

4.7 Normal Coordinate Analysis of SiH_3NCO

The data collected from the mid infrared nitrogen matrix spectra and the far infrared spectra were used in an

Fig.4.5 Far Infrared Spectrum of SiD_3NCO gas, 150 cm cell,
p = 70 mmHg, resolution 1·2 cm^{-1}

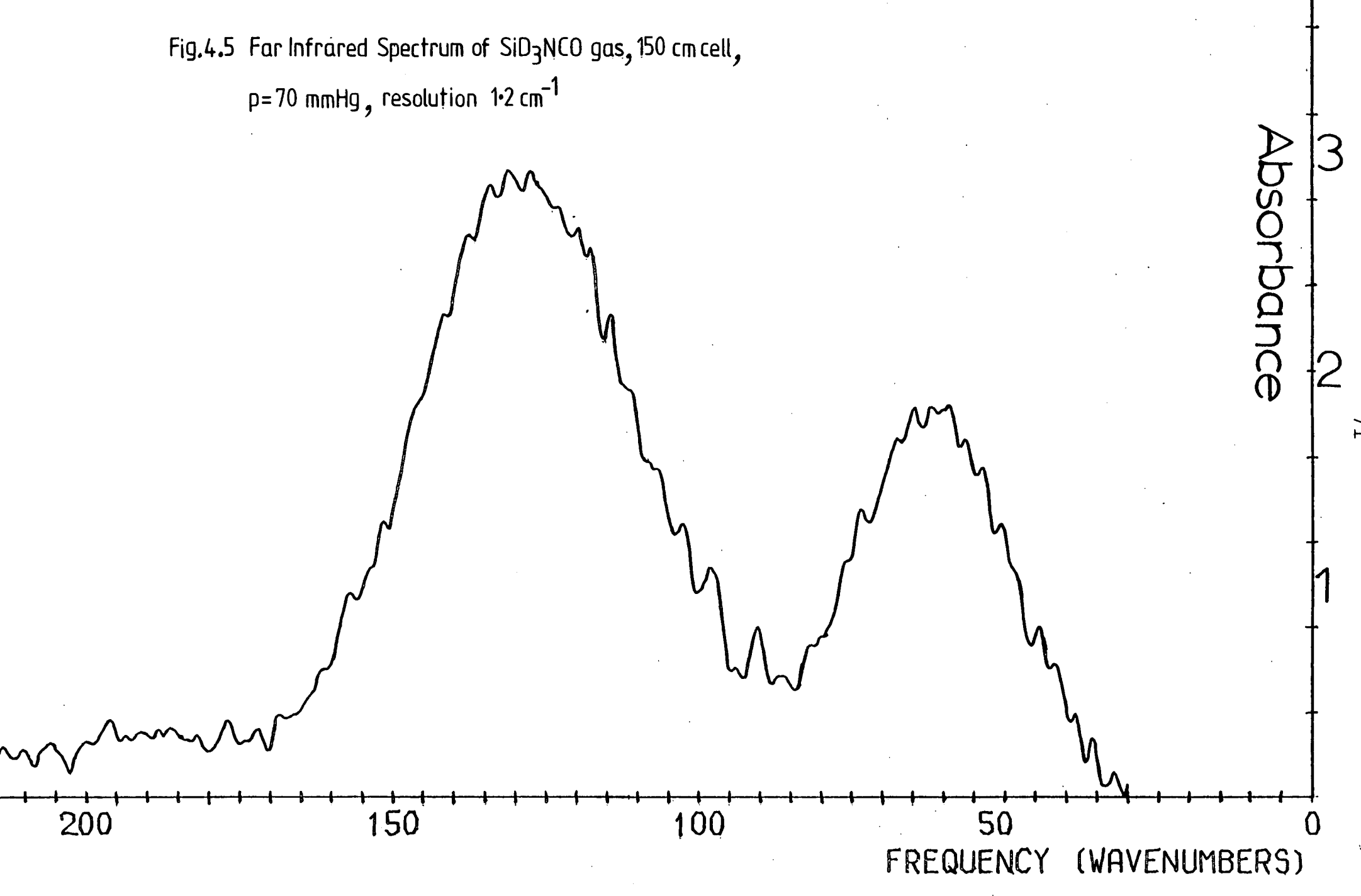

Fig. 4.6 Far Infrared Spectrum of SiD_3NCO gas, 150 cm cell, p = 70 mmHg, resolution 0·66 cm^{-1}

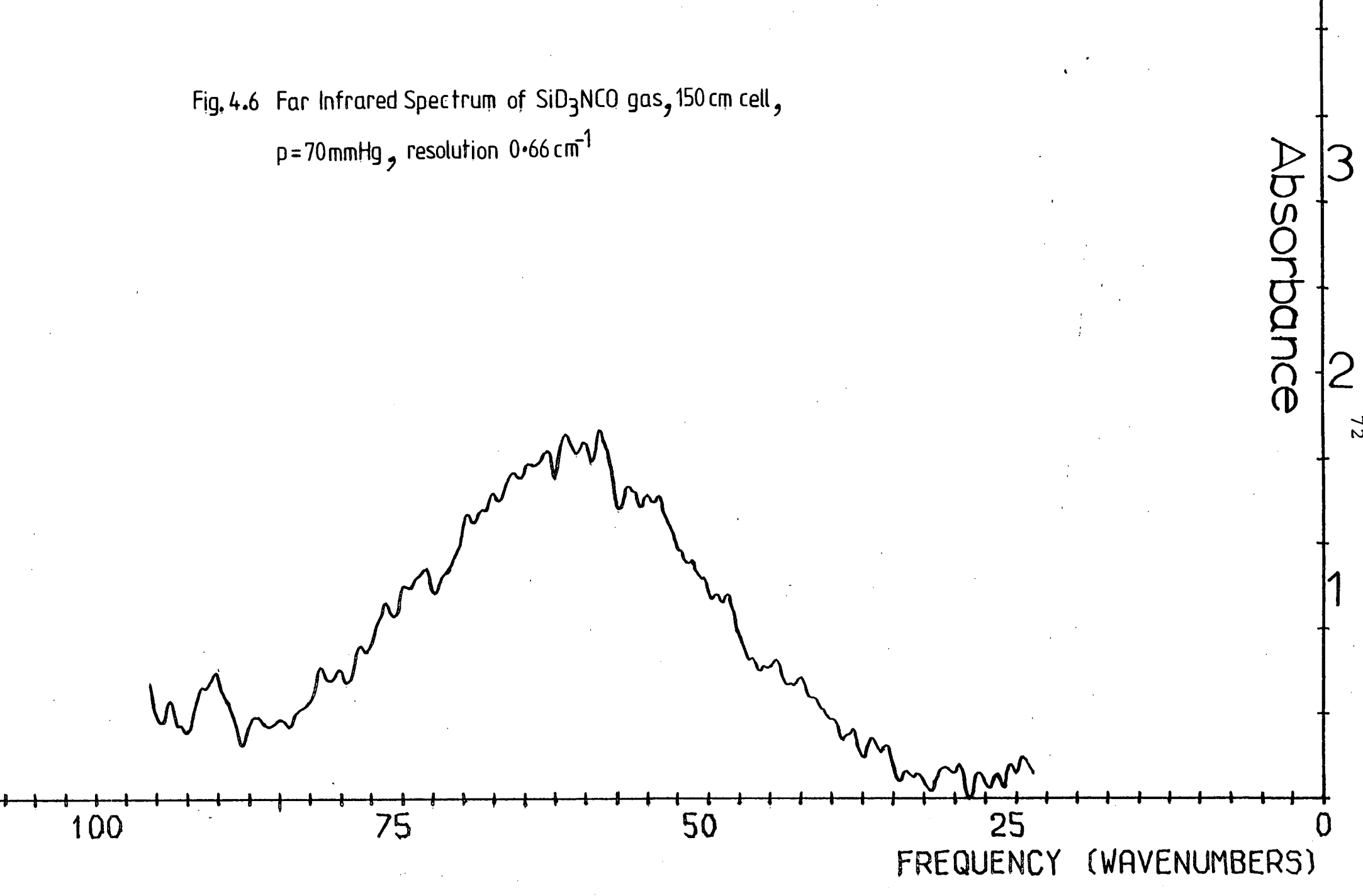

analysis of normal coordinates. Two separate analyses were carried out - one with the molecule in a C_s configuration (matrix) and one in a C_{3v} configuration (gas phase). The latter analysis was undertaken using slightly modified matrix data in order to make comparison with, and use of, previous gas phase studies.

4.7.1 Treatment of Fermi resonance, ν_3 with $2\nu_8$

In both C_s and C_{3v} configurations difficulty was encountered in reproducing the frequencies and shifts for the NCO symmetric stretch, ν_3. This was due to the Fermi resonance of ν_3 with $2\nu_8$. As in the gas phase, the band due to the symmetric NCO stretch is clearly double.

ν_8 is split into two components in the matrix spectrum, so $2\nu_8$ will be (at least) double. Twice either component of ν_8 has symmetry A', while their sum has symmetry A". Thus only the former combination will interact with the A' NCO symmetric stretch. The observed doublet was assumed to be ν_3, plus the closer component (in energy) of $2\nu_8$ in Fermi resonance. The more intense component was taken to be ν_3. In calculating the $2\nu_8$ frequencies it was assumed that the vibration is harmonic.

Below is a table of the observed frequencies and the calculated frequencies for $2\nu_8$.

ν_3 region of spectrum of SiH_3NCO - frequencies (cm^{-1})

	SiH_3NCO	$SiH_3{}^{15}NCO$	$SiH_3N^{13}CO$	SiD_3NCO
observed	(1463.5	1433*	1462	1460.2
	(1456.5*	1423 (sh)	1455*	
calculated	(1460.2	1457.4	1459.6	no Fermi resonance
$2\nu_8$	(1426.8	1424.6	1426.2	

In each case the * indicates the more intense component of the observed doublet and is therefore assigned to the 'fundamental'. Fermi resonance was assumed to occur only with the closer (in energy) component of $2\nu_8$. In order to make some form of adjustment to the observed frequencies, a first order interaction of ν_3 with $2\nu_8$ was assumed. On the basis of these assumptions it was possible to calculate unperturbed frequencies for ν_3. The calculated values are:

	SiH_3NCO	$SiH_3{}^{15}NCO$	$SiH_3N^{13}CO$	SiD_3NCO
ν_3	1459.8 cm^{-1}	1431.4 cm^{-1}	1457.4 cm^{-1}	1460.2 cm^{-1}
				(no adjustment)

A point in favour of this treatment is that the calculated frequency for SiH_3NCO of 1459.8 cm^{-1} is very close to the frequency of 1460.2 cm^{-1} for SiD_3NCO for which the Fermi resonance with $2\nu_8$ is removed. (It is not expected that ν_3 would shift in frequency by a significant amount on deuteration). The band in the spectrum of

SiD_3NCO shows no evidence of being double and is much sharper and more intense than in the other isotopic species.

4.7.2 Treatment of split 'degeneracies'

The normal coordinate analysis in the C_s configuration used all of the observed frequencies. In the C_{3v} configuration, it was found adequate to average the frequencies for the split 'degenerate' modes in all cases except the NCO bending region.

Observing the SiN stretching frequencies, the shift on ^{15}N substitution is small (0.6 cm^{-1}) and that on ^{13}C substitution is larger. While this is by no means impossible, the shift on ^{13}C substitution is abnormally large (9.6 cm^{-1}). It turns out that such a shift in frequency is acceptable for the molecule in a C_s configuration due to the interaction of the A' N-C-O bend (which has a large shift on ^{13}C substitution) with the A' Si-N stretch (see Figure 4.7).

The modes in question would be of different symmetries in a C_{3v} configuration and would therefore not interact, the SiN frequency shift on ^{13}C substitution then being much smaller. SiH_3NCS, which is known to be a (nearly) symmetric top in a matrix, shows a shift in frequency of the Si-N stretching mode on ^{13}C substitution of only 2.4 cm^{-1} [42]. Any attempt to refine the observed matrix data for SiH_3NCO in a C_{3v} configuration

Fig. 4.7 Infrared Spectrum of SiH_3NCO and Isotopically Substituted Species in a Nitrogen Matrix (560 - 680 cm^{-1})

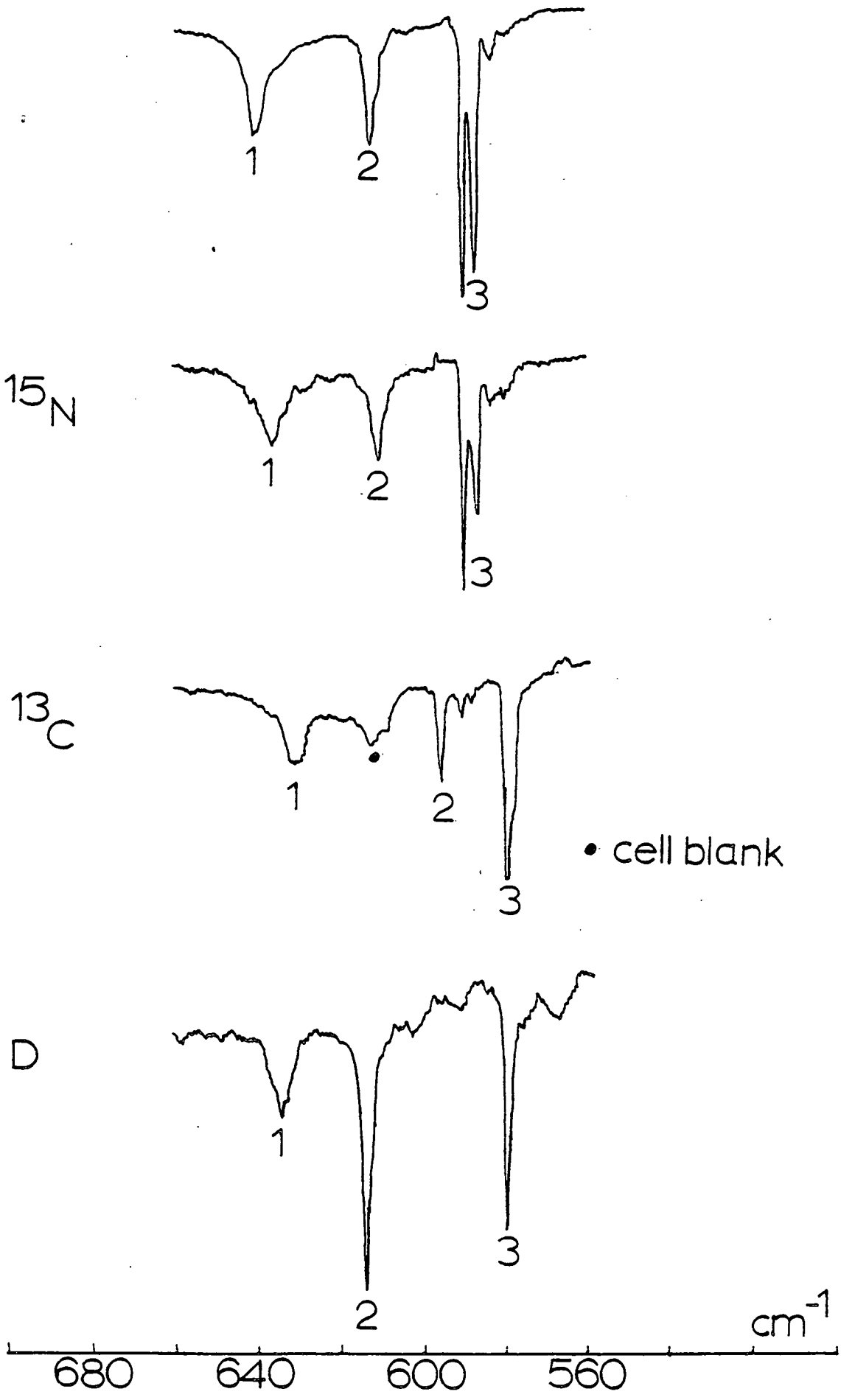

would therefore be futile without slight adjustments.

Of the two NCO bending modes, the one with the larger isotopic shift on ^{13}C substitution is taken as the A" mode. In the case of the normal isotopic species it is the band at 612.5 cm^{-1}. This frequency is not perturbed by any other levels close to it in energy so it (and the corresponding frequencies for the isotopic species) was used in the C_{3v} refinement. The other NCO bending mode (A') has a smaller shift due to its interaction with the SiN stretch (A'). It was possible, assuming a first order interaction, to calculate the perturbation on the A' NCO bend by comparison with the A" N-C-O bend and obtain a predicted ^{13}C shift for the SiN stretch in a C_{3v} configuration.

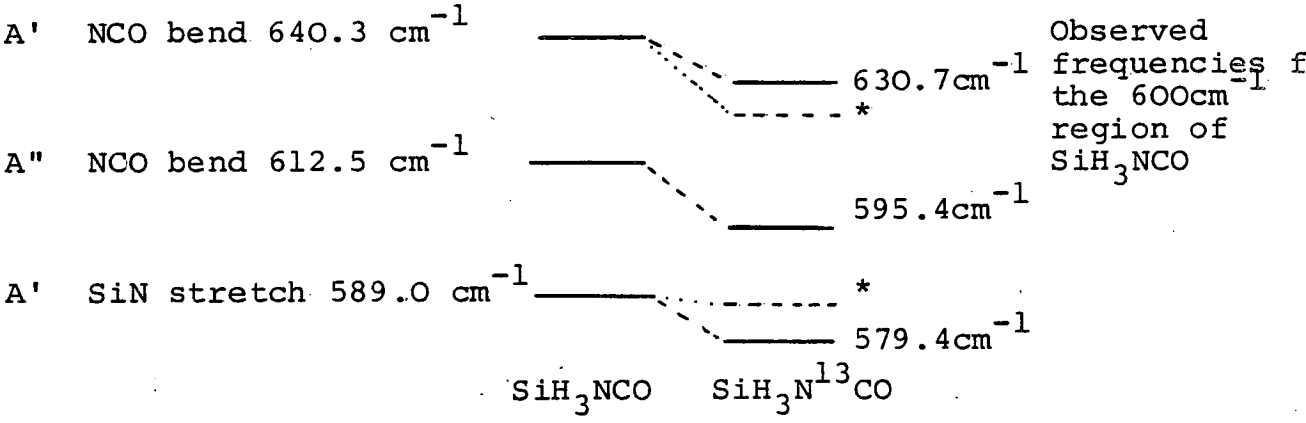

*unperturbed frequency

Shift of A" NCO bend = 17.3 cm^{-1}

Shift of A' NCO bend = 9.6 cm^{-1}

Perturbation on A' NCO bend = 17.3-9.6 = 7.7 cm^{-1}

Perturbed shift of A' SiN stretch = 9.6 cm^{-1}

Unperturbed shift of A' SiN stretch = 9.6-7.7 cm^{-1} = 1.9 cm^{-1}.

The value of 1.9 cm^{-1} was used as a shift for the SiN mode on ^{13}C substitution, for the molecule in a C_{3v} configuration. Shifts observed for the NCO bending modes on ^{15}N substitution and deuteration are much smaller than for ^{13}C substitution so the perturbations are likely to be small. The frequencies observed for these molecules were therefore left unaltered in the refinement.

4.7.3 Use of far infrared data in normal coordinate analysis

The harmonic approximation used in a force field analysis poses some problems when we consider the frequency values to use. In the absence of information about anharmonicities (e.g. from position of overtone bands), the fundamental transition frequency ($v = 0 \rightarrow v = 1$) is taken as the harmonic frequency.

The ν_{10} vibration of silyl isocyanate has a very anharmonic character, with the fundamental transition calculated[34] to be 20-25 cm^{-1}. Inserting a value in this range into a harmonic approximated calculation would clearly lead to incorrect results. The frequencies used for ν_{10} were 64 cm^{-1} for SiH_3NCO and 62 cm^{-1} for SiD_3NCO representing the room temperature observed band maxima in the gas phase. It is assumed in using these values that they are adequate overall 'harmonic' frequencies for ν_{10}.

4.7.4 Molecular structure, internal coordinate, symmetry coordinates

The molecular structure used was the same as that used in a previously published normal coordinate analysis[32]. The structural parameters were as follows: r(Si-N) 1.703 Å, r(Si-H) 1.488 Å, r(C-N) 1.216 Å, r(C-O) 1.164 Å, $\widehat{HSiH}$ 110°. For the analysis in the C_s configuration the angle at nitrogen was 151.7° which corresponds to the position of the potential minimum of the low frequency bend, calculated in an electron diffraction study[33]. The NCO group in this case was assumed to be trans to one of the silyl hydrogen atoms.

In the C_{3v} configuration the internal coordinates and symmetry coordinates were as follows:

Internal Coordinates

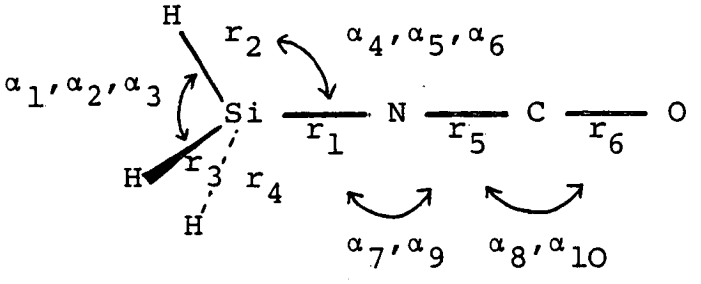

Symmetry Coordinates

$\underline{A}_1$

s_1: Δr_6

s_2: $\frac{1}{(3)^{\frac{1}{2}}}(\Delta r_2 + \Delta r_3 + \Delta r_4)$

s_3: Δr_5

s_4: $(3+3\nu^2)^{-\frac{1}{2}}\{r_2(\Delta\alpha_1+\Delta\alpha_2+\Delta\alpha_3) + \nu(r_1r_2)^{\frac{1}{2}}(\Delta\alpha_4+\Delta\alpha_5+\Delta\alpha_6)\}$

s_5: Δr_1

$$\nu = \frac{(3)^{\frac{1}{2}}\cos\alpha_4}{\cos\frac{\alpha_1}{2}}$$

E(1)

s_1: $\frac{1}{(6)^{\frac{1}{2}}}(2\Delta r_2-\Delta r_3-\Delta r_4)$

s_2: $\frac{r_2}{(6)^{\frac{1}{2}}}(-\Delta\alpha_1-\Delta\alpha_2+2\Delta\alpha_3)$

s_3: $\frac{(r_1r_2)^{\frac{1}{2}}}{(6)^{\frac{1}{2}}}(2\Delta\alpha_4-\Delta\alpha_5-\Delta\alpha_6)$

s_4: $(r_5r_6)^{\frac{1}{2}}\Delta\alpha_8$

s_5: $(r_1r_5)^{\frac{1}{2}}\Delta\alpha_7$

E(2)

s_1: $\frac{1}{(2)^{\frac{1}{2}}}(-\Delta r_3+\Delta r_4)$

s_2: $\frac{r_2}{(2)^{\frac{1}{2}}}(\Delta\alpha_1-\Delta\alpha_2)$

s_3: $\frac{(r_1r_2)^{\frac{1}{2}}}{(2)^{\frac{1}{2}}}(-\Delta\alpha_5+\Delta\alpha_6)$

s_4: $(r_5r_6)^{\frac{1}{2}}\Delta\alpha_{10}$

s_5: $(r_1r_5)^{\frac{1}{2}}\Delta\alpha_9$

There is a redundancy due to the fact that all angles around the silicon atom cannot increase simultaneously.

$$(3+3\nu^2)^{-\frac{1}{2}}\{r_2(\Delta\alpha_1+\Delta\alpha_2+\Delta\alpha_3)-\nu(r_1r_2)^{\frac{1}{2}}(\Delta\alpha_4+\Delta\alpha_5+\Delta\alpha_6)\} = 0.$$

In the C_s configuration the internal and symmetry coordinates were as follows:

Internal Coordinates

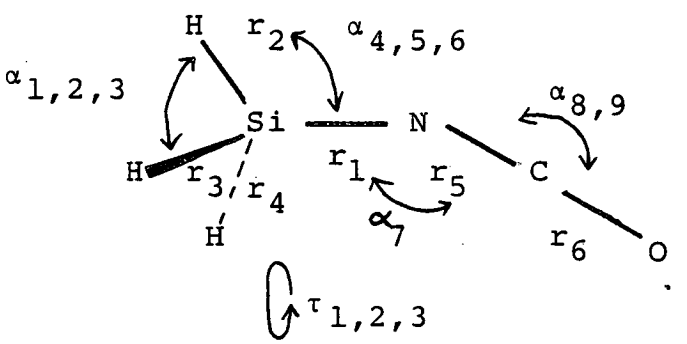

Symmetry Coordinates

A'

s_1: Δr_6

s_2: Δr_5

s_3: $(3+3\nu^2)^{-\frac{1}{2}}\{r_2(\Delta\alpha_1+\Delta\alpha_2+\Delta\alpha_3) + \nu(r_1r_2)^{\frac{1}{2}}(\Delta\alpha_4+\Delta\alpha_5+\Delta\alpha_6)\}$

s_4: $\frac{r_2}{(6)^{\frac{1}{2}}}(-\Delta\alpha_1-\Delta\alpha_2+2\Delta\alpha_3)$

s_5: $\frac{(r_1r_2)^{\frac{1}{2}}}{(6)^{\frac{1}{2}}}(2\Delta\alpha_4-\Delta\alpha_5-\Delta\alpha_6)$

s_6: $(r_5r_6)^{\frac{1}{2}}\Delta\alpha_9$

s_7: Δr_1

s_8: $(r_1r_5)^{\frac{1}{2}}\Delta\alpha_7$

A' SiH stretches

s_1: $\frac{1}{(3)^{\frac{1}{2}}}(\Delta r_2+\Delta r_3+\Delta r_4)$

s_2: $\frac{1}{(6)^{\frac{1}{2}}}(2\Delta r_2-\Delta r_3-\Delta r_4)$

A"

s_1: $\frac{1}{(2)^{\frac{1}{2}}}(-\Delta r_3+\Delta r_4)$

s_2: $\frac{r_2}{(2)^{\frac{1}{2}}}(\Delta\alpha_1-\Delta\alpha_2)$

s_3: $\frac{(r_1r_2)^{\frac{1}{2}}}{(2)^{\frac{1}{2}}}(-\Delta\alpha_5+\Delta\alpha_6)$

s_4: $(r_5r_6)^{\frac{1}{2}}\Delta\alpha_8$

s_5: $\frac{r_1}{(3)^{\frac{1}{2}}}(\Delta\tau_1+\Delta\tau_2+\Delta\tau_3)$

The A' SiH stretches were treated as a separate symmetry species due to computer programme formatting considerations. This is not likely to induce much error in the results of the analysis since these symmetry coordinates have negligible coupling with other coordinates in the normal mode.

4.7.6 Solution in C_{3v} configuration - discussion

Tables 4.3, 4.4 and 4.5 summarise the solutions for the A_1 and E symmetry species. The F matrix (mdynes $\mathring{A}^{-1}$), frequency fit, the potential energy distribution and the L matrix are all given. The calculated values U, P, L, K, RG, RALPHA are the same as those discussed in the chapter on theory.

In general, the frequency fit is good, except for the SiD modes in SiD_3NCO. This is due to the extremely large shifts observed and there being no correction for anharmonicity. In the refinement these shifts were given a reduced weighting. Any isotopic frequencies not observed were given zero weighting.

The A_1 solution potential energy distribution shows fairly 'pure' vibrations for the SiH stretch, SiH deformation and SiN stretch. The bands at 2308.3 cm^{-1} and 1459.8 cm^{-1} show considerable mixing of the CN and CO coordinates as expected, justifying their assignment as the asymmetric and symmetric NCO stretches.

Table 4.3

NORMAL COORDINATE SOLUTION FOR SIH NCO
SYMMETRY SPECIES - A1 3
F MATRIX AND FREQUENCIES FOR 4 ISOTOPIC SPECIES
P. E. DISTRIBUTION AND L MATRIX FOR 1ST ISOTOPIC SPECIES

F MATRIX

16.83771				
0.00000	2.90306			
2.05242	0.00000	12.70469		
0.00000	0.00000	0.00000	0.25169	
1.27588	0.00000	-0.30469	-0.28530	4.55942

F.OBS	F.CALC	DIFF	
2308.30	2308.30	0.00	
2224.00	2224.00	0.00	
1459.80	1459.80	0.00	SIH NCO
955.50	955.50	0.00	3
589.00	588.98	0.02	

F.OBS	F.CALC	DIFF	
2297.50	2295.83	1.67	
2224.00	2223.93	0.07	15
1431.40	1430.36	1.04	SIH NCO
955.60	955.47	0.13	3
588.40	587.94	0.46	

F.OBS	F.CALC	DIFF	
2252.20	2250.25	1.95	
2223.20	2222.42	0.78	13
1457.40	1459.35	-1.95	SIH N CO
955.60	955.45	0.15	3
587.10	585.00	2.10	

F.OBS	F.CALC	DIFF	
2306.00	2307.65	-1.65	
1593.50	1584.65	8.85	
1460.20	1455.91	4.29	SID NCO
714.70	698.74	15.96	3
579.90	578.91	0.99	

P.E. DISTRIBUTION

2308.30	2224.00	1459.80	955.50	589.00	
0.604	0.006	0.431	0.006	0.000	C-O STR.
0.007	0.992	0.000	0.000	0.000	SI-H SYM. STR.
0.476	0.004	0.330	0.007	0.207	C-N STR.
0.000	0.000	0.002	1.045	0.031	SI-H SYM. DEF.
0.022	0.000	0.182	0.021	0.881	SI-N STR.

L MATRIX

0.33551	0.03148	0.17917	-0.01375	0.00085
-0.08914	0.99762	-0.00795	0.00542	0.00590
-0.34295	-0.02945	0.18064	-0.01765	0.05765
0.00976	-0.05458	0.10521	1.49430	0.15799
0.12221	-0.01224	-0.22379	0.05019	0.19866

Table 4.4

NORMAL COORDINATE SOLUTION FOR SIH NCO
SYMMETRY SPECIES - E 3
F MATRIX AND FREQUENCIES FOR 4 ISOTOPIC SPECIES
P. E. DISTRIBUTION AND L MATRIX FOR 1ST ISOTOPIC SPECIES

F MATRIX

2.76714				
0.00000	0.21240			
0.00000	-0.05276	0.25031		
0.00000	0.00000	0.03125	0.47114	
0.00000	0.00000	0.00000	0.00000	0.01470

F.OBS	F.CALC	DIFF	
2212.00	2212.00	0.00	
946.10	946.10	-0.00	
721.75	721.70	0.05	SIH NCO
612.50	612.52	-0.02	3
64.00	64.00	0.00*	

F.OBS	F.CALC	DIFF	
2212.00	2212.00	0.00	
946.20	946.06	0.14	15
720.50	719.90	0.60	SIH NCO
610.80	609.75	1.05	3
-	62.70	-	

F.OBS	F.CALC	DIFF	
2211.00	2212.00	-1.00	
946.20	946.09	0.11	13
721.45	721.70	-0.25	SIH N CO
595.20	595.31	-0.11	3
-	63.92	-	

F.OBS	F.CALC	DIFF	
1623.50	1602.60	20.90	
688.80	686.38	2.42	
540.30	540.42	-0.12	SID NCO
614.00	613.96	0.04	3
62.00	60.89	1.11*	* GAS PHASE VALUE

P.E. DISTRIBUTION

2212.00	946.10	721.75	612.50	64.00	
0.999	0.001	0.001	0.000	0.000	SI-H ASYM. STR.
0.001	1.037	0.017	0.001	0.000	SI-H ASYM. DEF.
0.000	0.011	1.051	0.000	0.002	SI-H ROCK
0.000	0.000	0.008	0.984	0.017	N-C-O BEND
0.000	0.000	0.002	0.015	0.983	SI-N-C BEND

L MATRIX

1.01988	-0.01101	0.00764	0.00062	0.00005
0.08373	1.60425	0.15835	-0.03059	0.00006
-0.07047	0.15530	1.13478	-0.00130	-0.00424
0.00034	0.02008	-0.07240	0.67929	0.00919
-0.03615	-0.05781	0.19442	-0.48205	0.40155

Table 4.5

OBSERVED AND CALCULATED PARAMETERS
1ST ISOTOPIC SPECIES

CALCULATED AND OBSERVED CORIOLIS CONSTANTS

ZETA	6	7	8	9	10
OBS.	0.004	-0.190	0.220	-	-
CALC.	0.069	-0.188	0.212	0.991	0.931

INTERATOMIC DISTANCES AND AMPLITUDES - 0.00K

ATOMS	DIST(RA).	U	P	L	K	RG	RALPHA
SI-H	1.4880	0.0884	0.1542	0.0053	0.0160	1.4933	1.4773
SI-N	1.7030	0.0431	0.1330	0.0011	0.0104	1.7041	1.6937
C-N	1.2160	0.0366	0.0995	0.0011	0.0081	1.2171	1.2090
C-O	1.1640	0.0347	0.0993	0.0010	0.0085	1.1650	1.1566
SI..C	2.9190	0.0478	0.0654	0.0008	0.0015	2.9198	2.9183
N..O	2.3800	0.0401	0.1634	0.0007	0.0112	2.3807	2.3695
SI..O	4.0830	0.0470	0.0371	0.0005	0.0003	4.0835	4.0832
H..H	2.4408	0.1489	0.2105	0.0091	0.0182	2.4499	2.4317
H..N	2.5965	0.1199	0.2148	0.0055	0.0178	2.6021	2.5843
H..C	3.6776	0.1459	0.1540	0.0058	0.0064	3.6833	3.6769
H..O	4.7736	0.1668	0.1095	0.0058	0.0025	4.7794	4.7769

INTERATOMIC DISTANCES AND AMPLITUDES - 298.16K

ATOMS	DIST(RA).	U	P	L	K	RG	RALPHA
SI-H	1.4880	0.0884	0.2554	0.0053	0.0438	1.4933	1.4494
SI-N	1.7030	0.0448	0.3344	0.0012	0.0657	1.7042	1.6385
C-N	1.2160	0.0368	0.2156	0.0011	0.0382	1.2171	1.1789
C-O	1.1640	0.0347	0.2179	0.0010	0.0408	1.1650	1.1243
SI..C	2.9190	0.0502	0.1343	0.0009	0.0062	2.9199	2.9137
N..O	2.3800	0.0403	0.4167	0.0007	0.0730	2.3807	2.3077
SI..O	4.0830	0.0494	0.0852	0.0006	0.0018	4.0836	4.0818
H..H	2.4408	0.1498	0.3809	0.0092	0.0594	2.4500	2.3905
H..N	2.5965	0.1222	0.4848	0.0057	0.0905	2.6023	2.5118
H..C	3.6776	0.2182	0.2934	0.0129	0.0234	3.6905	3.6671
H..O	4.7736	0.2960	0.1268	0.0183	0.0034	4.7919	4.7886

The E solution was aided by the use of observed coriolis constants[30]. It was found that the calculated coriolis constants were very sensitive to the magnitude of the element F_{32}. The value of F_{32} = -0.05276 mdyne Å^{-1} was fixed in order to give the best values compared with the observed data for ζ_7 and ζ_8. The observed and calculated coriolis constants are given in Table 4.5.

The calculated parallel amplitudes compare well with both previously calculated[35] and experimental[33] values. Linear shrinkages derived from the K values in Table 4.5 are δ(Si...C) = 0.096 Å, δ(Si...O) = 0.140 Å and δ(N...O) = 0.005 Å at 298 K. These compare extremely well with experimental values[35] of δ(Si...C) = 0.086 Å and δ(Si...O) = 0.121 Å.

4.7.6 Solution in C_s configuration - discussion

The Tables 4.6 - 4.9 summarise the results for SiH_3NCO in a C_s configuration. The A' solution has a number of off-diagonal elements in the F matrix. These were given finite values to help the fit of the isotopic frequencies. It is notable that the observed matrix frequencies in the NCO bending and SiN stretching region are well reproduced by the solution in the C_s configuration for all the isotopic species. Here, there was no need for adjustments to the observed frequencies such as were made in the C_{3v} basis. The potential energy

distribution shows large mixing of the CN and CO coordinates. All the other modes are fairly 'pure' except those assigned to 640.3 cm^{-1} and 589.0 cm^{-1}. The 640.3 cm^{-1} mode is largely an NCO bend but also has significant contributions from the SiH_3 rock and SiN stretch. The mode at 589.0 cm^{-1} has contributions from the SiN stretch, CN stretch and NCO bend.

The A' Si-H stretches (treated as a separate symmetry species) are very 'pure' vibrations. The frequency fit for the SiD stretches is a little out because no connections were made for anharmonicity.

In the A" symmetry species a frequency value for the torsional vibration (which has not been observed in the matrix spectrum) must be supplied. The results are shown for a torsion frequency of 50 cm^{-1}. There is very little mixing of any of the symmetry coordinates. Two off-diagonal elements, F_{32} and F_{43} were inserted to give a more satisfactory potential energy distribution and isotopic frequency fit.

Some of the derived parameters given in Table 4.9 are sensitive to the supplied torsional frequency. Further calculations were carried out with a torsional frequency of 100 cm^{-1}. The resulting changes occurred in the parameters P and the related K values. The mean parallel amplitudes, U, were unaffected apart from those with components perpendicular to the plane of symmetry.

Table 4.6

NORMAL COORDINATE SOLUTION FOR SIH NCO
SYMMETRY SPECIES - A' 3
F MATRIX AND FREQUENCIES FOR 4 ISOTOPIC SPECIES
P. E. DISTRIBUTION AND L MATRIX FOR 1ST ISOTOPIC SPECIES

F MATRIX

16.22086							
1.35184	11.80265						
0.00000	0.00000	0.24425					
0.00000	0.00000	0.00000	0.20308				
0.00000	0.00000	0.00000	-0.02767	0.24672			
0.00000	0.00000	0.00000	0.01387	0.05643	0.52141		
0.70970	-1.32198	-0.18904	0.00000	0.09385	-0.16422	4.54278	
0.00000	0.00000	0.00000	0.00000	0.00000	0.00000	0.00000	0.01743

F.OBS	F.CALC	DIFF	
2308.30	2308.30	0.00	
1459.80	1459.79	0.01	
955.50	955.50	0.00	
946.10	946.10	0.00	SIH NCO
713.40	713.40	0.00	3
640.30	640.31	-0.01	
589.00	588.98	0.02	
64.00	64.00	-0.00*	

F.OBS	F.CALC	DIFF	
2297.50	2295.26	2.24	
1431.40	1430.26	1.14	
955.60	955.47	0.13	15
946.20	946.08	0.12	SIH NCO
712.30	713.13	-0.83	3
636.50	633.65	2.85	
588.40	588.04	0.36	
-	62.97	-	

F.OBS	F.CALC	DIFF	
2252.20	2248.93	3.27	
1457.40	1459.07	-1.67	
955.60	955.50	0.10	13
946.20	945.85	0.35	SIH N CO
713.10	711.80	1.30	3
630.70	629.79	0.91	
579.40	579.83	-0.43	
-	63.89	-	

F.OBS	F.CALC	DIFF	
2306.00	2308.22	-2.22	
1460.20	1458.46	1.74	
714.70	710.65	4.05	
685.90	689.06	-3.16	SID NCO
536.10	533.06	3.04	3
635.00	634.94	0.06	
579.90	580.28	-0.38	
62.00	61.00	1.00*	* GAS PHASE VALUE

P.E. DISTRIBUTION

2308.30	1459.80	955.50	946.10	713.40	640.30	589.00	64.00	
0.580	0.434	0.001	0.000	0.002	0.000	0.005	0.000	C-O STR.
0.448	0.280	0.000	0.001	0.005	0.081	0.235	0.001	C-N STR.
0.000	0.000	1.021	0.008	0.000	0.005	0.001	0.000	SI-H SYM. DEF.
0.000	0.000	0.008	0.978	0.024	0.010	0.001	0.000	SI-H ASYM. DEF.
0.000	0.004	0.002	0.058	0.844	0.132	0.013	0.003	SI-H ROCK
0.000	0.000	0.000	0.004	0.038	0.759	0.227	0.018	N-C-O BEND
0.020	0.176	0.018	0.000	0.001	0.322	0.569	0.003	SI-N STR.
0.000	0.000	0.000	0.000	0.000	0.019	0.001	0.980	SI-N-C BEND

L MATRIX

0.33493	0.18317	-0.00466	0.00273	0.00537	0.00203	0.00777	0.00003
-0.34510	0.17258	0.00223	0.00547	0.01083	0.04071	0.06372	0.00042
0.02072	0.00098	1.49928	-0.13181	-0.02306	0.07190	0.02639	0.00051
0.00272	-0.01948	0.14182	1.59321	-0.18874	-0.10726	0.02628	-0.00019
0.05754	-0.13909	0.06124	0.35222	1.01271	-0.36000	0.10557	-0.00564
0.01078	-0.01929	-0.01547	0.06348	0.14794	0.59285	-0.29827	0.00921
0.11688	-0.22050	0.04563	-0.00189	-0.00922	0.13075	0.16002	0.00128
0.02158	-0.03718	0.01711	-0.06710	0.02331	-0.51646	0.09735	0.36823

Table 4.7

```
NORMAL COORDINATE SOLUTION FOR SIH NCO
A' SI-H STRETCHES                    3
F MATRIX AND FREQUENCIES FOR 4 ISOTOPIC SPECIES
P. E. DISTRIBUTION AND L MATRIX FOR 1ST ISOTOPIC SPECIES

F MATRIX
  2.90336
  0.00000  2.76990

 F.OBS    F.CALC    DIFF
 2224.00  2224.00    0.00      SIH NCO
 2212.00  2212.00    0.00         3

 F.OBS    F.CALC    DIFF           15
 2224.00  2224.00    0.00      SIH   NCO
 2212.00  2212.00    0.00         3

 F.OBS    F.CALC    DIFF            13
 2223.20  2224.00   -0.80      SIH N  CO
 2211.00  2212.00   -1.00         3

 F.OBS    F.CALC    DIFF
 1593.50  1581.86   11.64      SID NCO
 1622.50  1600.44   22.06         3

P.E. DISTRIBUTION

   2224.00  2212.00

     1.000    0.000      SI-H SYM.STR.
     0.000    1.000      SI-H ASYM. STR.

L MATRIX
   1.00166 -0.00002
   0.00002  1.01997
```

Table 4.8

NORMAL COORDINATE SOLUTION FOR SIH NCO
SYMMETRY SPECIES - A'' 3
F MATRIX AND FREQUENCIES FOR 4 ISOTOPIC SPECIES
P. E. DISTRIBUTION AND L MATRIX FOR 1ST ISOTOPIC SPECIES

F MATRIX

2.76712				
0.00000	0.21251			
0.00000	-0.05361	0.25602		
0.00000	0.00000	0.02922	0.47529	
0.00000	0.00000	0.00000	0.00000	0.00057

F.OBS	F.CALC	DIFF	
2212.00	2212.00	-0.00	
946.10	946.06	0.04	
730.10	729.98	0.12	SIH NCO
612.50	612.51	-0.01	3
50.00	50.12	-0.12*	

F.OBS	F.CALC	DIFF	
2212.00	2212.00	-0.00	
946.20	946.02	0.18	15
728.70	728.14	0.56	SIH NCO
610.80	609.88	0.92	3
-	49.45	-	

F.OBS	F.CALC	DIFF	
2211.00	2212.00	-1.00	
946.20	946.05	0.15	13
729.80	729.98	-0.18	SIH N CO
595.20	595.25	-0.05	3
-	50.08	-	

F.OBS	F.CALC	DIFF	
1624.50	1602.61	21.89	
691.70	686.49	5.21	
544.50	545.43	-0.93	SID NCO
614.00	614.83	-0.83	3
-	43.94	-	

* ASSUMED VALUE

P.E. DISTRIBUTION

2212.00	946.10	730.10	612.50	50.00	
0.999	0.001	0.001	0.000	0.000	SI-H ASYM. STR.
0.001	1.037	0.018	0.001	0.000	SI-H ASYM. DEF.
0.000	0.011	1.051	0.000	0.001	SI-H ROCK
0.000	0.000	0.010	0.991	0.007	N-C-O BEND
0.000	0.000	0.001	0.007	0.993	SI-H3 TORSION

L MATRIX

1.01988	-0.01103	0.00780	0.00071	0.00002
0.08372	1.60395	0.16212	-0.02685	0.00002
-0.07068	0.15284	1.13506	0.01047	-0.00200
0.00034	0.01936	-0.07931	0.67858	0.00469
-0.10899	-0.17941	0.63435	-1.60236	1.60499

Table 4.9

CALCULATED PARAMETERS
1ST ISOTOPIC SPECIES

INTERATOMIC DISTANCES AND AMPLITUDES - 0.00K

ATOMS	DIST(RA).	U	P	L	K	RG	RALPHA
SI-H'	1.4880	0.0958	0.2204	0.0062	0.0326	1.4942	1.4615
SI-H''	1.4880	0.0891	0.1963	0.0053	0.0259	1.4933	1.4674
SI-N	1.7030	0.0434	0.1223	0.0011	0.0088	1.7041	1.6953
C-N	1.2160	0.0371	0.0944	0.0011	0.0073	1.2171	1.2098
C-O	1.1640	0.0348	0.0938	0.0010	0.0076	1.1650	1.1575
SI..C	2.8329	0.0654	0.0615	0.0015	0.0013	2.8344	2.8331
N..O	2.3800	0.0408	0.1511	0.0007	0.0096	2.3807	2.3711
SI..O	3.9626	0.0779	0.0366	0.0015	0.0003	3.9641	3.9638
H'..H''	2.4408	0.1491	0.3173	0.0091	0.0412	2.4499	2.4086
H'..N	2.5965	0.1178	0.2940	0.0053	0.0333	2.6019	2.5686
H'..C	3.8099	0.1228	0.2346	0.0040	0.0144	3.8139	3.7994
H'..O	4.9726	0.1251	0.1795	0.0031	0.0065	4.9757	4.9692
H''..N	2.5965	0.1196	0.2114	0.0055	0.0172	2.6020	2.5848
H''..C	3.4754	0.1735	0.1778	0.0087	0.0091	3.4840	3.4749
H''..O	4.4673	0.2175	0.1631	0.0106	0.0060	4.4779	4.4719

INTERATOMIC DISTANCES AND AMPLITUDES - 298.16K

ATOMS	DIST(RA).	U	P	L	K	RG	RALPHA
SI-H'	1.4880	0.1259	0.5232	0.0106	0.1839	1.4986	1.3147
SI-H''	1.4880	0.0906	0.4436	0.0055	0.1323	1.4935	1.3612
SI-N	1.7030	0.0450	0.3254	0.0012	0.0622	1.7042	1.6420
C-N	1.2160	0.0374	0.2129	0.0011	0.0373	1.2171	1.1799
C-O	1.1640	0.0348	0.2132	0.0010	0.0391	1.1650	1.1260
SI..C	2.8329	0.1279	0.1288	0.0058	0.0059	2.8387	2.8329
N..O	2.3800	0.0411	0.4094	0.0007	0.0704	2.3807	2.3103
SI..O	3.9626	0.1730	0.0894	0.0076	0.0020	3.9701	3.9681
H'..H''	2.4408	0.1592	0.7921	0.0104	0.2571	2.4512	2.1941
H'..N	2.5965	0.1366	0.7757	0.0072	0.2317	2.6037	2.3720
H'..C	3.8099	0.1509	0.5888	0.0060	0.0910	3.8159	3.7249
H'..O	4.9726	0.1587	0.4163	0.0051	0.0348	4.9776	4.9428
H''..N	2.5965	0.1227	0.5089	0.0058	0.0997	2.6023	2.5026
H''..C	3.4754	0.3411	0.4074	0.0335	0.0478	3.5088	3.4611
H''..O	4.4673	0.4943	0.3743	0.0547	0.0314	4.5220	4.4906

H' - IN PLANE
H''- OUT OF PLANE

Typically the mean perpendicular amplitude, P, showed values about half the magnitude of those calculated at torsion = 50 cm^{-1}, with a related change in the K values. It is difficult to draw comparisons between these derived parameters and experimental ones since the symmetries are different. The large K values in Table 4.9 result from the large values of the mean square perpendicular amplitudes. These values probably occur because of the rectilinear coordinates used in their calculation - an approximation which is more valid for high frequency vibrations.

4.8 Silyl Isocyanate in CO_2 and Allene Matrices

The reduction in symmetry of SiH_3NCO, from C_{3v} to C_s, in going from gas phase to matrix, led to experiments with other matrices with rigid linear molecular structures. Experiments were carried out with CO_2 and allene to observe if silyl isocyanate could be constrained to a linear configuration in these lattices.

CO_2 and allene, of course, have their own infrared active vibrations so it was necessary to run their infrared spectra in a pure state as a control.

The infrared spectrum of SiH_3NCO in CO_2 (see Figure 4.8) gave comparatively broad absorption bands. The matrix was annealed to 80 K (about 0.3 T_m) in the hope that the bands would sharpen. However, much of the

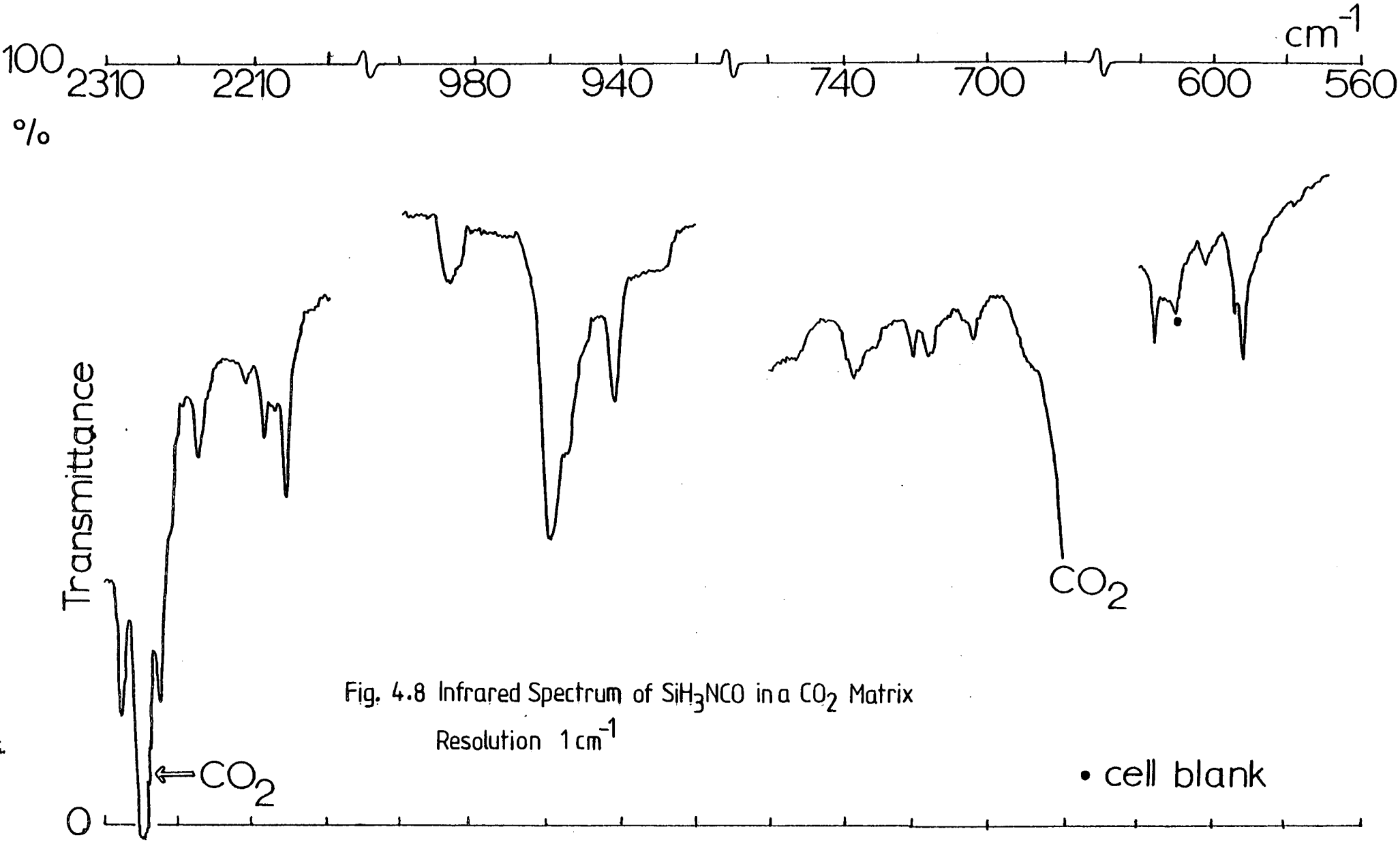

Fig. 4.8 Infrared Spectrum of SiH_3NCO in a CO_2 Matrix
Resolution 1 cm^{-1}

matrix sublimed and was lost. On annealing to 30 K the matrix again sublimed leaving little sample. It seems that CO_2 cannot be annealed under the pressure of the matrix isolation vacuum system, since in doing so the matrix sublimes and is pumped away. The spectrum shown in Figure 4.8 is therefore that immediately after spray-on to the cold window. Table 4.10 gives the observed frequencies and assignment of approximate mode of vibration. Assignments are given, still, in terms of a C_{3v} model.

The spectrum cannot be interpreted in terms of a linear heavy-atom chain since the split 'degeneracies' are still apparent. In the absence of an annealing experiment it is difficult to say which bands in the various multiplets are due to unstable site effects. Certainly the molecule appears to be occupying two different sites since the NCO asymmetric stretching mode shows two absorptions separated by 27 cm^{-1}. As to the symmetry of the molecule, it must be concluded that it is far from C_{3v} since the SiH asymmetric stretches are split by 16 cm^{-1}, the asymmetric deformation by 44.6 cm^{-1} and the SiH_3 rock into four components. The NCO bends also appear to be split by 13.1 cm^{-1}. We may conclude, also, that the silyl isocyanate molecules find it difficult to fit into a CO_2 lattice.

The first experiments with SiH_3NCO in an allene matrix used,as usual, a sample/matrix ratio of 1:1000.

Table 4.10

Observed frequencies (cm^{-1}) and assignment for SiH_3NCO, CO_2 matrix

2229	s	ν_1, NCO asymmetric stretch
2272	m.s.	
2248	w	ν_2, symmetric SiH stretch
2204	w	ν_6, asymmetric SiH stretch
2188	m.s.	
986.9	w	ν_7, asymmetric SiH deformation
959.7	s	ν_4, symmetric SiH deformation
942.3	m.s.	ν_7, asymmetric SiH deformation
738.1	w	ν_8, SiH_3 rock
721.9	w	
717.3	w	
705.4	w	
616.6	w	ν_9, NCO bend
603.5	v.w.	
529.5	m.s.	ν_5, SiN stretch

The infrared spectrum of the cold sample showed extremely intense absorption or scattering of the radiation above about 1500 cm^{-1}. Spectra could not be run in this region, and those in the region below 1500 cm^{-1} proved noisy (low signal to noise).

To overcome this, the matrix ratio was increased to 1:100 so that less matrix was required to obtain sample molecule bands. It is likely that many of the sample molecules would not be isolated completely at this ratio and therefore broad bands could be expected. In this case annealing the matrix was effective in sharpening the bands a little - a temperature of 40 K was necessary to anneal the matrix properly. The annealed matrix spectrum is shown in Figure 4.9.

The spectrum shows a very broad absorption at 2330 cm^{-1} associated with the asymmetric NCO stretch. The SiH stretches show very clearly at about 2200 cm^{-1}, and there is a very broad band associated with the SiH deformations at 937 cm^{-1}. In the two other important regions of the spectrum, between 700 and 750 cm^{-1} and 560-640 cm^{-1}, we have the familiar pattern of split 'degeneracies'.

The SiH_3 rocks are at 752.8 cm^{-1} and 718.5 cm^{-1} - a separation of 34.3 cm^{-1}. The NCO bends are at 623.7 cm^{-1} and 600.3 cm^{-1}, separation of 23.4 cm^{-1}. Here, the molecule is conclusively not a symmetric top.

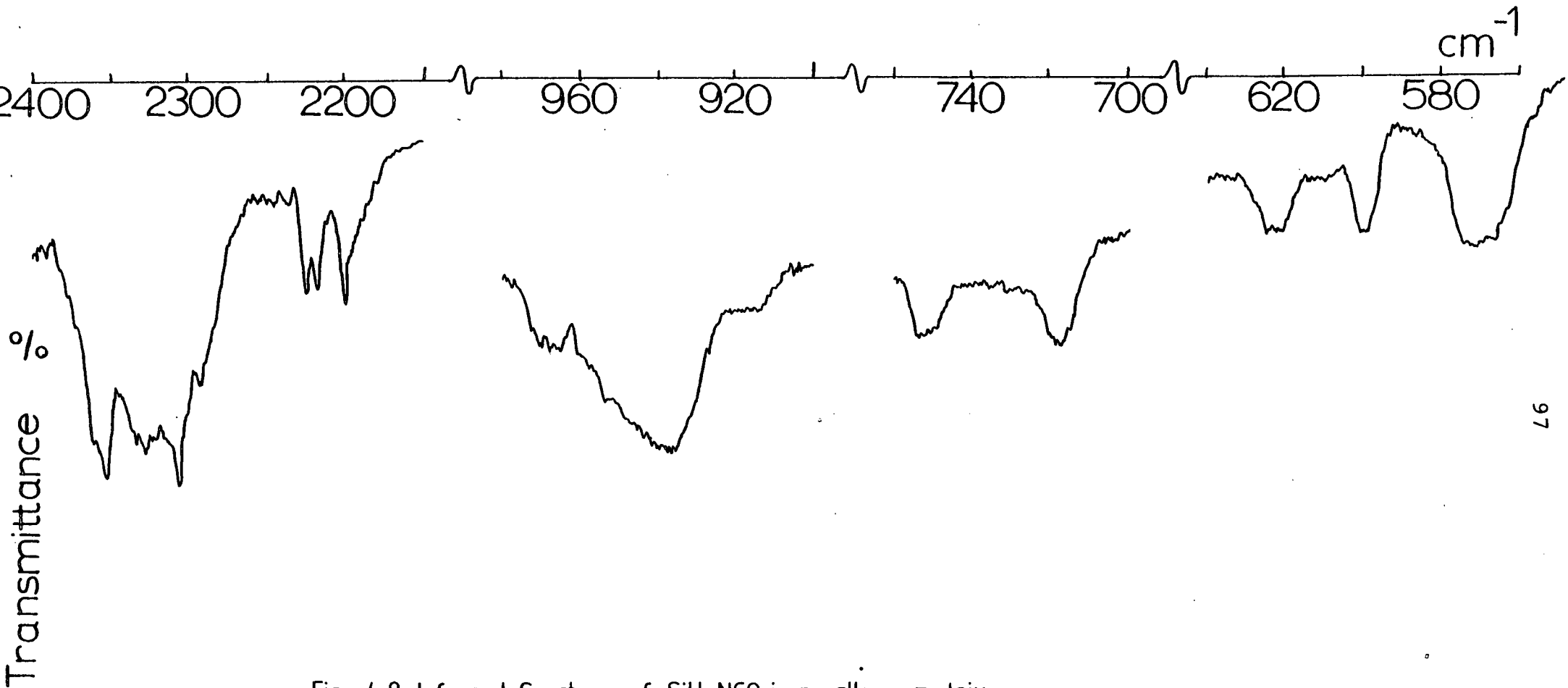

Fig. 4.9 Infrared Spectrum of SiH_3NCO in an allene matrix

Resolution $1\,cm^{-1}$

If anything, the splittings observed are larger than in a nitrogen matrix. The reason that neither CO_2 nor allene has been effective in making the heavy-atom chain linear in the matrix may be because they possess only a three atom chain. In order to constrain a four atom chain such as SiNCO to be linear, it may be necessary to use a matrix gas with a molecular chain of four or more atoms. Neither CO_2 nor allene crystallises with adjacent molecules 'end on', so long straight chains do not form[45].

A summary of the observed frequencies in an allene matrix are given in Table 4.11.

4.9 Conclusions

Silyl isocyanate gives sharp infrared absorption bands in a nitrogen matrix with evidence that its symmetry is C_s. The far infrared spectrum shows the potential for the low frequency bending mode to be anharmonic with a potential maximum at the linear heavy atom configuration. Since in a low temperature matrix the only populated level is v = 0, the molecule will assume a bent configuration (as observed) in such a potential.

A normal coordinate analysis in a C_{3v} configuration with slightly modified frequencies yields results in good agreement with experimentally observed coriolis

Table 4.11

Observed frequencies (cm^{-1}) and assignment for SiH_3NCO, allene matrix (1:100)

2330	s (broad)		ν_1, NCO asymmetric stretch
2227	m.s.		ν_2, SiH symmetric stretch
2218	m.s.	)	ν_6, SiH asymmetric stretches
2202	m.s.	)	
937.3	s (broad)		ν_4, ν_7, SiH deformations
752.8	w	)	ν_8, SiH_3 rock
718.5	w	)	
623.7	w	)	ν_9, NCO bend
600.3	w	)	
571.8	m.s.		ν_5, SiN stretch

constants, amplitudes of vibration and linear shrinkages. An analysis in a C_s configuration confirms the symmetry in the matrix by reproducing the observed frequencies. Attempts to constrain the SiNCO chain to a linear configuration using three atom rigid linear matrix molecules proved unsuccessful.

CHAPTER 5 - SILYL ISOSELENOCYANATE

5.1 Introduction

There have been few structural studies undertaken on silyl isoselenocyanate since it was first prepared[23]. This is mainly due to the relative instability of the species, which decomposes readily to give SiH_3CN, HCN and Se. The only technique which had proved successful in providing structural information when this work was begun was infrared spectroscopy.

The first assignment[30] of its infrared spectrum showed silyl isoselenocyanate to be a symmetric top in the gas phase. Q branches on the perpendicular bands showed an intensity alternation strong-weak-weak-strong indicative of a symmetric top. This was true of the silyl rocking band, which is the most likely to show signs of lifting of degeneracy.

The infrared spectrum showed the expected absorption bands due to a silyl group - silyl stretches near 2200 cm^{-1}, silyl deformations near 950 cm^{-1} and silyl rock near 700 cm^{-1}. There were also absorption bands due to the heavy-atom chain vibrations - CN stretch at 2068 cm^{-1}, CSe stretch at 868 cm^{-1} and the SiN stretch at 400 cm^{-1}. The band at 400 cm^{-1} was reported to be very broad. It was assumed that the band contained the combined intensities of the SiN stretch and the NCSe

bend. However, no definite assignment was made to either vibration.

No microwave study of silyl isoselenocyanate has yet been published. Apart from the problem of sample decomposition in the cell, there are numerous other difficulties. SiH_3NCSe has a large moment of inertia, I_B, so the J→J+1 transitions will be close together, making interpretation of the microwave spectrum difficult. The spectrum will also be complicated by the many different isotopic species present. Se has isotopic natural abundancies as follows: ^{74}Se 0.87%, ^{76}Se 9.02%, ^{77}Se 7.58%, ^{78}Se 23.52%, ^{80}Se 49.82%, ^{82}Se 9.19%. It was thought likely that SiH_3NCSe would have a low frequency bending vibration similar to that of SiH_3NCO. Such a vibration would complicate the microwave spectrum still further since most molecules would have a high vibrational quantum state occupied at room temperature.

One other isotopically labelled species has been studied - the deuterated molecule, SiD_3NCSe. Its infrared spectrum[30] showed the expected shifts for all the silyl group vibrations, with acceptable shifts for all the other modes. There was, however, still no definite assignment for ν_9, the NCSe bend.

A more direct method of determining molecular geometry is electron diffraction. There has been no published electron diffraction study on silyl

isoselenocyanate although work is in progress at Edinburgh.

There seems to be ample room for further study of silyl isoselenocyanate. The vibrational assignment has yet to be completed and studies in the far infrared have yet to be undertaken. Spectra of new isotopic species would lead to a better understanding of the normal modes of vibration through a normal coordinate analysis.

Experimental Results

5.2 Silyl Isoselenocyanate in an Argon Matrix

In general, the analysis of the matrix spectra posed certain problems in that there seemed to be more absorption bands than would be required to assign the nine fundamental modes expected in the mid infrared. Of course, extra bands can appear for numerous reasons; such as site splittings or cluster formation, both of which can be detected by annealing experiments. However, there was a band 'missing' in the spectrum around 400 cm^{-1} where the SiN stretch and the NCSe bend are expected - only one band was observed. We have, then, the same problem as encountered in the gas phase spectra, only now we must consider whether the SiN stretch and NCSe bend are accidentally degenerate.

Figure 5.1 shows the important regions of the

infrared spectrum of SiH_3NCSe in an argon matrix. The bands in the spectrum are fairly easily assigned but several are a little broad. In the 2200 cm^{-1} region are the SiH stretches - the symmetric stretch shows as a moderately strong band with the asymmetric stretch as a shoulder. The very strong band at 2059 cm^{-1} is the CN stretching mode. The silyl deformations are at 939.7 cm^{-1} and the CSe stretch at 899.9 cm^{-1}. At 713.5 cm^{-1} we have a broad band due to the silyl rock, with the SiN stretch at 390.8 cm^{-1}.

From the spectrum it is difficult to draw any conclusions as to the structure of the molecule. In particular, the rocking band at 713.5 cm^{-1} is very broad. The SiH asymmetric deformation modes at 939.7 cm^{-1} are degenerate and also accidentally degenerate with the symmetric deformation mode.

There are impurity bands in the spectrum at 2210 cm^{-1}, 962 cm^{-1} and 949.8 cm^{-1} due to $(SiH_3)_2O$. The band at 416.1 cm^{-1} was thought to be the absorption due to the NCSe bend. It was noted, however, that its intensity varied from sample to sample (as did an unassigned band at 1958 cm^{-1}). Further experiments with wet argon as a matrix caused these two bands to increase dramatically in intensity and they were assigned to the hydrolysis product HNCSe. HNCSe seems to be just stable enough to be deposited to some extent on the cold window

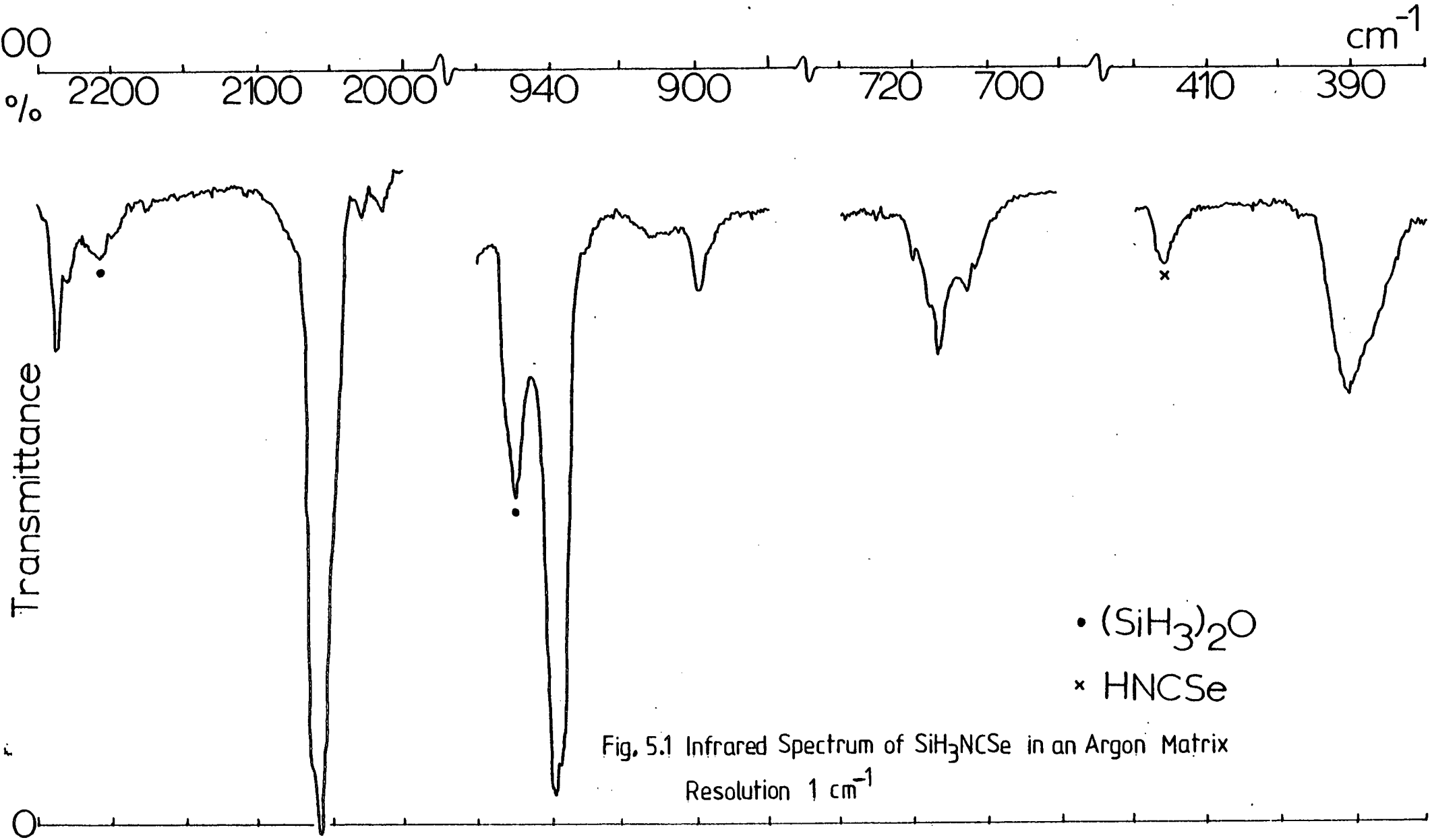

Fig. 5.1 Infrared Spectrum of SiH_3NCSe in an Argon Matrix
Resolution 1 cm^{-1}

when spraying on.

Annealing experiments indicated that molecular clusters formed easily in the matrix - bands at 903.3 cm^{-1} and 859.8 cm^{-1} appeared and the 390.8 cm^{-1} band developed a shoulder to low frequency. These frequencies are close in energy to the fundamental modes at 899.9 cm^{-1} and 390.8 cm^{-1} which are associated with the C-Se stretch and the Si-N stretch respectively and which one would expect to be affected most by intermolecular association. Association will probably occur in a similar way to that in SiH_3NCO with strong N...Si interactions between different molecules.

In all, four isotopic species were studied in an argon matrix. In assigning the bands for the different isotopic species, account must be taken of the effects of the many naturally occurring Se isotopes. A normal coordinate analysis showed that the only modes of vibration significantly affected by Se isotopes are the CN, CSe and SiN vibrations. On changing from ^{80}Se to ^{78}Se their respective shifts are approximately 0.15 cm^{-1}, 1.0 cm^{-1} and 1.5 cm^{-1}. It is probable that, at a resolution of about 1 cm^{-1} (at which most of the spectra were run) only the SiN mode might show resolvable detail. No such splitting was detected, so the SiN band at 390.8 cm^{-1} may be inherently broad.

Since no isotopic features due to Se were observed

it is assumed that each band maximum corresponds to the most abundant isotopic species, i.e. that containing ^{80}Se. Table 5.1 summarises the observed frequencies and assignment of approximate mode of vibration. Assignment is on the basis of a C_{3v} model.

The band at 390.8 cm^{-1} (SiH_3NCSe) was assigned to the SiN stretch rather than the NCSe bend due to its larger shift on deuteration. In contrast with the gas phase spectra of SiH_3NCSe, the matrix spectra show very clearly and separately the fundamentals around 900 cm^{-1} - the silyl deformations and the CSe stretch.

5.3 Silyl Isoselenocyanate in a Nitrogen Matrix

Nitrogen matrix spectra of SiH_3NCSe showed basically the same infrared absorptions as the argon matrix spectra, although in slightly different frequency positions. The bands observed, however, were sharper, especially in the SiH_3 rocking region and the SiH stretching region (see Figures 5.2 and 5.3).

The SiH stretches show very sharp bands - a strong band for the symmetric mode and a weaker one to low frequency for the asymmetric mode (similar in position to gas phase spectrum). Again the CN stretch gives a very strong band and there are corresponding bands due to the natural abundance of ^{13}C and ^{15}N. The most striking features of this spectrum are the separate

Table 5.1

Observed frequencies (cm^{-1}) and assignment for SiH_3NCSe, argon matrix

SiH_3NCSe	$SiH_3{}^{15}NCSe$	$SiH_3N{}^{13}CSe$	SiD_3NCSe		
2237	2238	2237	1603	s	ν_1, SiH symmetric stretch
2231	2230	2231	1633.5	w	ν_6, SiH asymmetric stretch
2059	2029	2015.5	2059	v.s.	ν_2, CN stretch
939.7	939.3	939.5	687.4	v.s.	ν_3, ν_7, SiH deformations
899.9	888.2	886.7	899.7	m.w.	ν_4, CSe stretc
713.5	711.9	713.4	542.1	m.s.(br)	ν_8, SiH_3 rock
390.8	390.0	388.8	380.9	s	ν_5, SiN stretc

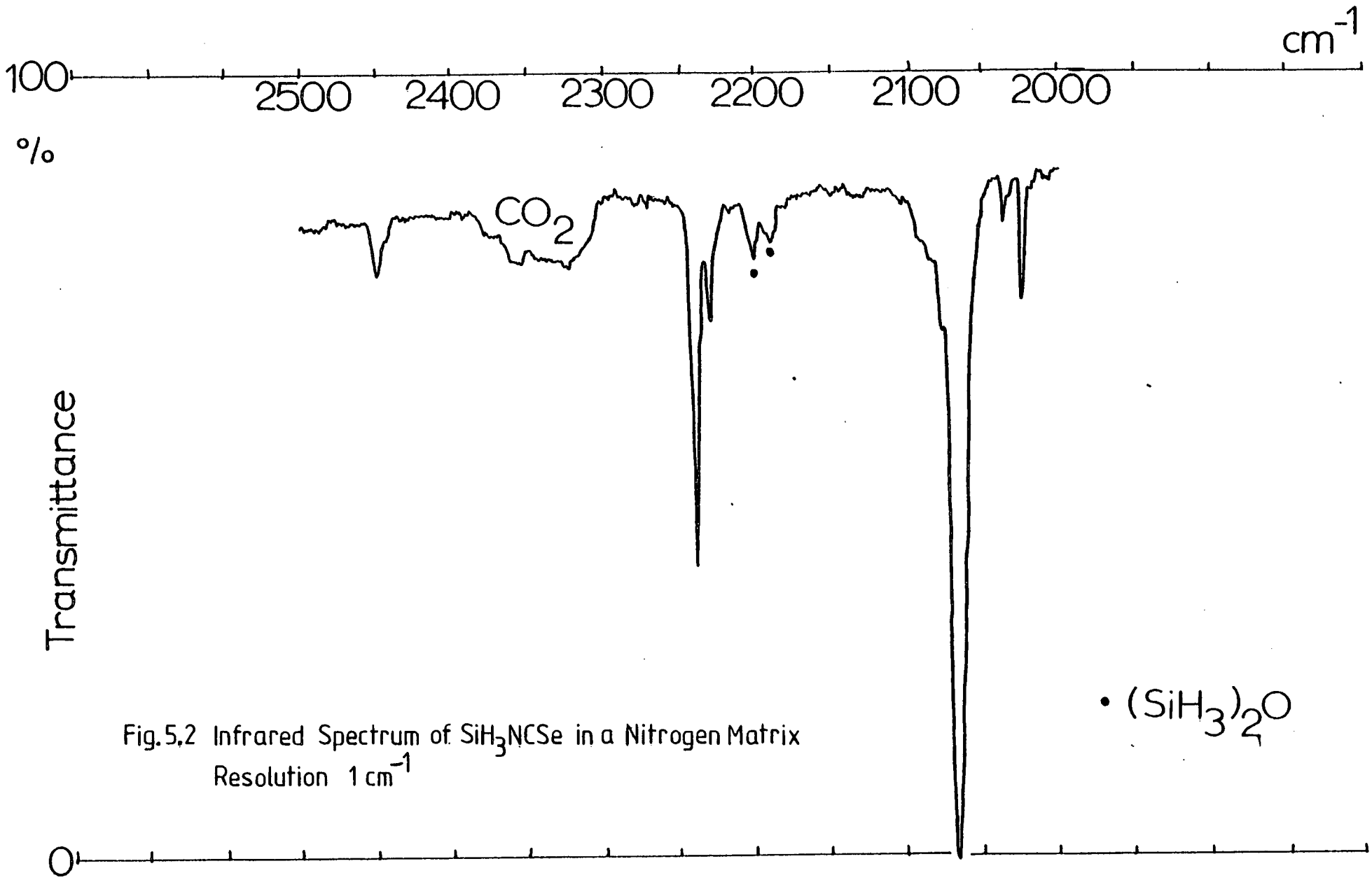

Fig. 5.2 Infrared Spectrum of SiH_3NCSe in a Nitrogen Matrix
Resolution 1 cm^{-1}

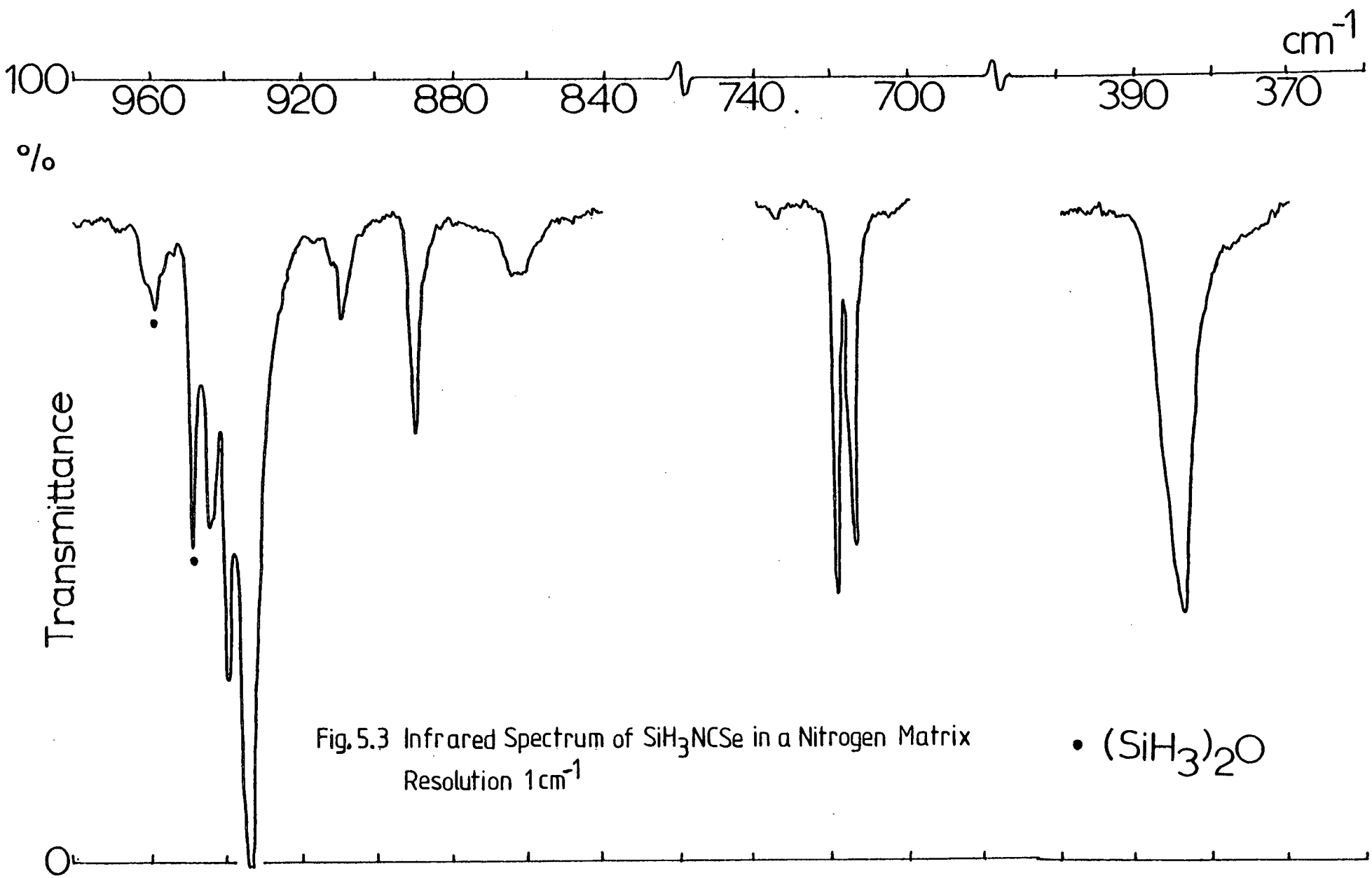

Fig. 5.3 Infrared Spectrum of SiH_3NCSe in a Nitrogen Matrix
Resolution 1 cm^{-1}

absorptions of the SiH asymmetric deformations at 944.3 cm^{-1} and 939.6 cm^{-1} (separation 4.7 cm^{-1}) and the two components of the SiH_3 rock at 719.6 cm^{-1} and 715.0 cm^{-1} (separation 4.6 cm^{-1}). Since the splitting in the rocking mode is small (compared to that in SiH_3NCO certainly) it would seem that the heavy-atom chain is not far from linear. It is unfortunate that the NCSe bend does not appear in the matrix spectrum - it would be a good further indication of the symmetry of the molecule.

Since the splittings of the E modes are small (less than 5 cm^{-1}) the SiH_3NCSe molecule can be assumed to be a symmetric top in the matrix, as in the gas phase. The small splittings can be explained in terms of the non-isotropic matrix cage interacting differently with the two degenerate components. As in the argon matrix spectrum there are bands due to sample molecule clusters - at 909.5 cm^{-1} and 863.3 cm^{-1}. These are observed to grow in intensity on annealing the sample at the expense of the band at 890.1 cm^{-1} due to isolated molecules. The SiN stretch has a frequency of 384.45 cm^{-1}. One feature which had not previously been observed in a matrix spectrum was the appearance of a combination band near 2450 cm^{-1} ($\nu_2 + \nu_5$). Table 5.2 contains a full list of frequencies for all four isotopic species of SiH_3NCSe studied.

After studies in two different matrices there was

Table 5.2

Observed frequencies (cm^{-1}) and assignment for SiH_3NCSe, nitrogen matrix

SiH_3NCSe	$SiH_3{}^{15}NCSe$	$SiH_3N{}^{13}CSe$		SiD_3NCSe		
2451.5	2420	2409		2444	w	$\nu_2 + \nu_5$
2239.5	2238	2239		1600.5	s	ν_1, SiH symmetric stretch
2230.0	2229	2230		1635.2	w	ν_6, SiH asymmetric stretch
2067.5	2037	2024		2069	v.s.	ν_2, CN stretch
944.3	944.3	943.7	s			ν_7, asymmetric
939.6	939.5	940.0	s	683.7	v.s.	SiH deformation
934.1	933.9	933.7			v.s.	ν_3, symmetric SiH deformation
890.3	878.7	876.5		889.3	s	ν_4, CSe stretch
719.6	717.6	719.5		546.2	s	ν_8, SiH_3 rock
715.0	713.3	714.6		541.9	s	
384.45	385.8	384.1		374.9	s	ν_5, SiN stretch

still no assignment for the NCSe bend. At first it was postulated that the SiN stretch and the NCSe bend were accidentally degenerate. Close examination of the band at 384.45 cm^{-1} revealed a slight asymmetry with tailing off to higher frequency which might support this view. Among the isotopic species one would expect the shift for the deuterated species to separate the two modes substantially. The band at 374.9 cm^{-1} in SiD_3NCSe is indeed double.

A set of estimated frequencies and isotopic shifts was compiled based on this idea. However, when trying to refine them in the normal coordinate analysis, the fit was unsatisfactory. The asymmetry apparent in the band around 380 cm^{-1} (and to some extent in the band at 890.3 cm^{-1}) was then attributed to the Se isotope natural abundances which would give a tail to higher frequency. Any doubling of the SiN stretch could be due to some association of the sample molecules in the matrix. There is some evidence for this in the annealed spectra.

Attention reverted to the gas phase infrared spectrum. It was noted in running purity checks that the band around 400 cm^{-1} showed a different contour with different isotopic species. The KBr plate absorption made it difficult to study this region, so CsI plates were subsequently used.

On close examination of the gas phase infrared

spectrum in this region it was discovered that there is a band to low frequency of the SiN stretch (see Figure 5.4). Although the band is weak and appears in a position where the rotational spectrum of H_2O is strong, it was possible to prove that this is a genuine band of SiH_3NCSe by flushing the spectrometer with dry nitrogen, and observing its shift with different isotopic species. Below are the frequencies of the NCSe bend in the gas phase for all the isotopic species studied.

SiH_3NCSe	$SiH_3{}^{15}NCSe$	$SiH_3N{}^{13}CSe$	SiD_3NCSe	
372.9 cm^{-1}	367.2 cm^{-1}	362.5 cm^{-1}	372.4 cm^{-1}	v.w. ν_9, NCSe bend.

A further examination of the matrix spectra to low frequency of the SiN stretch did not reveal conclusive evidence for an absorption due to the NCSe bend.

5.4 Far Infrared Spectrum of Silyl Isoselenocyanate

Far infrared spectra were run on both SiH_3NCSe and SiD_3NCSe in a 150 cm cell at a pressure of 8 mmHg (maximum vapour pressure at room temperature). Figures 5.5 and 5.6 show the spectra obtained. In the range 250-10 cm^{-1} two bands were observed centred at 122 cm^{-1} and 65 cm^{-1} for SiH_3NCSe, and 116 cm^{-1} and 62 cm^{-1} for SiD_3NCSe. The intensities of the lower band ($\Delta v = 1$, $\Delta l = \pm 1$ transitions) and upper band ($\Delta v = 2$, $\Delta l = 0,2$)

Fig. 5.4 Infrared Spectrum of SiH_3NCSe gas and Isotopically Substituted Species (350 – 450 cm^{-1}), 10 cm cell, p = 8 mmHg

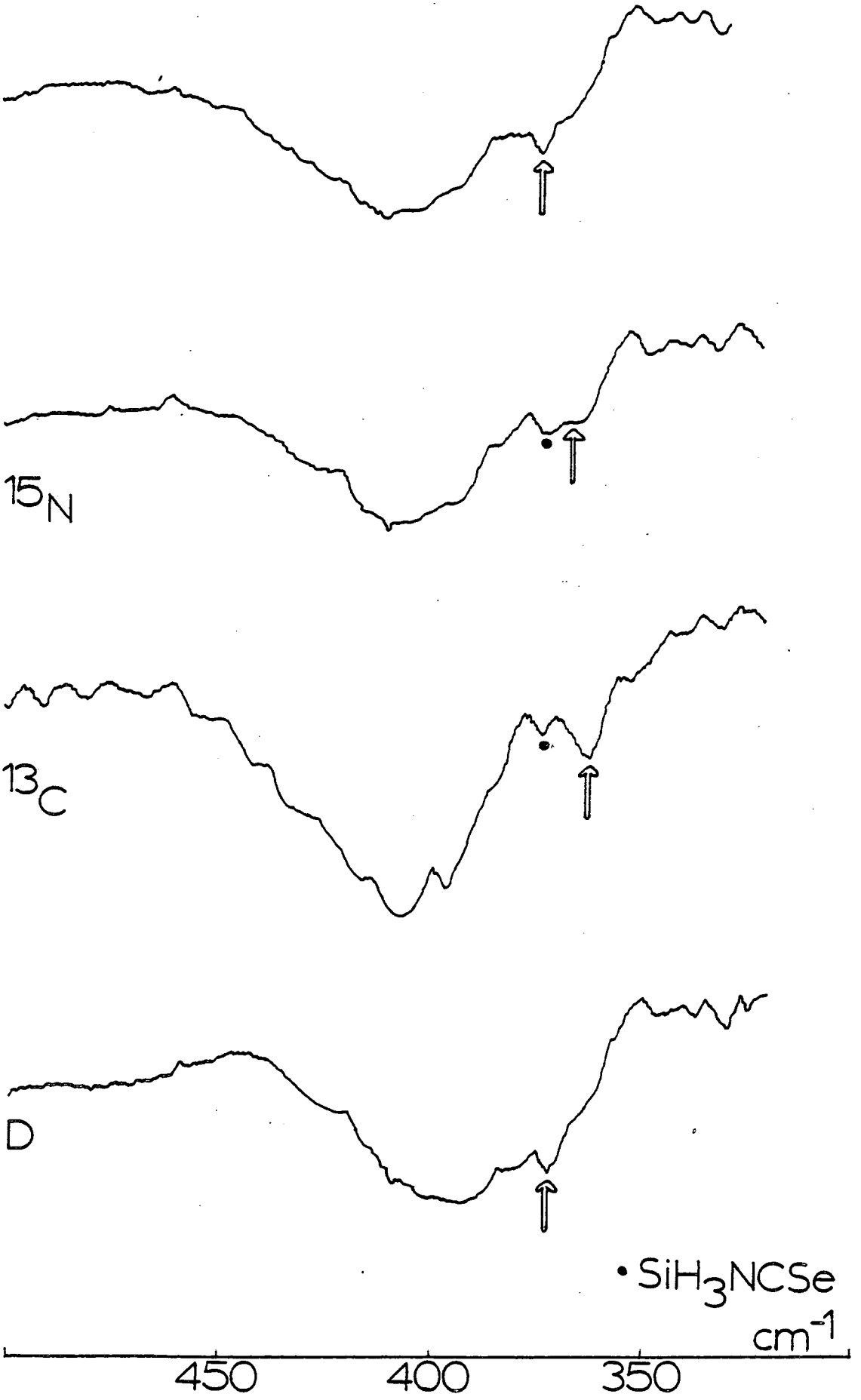

are comparable. These bands are due to the SiNC bending motion.

In general, the spectra are similar to those observed in SiH_3NCO. However, the bands are narrower in this case, even allowing for the reduced absorbance, and are more intense in absolute terms. There is no structure on the bands similar to that in the SiH_3NCO spectrum. The apparent structure on the lower frequency band in Figure 5.5 is due to the rotational spectrum of a small amount of HCN impurity.

The higher frequency bands show a distinct parallel band shape with P branch heading. It can be deduced from this that the many individual transitions which make up the band must be closely overlapping in order to produce such an overall band contour. It contrasts well with the case of SiH_3NCO where the individual transitions do not overlap but are staggered. One can say, then, that since the vibrational intervals are approximately equal in magnitude the potential governing the vibration is approximately harmonic.

It is possible to rationalise the observations in the far infrared with the behaviour in the matrix. The far infrared spectrum indicates that the potential governing the low frequency SiNC bend is harmonic, or nearly so, and that it therefore has a potential minimum or at most a very small maximum, at the linear

Fig.5.5 Far Infrared Spectrum of SiH_3NCSe gas, 150 cm cell,
p= 8 mmHg, resolution 1·2 cm^{-1}

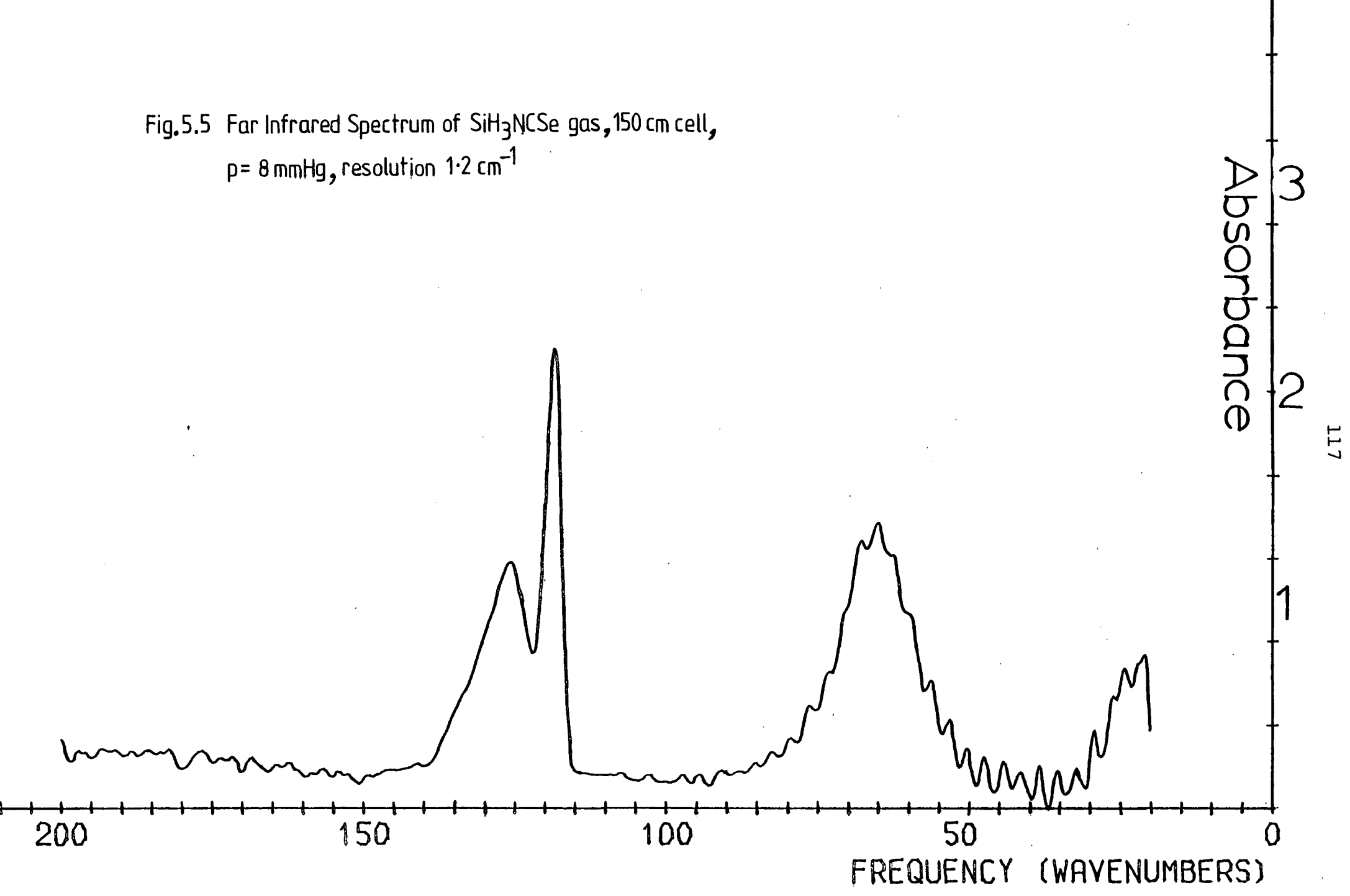

Fig. 5.6 Far Infrared Spectrum of SiD_3NCSe, 150 cm cell,
p = 8 mmHg, resolution 1·2 cm^{-1}

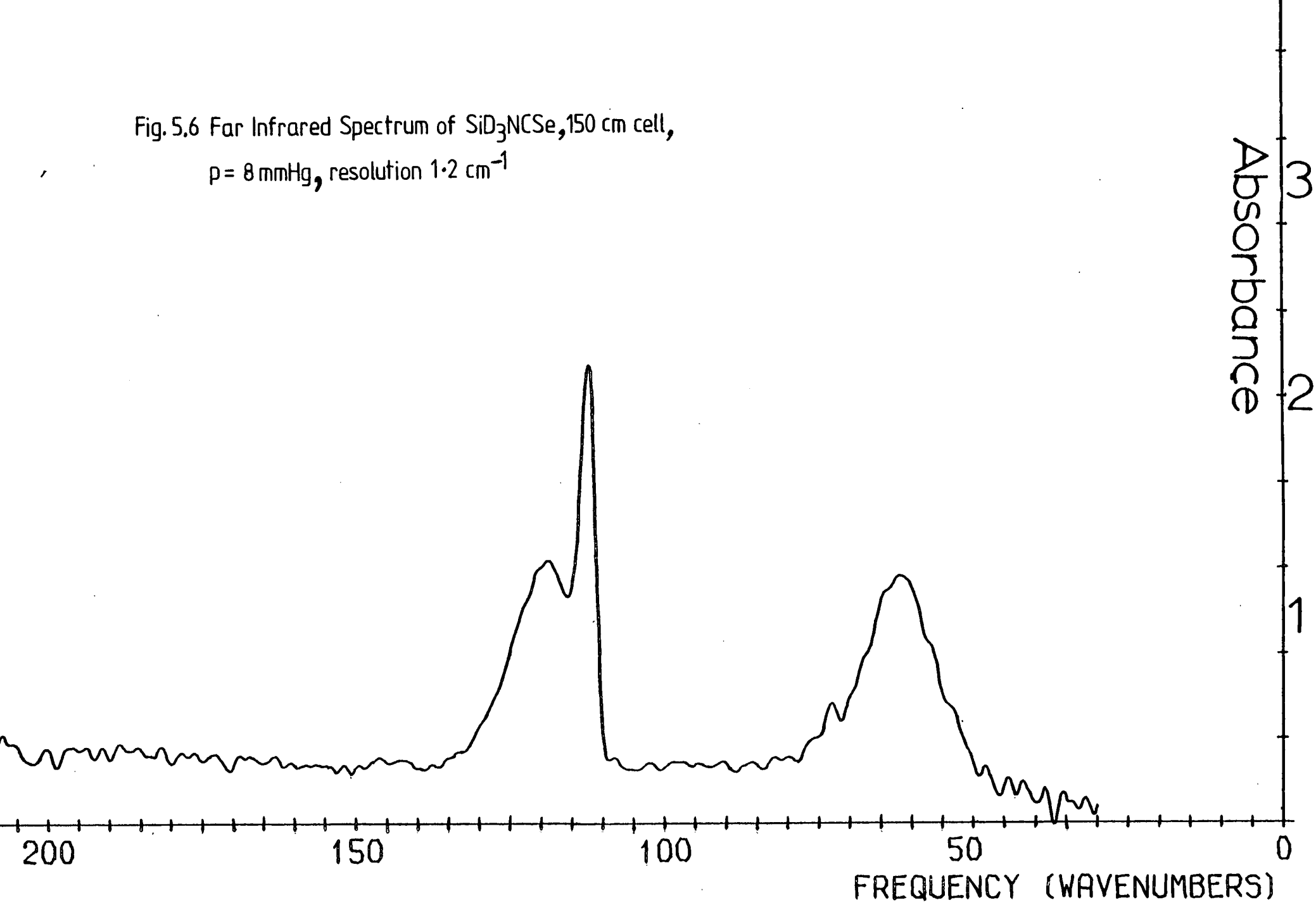

configuration. In the matrix spectra there is evidence for a very small perturbation to the C_{3v} symmetry suggested by its gas phase spectrum. This would suggest that there is little or no potential maximum at a linear configuration for either of the skeletal bending modes.

5.5 Normal Coordinate Analysis of SiH_3NCSe

An analysis of normal coordinates was carried out for SiH_3NCSe in a C_{3v} reference configuration. The frequency data were taken from the nitrogen matrix spectra, apart from values for the NCSe bend and the SiNC bend, which were taken from the gas phase spectra. The frequencies for the slightly split 'degenerate' modes were averaged for use in the refinement. Values of 65 cm^{-1} (SiH_3NCSe) and 62 cm^{-1} (SiD_3NCSe) were used for ν_{10}, corresponding to the observed band maximum in the gas phase at room temperature. The band maxima were assumed to be close to the 'harmonic' frequency of the vibration.

5.5.1 Molecular structure, internal coordinates and symmetry coordinates

Parameters for the molecular structure, in the absence of a published electron diffraction structure, were adapted from a structure for SiH_3NCS[40]. All parameters were assumed to be the same except the C-N distance and C-Se distance. The parameters used were:

r(SiH) 1.498 Å, r(Si-N) 1.673 Å, r(C-N) 1.21 Å, r(C-Se) 1.71 Å, H-$\hat{Si}$-N = 107.1°. The C-N and C-Se distances agree well with structure calculations on NCSe groups in other species.

Internal Coordinates

These were defined as follows:

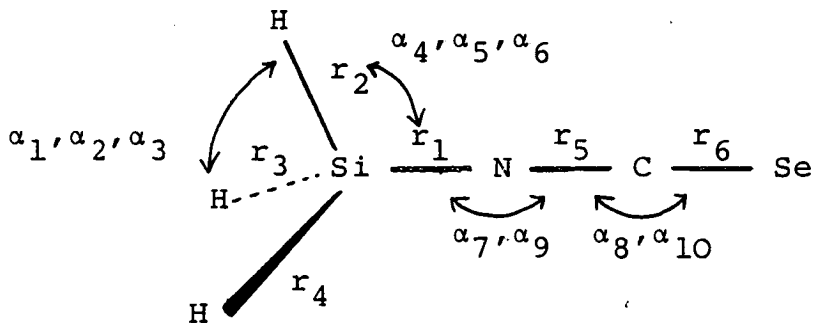

Symmetry Coordinates

The normal coordinate solution was obtained in terms of the following symmetry coordinates:

$\underline{A}_1$ $\quad s_1 : \frac{1}{(3)^{\frac{1}{2}}} (\Delta r_2 + \Delta r_3 + \Delta r_4)$

$s_2 : \Delta r_5$

$s_3 : (3+3\nu^2)^{-\frac{1}{2}} \{ r_2(\Delta\alpha_1 + \Delta\alpha_2 + \Delta\alpha_3) + \nu(r_1 r_2)^{\frac{1}{2}} (\Delta\alpha_4 + \Delta\alpha_5 + \Delta\alpha_6) \}$

$s_4 : \Delta r_6$

$s_5 : \Delta r_1$

$$\nu = \frac{(3)^{\frac{1}{2}} \cos \alpha_4}{\cos \frac{\alpha_1}{2}}$$

E(1)	E(2)
$s_1 : \frac{1}{(6)^{\frac{1}{2}}}(2\Delta r_2-\Delta r_3-\Delta r_4)$	$s_1 : \frac{1}{(2)^{\frac{1}{2}}}(-\Delta r_3+\Delta r_4)$
$s_2 : \frac{r_2}{(6)^{\frac{1}{2}}}(-\Delta\alpha_1-\Delta\alpha_2+2\Delta\alpha_3)$	$s_2 : \frac{r_2}{(2)^{\frac{1}{2}}}(\Delta\alpha_1-\Delta\alpha_2)$
$s_3 : \frac{(r_1r_2)^{\frac{1}{2}}}{(6)^{\frac{1}{2}}}(2\Delta\alpha_4-\Delta\alpha_5-\Delta\alpha_6)$	$s_3 : \frac{(r_1r_2)^{\frac{1}{2}}}{(2)^{\frac{1}{2}}}(\Delta\alpha_5-\Delta\alpha_6)$
$s_4 : (r_5r_6)^{\frac{1}{2}}\Delta\alpha_8$	$s_4 : (r_5r_6)^{\frac{1}{2}}\Delta\alpha_{10}$
$s_5 : (r_1r_5)^{\frac{1}{2}}\Delta\alpha_7$	$s_5 : (r_1r_5)^{\frac{1}{2}}\Delta\alpha_9$

5.5.2 Normal coordinate solution for SiH_3NCSe - discussion

Tables 5.3, 5.4 and 5.5 contain the results of this normal coordinate analysis.

The frequency fit in the A_1 symmetry species is excellent apart from the silyl stretches in the deuterated species. This is due to there being no correction for anharmonicity. Consequently this shift was given a smaller weighting in the refinement. The F matrix has a number of off-diagonal elements, the largest of which is F_{42}, coupling the CN and CSe stretching coordinates. The elements F_{54} and F_{53} were given finite values in order to reproduce the observed shifts for the CSe and SiN modes, especially for the deuterated species.

The potential energy distribution indicates that the

Table 5.3

```
NORMAL COORDINATE SOLUTION FOR SIH NCSE
SYMMETRY SPECIES - A1              3
F MATRIX AND FREQUENCIES FOR 4 ISOTOPIC SPECIES
P. E. DISTRIBUTION AND L MATRIX FOR 1ST ISOTOPIC SPECIES

F MATRIX
  2.94766
  0.00000 15.62954
  0.00000  0.00000  0.25348
  0.00000  1.61490 -0.04999  6.07751
  0.00000  0.09014 -0.20798 -0.14691  3.41623

 F.OBS   F.CALC    DIFF
 2239.50 2239.49    0.01
 2067.50 2067.49    0.01
  934.10  934.10    0.00      SIH NCSE
  890.30  890.30   -0.00         3
  384.45  384.45    0.00

 F.OBS   F.CALC    DIFF
 2238.00 2239.48   -1.48
 2037.00 2036.28    0.72          15
  933.90  933.81    0.09      SIH   NCSE
  878.70  877.15    1.55         3
  383.80  384.31   -0.51

 F.OBS   F.CALC    DIFF
 2239.00 2239.49   -0.49
 2024.00 2024.04   -0.04           13
  933.70  933.61    0.09      SIH N  CSE
  876.50  877.30   -0.80         3
  384.10  384.44   -0.34

 F.OBS   F.CALC    DIFF
 1600.50 1592.65    7.85
 2069.00 2067.14    1.86
  683.70  682.65    1.05      SID NCSE
  889.30  890.02   -0.72         3
  374.90  374.39    0.51

P.E. DISTRIBUTION

  2239.50  2067.50   934.10   890.30   384.45

    0.999    0.000    0.000    0.000    0.000     SI-H SYM. STR.
    0.000    0.958    0.002    0.000    0.068     C-N STR.
    0.000    0.000    1.002    0.041    0.012     SI-H SYM. DEF.
    0.000    0.113    0.020    0.555    0.345     C-SE STR.
    0.001    0.047    0.001    0.416    0.590     SI-N STR.

L MATRIX
  1.00056 -0.01854  0.00413 -0.00628  0.00234
  0.00728  0.39273 -0.00848  0.00224  0.01953
 -0.04913  0.03005  1.42531 -0.27388  0.06446
 -0.00304 -0.21592  0.04093  0.20639  0.07030
 -0.02346 -0.18594  0.00954 -0.23854  0.12264
```

Table 5.4

NORMAL COORDINATE SOLUTION FOR SIH NCSE
SYMMETRY SPECIES - E 3
F MATRIX AND FREQUENCIES FOR 4 ISOTOPIC SPECIES
P. E. DISTRIBUTION AND L MATRIX FOR 1ST ISOTOPIC SPECIES

F MATRIX

2.81004				
0.00000	0.20242			
0.00000	-0.04212	0.25089		
0.00000	0.00000	0.06090	0.12654	
0.00000	0.00000	0.00000	-0.02298	0.04077

F.OBS	F.CALC	DIFF	
2230.00	2230.00	-0.00	
941.95	941.94	0.01	
717.30	717.30	0.00	SIH NCSE
372.90	372.90	-0.00*	3
65.00	64.99	0.01*	

F.OBS	F.CALC	DIFF	
2229.00	2230.00	-1.00	
941.90	941.92	-0.02	15
715.45	716.13	-0.68	SIH NCSE
367.20	368.58	-1.38*	3
-	63.99	-	

F.OBS	F.CALC	DIFF	
2230.00	2230.00	-0.00	
941.85	941.93	-0.08	13
717.05	716.91	0.14	SIH N CSE
362.50	363.62	-1.12*	3
-	64.30	-	

F.OBS	F.CALC	DIFF		
1635.20	1616.20	19.00		
683.70	681.14	2.56		
544.05	540.03	4.02	SID NCSE	
372.40	371.98	0.42*	3	
62.00	61.33	0.67*		* GAS PHASE VALUE

P.E. DISTRIBUTION

2230.00	941.95	717.30	372.90	65.00	
0.999	0.001	0.001	0.000	0.000	SI-H ASYM. STR.
0.001	1.030	0.004	0.005	0.002	SI-H ASYM. DEF.
0.000	0.015	1.017	0.069	0.096	SI-H ROCK
0.000	0.000	0.000	0.681	0.606	N-C-SE BEND
0.000	0.000	0.002	0.177	0.952	SI-N-C BEND

L MATRIX

1.02033	-0.01034	0.00766	-0.00032	0.00006
0.08673	1.63057	0.07928	-0.04508	-0.00514
-0.06968	0.17914	1.10826	-0.15056	-0.03077
0.00038	0.01861	0.00148	0.66401	0.10917
-0.03655	-0.05208	0.12524	-0.59705	0.24100

Table 5.5

OBSERVED AND CALCULATED PARAMETERS
1ST ISOTOPIC SPECIES

CALCULATED AND OBSERVED CORIOLIS CONSTANTS

ZETA	6	7	8	9	10
OBS.	0.000	-0.167	0.225	-	-
CALC.	0.069	-0.189	0.207	0.998	0.921

INTERATOMIC DISTANCES AND AMPLITUDES - 0.00K

ATOMS	DIST(RA).	U	P	L	K	RG	RALPHA
SI-H	1.4980	0.0881	0.1567	0.0052	0.0164	1.5032	1.4868
SI-N	1.6730	0.0450	0.1285	0.0012	0.0099	1.6742	1.6643
C-N	1.2100	0.0357	0.0840	0.0011	0.0058	1.2111	1.2052
C-SE	1.7100	0.0379	0.1027	0.0008	0.0062	1.7108	1.7047
SI..C	2.8830	0.0479	0.1170	0.0008	0.0047	2.8838	2.8790
N..SE	2.9200	0.0381	0.1097	0.0005	0.0041	2.9205	2.9164
SI..SE	4.5930	0.0451	0.0205	0.0004	0.0001	4.5934	4.5933
H..H	2.4799	0.1480	0.2163	0.0088	0.0189	2.4887	2.4699
H..N	2.5528	0.1219	0.2115	0.0058	0.0175	2.5586	2.5411
H..C	3.6188	0.1414	0.1950	0.0055	0.0105	3.6243	3.6138
H..SE	5.2331	0.1647	0.1247	0.0052	0.0030	5.2383	5.2354

INTERATOMIC DISTANCES AND AMPLITUDES - 298.16K

ATOMS	DIST(RA).	U	P	L	K	RG	RALPHA
SI-H	1.4980	0.0881	0.2617	0.0052	0.0457	1.5032	1.4575
SI-N	1.6730	0.0479	0.3130	0.0014	0.0586	1.6744	1.6158
C-N	1.2100	0.0358	0.1056	0.0011	0.0092	1.2111	1.2018
C-SE	1.7100	0.0392	0.2332	0.0009	0.0318	1.7109	1.6791
SI..C	2.8830	0.0515	0.2751	0.0009	0.0262	2.8839	2.8577
N..SE	2.9200	0.0401	0.2684	0.0005	0.0247	2.9205	2.8959
SI..SE	4.5930	0.0526	0.0454	0.0006	0.0004	4.5936	4.5931
H..H	2.4799	0.1489	0.3973	0.0089	0.0637	2.4889	2.4252
H..N	2.5528	0.1261	0.4650	0.0062	0.0847	2.5590	2.4743
H..C	3.6188	0.1869	0.4204	0.0096	0.0488	3.6284	3.5796
H..SE	5.2331	0.2822	0.2042	0.0152	0.0080	5.2484	5.2404

vibrational modes are fairly 'pure' except those at 890.3 cm^{-1} and 384.45 cm^{-1}. Here there is a strong mixing of the CSe and SiN coordinates.

In the E symmetry species the off-diagonal element F_{32} = -0.04212 is inserted to give the best fit for the observed[30] and calculated coriolis constants. F_{54} is given a finite value in order to give a better fit of isotopic frequencies. The potential energy distribution indicates 'pure' vibrations with some mixing of the SiNC and NCSe bending coordinates.

Table 5.5 gives observed and calculated parameters for SiH_3NCSe. The coriolis coupling constants are in reasonable agreement. It should be noted, however, that the observed values were calculated on the assumption that $\zeta_6 = 0$, which is likely to be nearly true by comparison with other silyl compounds. Calculated linear shrinkage effects are δ(Si...C) = 0.040 Å, δ(N...Se) = 0.015 Å, δ(Si...Se) = 0.096 Å at 298 K.

5.6 Conclusions

The matrix isolated spectra of silyl isoselenocyanate indicate that the molecule is a symmetric top. All of the fundamental bands except ν_9 and ν_{10} were observed in these spectra. ν_9 has been assigned in the gas phase with help from isotopic labelling. The far infrared spectrum in the gas phase gives two bands, the

lower frequency band due to the $\Delta v = 1$, $\Delta l = \pm 1$ transitions, the higher frequency band due to the $\Delta v = 2$, $\Delta l = 0,2$ transitions of the SiNC bending mode. The simplicity of the 'overtone' band contour indicates a harmonic, or nearly harmonic, potential for the low frequency skeletal bend. A normal coordinate analysis in a C_{3v} configuration confirmed the assignment and led to the refinement of the force field.

CHAPTER 6 - GERMYL ISOCYANATE (GeH_3NCO) AND GERMYL ISOTHIOCYANATE (GeH_3NCS)

6.1 Introduction

6.1.1 Germyl isocyanate

Germyl isocyanate has been the subject of many studies since its first preparation[25]. The infrared spectral studies have on occasion led to incorrect conclusions about the assignment of the bands and about the presence of different isomers.

The first extensive infrared study[47] gave fairly accurate general conclusions but with some small errors in detail. The symmetry of the molecule in the gas phase was thought to be C_s i.e. a non-linear GeNCO chain. This conclusion was reached since two different frequencies were observed for the germyl rocking modes (667.5 cm^{-1} and 656 cm^{-1})). The absolute frequencies observed for the heavy-atom skeletal modes supported the view that the molecule was in the iso form, although a few bands were tentatively assigned to a small proportion of GeH_3OCN. ν(C-O) = 1284 cm^{-1}, ν(C≡N) 2374 cm^{-1}.

The GeH modes showed some structure due to a series of Q branches, similar to that in symmetric top molecules. These Q branch spacings were, however, not regular and therefore did not fit well with the symmetric top formula for perpendicular band Q branches. The structure was

attributed to the nearly-free rotation of the GeH_3 group. There appeared to be a very small barrier to internal rotation.

An assignment of the NCO bending modes to a band at 483 cm^{-1} was made. This can immediately be considered doubtful since the NCO bends in the closely related compound SiH_3NCO are near 600 cm^{-1}. The GeNC bend was placed at 115 cm^{-1}.

A later combined n.m.r. and infrared study of GeH_3NCO[48] helped to clarify certain points. The ^1H and ^{14}N n.m.r. spectra showed peaks due to only one type of molecule - the isocyanate. No resonances were observed that could be assigned to GeH_3OCN. The infrared spectrum was again consistent with a non-symmetric top molecular structure.

Solid phase spectra showed, apart from all the previously observed bands, four separate bands in the region 600-700 cm^{-1}. These were assigned to the germyl rocks (higher frequency pair) and the two NCO bends (lower frequency pair). A definite assignment of these bands to A' and A" modes was not attempted.

The most recent and comprehensive study of the infrared and Raman spectra[49] has led to a similar assignment for the NCO bends. The A" NCO bend is reported at 630 cm^{-1} with the A' mode at 611 cm^{-1} in the solid phase. There appears to be no Raman polarisation

data for the normal species GeH_3 rocking bands. Raman polarisation data were obtained from liquid and gas phase studies to aid in the assignment of the solid phase spectrum.

The absorption band previously reported[25] at 115 cm^{-1} is, in fact, the 'overtone' of the GeNC bend reported here[49] at 106 cm^{-1}, with a less intense bend at 55 cm^{-1}. The lower frequency band was assigned to the GeNC bend since the shift factor for the deuterated species was not consistent with that expected for the GeH_3 torsion. A fairly harmonic potential for this vibration was postulated since there was no fine structure on either of the bands.

A normal coordinate analysis carried out in the course of this work[49] served to confirm the vibrational spectrum in broad terms. It reproduced the observed frequencies for the normal and deuterated species with an average deviation of about 10 cm^{-1}.

The only microwave study to be carried out on germyl isocyanate[50] certainly indicated a non-linear GeNCO chain since transitions involving the GeH_3 internal rotation were observed. It was concluded that there was no significant bending of the heavy-atom chain. The complications induced by the presence of internal rotations have made detailed study of the microwave spectrum impossible. There are also further complexities

caused by significant populations of the excited states of the low frequency bend, and the many naturally occurring Ge isotopes.

A recent electron diffraction study of GeH_3NCO[51] has refined the observed molecular structural parameters at room temperature. The structural parameters are as expected with the GeNC angle observed to be 141.3°. Even with an equilibrium linear configuration for the GeNCO chain the electron diffraction structure would appear non-linear due to shrinkage effects. We must be careful, then, in drawing conclusions about linearity from an electron diffraction structure. However, the observed GeNC angle deviates from linearity to such an extent that it cannot be explained by shrinkage effects.

Most of the detailed infrared spectral data have been obtained from the solid phase where there are interactions between sample molecules. A matrix spectrum would combine the advantages of a solid phase spectrum (sharp lines) with the isolation of the sample molecules. It would also be possible to obtain some structural information from such a spectrum. The synthesis of more isotopically labelled species would lead to a more accurate and more precisely defined normal coordinate analysis.

6.1.2 Germyl isothiocyanate

A full and detailed study of GeH_3NCS has been carried

out only very recently[52]. Preliminary studies after its first synthesis[25] indicated that GeH_3NCS is a liquid of very low volatility at room temperature. The vapour pressure at room temperature is approximately 3 mmHg. The low volatility makes studies of the infrared spectrum in the gas phase very difficult.

The first structural information obtained on GeH_3NCS was from an infrared study[53]. In this work it was concluded that the molecule had C_s symmetry due to the 'parallel' and 'perpendicular' type contours for the two germyl rocks, and the irregular Q branch intervals on the 'perpendicular' GeH stretches. The positions of the bands associated with the GeH_3 group were as expected. The CN and GeN stretching modes were easily assigned.

However, the CS stretch appeared to have very low intensity and it was assigned only in the solid phase at 940 cm^{-1}. The NCS bending mode also had low intensity and was assigned to an absorption band at 460 cm^{-1}. A number of bands was observed between 100 cm^{-1} and 200 cm^{-1} and these were assigned to the GeNC bend and the germyl torsion. This has since been shown to be in error - there are no GeH_3NCS bands in the region. It is possible that those bands were due to impurities.

The more recent detailed study[52] of GeH_3NCS also contained a microwave analysis. The microwave study used an isotopically enriched sample with ^{74}Ge - this spectrum

could only be analysed using a C_{3v} model for the molecule. Hence, there is disagreement with the previously obtained results. Intensity calculations on the microwave bands indicated a low frequency vibration for the molecule at about 50 cm^{-1}, presumably associated with the GeNC bend. The associated infrared study gave essentially the same assignment to the fundamental bands. The NCS bend was assigned to 464 cm^{-1} with the GeN stretch at 388 cm^{-1}. In the deuterated species gas phase spectrum the CS stretch was reported at 911 cm^{-1}. The GeNC bending absorption was not observed in the far infrared due to the very low vapour pressure at room temperature.

Experimental Results

6.2 Germyl Isocyanate in an Argon Matrix

In studying the matrix isolated infrared spectra of germanium compounds one must be aware of the natural abundance of the isotopes. It is possible that a number of the modes of vibration will show isotopic splitting patterns if the individual lines are resolved. The natural abundances of the germanium isotopes are as follows:

^{74}Ge 36.54%, ^{72}Ge 27.43%, ^{70}Ge 20.52%, ^{73}Ge 7.76%, ^{76}Ge 7.76%.

It is useful in cases like this to have some

information on the modes expected to be affected significantly by the different isotopes. This can be achieved by performing a normal coordinate analysis with an approximate force field to give predicted shifts. The modes significantly affected by the different isotopes are few. Those which give a shift of greater than 0.1 cm^{-1} on going from ^{74}Ge to ^{72}Ge are: asymmetric GeH stretches ~0.5 cm^{-1}, symmetric GeH stretches ~0.14 cm^{-1}, GeH_3 rock ~0.4 cm^{-1}, symmetric GeH deformation ~0.5 cm^{-1}, GeN stretch ~1.5 cm^{-1}. None of these is likely to be resolved.

Argon matrix spectra were run for only the normal isotopic species of GeH_3NCO. As found for SiH_3NCO, argon proved to be unsatisfactory as a matrix material. However, the argon matrix spectrum is shown in Figure 6.1. In general the bands in the spectrum are a little broad especially in the region 600-670 cm^{-1}. It is difficult to draw any conclusion about the molecular symmetry. Of the 'degenerate' modes which are well-defined, there does not appear to be any large splitting in energy. The best criterion by which to judge the molecular symmetry, the germyl rock (656.0 cm^{-1}) is very broad.

The strong band in the region near 2270 cm^{-1} is associated with the NCO asymmetric stretch. The double maximum is thought to be due to a Fermi resonance with a combination band (see later). The GeH stretches near

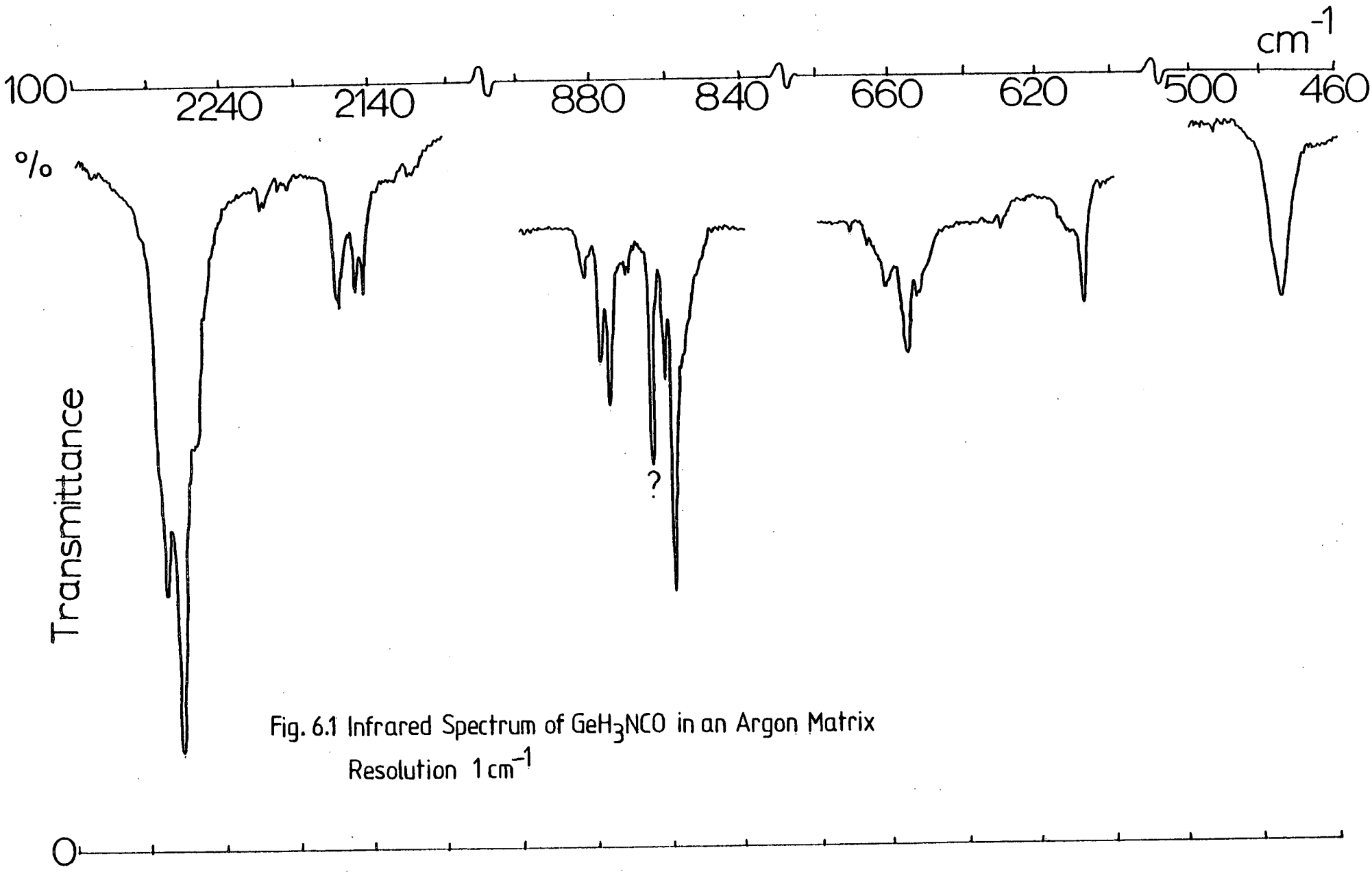

Fig. 6.1 Infrared Spectrum of GeH_3NCO in an Argon Matrix
Resolution 1 cm^{-1}

2150 cm^{-1} show the single higher frequency band due to the symmetric mode, and the two slightly split bands due to the two asymmetric modes. In the 800-900 cm^{-1} region there are the GeH deformations - the strong band assigned to the symmetric and the two higher frequency bands to the asymmetric modes. The three remaining absorptions are the GeH_3 rock (656.0 cm^{-1}), NCO bends (608.5 cm^{-1}) and the GeN stretch (475.5 cm^{-1}). The 600-670 cm^{-1} region does not show the expected four bands for a C_s GeH_3NCO molecule; however, the bands are broad. Table 6.1 summarises the argon matrix spectrum of GeH_3NCO. The bands are not assigned on the basis of any particular reference configuration.

6.3 Germyl Isocyanate in a Nitrogen Matrix

The infrared spectrum of germyl isocyanate in a nitrogen matrix shows more detail than the argon matrix spectrum. The interpretation of the spectrum, especially of the bands between 600 and 700 cm^{-1}, requires a set of spectra of different isotopic species. Figure 6.2 shows the spectra of GeH_3NCO in a nitrogen matrix. In this case annealing the matrix gives little change in the spectrum.

In the region around 2200 cm^{-1} there is the strong band due to the NCO asymmetric stretch - double maximum as before. The double maximum is not nearly so pronounced in any of the other isotopic species studied. This would suggest that Fermi resonance is involved with an overtone

Table 6.1

Observed frequencies (cm^{-1}) and assignment for GeH_3NCO, argon matrix

2279	s	Fermi resonance?
2270	v.s.	NCO asymmetric stretch
2163	m.s.	symmetric GeH stretch
2151	m.s.)	asymmetric GeH stretches
2146	m.s.)	
878.5	m.s.)	asymmetric GeH deformations
876.1	m.s.)	
858.9	s	symmetric GeH deformation
656.0	m.s.(br)	GeH_3 rock(s)
608.5	m.s.	NCO bend(s)
475.5	s	GeN stretch

Note: the absorption due to the NCO symmetric stretch, expected near 1400 cm^{-1}, was not observed.

or combination. The most plausible combination would be that of 3 x NCO bend + GeN stretch.

The GeH stretching bands near 2150 cm^{-1} show quite an interesting pattern. The three bands at 2165 cm^{-1}, 2158 cm^{-1} and 2151 cm^{-1} have intensities which at first sight could indicate the different bands associated with the naturally occurring Ge isotopes. However, the spacing of the bands (7 cm^{-1}) is too large to be due to a Ge isotopic shift; also, the relative absorbances do not match the relative natural abundancies. These three bands were therefore all assigned to the symmetric GeH stretch, with sample molecules in different stable sites. The fourth band to lower frequency is slightly broad, indicating that there may be more than one component. This band was therefore assigned to the two (closely overlapping) GeH asymmetric stretches.

The bands near 850 cm^{-1} have a very clear interpretation - two components with similar intensities of the GeH asymmetric deformation and the stronger band associated with the symmetric GeH deformation. In the region 600-670 cm^{-1} there are clearly three bands. For a GeH_3NCO molecule in a C_{3v} configuration we would expect two bands (NCO bend and GeH_3 rock), and in a C_s configuration four bands (2 x NCO bend and 2 x GeH_3 rock) in this region. It is clear that the molecule is not C_{3v}, although there is a band 'missing'. The

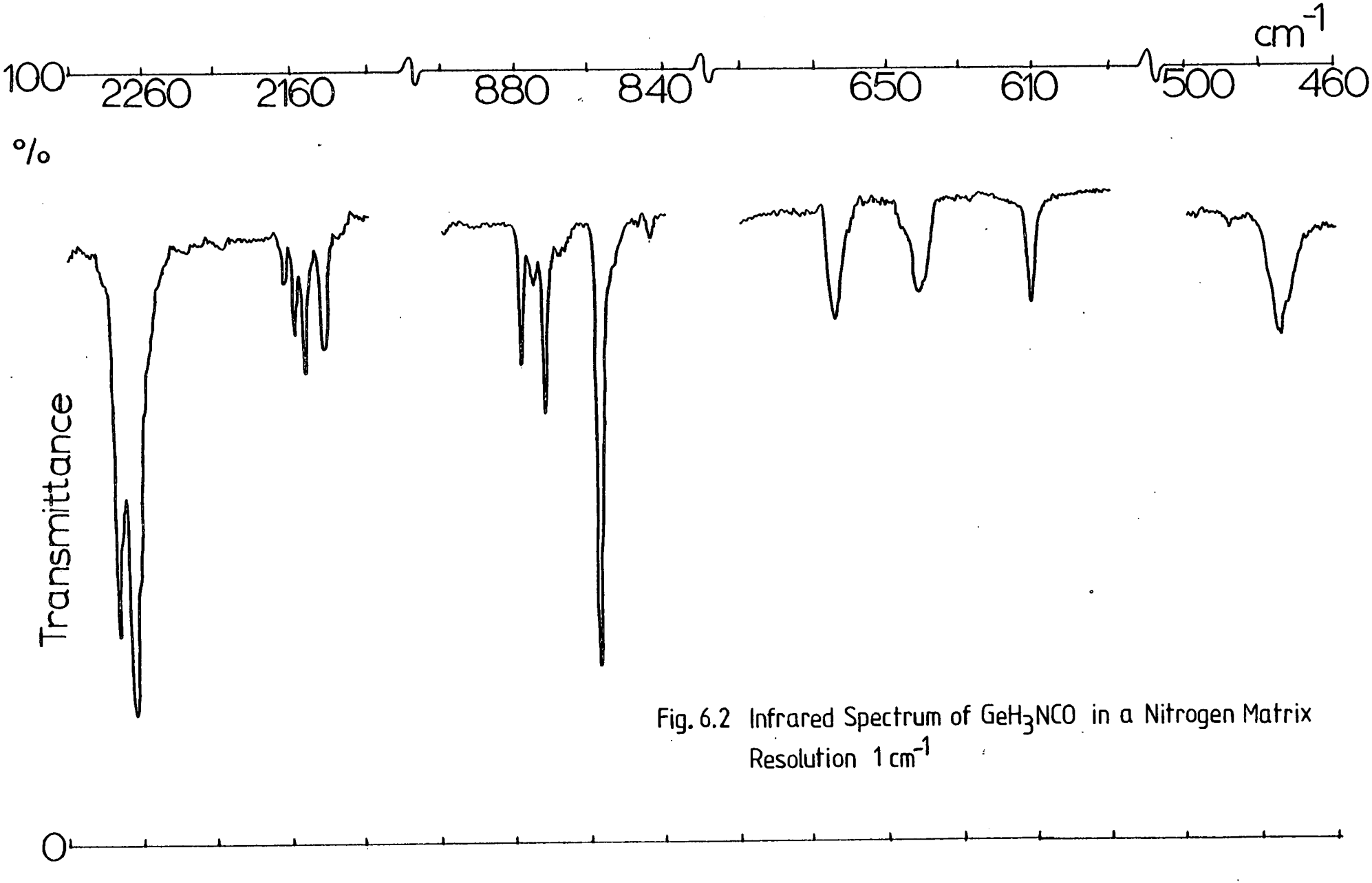

Fig. 6.2 Infrared Spectrum of GeH_3NCO in a Nitrogen Matrix
Resolution 1 cm^{-1}

possibilities are that two modes are degenerate or that one of the bands is weak and not observed. The former is true in this case (see later). The GeN stretch, lastly, is at 475.1 cm^{-1}. Again, the symmetric NCO stretch was not observed.

Assignment of the bands in the region 600-670 cm^{-1} was clarified using isotopically substituted species, and the predicted shifts from a normal coordinate analysis in the case of GeD_3NCO. Figure 6.3 shows the region 600-670 cm^{-1} for all the isotopic species of GeH_3NCO studied. It was not expected that the germyl rocks would be shifted much on ^{15}N or ^{13}C substitution. Therefore the bands at 664.7 cm^{-1} and 642.2 cm^{-1} (GeH_3NCO) were assigned as such. The spectrum of the ^{13}C substituted species provides the key to the assignment of the NCO bends. As the figure indicates, there is an extra band in the spectrum of $GeH_3N^{13}CO$, so there are now four as expected. The 'new' band at 626.7 cm^{-1} has shifted down in frequency from 'under' the germyl rocking band at 642.2 cm^{-1} in the normal species. This is a shift of 15.5 cm^{-1} - about right for an NCO bend. The other NCO bend at 611.9 cm^{-1} (normal isotopic species) shifts 17.1 cm^{-1} on ^{13}C substitution.

The NCO bend at 611.9 cm^{-1} was assigned to the in-plane (A') mode in accordance with Raman polarisation data[49]. The GeH_3 rock which is accidentally degenerate

Fig. 6.3 Infrared Spectrum of GeH_3NCO and Isotopically Substituted Species in a Nitrogen Matrix (570 - 690 cm^{-1})

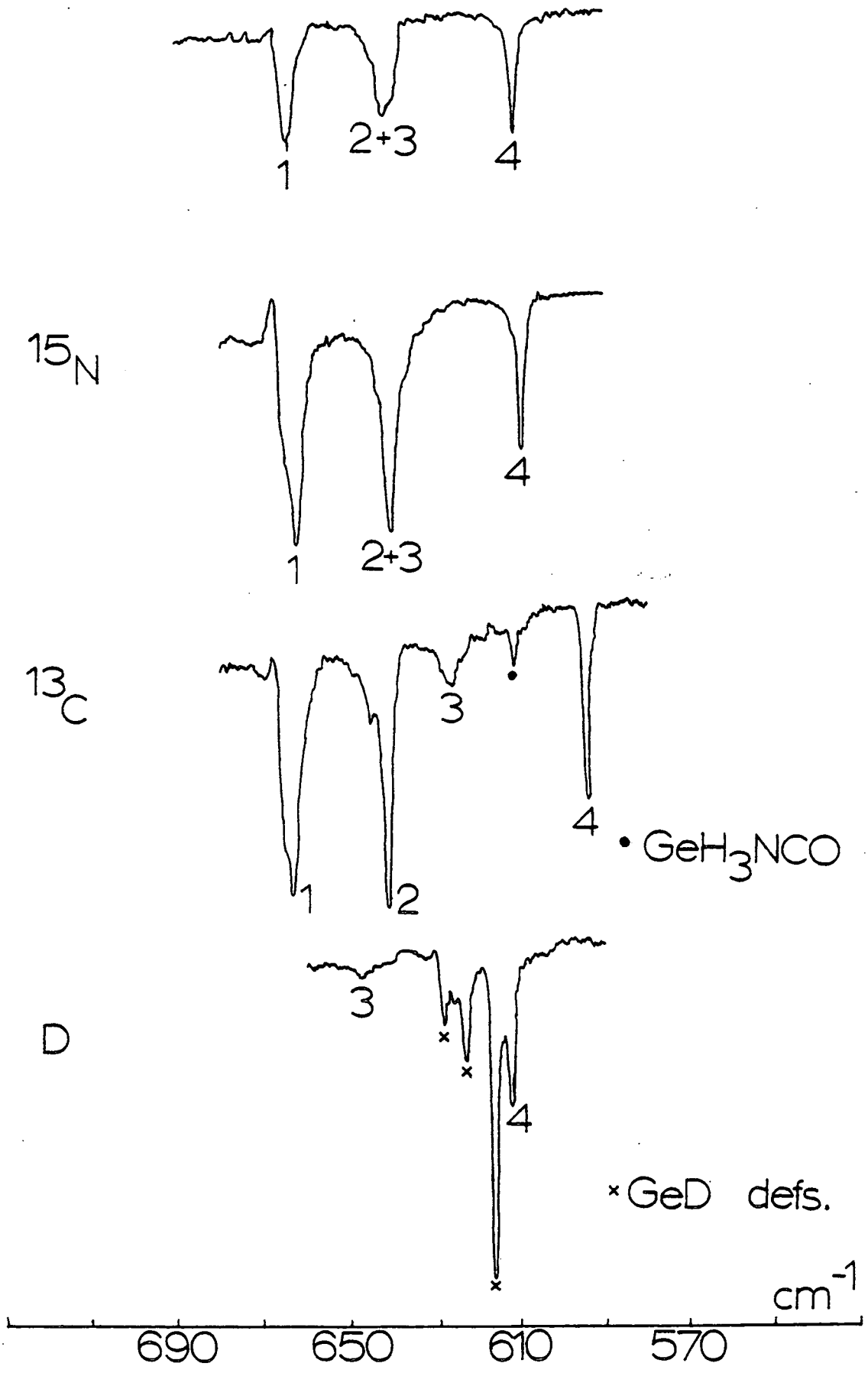

with the A" NCO bend in the normal species was assigned to the A' mode. This leaves the higher frequency GeH_3 rock as the A" mode. The accidental degeneracy is not removed on ^{15}N substitution since neither the A" NCO bend nor the A' GeH_3 rock is shifted by a large amount.

The GeD_3NCO spectrum proved more difficult to interpret. It was hoped that the large shift of the germyl rocks on deuteration would leave the region around 600 cm^{-1} with only the two NCO bends. Deuteration does indeed shift the germyl rocking bands to lower frequency but also shifts the GeD deformations to the 600 cm^{-1} region. Thus the result was more complex than anticipated, but analysis of the shifts served to confirm the assignment already made.

In order to assign the spectrum of the deuterated species a normal coordinate analysis was carried out with a force field refined from the data for GeH_3NCO, $GeH_3{}^{15}NCO$ and $GeH_3N{}^{13}CO$. From this analysis the predicted frequencies for GeD_3NCO were obtained. The assignment of the GeD deformations was fairly easy - the two components of the asymmetric mode at 628.6 cm^{-1} and 623.6 cm^{-1}, and the more intense symmetric mode at 616.7 cm^{-1}.

The predicted frequencies for the NCO bending modes showed that the A' mode shifted up in frequency by 0.4 cm^{-1} to 612.3 cm^{-1} and the A" mode shifted up by

7.2 cm^{-1} to 649.4 cm^{-1} on deuteration (relative to the normal isotopic species). This matches well with the observed GeD_3NCO spectrum - a band is observed at 612.4 cm^{-1} and a very weak one at 649.0 cm^{-1}. The latter band is not absolutely clear in the expansion shown in Figure 6.3 but shows well in a survey scan. Thus for GeD_3NCO the A' NCO bend is at 612.4 cm^{-1}, the A" NCO bend at 649.0 cm^{-1}. The assignment of the A" NCO bend is not unreasonable since the A" NCO absorptions are also weak in all the other isotopic species studied.

Table 6.2 gives a summary of the observed frequencies and assignment of approximate mode of vibration for all the isotopic species studied. The assignment was made for the molecule in a C_s configuration.

The symmetric NCO stretch, ν_4, was not observed in the matrix spectra. Gas phase values obtained were as follows:

GeH_3NCO	$GeH_3{}^{15}NCO$	$GeH_3N{}^{13}CO$	GeD_3NCO	
1412.8 cm^{-1}	1386.2	1410.3	(1412.8)*	w, ν_4, N-C-O symmetric stretch

*This value was not observed due to impurity bands but was assigned the same value as the normal isotopic species.

There can be no doubt that GeH_3NCO is not a symmetric top in a low temperature matrix. The splitting

Table 6.2

Observed frequencies (cm^{-1}) and assignment for GeH_3NCO, nitrogen matrix

GeH_3NCO	$GeH_3{}^{15}NCO$	$GeH_3N{}^{13}CO$	GeD_3NCO		
2277	-	-	-		Fermi resonance[μ]
2266	2258	2209	2266	v.s.	ν_1, NCO asymmetric stretch
2165	2165	2165	1560	m.w.	ν_2, symmetric GeH stretch (multiple site)
2158	2157	2158	1555	s	
2151	2151	2151	1550	s	
2138	2138	2137	1534	s	ν_3, ν_{11}, asymmetric GeH stretches
878.5	878.6	878.7	628.6	s	ν_5, GeH asymmetric deformation
872.1	872.4	872.5	623.6	s	ν_{12}, GeH asymmetric deformation
857.5	857.5	857.5	616.7	v.s.	ν_6, symmetric GeH deformation
664.7	662.1	664.2	495.9	s	ν_{13}, GeH_3 rock
642.2[1,2]	640.3[1,2]	641.6[1]	474.4[1]	s	ν_7, GeH_3 rock[1]
-	-	626.7[2]	649.0[2]	w	ν_{14}, NCO bend[2]
611.9	609.8	594.8	612.4	s	ν_8, NCO bend
475.1	471.0	470.7	463.5	s	ν_4, GeN stretch

between the germyl rocking bands is in excess of 20 cm^{-1}, with the NCO bending modes split by 30 cm^{-1}. This conclusion is well supported by a normal coordinate analysis in a C_s configuration which predicted the frequencies of the deuterated species, and reproduced all the observed data.

The modes ν_{10} (GeNC bend) and ν_{15} (GeH_3 torsion) were not observed in the matrix spectra; they are likely to absorb in the far infrared.

6.4 Far Infrared Spectra of Germyl Isocyanate

Assuming, as is likely, that GeH_3NCO has C_s symmetry, i.e. is non-linear at the nitrogen atom, two low frequency modes are expected. One is the GeNC bend, the other is the GeH_3 torsion. These modes will absorb in the far infrared region of the spectrum. The observed far infrared spectrum is shown in Figure 6.4.

There are two broad bands in the spectrum, one centred at 53.1 cm^{-1}, and the other at 107.4 cm^{-1}. One band centre is approximately twice the frequency of the other indicating that the lower band represents the $\Delta v = 1$, $\Delta l = \pm 1$ transitions and the upper band is the $\Delta v = 2$, $\Delta l = 0,2$ transitions of a low frequency vibration. There appear to be no fine structure features on either band, suggesting an approximately harmonic potential. The bands are broad which suggests some degree of

Fig. 6.4 Far Infrared Spectrum of GeH_3NCO gas, 150 cm cell,
p = 20 mmHg, resolution 1·2 cm^{-1}

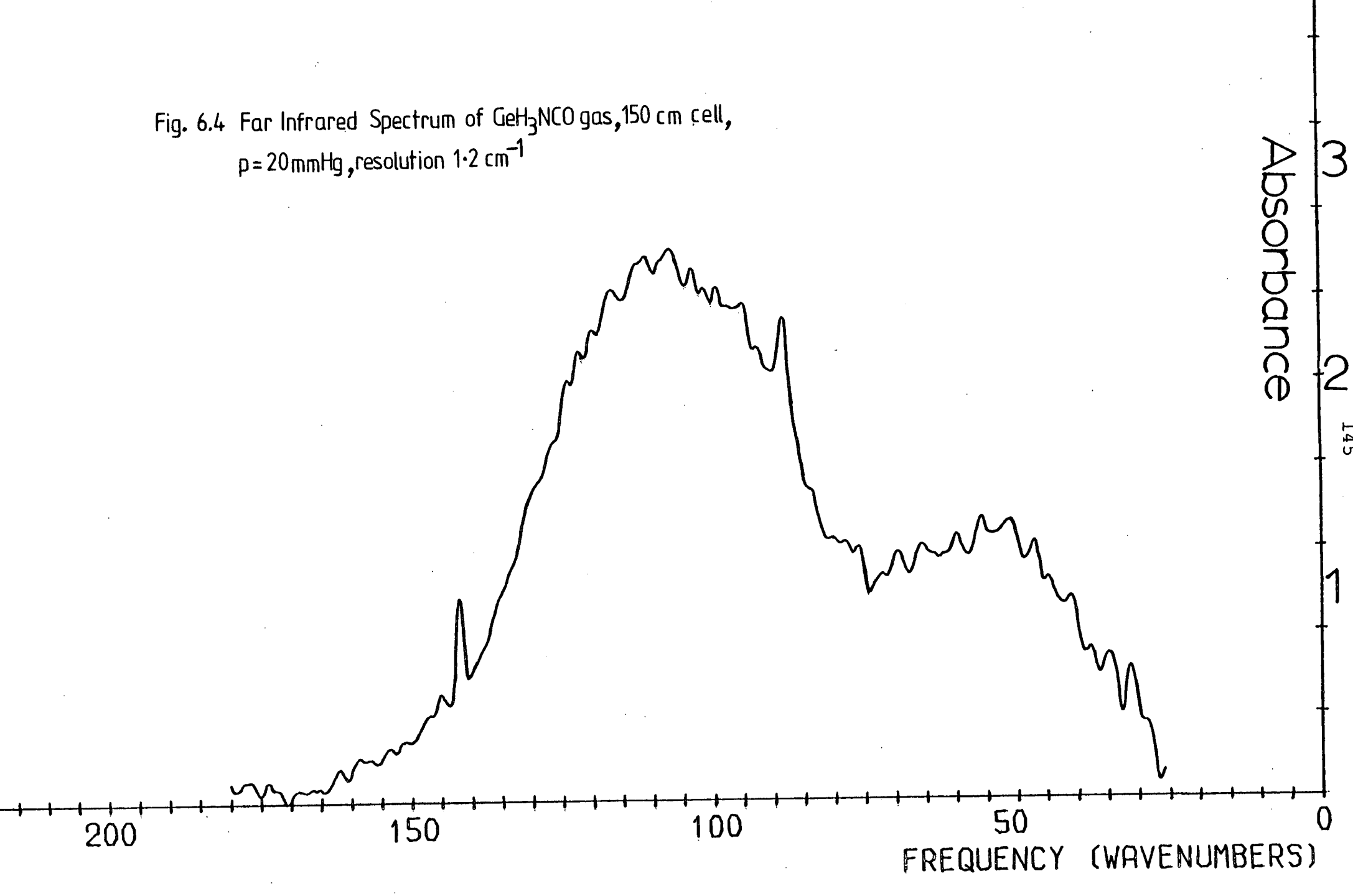

anharmonicity. The intensity of the higher frequency band is much greater than that of the lower frequency band, which is difficult to explain in simple terms. There are two visible sharp bands due to Q branches of the HNCO rotational spectrum.

The spectrum could be interpreted as one band being the torsional mode and the other the GeNC bending mode but this has been shown not to be the case by observing the shifts of these bands on deuteration[49]. Thus the GeNC bend was assigned to the band at 53.1 cm^{-1} with its 'overtone' at 107.4 cm^{-1}.

A spectrum in the range 500-50 cm^{-1} was run to check that there were no other bands which could be assigned to the torsion (see Figure 6.5). This spectrum shows the very strong GeN stretch at 491.9 cm^{-1} and a moderately strong band at 395.5 cm^{-1}, together with the already observed band at 107.4 cm^{-1}. The band at 395.5 cm^{-1} could be assigned to the GeH_3 torsion but is more likely to be the difference band of the absorptions at 491.9 and 107.4 cm^{-1} (491.9 - 107.4 = 384.5 cm^{-1}). It was concluded then, that the GeH_3 torsion was not observed.

6.5 Normal Coordinate Analysis of GeH_3NCO

6.5.1 Observed data

Most of the frequency data used in the normal coordinate analysis were taken from the matrix isolated

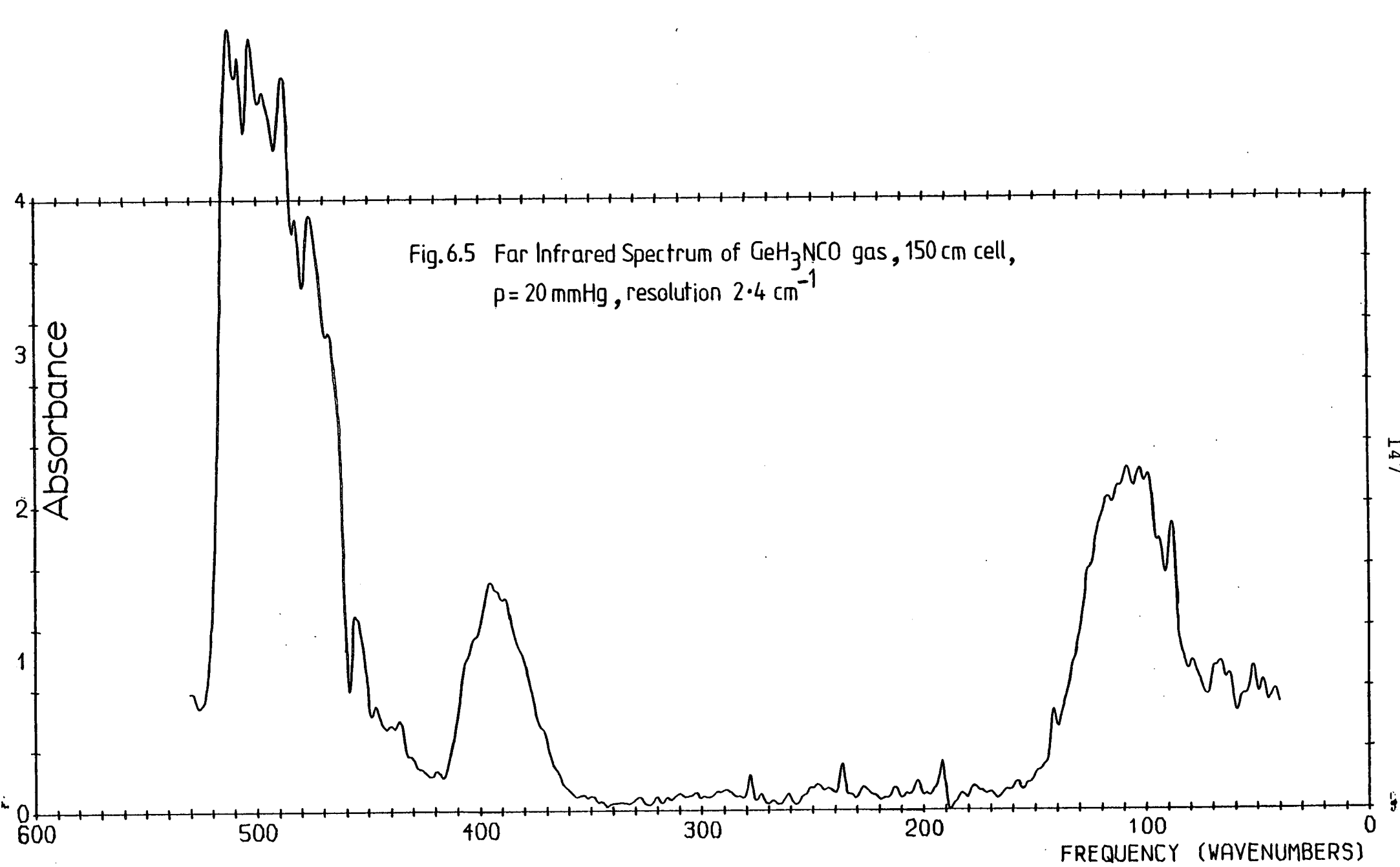

Fig. 6.5 Far Infrared Spectrum of GeH_3NCO gas, 150 cm cell, p = 20 mmHg, resolution 2·4 cm^{-1}

GEH3NCO PATH LENGTH 1.5M - 20 TORR (GN06)

spectrum, the assignment of which is given in Table 6.2. The solution to the frequency data was carried out in a C_s configuration with the NCO group trans to one of the hydrogen atoms. Data for the NCO symmetric stretch, ν_4, were taken from gas phase spectra, as was the frequency for the low frequency GeNC bend. The band maximum at 53.1 cm^{-1} in the far infrared gas phase spectrum was assumed to be close to the 'harmonic' frequency for the GeNC vibration.

The normal coordinate analysis was carried out using a mass value for germanium of the isotope ^{74}Ge, the most naturally abundant species. This assumes, then, that the infrared band maxima in the matrix spectra and far infrared correspond to the frequencies of vibration of the most naturally abundant species. It was necessary to supply a frequency value for the unobserved GeH_3 torsion. The results given for the analysis assumed a value of 50 cm^{-1} although any changes in the results were noted for a value of 100 cm^{-1}.

6.5.2 Molecular structure, internal coordinates, symmetry coordinates

Molecular Structure

The molecular structure parameters used were taken from an electron diffraction study[51]. Structural parameters were as follows: r(Ge-H) 1.532 Å,

r(Ge-N) 1.831 Å, r(C-N) 1.190 Å, r(C-O) 1.182 Å, Ge-$\hat{N}$-C 141.3°, H-$\hat{Ge}$-N 110°.

Internal Coordinates

The internal coordinates were defined as follows:

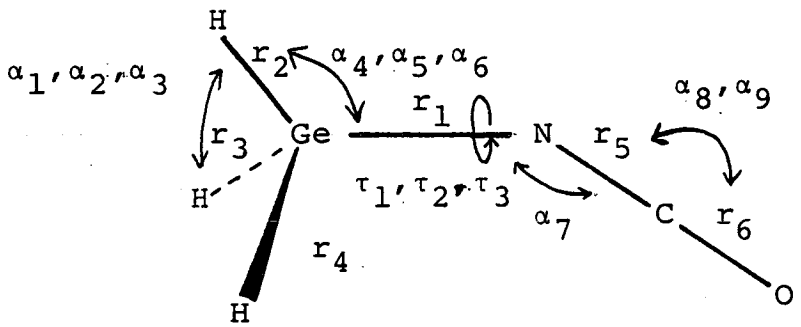

Symmetry Coordinates

The solution was refined using the following symmetry coordinate basis. The A' Ge-H stretches were treated as a separate symmetry species for reason of computer programme formatting. Since these coordinates do not couple to any great extent with other coordinates, this was assumed not to incur any error.

A' $s_1 : \Delta r_6$

$s_2 : \Delta r_5$

$s_3 : \frac{1}{(6)^{\frac{1}{2}}}(r_1 r_2)^{\frac{1}{2}}(-\Delta\alpha_1 - \Delta\alpha_2 + 2\Delta\alpha_3)$

$s_4 : (3+3\nu^2)^{-\frac{1}{2}}\{r_2(\Delta\alpha_1+\Delta\alpha_2+\Delta\alpha_3)+\nu(r_1 r_2)^{\frac{1}{2}}(\Delta\alpha_4+\Delta\alpha_5+\Delta\alpha_6)\}$

$s_5 : \frac{1}{(6)^{\frac{1}{2}}}(r_1 r_2)^{\frac{1}{2}}(2\Delta\alpha_4 - \Delta\alpha_5 - \Delta\alpha_6)$

$$s_6 : (r_5 r_6)^{\frac{1}{2}} \Delta\alpha_9$$

$$s_7 : \Delta r_1$$

$$s_8 : (r_1 r_5)^{\frac{1}{2}} \Delta\alpha_7$$

A' Ge-H stretches

$$s_1 : \frac{1}{(3)^{\frac{1}{2}}}(\Delta r_2 + \Delta r_3 + \Delta r_4)$$

$$s_2 : \frac{1}{(6)^{\frac{1}{2}}}(2\Delta r_2 - \Delta r_3 - \Delta r_4)$$

A"

$$s_1 : \frac{1}{(2)^{\frac{1}{2}}}(-\Delta r_3 + \Delta r_4)$$

$$s_2 : \frac{r_2}{(2)^{\frac{1}{2}}}(\Delta\alpha_1 - \Delta\alpha_2)$$

$$s_3 : \frac{(r_1 r_2)^{\frac{1}{2}}}{(2)^{\frac{1}{2}}}(\Delta\alpha_5 - \Delta\alpha_6)$$

$$s_4 : (r_5 r_6)^{\frac{1}{2}} \Delta\alpha_8$$

$$s_5 : \frac{r_1}{(3)^{\frac{1}{2}}}(\Delta\tau_1 + \Delta\tau_2 + \Delta\tau_3)$$

6.5.3 Normal coordinate solution for GeH_3NCO

The results of the normal coordinate anlysis of GeH_3NCO are given in Tables 6.3 - 6.6. The A' solution summarised in Table 6.3 omits the GeH stretches as mentioned earlier. All the vibrational modes are fairly 'pure' with the exceptions of those associated with the frequencies 2266.00 and 1412.80. Hence there is a mixing

of the CN and CO stretching coordinates, which supports the assignment of NCO asymmetric and symmetric stretches to these frequencies.

The A' GeH stretches (Table 6.4) result in a very simple solution showing no mixing of the coordinates. The apparently inferior fit for GeD_3NCO is due to the large observed shift for which there was no anharmonicity correction.

A frequency of 50 cm^{-1} was assumed for the GeH_3 torsional mode in the A" symmetry species solution (Table 6.5). There is the expected off-diagonal element F_{32} coupling the GeH asymmetric deformation and the GeH_3 rock, and also a finite element F_{43} coupling the GeH_3 rock and the NCO bend. The latter is not unusual since there is similar coupling in related molecules, e.g. SiH_3NCO, and the vibrational modes are very close in energy. The frequency fit exhibits, again, the absence of anharmonicity corrections for the deuterated species. In the potential energy distribution there is some contribution from the NCO bend to the principally GeH_3 rocking mode and vice versa.

Table 6.6 contains some calculated parameters from the normal coordinate analysis. Some of the quoted parameters are sensitive to the frequency value used for the GeH_3 torsional mode. These are mainly the mean perpendicular amplitudes, P, although some of the

Table 6.3

NORMAL COORDINATE SOLUTION FOR GEH NCO
SYMMETRY SPECIES - A' 3
F MATRIX AND FREQUENCIES FOR 4 ISOTOPIC SPECIES
P. E. DISTRIBUTION AND L MATRIX FOR 1ST ISOTOPIC SPECIES

F MATRIX

16.49355							
1.38660	11.24830						
0.00000	0.00000	0.17638					
0.00000	0.00000	0.00000	0.18805				
0.00000	-0.01231	-0.01846	0.00000	0.21874			
0.00000	0.00000	0.00448	0.00000	0.01425	0.48964		
0.23280	-1.19635	0.00000	0.00000	0.11456	-0.25483	3.37011	
0.00000	0.00000	0.00000	0.00000	0.00000	0.00000	0.00000	0.01616

F.OBS	F.CALC	DIFF	
2266.00	2265.98	0.02	
1412.80	1413.32	-0.52*	
878.50	878.41	0.09	
857.50	857.39	0.11	GEH NCO
642.20	642.27	-0.07	3
611.90	611.76	0.14	
475.10	475.25	-0.15	
53.10	53.13	-0.03*	

F.OBS	F.CALC	DIFF	
2258.00	2256.82	1.18	
1386.20	1383.20	3.00*	
878.60	878.40	0.20	15
857.50	857.37	0.13	GEH NCO
640.30	640.76	-0.46	3
609.80	609.11	0.69	
471.00	468.97	2.03	
-	52.42	-	

F.OBS	F.CALC	DIFF	
2209.00	2205.55	3.45	
1410.30	1413.26	-2.97*	
878.70	878.37	0.33	13
857.50	857.38	0.12	GEH N CO
641.60	641.57	0.03	3
594.80	595.79	-1.00	
470.70	471.46	-0.76	
-	52.96	-	

F.OBS	F.CALC	DIFF	
2266.00	2265.93	0.07	
1412.80	1412.12	0.68*	
628.60	626.84	1.76	
616.70	622.39	-5.69	GED NCO
474.40	476.99	-2.59	3
612.40	612.65	-0.25	
463.50	464.49	-0.99	
-	51.71	-	* GAS PHASE VALUE

P.E. DISTRIBUTION

2266.00	1412.80	878.50	857.50	642.20	611.90	475.10	53.10	
0.661	0.346	0.001	0.000	0.002	0.000	0.005	0.000	C-O STR.
0.411	0.394	0.002	0.002	0.003	0.009	0.231	0.002	C-N STR.
0.000	0.000	0.922	0.001	0.071	0.015	0.000	0.000	GE-H ASYM. DEF.
0.000	0.000	0.001	0.993	0.000	0.000	0.006	0.000	GE-H SYM. DEF.
0.000	0.007	0.142	0.000	0.839	0.034	0.009	0.001	GE-H ROCK
0.000	0.000	0.000	0.000	0.084	0.942	0.004	0.019	N-C-O BEND
0.008	0.104	0.000	0.005	0.020	0.058	0.907	0.009	GE-N STR.
0.000	0.000	0.000	0.000	0.004	0.016	0.004	0.977	GE-N-C BEND

L MATRIX

0.34801	0.15703	0.00375	0.00190	0.00511	0.00077	0.00611	0.00005
-0.33226	0.20296	0.00940	0.00925	0.00860	0.01357	0.05222	0.00054
0.00454	-0.03468	1.54135	-0.05386	-0.31315	-0.13463	-0.01772	0.00010
0.00970	-0.03831	0.04972	1.51197	-0.00423	-0.00719	-0.06358	-0.00031
0.06814	-0.19309	0.54259	-0.02274	0.96545	0.18621	-0.07489	-0.00330
0.00810	-0.01351	0.01467	0.00021	-0.20416	0.65102	-0.03427	0.00797
0.08307	-0.19072	-0.00393	0.02466	-0.03836	0.06135	0.18922	0.00211
0.02933	-0.06327	-0.00872	-0.01033	0.23180	-0.46380	-0.17436	0.31700

Table 6.4

```
NORMAL COORDINATE SOLUTION FOR GEH NCO
A' GE-H STRETCHES                    3
F MATRIX AND FREQUENCIES FOR 4 ISOTOPIC SPECIES
P. E. DISTRIBUTION AND L MATRIX FOR 1ST ISOTOPIC SPECIES

F MATRIX
  2.73308
  0.00000  2.66495

 F.OBS    F.CALC    DIFF
 2151.00 2151.00    0.00      GEH NCO
 2138.00 2138.00    0.00         3

 F.OBS    F.CALC    DIFF           15
 2151.00 2151.00    0.00      GEH   NCO
 2138.00 2138.00    0.00         3

 F.OBS    F.CALC    DIFF           13
 2151.00 2151.00    0.00      GEH N  CO
 2137.00 2138.00   -1.00         3

 F.OBS    F.CALC    DIFF
 1550.00 1525.20   24.80      GED NCO
 1534.00 1525.73    8.27         3

P.E. DISTRIBUTION

  2151.00  2138.00

    1.000    0.000     GE-H SYM. STR.
    0.000    1.000     GE-H ASYM. STR.

L MATRIX
  0.99850 -0.00000
  0.00000  1.00508
```

Table 6.5

```
NORMAL COORDINATE SOLUTION FOR GEH NCO
SYMMETRY SPECIES - A''            3
F MATRIX AND FREQUENCIES FOR 4 ISOTOPIC SPECIES
P. E. DISTRIBUTION AND L MATRIX FOR 1ST ISOTOPIC SPECIES

F MATRIX
  2.66465
  0.00000  0.17743
  0.00000 -0.02500  0.22162
  0.00000  0.00000  0.02869  0.52928
  0.00000  0.00000  0.00000  0.00000  0.00088

 F.OBS    F.CALC     DIFF
 2138.00  2138.00     0.00
  872.10   872.10    -0.00
  664.70   664.70    -0.00      GEH NCO
  642.20   642.20     0.00         3
   50.00    50.00     0.00*

 F.OBS    F.CALC     DIFF
 2138.00  2138.00     0.00
  872.40   872.05     0.35           15
  662.10   661.46     0.64      GEH   NCO
  640.30   640.89    -0.59         3
     -      49.48      -

 F.OBS    F.CALC     DIFF
 2137.00  2138.00    -1.00
  872.50   872.09     0.41           13
  664.20   662.97     1.23      GEH N  CO
  626.70   625.74     0.96         3
     -      49.97      -

 F.OBS    F.CALC     DIFF
 1534.00  1525.98     8.02
  623.60   619.31     4.29
  495.90   490.58     5.32      GED NCO
  649.00   648.23     0.77         3
     -      42.14      -                  * ASSUMED VALUE

P.E. DISTRIBUTION

   2138.00    872.10    664.70    642.20     50.00

      1.000     0.000     0.000     0.000     0.000     GE-H ASYM. STR.
      0.000     0.952     0.046     0.018     0.000     GE-H ASYM. DEF.
      0.000     0.140     0.742     0.141     0.000     GE-H ROCK
      0.000     0.000     0.232     0.769     0.006     N-C-O BEND
      0.000     0.000     0.002     0.003     0.994     GE-H3 TORSION

L MATRIX
  1.00507 -0.00206  0.00278  0.00146  0.00001
  0.02909  1.55013 -0.25998 -0.15824  0.00016
 -0.02652  0.53166  0.93344  0.39315 -0.00168
  0.00008  0.00398 -0.33791  0.59413  0.00398
 -0.02558  0.01978  0.84460 -0.97764  1.28961
```

Table 6.6

CALCULATED PARAMETERS
1ST ISOTOPIC SPECIES

INTERATOMIC DISTANCES AND AMPLITUDES - 0.00K

ATOMS	DIST(RA).	U	P	L	K	RG	RALPHA
GE-H'	1.5320	0.0915	0.2405	0.0055	0.0377	1.5375	1.4997
GE-H''	1.5320	0.0890	0.2175	0.0052	0.0309	1.5372	1.5063
GE-N	1.8310	0.0437	0.1031	0.0010	0.0058	1.8320	1.8262
C-N	1.1900	0.0377	0.0919	0.0012	0.0071	1.1912	1.1841
C-O	1.1820	0.0346	0.0930	0.0010	0.0073	1.1830	1.1757
GE..C	2.8583	0.0718	0.0503	0.0018	0.0009	2.8601	2.8592
N..O	2.3720	0.0410	0.1472	0.0007	0.0091	2.3727	2.3636
GE..O	3.9696	0.0916	0.0485	0.0021	0.0006	3.9717	3.9711
H'..H''	2.4935	0.1538	0.3547	0.0095	0.0504	2.5030	2.4525
H'..N	2.7601	0.1210	0.3008	0.0053	0.0328	2.7654	2.7327
H'..C	3.9435	0.1193	0.2484	0.0036	0.0156	3.9471	3.9314
H'..O	5.1219	0.1181	0.2007	0.0027	0.0079	5.1246	5.1167
H''..N	2.7601	0.1245	0.2198	0.0056	0.0175	2.7658	2.7482
H''..C	3.5125	0.1806	0.1998	0.0093	0.0114	3.5218	3.5104
H''..O	4.4531	0.2328	0.1938	0.0122	0.0084	4.4652	4.4568

INTERATOMIC DISTANCES AND AMPLITUDES - 298.16K

ATOMS	DIST(RA).	U	P	L	K	RG	RALPHA
GE-H'	1.5320	0.1062	0.5905	0.0074	0.2276	1.5394	1.3118
GE-H''	1.5320	0.0891	0.5134	0.0052	0.1721	1.5372	1.3651
GE-N	1.8310	0.0471	0.2846	0.0012	0.0442	1.8322	1.7880
C-N	1.1900	0.0380	0.2104	0.0012	0.0372	1.1912	1.1540
C-O	1.1820	0.0346	0.2178	0.0010	0.0401	1.1830	1.1429
GE..C	2.8583	0.1712	0.0958	0.0103	0.0032	2.8685	2.8653
N..O	2.3720	0.0414	0.4118	0.0007	0.0715	2.3727	2.3012
GE..O	3.9696	0.2419	0.1309	0.0147	0.0043	3.9844	3.9801
H'..H''	2.4935	0.1608	0.9172	0.0104	0.3374	2.5038	2.1664
H'..N	2.7601	0.1307	0.8001	0.0062	0.2319	2.7663	2.5344
H'..C	3.9435	0.1227	0.6281	0.0038	0.1000	3.9473	3.8472
H'..O	5.1219	0.1215	0.4724	0.0029	0.0436	5.1248	5.0812
H''..N	2.7601	0.1282	0.5425	0.0060	0.1066	2.7661	2.6595
H''..C	3.5125	0.3706	0.4795	0.0391	0.0655	3.5516	3.4861
H''..O	4.4531	0.5596	0.4698	0.0703	0.0496	4.5234	4.4738

H' - IN PLANE
H''- OUT OF PLANE

interatomic parallel amplitudes, U, are affected if they have components perpendicular to the plane of symmetry. The K values, which are measures of the perpendicular distance corrections of electron diffraction distances, are reduced to about half their value with ν_{15} = 100 cm^{-1} instead of 50 cm^{-1}.

Of the refined parallel amplitudes from electron diffraction[51], most show good agreement with calculated values. Some of the calculated K values at room temperature are very large - undoubtedly due to the use of rectilinear coordinates in their calculation. Such an approximation does not hold well for very low frequency vibrations. From Table 6.6 the calculated linear shrinkage δ(N...O) is 0.004 Å compared to the electron diffraction value[51] of 0.008 Å.

6.6 Conclusions

Germyl isocyanate has an infrared spectrum in an argon matrix (concn 1:1000) showing all the major features expected. Due to the broadness of some of the bands, however, it is difficult to draw conclusions about molecular symmetry. The infrared spectrum in a nitrogen matrix (1:1000) is much more detailed and can be interpreted only in terms of a C_s molecular model. The far infrared gas phase spectrum of GeH_3NCO shows the absorption due to the GeNC band, the potential of which

is likely to have some anharmonicity. The GeH_3 torsion was not observed. A detailed normal coordinate analysis of GeH_3NCO in a C_s configuration reproduces well the observed frequencies for four isotopic species and serves to confirm the vibrational assignment.

6.7 Germyl Isothiocyanate - Preliminary Study

Germyl isothiocyanate, GeH_3NCS, is a very involatile compound with a vapour pressure at room temperature of about 3 mmHg. This makes gas phase studies difficult; however, studies in matrix isolation are relatively easy due to the small amounts required.

GeH_3NCS was studied in a nitrogen matrix and the spectrum obtained is shown in Figure 6.6. The highest frequency band observed, at 2454 cm^{-1}, was assigned to a combination. In the region 2050-2200 cm^{-1} we see the symmetric GeH stretch as a strong band at 2168 cm^{-1} with a weak band to lower frequency associated with the asymmetric GeH stretches. The very strong band due to the CN stretch is at 2092 cm^{-1}.

The germyl deformations occur between 830 and 870 cm^{-1}. The very strong band is the symmetric GeH deformation and the broadish weaker band to higher frequency is due to the asymmetric GeH deformation. As indicated in the figure, the two components are not resolved. The germyl rocking band near 655 cm^{-1} shows

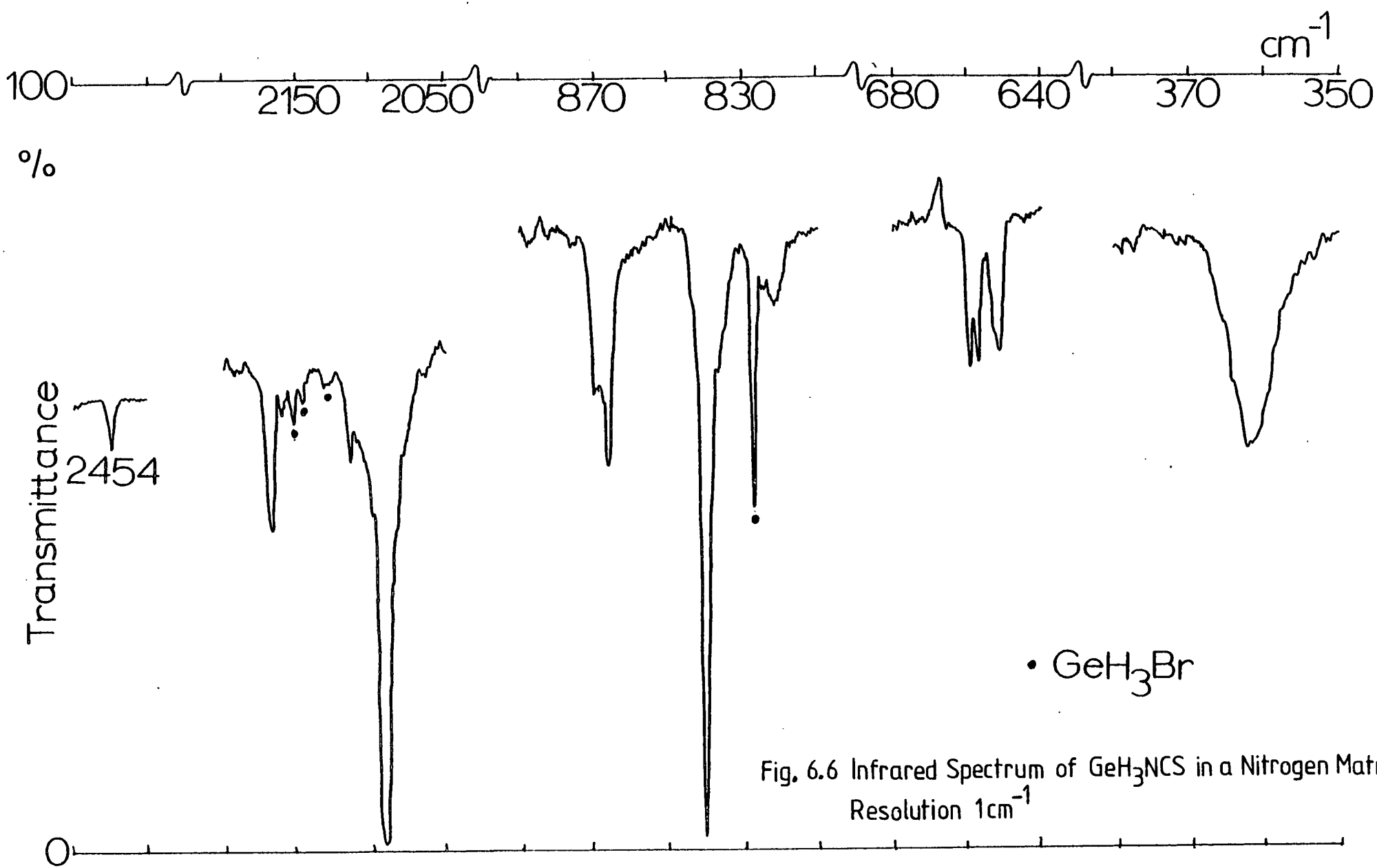

Fig. 6.6 Infrared Spectrum of GeH_3NCS in a Nitrogen Matrix
Resolution $1cm^{-1}$

some splitting, which does not disappear on annealing the sample. The difference in frequency between the highest and lowest band is 7.8 cm^{-1}.

It is possible to account for a small splitting of 'degenerate' modes by recognising the non-isotropic nature of the matrix cage. This splitting is usually <5 cm^{-1}. In the case of GeH_3NCS, therefore, the splitting of the germyl rocks indicates a slight non-linearity in the heavy-atom chain. Lastly, the GeN stretching absorption is observed at 361.9 cm^{-1} as a strong band. Table 6.7 gives a summary of GeH_3NCS bands and assignment of approximate mode of vibration. The assignment is given in terms of a C_{3v} model.

Taking the matrix isolated infrared spectrum of GeH_3NCS as a whole, it seems likely that the molecule is a nearly symmetric top. The GeH stretches show a simple pattern - strong and weak bands, symmetric and asymmetric. The asymmetric components of the GeH deformation are nearly degenerate. In the germyl rocking band we have a larger splitting than, for example, for the silyl rock in SiH_3NCSe. In the case of SiH_3NCSe the splitting can be explained in terms of a non-isotropic matrix cage. The splitting of the germyl rock in GeH_3NCS is, however, smaller than that for GeH_3NCO or for the silyl rock in SiH_3NCO, both of which must be explained in terms of a non-linear heavy-atom chain. In GeH_3NCS, then, we may

Table 6.7

Observed frequencies (cm^{-1}) and assignment for GeH_3NCS, nitrogen matrix

2454	v.w.	$\nu_2 + \nu_5$
2168	s	ν_1, symmetric GeH stretch
2161	v.w.	ν_6, asymmetric GeH stretch
2092	v.s.	ν_2, CN stretch
869.7(sh)	s	ν_7, asymmetric GeH deformations
866.7	s	
840.4	v.s.	ν_4, symmetric GeH deformation
659.0	s	ν_8, GeH rock
656.8	s	
651.2	s	
361.9	s	ν_5, GeN stretch

have a slightly bent heavy-atom chain.

The CS stretching absorption, ν_3, was not observed in the matrix isolated infrared spectrum. This band was expected between 850 and 1050 cm^{-1}. The NCS band, ν_9, was not observed either. The only band which could be assigned to ν_9 was at 361.9 cm^{-1}; however, this was assigned to ν_5, the GeN stretch due to the similarity in intensity to the corresponding band of GeH_3NCO.

In order to obtain further information about the unassigned GeH_3NCS fundamentals, an infrared spectrum was run in the gas phase using a long path cell (path length = 1.25 m, pressure = 0.7 mmHg). The NCS bend can be assigned to a very weak band at 470 cm^{-1}. In the region where the CS stretch is expected the GeH deformations dominate the spectrum. There appears to be only one extremely weak band at 975 cm^{-1} which could be assigned to the CS stretch.

6.8 Far Infared Spectrum of Germyl Isothiocyanate

The low vapour pressure, again, has been the limiting factor in the study of GeH_3NCS in the far infrared. In the 150 cm cell, however, it was possible that an absorption might be observed. The observed spectrum in the range 250-10 cm^{-1} is shown in Figure 6.7.

Two bands were observed, one centred at 49.4 cm^{-1}, the other at 92.2 cm^{-1}. The bands are of comparable

Fig. 6.7 Far Infrared Spectrum of GeH_3NCS gas, 150 cm cell,
p = 3 mmHg, resolution 1·2 cm^{-1}

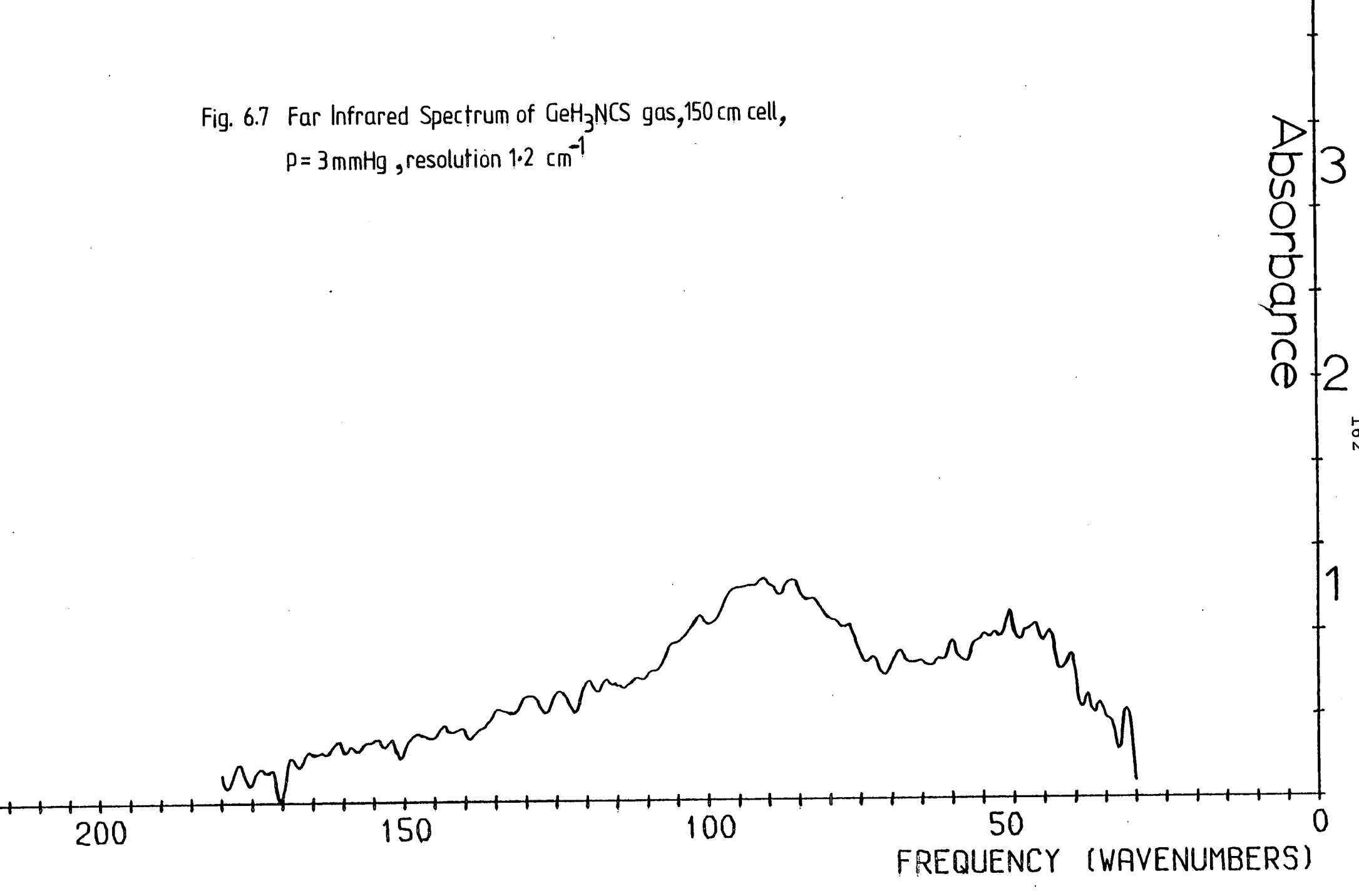

intensity, one approximately twice the frequency of the other. As with similar molecules studied, the lower band is concluded to be due to the $\Delta v = 1$, $\Delta l = \pm 1$ transitions of a low frequency bend, with the upper band the $\Delta v = 2$, $\Delta l = 0,2$ transitions. The absorption is principally associated with the GeNC bending mode.

It is difficult to see if there are any fine structure features on either band due to the poor signal to noise, although there seems no suggestion of underlying features. The bands are broad which suggests some degree of anharmonicity in the vibration. The former prediction of 50 cm^{-1} for the low frequency bending mode of this molecule was very accurate.

6.9 Conclusions

The matrix isolated spectrum of GeH_3NCS suggests that the molecule is a nearly symmetric top with deviations from linearity of the GeNCS chain very small. Two of the fundamental absorptions, ν_3 and ν_9, do not show in the matrix isolated spectrum although ν_9 can be assigned in the gas phase spectrum. The assignment of ν_3 is still uncertain. The far infrared spectrum of GeH_3NCS in the gas phase shows the 'fundamental' and 'overtone' of the low frequency GeNC bending vibration, with a 'fundamental' band maximum, at room temperature, of 49.4 cm^{-1}.

CHAPTER 7 - SILYL CYANIDE, SiH_3CN and $SiH_2(NCO)_2$

7.1 Introduction

Silyl cyanide was first prepared by passing silyl iodide vapour over silver cyanide[29]. The only physical property reported at that time was its melting point of 34°C. Although there was no attempt to determine the molecular structure, it was assumed that the CN group was bonded to silicon through the carbon atom. A later study[38] reported that the reaction of silyl iodide with silver cyanide gave silyl isocyanide, SiH_3NC, analogous to the methyl compound CH_3NC. There was, however, no evidence to support either structure.

The first detailed infrared study of silyl cyanide[54] reported the bands due to seven of the eight fundamentals. The low frequency bending of the SiCN chain, ν_8, was assumed to occur at a frequency of about 235 cm^{-1} by observation of its overtone. Silyl cyanide was assumed to be a symmetric top in accordance with the gas phase infrared spectrum. Observation of the ^{13}C and ^{15}N isotopic shifts for SiD_3CN on the CN stretching band led to the conclusion that the molecule was the normal cyanide, SiH_3CN.

Further evidence for the normal cyanide molecular structure came from preliminary microwave studies[55,56]. The B rotational constant was much closer to that

expected for SiH_3CN than SiH_3NC. Also, the quadrupolar couplings observed due to ^{14}N could only occur in the SiH_3CN form. By analogy with CH_3NC, the ^{14}N quadrupole couplings were unlikely to be resolved for SiH_3NC.

One further infrared study has been published[57] in which a number of the perpendicular band structures were analysed. This yielded a ζ constant for ν_7. ν_8 was observed directly at 247.2 cm^{-1} which, when considered along with the position of the overtone, indicated significant anharmonicity in this vibration.

The most recent spectroscopic study of silyl cyanide was in the microwave region[58]. A full vibrational/rotational analysis was carried out for the molecule in the ground state and the first four excited states of ν_8. There is also analysis giving the rotational constant in the first excited state of ν_3, ν_4 and ν_7. The microwave spectrum was interpreted in terms of a symmetric top model for silyl cyanide.

Work has been carried out at Edinburgh on the equilibrium structure, r_e, of silyl cyanide, for which a normal coordinate analysis was required. SiH_3CN was studied in matrix isolation together with three isotopically labelled species, and the resulting data used in a normal coordinate analysis. The infrared spectrum of SiH_3CN in the gas phase was also run at a

resolution of 0.06 cm^{-1} to enable analysis of the rotational structure of the individual bands. This, it was hoped, would give values for α_B for the different vibrational modes.

The infrared spectrum of $SiH_2(NCO)_2$ was run in the gas phase and in matrix isolation. The matrix isolated spectrum proved very successful in resolving the many closely spaced bands.

Experimental Results

7.2 Silyl Cyanide in a Nitrogen Matrix

Two isotopic species, SiH_3CN and $SiH_3C^{15}N$, had already been studied by infrared spectroscopy in a nitrogen matrix[59]. Silyl cyanide was not expected to be significantly removed from the C_{3v} symmetry found in the gas phase on matrix isolation. The matrix isolated infrared spectrum of $SiH_3{}^{13}C^{15}N$ is shown in Figure 7.1.

The SiH stretching region near 2200 cm^{-1} shows the usual pattern of a strong band due to the symmetric mode and a weaker band to low frequency associated with the asymmetric mode. The CN stretch appears at 2122 cm^{-1} as a sharp line of moderate intensity. In the region 900-940 cm^{-1} there is a very strong band due to the symmetric SiH deformation with a broad multiplet for the asymmetric SiH deformation.

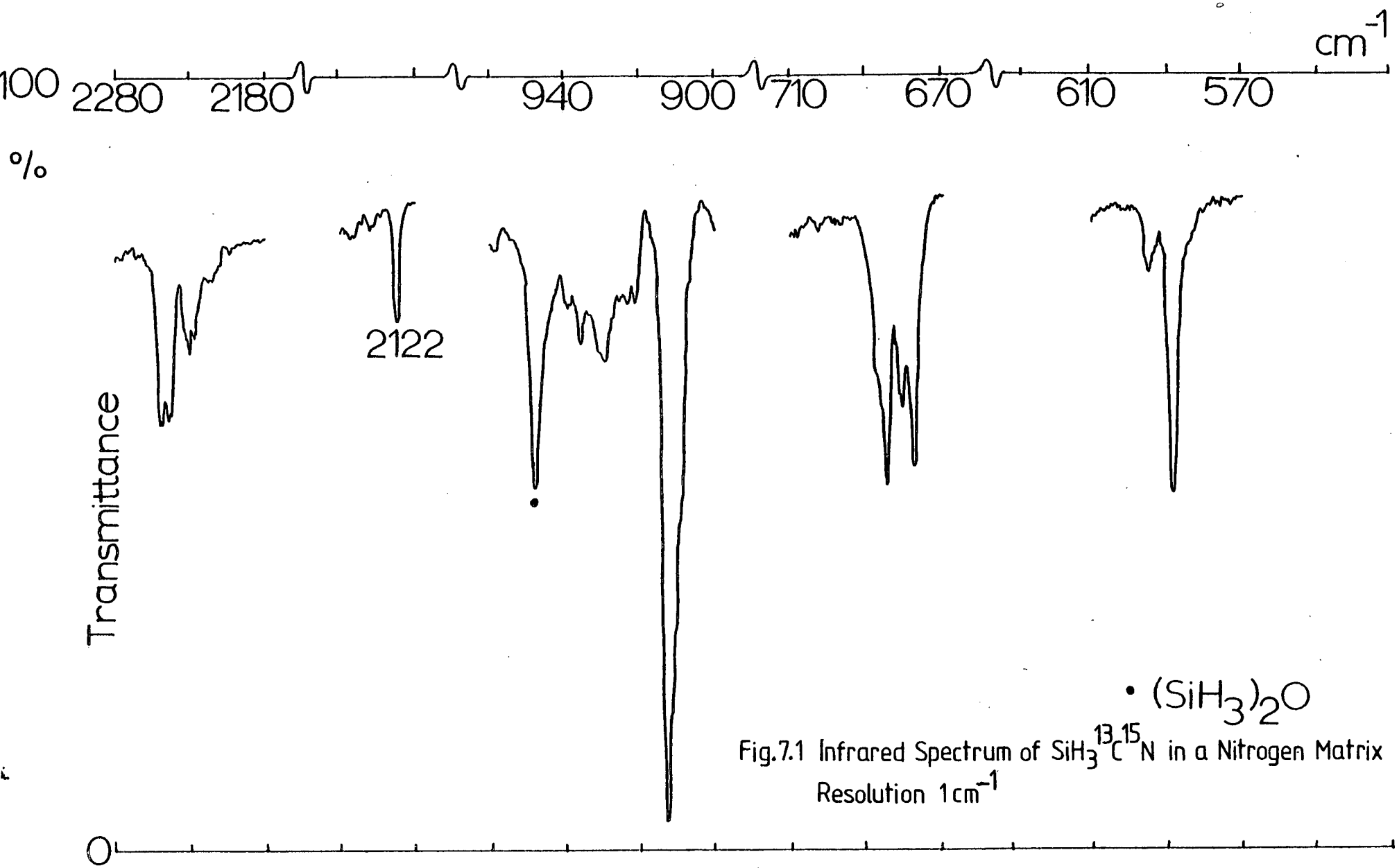

Fig.7.1 Infrared Spectrum of $SiH_3{}^{13}C^{15}N$ in a Nitrogen Matrix
Resolution 1 cm^{-1}

There is evidence for clusters of sample molecules, with bands between 880 and 900 cm^{-1}. These are observed to grow in intensity on annealing.

The SiH rocking band appears as a doublet with a separation of about 8 cm^{-1}. The SiC stretching mode gives a strong sharp absorption at 588.2 cm^{-1}. From the splitting of the components of the silyl rock it must be assumed that there is some bending at the carbon atom in the matrix.

All of the fundamental transitions are observed in the matrix isolated infrared spectrum except the lowest energy one associated with the SiCN bending. It is difficult to account for this, since the gas phase absorption is fairly strong. Some of the bands in the spectrum are broad, notably those due to the asymmetric SiH deformations and the SiH_3 rock. It may be that there is a significant proportion of the sample molecules in clusters, even at a matrix ratio of 1:1000, causing this effect.

Evidence for a significant degree of aggregation of sample molecules in the matrix can be seen in the associated bands in the infrared spectrum. The spectrum recorded immediately after spray-on to the cold window, i.e. with no annealing, showed a fairly strong cluster band at 898.7 cm^{-1}. Annealing to the matrix causes this band to increase in intensity.

The tendency of SiH_3CN molecules to interact with each other strongly is not surprising in view of the compound's behaviour in a pure state. It does not

liquefy when handled in a vacuum system, and has a high latent heat of vaporisation. The origin of the strong intermolecular attraction is the affinity of the nitrogen lone pair for the silicon atom of a neighbouring molecule. This explains the appearance of extra bands in the SiH deformation region and the SiC stretching region on annealing the matrix - these modes are most likely to change in frequency if a cluster forms. The strong intermolecular force between nitrogen and silicon atoms is also exhibited in the crystal structure of SiH_3CN. Long chains Si-C-N...Si are found.

Table 7.1 summarises the observed frequencies and the assignment of the approximate mode of vibration for all the isotopic species studied. The assignment assumes a C_{3v} point group for SiH_3CN. The absorption associated with the SiCN bend was observed only in the gas phase using a cell with CsI windows. The observed frequencies were as follows:

SiH_3CN	$SiH_3C^{15}N$	$SiH_3{}^{13}C^{15}N$	SiD_3CN		
246.6 cm^{-1}	244.8	239.6	229.2	s	ν_8, SiCN bend.

7.3 Silyl Cyanide, ν_8 Band Shape

The gas phase band, ν_8, of silyl cyanide shows evidence of a hot-band transition. The proportion of

Table 7.1

Observed frequencies (cm^{-1}) and assignment for SiH_3CN, nitrogen matrix

SiH_3CN	$SiH_3C^{15}N$	$SiH_3{}^{13}C^{15}N$	SiD_3CN		
2248.3	2247.1	2248.0	1603	m.s.	ν_1, SiH symmetric stretch
2243.0	2242.4	2243.0		m.s.	
2231.0	2229.8	2231	1643	w	ν_5, SiH asymmetric stretch
2200.4	2171.0	2122	2201	m.s.	ν_2, CN stretch
934.9	934.3	936.2	679.6	m.s.	ν_6, SiH asymmetric stretch
			677.4		
930.4	930.1	930.2	674.2	m.s.	
913.9	913.7	913.4	687.3	s	ν_3, SiH symmetric deformation
690.5	690.5	687.3(sh)		s	ν_7, SiH_3 rock
688.1	687.9	684.5	541.0	s	
683.6	682.8	680.9	537.3	s	
681.1	680.7	677.2		s	
601.5	595.6	588.2	573.8	s	ν_4, SiC stretch

molecules in state $v_8 = 1$ at room temperature is about 30% of the ground state population. There is also a proportion of about 10% of the ground state population in state $v_8 = 2$. In order to see any hot bands separately the vibration would require to be anharmonic.

Figure 7.2 shows the gas phase infrared spectrum of SiH_3CN from 500-100 cm^{-1}. The fundamental absorption occurs at 246.5 cm^{-1} and the overtone is centred at 475.0 cm^{-1}. The apparent structure on the overtone band is probably due to incorrect ratioing of background/sample + background. From the positions of the two bands it is obvious that the vibration is anharmonic.

Most of the intensity from the lower frequency band will be from the two transitions $v_8 = 0 \rightarrow v_8 = 1$ and $v_8 = 1 \rightarrow v_8 = 2$, while the 'overtone' will have contributions largely from $v_8 = 0 \rightarrow v_8 = 2$ and $v_8 = 1 \rightarrow v_8 = 3$. In view of the anharmonicity of the vibration, the spike to low frequency of the fundamental band was assigned to the hot-band transition $v_8 = 1 \rightarrow v_8 = 2$ (237.5 cm^{-1}). It is unlikely that this band is the P branch of the fundamental band. Calculations of the fundamental band shape (see Appendix) do not give results similar to the observed spectrum.

7.4 Normal Coordinate Analysis of SiH_3CN

A normal coordinate analysis of SiH_3CN was carried

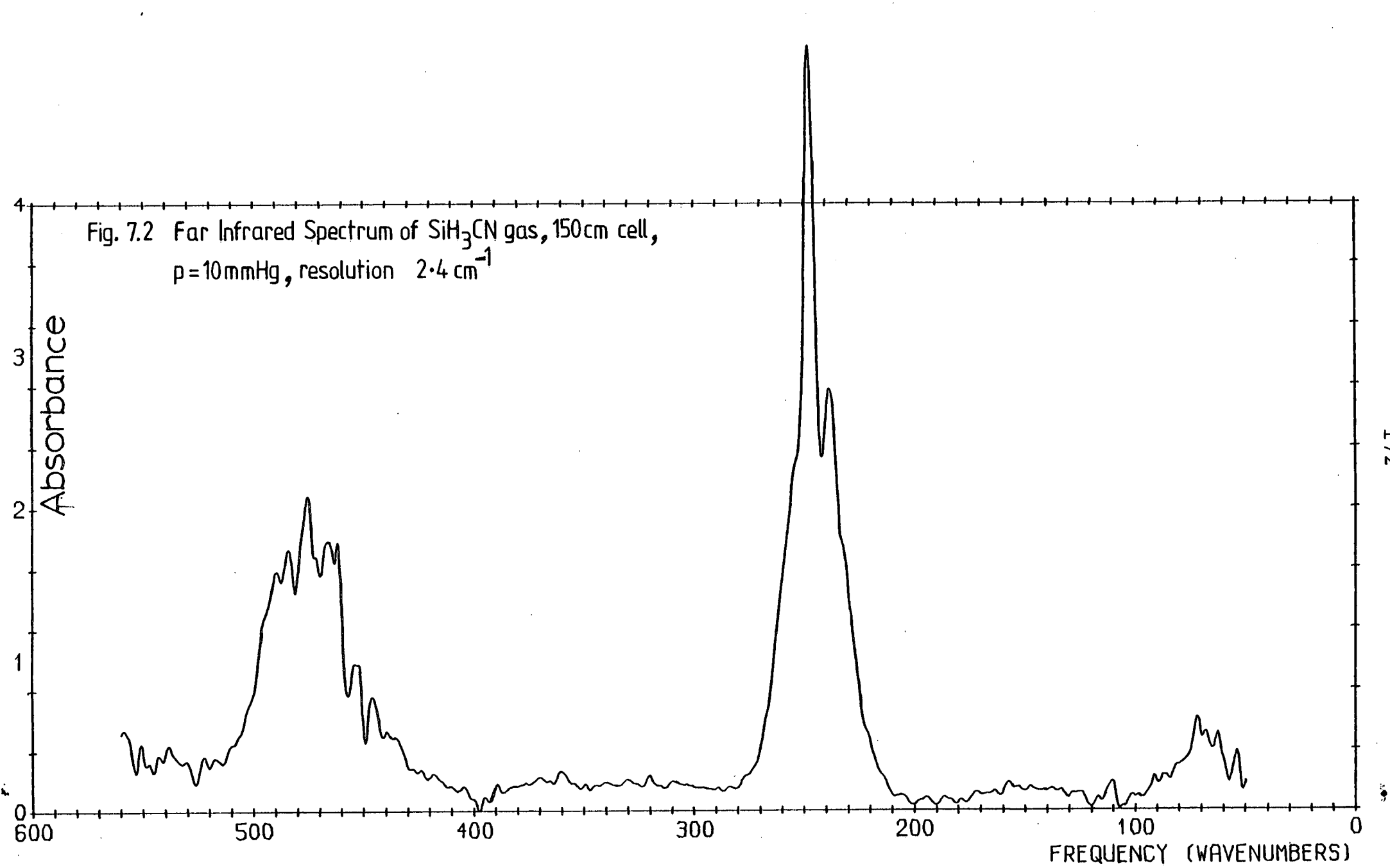

Fig. 7.2 Far Infrared Spectrum of SiH_3CN gas, 150cm cell, p = 10mmHg, resolution $2{\cdot}4\ cm^{-1}$

out using the nitrogen matrix infrared frequencies for the four isotopic species studied. The analysis was carried out with the molecule in a C_{3v} configuration. Any split 'degeneracies' in the matrix data were averaged for use in the refinement. Frequency values for ν_8 were taken from gas phase spectra for all isotopic species.

7.4.1 Molecular structure, internal coordinates, symmetry coordinates

Molecular Structure

The molecular structure parameters were taken from a microwave paper[55]. These parameters are quoted therein as being identical to an unpublished electron diffraction study. Structural parameters used were as follows: r(Si-H) 1.49 Å, r(C-N) 1.158 Å, r(Si-C) 1.847 Å, C-$\hat{\text{Si}}$-H 107.5°, Si-$\hat{\text{C}}$-N 180°.

Internal Coordinates

The internal coordinates used were defined as follows:

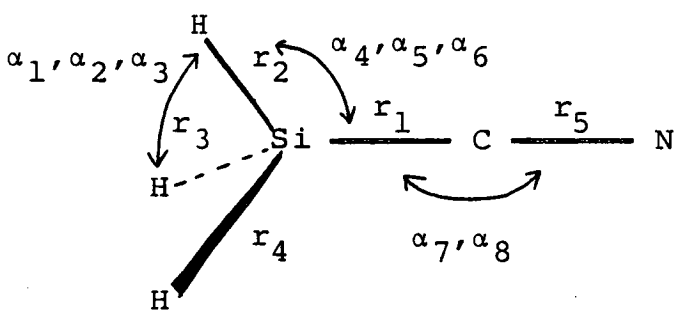

Symmetry Coordinates

The force field solution was refined using the following symmetry coordinate basis:

$\underline{A_1}$ $s_1 : \frac{1}{(3)^{\frac{1}{2}}}(\Delta r_2+\Delta r_3+\Delta r_4)$

$s_2 : \Delta r_5$

$s_3 : (3+3\nu^2)^{-\frac{1}{2}}\{r_2(\Delta\alpha_1+\Delta\alpha_2+\Delta\alpha_3)+\nu(r_1r_2)^{\frac{1}{2}}(\Delta\alpha_4+\Delta\alpha_5+\Delta\alpha_6)\}$

$$\nu = \frac{(3)^{\frac{1}{2}} \cos \alpha_4}{\cos \frac{\alpha_1}{2}}$$

$s_4 : \Delta r_1$

$\underline{E(1)}$ $s_1 : \frac{1}{(6)^{\frac{1}{2}}}(2\Delta r_2-\Delta r_3-\Delta r_4)$

$s_2 : \frac{r_2}{(6)^{\frac{1}{2}}}(-\Delta\alpha_1-\Delta\alpha_2+2\Delta\alpha_3)$

$s_3 : \frac{(r_1r_2)^{\frac{1}{2}}}{(6)^{\frac{1}{2}}}(2\Delta\alpha_4-\Delta\alpha_5-\Delta\alpha_6)$

$s_4 : (r_1r_5)^{\frac{1}{2}}\Delta\alpha_7$

$\underline{E(2)}$ $s_1 : \frac{1}{(2)^{\frac{1}{2}}}(-\Delta r_3+\Delta r_4)$

$s_2 : \frac{r_2}{(2)^{\frac{1}{2}}}(\Delta\alpha_1-\Delta\alpha_2)$

$s_3 : \frac{(r_1r_2)^{\frac{1}{2}}}{(2)^{\frac{1}{2}}}(\Delta\alpha_5-\Delta\alpha_6)$

$s_4 : (r_1r_5)^{\frac{1}{2}}\Delta\alpha_8$

7.4.2 Normal coordinate solution for SiH_3CN

The solution for SiH_3CN proved easy to refine since the $\underline{F}$ matrix for each symmetry species was only a 4x4. Tables 7.2-7.4 give the results of the least squares refinement for SiH_3CN.

Table 7.2

```
NORMAL COORDINATE SOLUTION FOR SIH CN
SYMMETRY SPECIES - A1              3
F MATRIX AND FREQUENCIES FOR 4 ISOTOPIC SPECIES
P. E. DISTRIBUTION AND L MATRIX FOR 1ST ISOTOPIC SPECIES

F MATRIX
  2.96140
  0.00000 17.43146
  0.00000  0.00000  0.22090
  0.00000  0.00000 -0.11941  3.18777

 F.OBS    F.CALC    DIFF
 2245.65  2245.65    0.00
 2200.40  2200.39    0.01      SIH CN
  913.90   913.90   -0.00         3
  601.50   601.50   -0.00

 F.OBS    F.CALC    DIFF
 2244.75  2245.46   -0.71           15
 2171.00  2170.38    0.62      SIH C  N
  913.70   913.90   -0.20         3
  595.60   594.38    1.22

 F.OBS    F.CALC    DIFF
 2245.50  2245.32    0.18          13 15
 2122.00  2119.31    2.69      SIH   C  N
  913.40   913.90   -0.50         3
  588.20   589.82   -1.62

 F.OBS    F.CALC    DIFF
 1603.00  1597.01    5.99
 2201.00  2200.86    0.14      SID CN
  687.30   689.14   -1.84         3
  573.80   575.82   -2.02

P.E. DISTRIBUTION

   2245.65  2200.40   913.90   601.50

     0.988    0.011    0.000    0.000     SI-H SYM. STR.
     0.010    0.931    0.000    0.059     C-N STR.
     0.000    0.000    1.020    0.000     SI-H SYM. DEF.
     0.002    0.057    0.020    0.941     SI-C STR.

L MATRIX
  0.99540 -0.10520  0.00584  0.00493
  0.04112  0.39030 -0.00011  0.02681
 -0.05287  0.00584  1.50741  0.00207
 -0.04416 -0.22608  0.05558  0.25085
```

Table 7.3

NORMAL COORDINATE SOLUTION FOR SIH CN
SYMMETRY SPECIES - E 3
F MATRIX AND FREQUENCIES FOR 4 ISOTOPIC SPECIES
P. E. DISTRIBUTION AND L MATRIX FOR 1ST ISOTOPIC SPECIES

F MATRIX

```
  2.81347
  0.00000  0.19795
  0.00000 -0.03000  0.19205
  0.00000  0.00000  0.02469  0.08987
```

F.OBS	F.CALC	DIFF	
2231.00	2231.00	-0.00	
932.65	932.65	-0.00	SIH CN
685.83	685.83	0.00	3
246.60	246.60	0.00*	

F.OBS	F.CALC	DIFF	
2229.80	2231.00	-1.20	15
932.20	932.65	-0.45	SIH C N
685.48	685.73	-0.25	3
244.80	244.53	0.27*	

F.OBS	F.CALC	DIFF	
2231.00	2231.00	-0.00	13 15
933.20	932.65	0.55	SIH C N
682.48	681.99	0.49	3
239.60	238.79	0.81*	

F.OBS	F.CALC	DIFF	
1643.00	1616.51	26.49	
676.35	671.44	4.91	SID CN
539.15	539.13	0.02	3
229.20	228.87	0.33*	

* GAS PHASE VALUE

P.E. DISTRIBUTION

2231.00	932.65	685.83	246.60	
0.999	0.000	0.001	0.000	SI-H ASYM. STR.
0.000	1.024	0.000	0.000	SI-H ASYM. DEF.
0.000	0.027	0.911	0.125	SI-H ROCK
0.000	0.000	0.027	1.010	SI-C-N BEND

L MATRIX

```
  1.02024 -0.00918  0.00707  0.00024
  0.08476  1.62808 -0.01008 -0.00824
 -0.06730  0.26654  1.14605 -0.15279
 -0.03477 -0.02294  0.28953  0.63449
```

Table 7.4

OBSERVED AND CALCULATED PARAMETERS
1ST ISOTOPIC SPECIES

OBSERVED AND CALCULATED CORIOLIS CONSTANTS

ZETA	5	6	7	8
OBS.	-0.001	-0.202	0.324	0.890
CALC.	0.067	-0.217	0.306	0.874

INTERATOMIC DISTANCES AND AMPLITUDES - 0.00K

ATOMS	DIST(r_a)	U.	P	L	K	RG	RALPHA
SI-H	1.4900	0.0880	0.1403	0.0052	0.0132	1.4952	1.4820
SI-C	1.8470	0.0472	0.0671	0.0012	0.0024	1.8482	1.8458
C-N	1.1580	0.0346	0.0947	0.0010	0.0077	1.1590	1.1513
SI..N	3.0050	0.0492	0.0320	0.0008	0.0003	3.0058	3.0055
H..H	2.4613	0.1485	0.1844	0.0090	0.0138	2.4703	2.4565
H..C	2.6994	0.1266	0.1449	0.0059	0.0078	2.7053	2.6975
H..N	3.7340	0.1466	0.1090	0.0058	0.0032	3.7398	3.7366

INTERATOMIC DISTANCES AND AMPLITUDES - 298.16K

ATOMS	DIST(r_a)	U.	P	L	K	RG	RALPHA
SI-H	1.4900	0.0880	0.1529	0.0052	0.0157	1.4952	1.4795
SI-C	1.8470	0.0493	0.0888	0.0013	0.0043	1.8483	1.8440
C-N	1.1580	0.0347	0.1285	0.0010	0.0142	1.1590	1.1448
SI..N	3.0050	0.0517	0.0431	0.0009	0.0006	3.0059	3.0053
H..H	2.4613	0.1495	0.2071	0.0091	0.0174	2.4704	2.4530
H..C	2.6994	0.1309	0.1732	0.0063	0.0111	2.7057	2.6946
H..N	3.7340	0.1642	0.1118	0.0072	0.0033	3.7412	3.7379

The A_1 solution has only one off-diagonal F matrix element, F_{43}. This was required to reproduce the isotopic shifts in the rocking mode and the SiC stretching mode for the deuterated species. Refining all five non-zero elements simultaneously produced the fit shown in Table 7.2. The shift for the SiH stretch on deuteration was given a smaller weighting in the refinement. The potential energy distribution shows all the modes of vibration to be fairly 'pure'.

The solution for the E symmetry species gives a good fit for the frequencies. F_{32}, coupling the asymmetric SiH deformation and the SiH_3 rock, was given a fixed value which best reproduced the observed coriolis constants[57,58]. Here the vibrational modes are also fairly 'pure'. Table 7.4 shows the observed and calculated coriolis constants. This table also gives a number of interatomic amplitudes and derived parameters calculated from the normal coordinate analysis. The calculated linear shrinkage from Table 7.4 is δ(Si...N) = 0.017 Å (room temperature).

7.5 High Resolution Gas Phase Infrared Spectra of SiH_3CN

All of the major bands with frequency greater than 500 cm^{-1} were studied in the gas phase at a resolution of 0.06 cm^{-1} or 0.09 cm^{-1}. This meant that the J structure of many of the bands showed up clearly, since

2B for SiH_3CN is about 0.32 cm^{-1}.

Spectra were run at two different gas pressures in a 10 cm cell. The regions 890-970 cm^{-1} (silyl deformations) and 2200 cm^{-1} - 2260 cm^{-1} (silyl stretches and CN stretch) were run at low pressure, about 4 mmHg. The spectral range was extended to higher and lower frequency on both regions, plus the region 570-750 cm^{-1}, in the high pressure spectrum (15 mmHg).

7.5.1 2250 cm^{-1} region

At low pressure the infrared spectrum is dominated by the sharp Q branches of the perpendicular band associated with the SiH asymmetric stretch, ν_5. They also show up very clearly in the high pressure spectrum. This region also has the absorptions due to the SiH symmetric stretch, ν_1, and the CN stretch, ν_2 (parallel bands).

The low pressure spectrum has no assignable J structure for either of the parallel bands. However, there is a Q branch at 2202.3 cm^{-1} which can be assigned to the CN stretching band. The Q branch for the SiH symmetric stretch may be at 2205 cm^{-1}, very close to one of the SiH asymmetric stretch Q branches.

The J structure associated with the parallel bands will be well-defined only if the K sub-bands closely overlap, i.e. if B'-B" is small. For the SiH and CN

stretches this is likely to be the case. However, if the Q branches are close together there will be a large overlap of the P and R branches for the two bands. This made assignment of the J structure impractical. The situation is further complicated by the overlapping perpendicular band due to the asymmetric SiH stretch, with its series of Q branches, and each with its associated P and R branches. It is possible to assign some of the P and R branch lines for the sub-bands of the perpendicular band, ν_5. Unfortunately this is possible only for the higher K sub-bands where the ^{P}P and ^{R}R lines become relatively more intense, and where there is no interference from either of the parallel bands. Any calculation on the B' and B" values for the perpendicular band would require a clear assignment of both the P and R branches of any one sub-band.

The Q branches on the perpendicular band were assigned on the basis of the strong-weak-weak-strong alternation together with observation of the number of missing ^{R}R and ^{P}P lines for individual sub-bands. $^{R}Q_{O}$ was assigned to 2226.25 cm^{-1}. Only the Q branch series for ν_5 was assigned and least squares fitted to give the following parameters:

$$\nu_0 + \{A'(1-2\zeta_i)-B'\} = 2226.26404 \pm 0.06802 \text{ cm}^{-1}$$

$$2\{A'(1-\zeta_i)-B'\} = 5.18718 \pm 0.00962 \text{ cm}^{-1}$$

$$(A'-B') - (A''-B'') = -0.01735 \pm 0.00415 \text{ cm}^{-1}$$

Table 7.5 shows the least squares fit for the Q branches of silyl cyanide, ν_5.

7.5.2 950 cm^{-1} region

This region contains two absorption bands - the symmetric SiH deformation ν_3, and the asymmetric SiH deformation, ν_6. Both bands are in Fermi resonance with the combination $\nu_7 + \nu_8$. The combination band will have both A_1 and E components and will therefore perturb both ν_3 and ν_6.

The parallel band, ν_3, shows up well in the low pressure spectrum as a P and R branch with J structure. The P and R branch lines, however, are not regular and cannot be assigned. The Q branch of ν_3 is at 922.2 cm^{-1} and does not lie directly between the P and R branches but is displaced to higher frequency.

Q branches of the perpendicular band, ν_6, are not observed near the parallel band maximum. However, above 940 cm^{-1} and below 900 cm^{-1} they are easily observed and assigned. The assignment was again made with help from the strong-weak-weak-strong intensity alternation and by counting the missing lines in the P

Table 7.5

Q branch frequencies (cm^{-1}) for SiH_3CN, ν_5

P Q	FREQ.OBS.	FREQ.CALC.	OBS.-CALC.
16	2138.98	2138.83	0.15
15	2144.63	2144.55	0.08
14	2150.28	2150.24	0.04
13	2155.90	2155.90	0.00
12	2161.50	2161.52	-0.02
11	2167.03	2167.11	-0.08
10	2172.58	2172.66	-0.08
9	2178.08	2178.17	-0.09
8	2183.48	2183.66	-0.18
7	2189.15	2189.10	0.05
6	2194.50	2194.52	-0.02
5	2199.88	2199.89	-0.01
4	2205.23	2205.24	-0.01
3	2210.49	2210.55	-0.06
2	2215.79	2215.82	-0.03
1	2221.05	2221.06	-0.01
R Q			
0	2226.25	2226.26	-0.01
1	2231.45	2231.43	0.02
2	2236.60	2236.57	0.03
3	2241.69	2241.67	0.02
4	2246.79	2246.74	0.05
5	2251.82	2251.77	0.05
6	2256.83	2256.76	0.07
7	2261.80	2261.72	0.08
8	2266.72	2266.65	0.07
9	2271.60	2271.54	0.06
10	2276.47	2276.40	0.07
11	2281.26	2281.22	0.04
12	2285.97	2286.01	-0.04
13	2290.75	2290.77	-0.02
14	2295.41	2295.48	-0.07
15	2300.03	2300.17	-0.14

RMS DEVIATION = 0.068

DERIVED PARAMETERS:

1.	2226.26404	± 0·06802	cm^{-1}
2.	5.18718	± 0·00962	cm^{-1}
3.	-0.01735	± 0·00415	cm^{-1}

and R branches of the sub-bands. Unfortunately it was possible only to assign the ^{R}R lines and the ^{P}P lines for high K values since the ^{R}P and ^{P}R lines are relatively weak.

A least squares fit of all observed Q branches for ν_6 shows the perturbation caused by $\nu_7 + \nu_8$. The fit close to $^{R}Q_0$ is not satisfactory (see Table 7.6) - there is a high r.m.s. deviation. Derived parameters from the fit were as follows:

$$\nu_0 + \{A'(1-2\zeta_i)-B'\} = 943.70841 \pm 1.61752 \text{ cm}^{-1}$$

$$2\{A'(1-\zeta_i)-B'\} = 6.32794 \pm 1.09195 \text{ cm}^{-1}$$

$$(A'-B') - (A''-B'') = -0.00012 \pm 1.04466 \text{ cm}^{-1}$$

Assuming the centre of the Fermi resonance perturbation to be at 930 cm^{-1}, we can exclude all observed Q branches $\pm$ 50 cm^{-1} from this value. This markedly reduces the r.m.s. deviation, although it also reduces the number of observed values used in the fit. The derived parameters are now:

$$\nu_0 + \{A'(1-2\zeta_i)-B'\} = 945.56625 \pm 0.35024 \text{ cm}^{-1}$$

$$2\{A'(1-\zeta_i)-B'\} = 6.31738 \pm 0.03986 \text{ cm}^{-1}$$

$$(A'-B') - (A''-B'') = -0.01041 \pm 0.00555 \text{ cm}^{-1}$$

(see Table 7.7).

Table 7.6

Q Branch Frequencies (cm^{-1}) for SiH_3CN, ν_6

P Q	FREQ.OBS.	FREQ.CALC.	OBS.-CALC.
18	828.05	829.77	-1.72
17	834.82	836.10	-1.28
16	841.65	842.43	-0.78
15	848.42	848.76	-0.34
14	855.07	855.09	-0.02
13	862.03	861.42	0.61
12	868.80	867.76	1.04
11	875.50	874.09	1.41
10	882.20	880.42	1.78
9	888.91	886.75	2.16
8	895.52	893.08	2.44
7	-	899.41	-
6	-	905.74	-
5	-	912.07	-
4	-	918.39	-
3	-	924.72	-
2	-	931.05	-
1	-	937.38	-
R Q			
0	-	943.71	-
1	944.78	950.04	-5.26
2	952.97	956.36	-3.39
3	961.36	962.69	-1.33
4	968.72	969.02	-0.30
5	975.61	975.35	0.26
6	982.41	981.67	0.74
7	988.76	988.00	0.76
8	995.18	994.32	0.86
9	1001.51	1000.65	0.86
10	1007.80	1006.98	0.82
11	1014.00	1013.30	0.70
12	1020.08	1019.63	0.45
13	1026.18	1025.95	0.23
14	1032.12	1032.28	-0.16
15	1038.04	1038.60	-0.56

RMS DEVIATION = 1.618

DERIVED PARAMETERS

1.	943.70841	± 1·61752 cm^{-1}
2.	6.32794	± 1·09195 cm^{-1}
3.	-0.00012	± 1·04466 cm^{-1}

Table 7.7

Q Branch Frequencies (cm^{-1}) for SiH_3CN, ν_6

P Q	FREQ.OBS.	FREQ.CALC.	OBS.-CALC.
18	828.05	828.48	-0.43
17	834.82	835.16	-0.34
16	841.65	841.82	-0.17
15	848.42	848.46	-0.04
14	855.07	855.08	-0.01
13	862.03	861.68	0.35
12	868.80	868.26	0.54
11	875.50	874.82	0.68
10	-	881.35	-
9	-	887.87	-
8	-	894.36	-
7	-	900.83	-
6	-	907.29	-
5	-	913.72	-
4	-	920.13	-
3	-	926.52	-
2	-	932.89	-
1	-	939.24	-
R Q			
0	-	945.57	-
1	-	951.87	-
2	-	958.16	-
3	-	964.42	-
4	-	970.67	-
5	-	976.89	-
6	982.41	983.10	-0.69
7	988.76	989.28	-0.52
8	995.18	995.44	-0.26
9	1001.51	1001.58	-0.07
10	1007.80	1007.70	0.10
11	1014.00	1013.80	0.20
12	1020.08	1019.88	0.20
13	1026.18	1025.93	0.25
14	1032.12	1031.97	0.15
15	1038.04	1037.98	0.06

RMS DEVIATION = 0.350

DERIVED PARAMETERS

1.	945.56625	± 0.35024 cm^{-1}
2.	6.31738	± 0.03986 cm^{-1}
3.	-0.01041	± 0.00555 cm^{-1}

7.5.3 570-750 cm^{-1} region

In this region we have the silyl rock, ν_7, and the SiC stretch, ν_4. The former is a perpendicular band and the latter a parallel band. The silyl rocking band is overlapped by HCN and CO_2 lines. HCN was present in the sample as a decomposition product. CO_2 bands arose since the instrument was not purged while running the spectrum. The sample spectrum was ratioed against a straight line background.

It was, however, possible to pick a way through the many lines to assign the perpendicular Q branch series for ν_7. The least squares fit to the usual symmetric top formula for perpendicular band Q branches is shown in Table 7.8. The derived parameters for SiH_3CN, ν_7 Q branch series are as follows:

$$\nu_0 + \{A'(1-2\zeta_i)-B'\} = 682.51240 \pm 0.06590 \text{ cm}^{-1}$$

$$2\{A'(1-\zeta_i)-B'\} = 3.40469 \pm 0.01359 \text{ cm}^{-1}$$

$$(A'B') - (A''-B'') = 0.01543 \pm 0.00866 \text{ cm}^{-1}$$

In ν_4 of SiH_3CN we had a band which was clear of all impurity peaks and other overlapping fundamentals. Since it is a parallel band we see a Q branch and a P and R branch series. This indicates that the individual K sub-bands are closely overlapping, i.e. B'-B" is small.

By the method of combination of differences it was

Table 7.8

Q Branch Frequencies (cm^{-1}) for SiH_3CN, ν_7

P Q	FREQ.OBS.	FREQ.CALC.	OBS.-CALC.
15	635.00	634.91	0.09
14	637.92	637.87	0.05
13	640.90	640.86	0.04
12	643.87	643.88	-0.01
11	646.91	646.93	-0.02
10	649.97	650.01	-0.04
9	653.06	653.12	-0.06
8	656.21	656.26	-0.05
7	659.38	659.44	-0.06
6	662.58	662.64	-0.06
5	665.82	665.87	-0.05
4	669.10	669.14	-0.04
3	672.40	672.44	-0.04
2	675.77	675.76	0.01
1	679.14	679.12	0.02
R Q			
0	682.52	682.51	0.01
1	685.97	685.93	0.04
2	689.43	689.38	0.05
3	692.92	692.87	0.05
4	696.46	696.38	0.08
5	700.02	699.92	0.10
6	703.57	703.50	0.07
7	707.16	707.10	0.06
8	710.78	710.74	0.04
9	714.33	714.40	-0.07
10	717.90	718.10	-0.20

RMS DEVIATION = 0.066

DERIVED PARAMEERS

1.	682.51240	$\pm$ 0·06590 cm^{-1}
2.	3.40469	$\pm$ 0·01359 cm^{-1}
3.	0.01543	$\pm$ 0·00866 cm^{-1}

possible to calculate B', B" and B'-B". A plot of R(J)-P(J) against J gave a straight line of slope 4B'. Similarly R(J-1)-P(J+1) plotted against J gave a line of slope 4B". From the derived values of B' and B", B'-B" can be obtained by direct subtraction. However, in order to obtain a more accurate value for B'-B", R(J-1)+P(J) was plotted against J^2 to give a straight line of slope 2(B'-B") and an intercept of $2\nu_0$.

Table 7.9 summarises the assignment of the R and P branch lines for SiH_3CN, ν_4. The quantities R(J)-P(J), R(J-1)-P(J+1) and R(J-1)+P(J) are also given. Parameters derived from the least squares fit of the data as outlined above gave the following parameters:

$$B" = 0.16576 \pm 0.00014 \quad cm^{-1}$$

$$B' = 0.16498 \pm 0.00012 \quad cm^{-1}$$

$$B'-B" = -0.000676 \pm 0.000005 \quad cm^{-1}$$

$$\nu_0 = 608.307 \pm 0.006 \quad cm^{-1}$$

These values of B", B' and B'-B" agree well with those derived by microwave study[58]. The values found from the microwave study are:

$$B" = 0.1658817 \pm 0.0000005 \quad cm^{-1}$$

$$B' = 0.1651977 \pm 0.0000007 \quad cm^{-1}$$

$$B'-B" = -0.0006840.$$

Table 7.9

P and R Branch Assignment (cm^{-1}) for SiH_3CN, ν_4

J	R(J)	P(J)	R(J)-P(J)	R(J-1)-P(J+1)	R(J-1)+P(J)
0	608.58				
1	608.93	607.85	1.08	1.07	1216.43
2	609.31	607.51	1.80	1.79	1216.44
3	609.65	607.14	2.51	2.46	1216.45
4	610.03	606.85	3.18	3.17	1216.50
5	610.44	606.48	3.96	3.85	1216.51
6	610.77	606.18	4.59	4.62	1216.62
7	611.10	605.82	5.28	5.29	1216.59
8	611.42	605.48	5.94	5.97	1216.58
9	611.73	605.13	6.60	6.62	1216.55
10	612.04	604.80	7.24	7.27	1216.53
11	612.36	604.46	7.90	7.94	1216.50
12	612.68	604.10	8.58	8.62	1216.46
13	612.98	603.74	9.24	9.29	1216.42
14	613.29	603.39	9.90	9.96	1216.37
15	613.59	603.02	10.57	10.61	1216.31
16	613.91	602.68	11.23	11.26	1216.27
17	614.22	602.33	11.89	11.93	1216.24
18	614.53	601.98	12.55	12.59	1216.20
19	614.84	601.63	13.21	13.25	1216.16
20	615.14	601.28	13.86	13.92	1216.12
21	615.43	600.92	14.51	14.59	1216.06
22	615.72	600.55	15.17	15.24	1215.98
23	616.02	600.19	15.83	15.90	1215.91
24	616.32	599.82	16.50	16.54	1215.84
25	616.60	599.48	17.12	17.21	1215.80
26	616.92	599.11	17.81	17.86	1215.71
27	617.20	598.74	18.46	18.54	1215.66
28	617.48	598.38	19.10	19.20	1215.58
29	617.77	598.00	19.77	19.85	1215.48
30	618.06	597.63	20.43	20.50	1215.40
31	618.35	597.27	21.08	21.16	1215.33
32	618.64	596.90	21.74	21.83	1215.25
33	618.91	596.52	22.39	22.51	1215.16
34	619.20	596.13	23.07	23.13	1215.04
35	619.49	595.78	23.71	23.82	1214.98
36	619.78	595.38	24.40	24.50	1214.87
37	620.03	594.99	25.04	25.16	1214.77
38	620.32	594.62	25.70	25.80	1214.65
39	620.58	594.23	26.35	26.47	1214.55
40	620.85	593.85	27.00	27.10	1214.43
41	621.13	593.48	27.65	27.76	1214.33
42	621.42	593.09	28.33	28.44	1214.22
43	621.70	592.69	29.01	29.12	1214.11
44	621.97	592.30	29.67	29.79	1214.00
45	622.22	591.91	30.31	30.46	1213.88
46	622.48	591.51	30.97	31.10	1213.73
47	622.70	591.12	31.58	31.75	1213.60
48	622.99	590.73	32.26	32.35	1213.43
49	623.28	590.35	32.93	33.02	1213.34
50	623.55	589.97	33.58	33.72	1213.25
51	623.84	589.56	34.28	34.43	1213.11
52		589.12			1212.96

7.6 Conclusions

The fundamental bands of SiH_3CN are easily assigned in a matrix isolated infrared spectrum. Some of the bands are broad which may be explained in terms of cluster formation due to strong intermolecular attractions. The fundamental band, ν_8, does not appear in the matrix infrared spectrum but is strong in the gas phase spectrum. A hot-band transition is observed to low frequency of ν_8 in the gas phase indicating anharmonicity in the vibration. Accurate normal coordinates have been obtained using data from four isotopic species of SiH_3CN.

7.7 Infrared Spectra of Silyl bis-Isocyanate

As detailed in the experimental chapter, a sample of $SiH_2(NCO)_2$ was purified, together with some $SiH(NCO)_3$. The corresponding deuterated species were also isolated. Studies in the infrared were most successful with the $SiH_2(NCO)_2$ sample - a note on the work with $SiH(NCO)_3$ will be inserted at the end of the chapter.

For the purposes of analysis of the infrared spectrum and assignment of absorption bands, $SiH_2(NCO)_2$ was assumed to have C_{2v} symmetry, and the SiNCO chains were assumed linear. In describing the heavy-atom chains in this manner we assume also that the bonding of the NCO groups to silicon is through the nitrogen atoms as

with SiH_3NCO.

In a C_{2v} configuration the vibrational modes expected in terms of symmetry classes are $8A_1 + 3A_2 + 4B_1 + 6B_2$. The A_2 modes are infrared inactive.

7.7.1 Gas phase spectrum of $SiH_2(NCO)_2$ - mid infrared

The gas phase infrared spectrum was easily obtained in a 10 cm cell with KBr windows. The vapour pressure of $SiH_2(NCO)_2$ is about 18 mmHg at room temperature. In general, the spectrum is similar to that of SiH_3NCO since there are the same groups present.

For a C_{2v} molecule three different types of infrared band contour are observed in the gas phase - A, B and C. These correspond to dipole changes along the least, intermediate and largest moment of inertia respectively. Using an assumed molecular structure, it is a simple task to calculate the directions of A, B and C. In this case, vibrations of symmetry A_1 will give B type bands, those of symmetry B_1 will give C type bands and those of symmetry B_2 will give A type bands.

Each type of band has a characteristic shape which helps in the assignment of vibrations. Type A bands have a central maximum with P and R branches (similar to a symmetric top parallel band). Type B bands have a central minimum for a small value of

I_A/I_B (as is the case here). Type C bands give a single broad maximum for small I_A/I_B.

In the gas phase infrared spectrum of $SiH_2(NCO)_2$, the region 2100-2400 cm^{-1} exhibits a number of bands. There is a strong band at 2291 cm^{-1} with a high frequency shoulder due to the two NCO asymmetric stretches (A_1 and B_2). Here the band shapes are unclear. In the same region, there is a possible B type band at 2224 cm^{-1} (SiH symmetric stretch, A_1) and a C type band at 2196 cm^{-1} (SiH asymmetric stretch, B_1). The NCO symmetric stretches (A_1 and B_2) overlap at 1460 cm^{-1}. Again, there was no information available on band shapes from the spectrum.

The region 900-1000 cm^{-1} contains the absorptions due to the SiH_2 wag and the SiH_2 deformation. A strong band at 913 cm^{-1} shows a definite A type contour and is assigned to the SiH_2 wag (B_2). The other band, at 969 cm^{-1}, is assigned to the SiH_2 deformation (A_1). This band does not have a B type contour as expected; however, it may be perturbed by a Fermi resonance as in other di-halosilanes.

The remainder of the infrared spectrum, between 550 and 750 cm^{-1} consists of a very broad band with two slight maxima. In this region we expect the absorptions due to the SiH_2 rock (B_1), SiN_2 asymmetric stretch (B_2) and the three infrared active NCO bends

(A_1, B_1, B_2). Only limited information can be obtained in this region. There is a type C band at 678 cm^{-1} (SiH_2 rock), a type C band at 621 cm^{-1} (NCO bend) and a type B band at 615 cm^{-1} (NCO bend).

7.7.2 Infrared spectrum of $SiH_2(NCO)_2$ in a nitrogen matrix

Studying the molecule in a matrix enabled the assignment of all the fundamental bands in the mid infrared to be made. Annealing the sample to 25 K greatly improved the spectrum by removing site splittings and sharpening the infrared absorption bands. The important regions of the annealed spectrum are shown in Figures 7.3 and 7.4.

Much use was made of the infrared spectrum in a nitrogen matrix of the deuterated species, $SiD_2(NCO)_2$, in assigning the bands. A preliminary assignment was made first of all and then the normal coordinate analysis programme was used to make improvements. The region where assignments were most difficult was 570-700 cm^{-1}.

In the region 2200-2350 cm^{-1} are the absorptions due to the two NCO asymmetric stretches (A_1 and B_2) and the two SiH stretches (A_1 and B_1). By comparison with the spectrum of the deuterated species the strong absorptions at 2324 cm^{-1} and 2284 cm^{-1} were assigned to the NCO asymmetric stretches. Each of these bands shows satellites due to natural abundance ^{13}C at

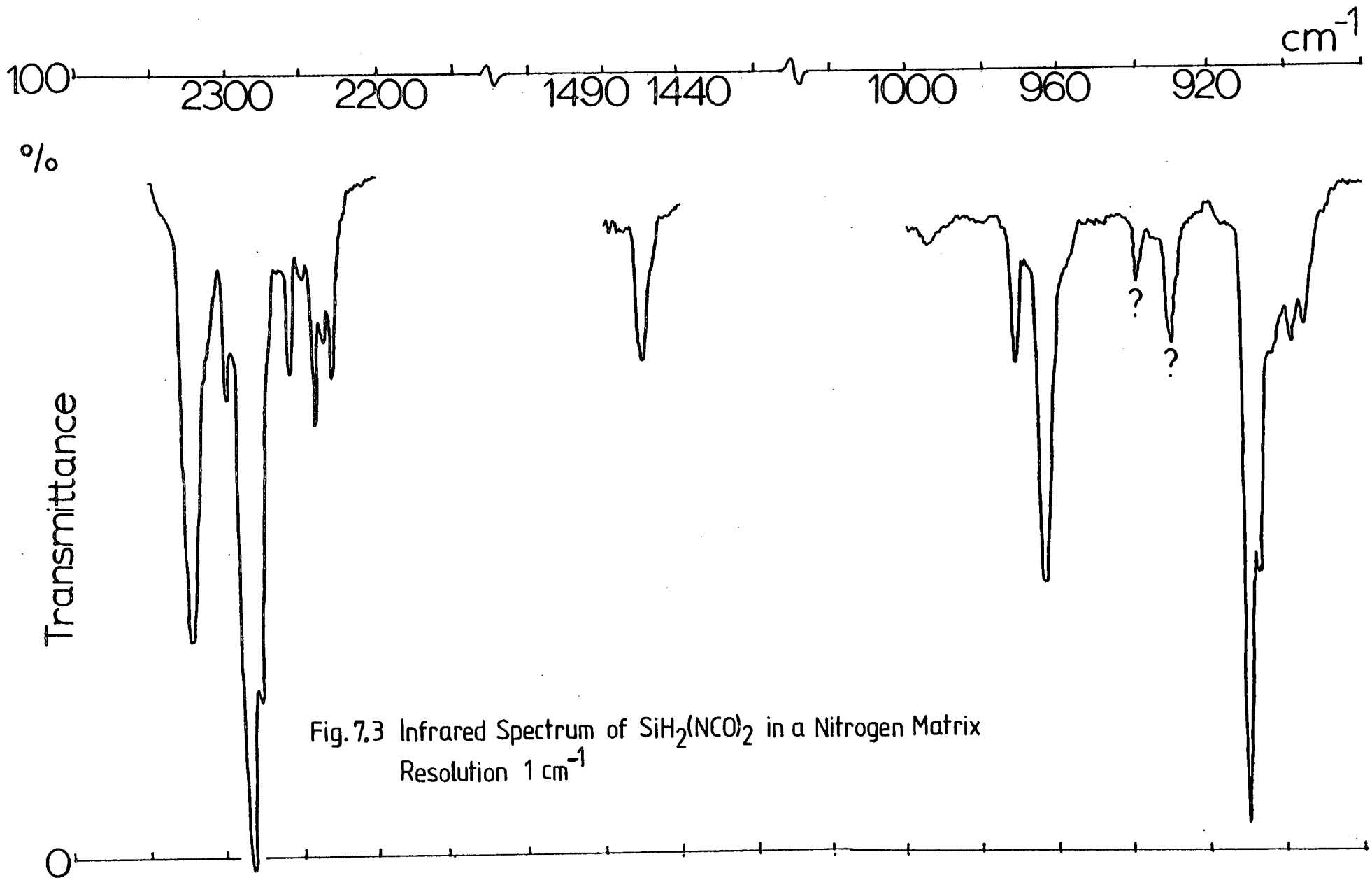

Fig. 7.3 Infrared Spectrum of $SiH_2(NCO)_2$ in a Nitrogen Matrix
Resolution 1 cm^{-1}

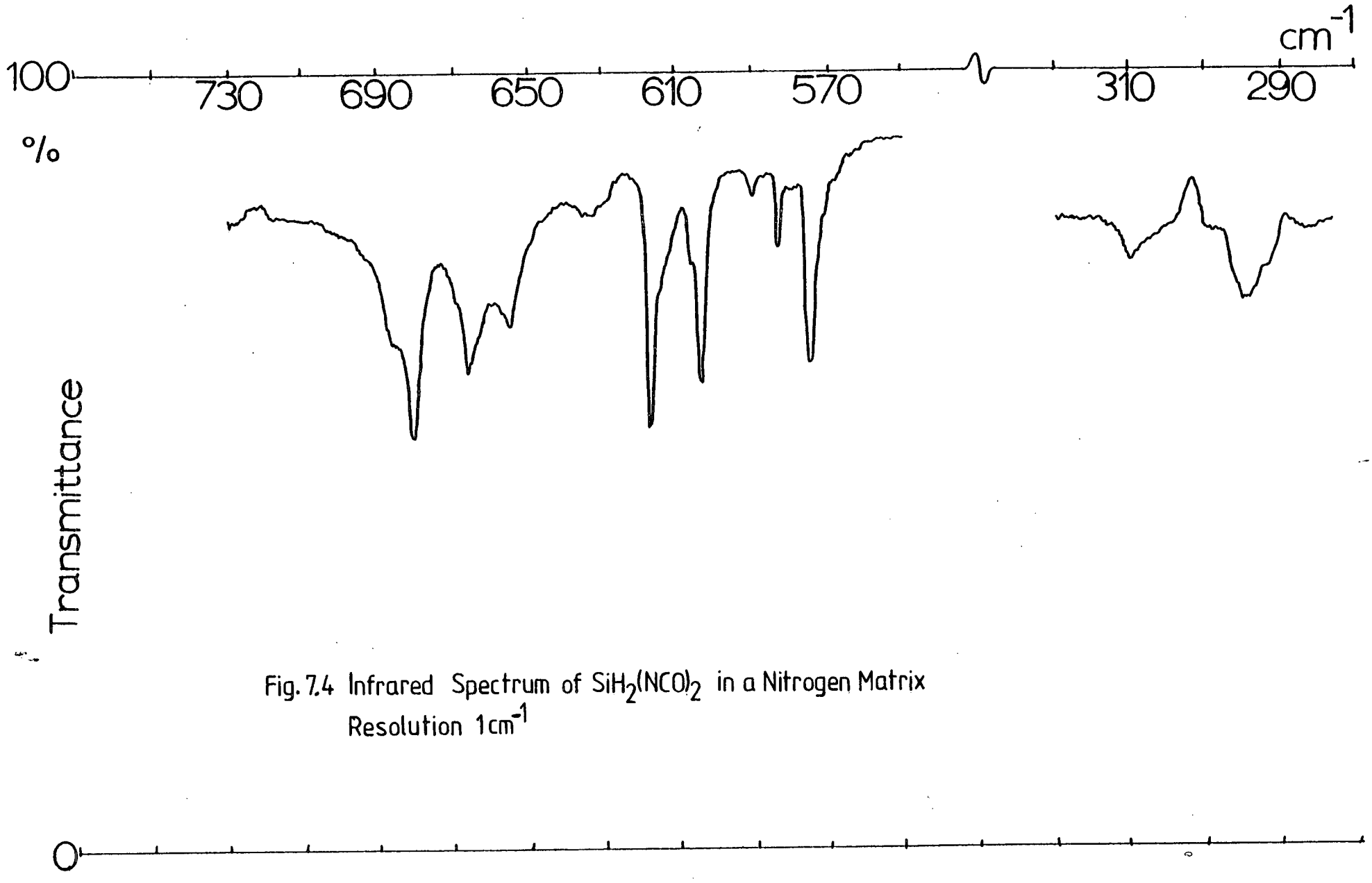

Fig. 7.4 Infrared Spectrum of $SiH_2(NCO)_2$ in a Nitrogen Matrix
Resolution $1 cm^{-1}$

2300 cm^{-1} and 2258 cm^{-1} respectively. The SiH stretches were assigned to the two remaining strong bands at 2241 cm^{-1} and 2230 cm^{-1}. At 1466 cm^{-1} is a broadish band due to the two NCO symmetric stretches (A_1 and B_2).

In the region 880-990 cm^{-1} there are two strong bands which can be assigned to the SiH_2 deformation (A_1) and the SiH_2 wag (B_2). Here, the spectrum of the deuterated species and the computer predictions for isotopic shifts led to the assignment of the band at 964.0 cm^{-1} to the SiH_2 deformation and of that at 910.0 cm^{-1} to the SiH_2 wag. This agrees well with the gas phase assignment and band contours. The two weak bands at 939 cm^{-1} and 930.6 cm^{-1} were unassigned and may be due to impurities.

Between 560 and 700 cm^{-1} there are five main bands as we would expect. The highest frequency band at 681.2 cm^{-1} was assigned to the SiH_2 rock (B_1) since it alone gave a large enough shift (as predicted by the computer) with a band in the spectrum of the deuterated species. This effectively assigned the band at 533.7 cm^{-1} in the spectrum of $SiD_2(NCO)_2$ to the SiD_2 rock. The three bands of similar intensity between 570 cm^{-1} and 630 cm^{-1} were assigned to the infrared active NCO bends (A_1,B_1,B_2). It is not unreasonable to make this assignment since one would not expect the NCO bending coordinates to mix significantly with other coordinates.

They would, therefore, have similar vibrational frequencies. The one remaining broad band at 666.2 cm^{-1} was assigned to the NSiN asymmetric stretch (B_2).

The final assignment of the NCO bends to the different symmetry classes was made with help from computer isotopic shift predictions. Using all the information available the expected shifts of the three NCO bends on deuteration were calculated. It was found that the A_1 NCO bend would have a slightly smaller shift (~8 cm^{-1}) than the B_2 NCO Bend (~12 cm^{-1}). The B_1 NCO bend was predicted to increase in frequency by about 3 cm^{-1}. It was possible to make a plausible assignment using this information. The assignment was as follows:

	$SiH_2(NCO)_2$	$SiD_2(NCO)_2$	Observed Shift	Predicted Shift
A_1 NCO bend	575.4 cm^{-1}	568.7 cm^{-1}	6.7 cm^{-1}	8 cm^{-1}
B_1 NCO bend	617.9 cm^{-1}	618.9 cm^{-1}	-1.0 cm^{-1}	-3 cm^{-1}
B_2 NCO bend	604.4 cm^{-1}	590.7 cm^{-1}	13.7 cm^{-1}	12 cm^{-1}

The two remaining weak bands in the spectrum were at 310.6 cm^{-1} and 295.1 cm^{-1}, assigned to the NSiN symmetric stretch (A_1) and the NSiN deformation (A_1) respectively. These two bands are very weak but are nevertheless real bands of $SiH_2(NCO)_2$ since they show shifts in frequency in the $SiD_2(NCO)_2$ spectrum. A summary of all the infrared

bands observed in a nitrogen matrix are given in Table 7.10.

7.7.3 Far infrared spectrum of Gaseous $SiH_2(NCO)_2$

The gas phase spectra of $SiH_2(NCO)_2$ and $SiD_2(NCO)_2$ were run in the range 400-80 cm^{-1} in the 150 cm cell. The maximum gas pressure attained for the normal isotopic species was 3 mmHg, and that for the deuterated species was 7 mmHg. In the latter case more sample was available. The spectra obtained are shown in Figures 7.5 and 7.6.

The two maxima on the bands observed near 300 cm^{-1} were assigned to different modes of vibration since the matrix isolated infrared spectrum shows two absorptions in this region. In the normal isotopic species spectrum the maxima are at 286 cm^{-1} and 307 cm^{-1}, and in the deuterated species at 283 cm^{-1} and 303 cm^{-1}. The higher frequency band was assigned to the symmetric SiN stretch (A_1) and the lower frequency band to the SiN_2 deformation (A_1).

To lower frequency there appeared a broad absorption at about 130 cm^{-1} in both spectra. This may be due to a small residual amount of SiH_3NCO (or SiD_3NCO) present in the sample, or may be a genuine $SiH_2(NCO)_2$ ($SiD_2(NCO)_2$) band. Since SiH_3NCO has a band in this position (the 'overtone' of the SiNC band) it is reasonable to assume that $SiH_2(NCO)_2$ will have absorptions due to the three

Table 7.10

Observed frequencies (cm^{-1}) and assignment for $SiH_2(NCO)_2$, nitrogen matrix

$SiH_2(NCO)_2$	$SiD_2(NCO)_2$		
2324	2322	s	NCO asymmetric stretch (B_2)
2284	2283	v.s.	NCO asymmetric stretch (A_1)
2241	1617	m.s.	SiH symmetric stretch (A_1)
2230	1646	m.s.	SiH asymmetric Stretch (B_1)
1466	1467(br)	m.s.	NCO symmetric stretches (A_1 and B_2)
964.0	705.0	s	SiH_2 deformation (A_1)
910.0	712.2	v.s.	SiH_2 wag (B_2)
681.2	533.7	s	SiH_2 rock (B_1)
662.2	639.1	m.s.	SiN asymmetric stretch (B_2)
617.9	618.9	s	NCO bend (B_2)
604.4	590.7	s	NCO bend (B_2)
575.4	568.7	s	NCO bend (A_1)
310.6	307.3	v.w.	SiN symmetric stretch (A_1)
295.1	293.6	w	NSiN deformation (A_1)

Fig. 7.5 Far Infrared Spectrum of $SiH_2(NCO)_2$ gas, 150 cm cell, p= 3 mmHg, resolution 2·4 cm^{-1}

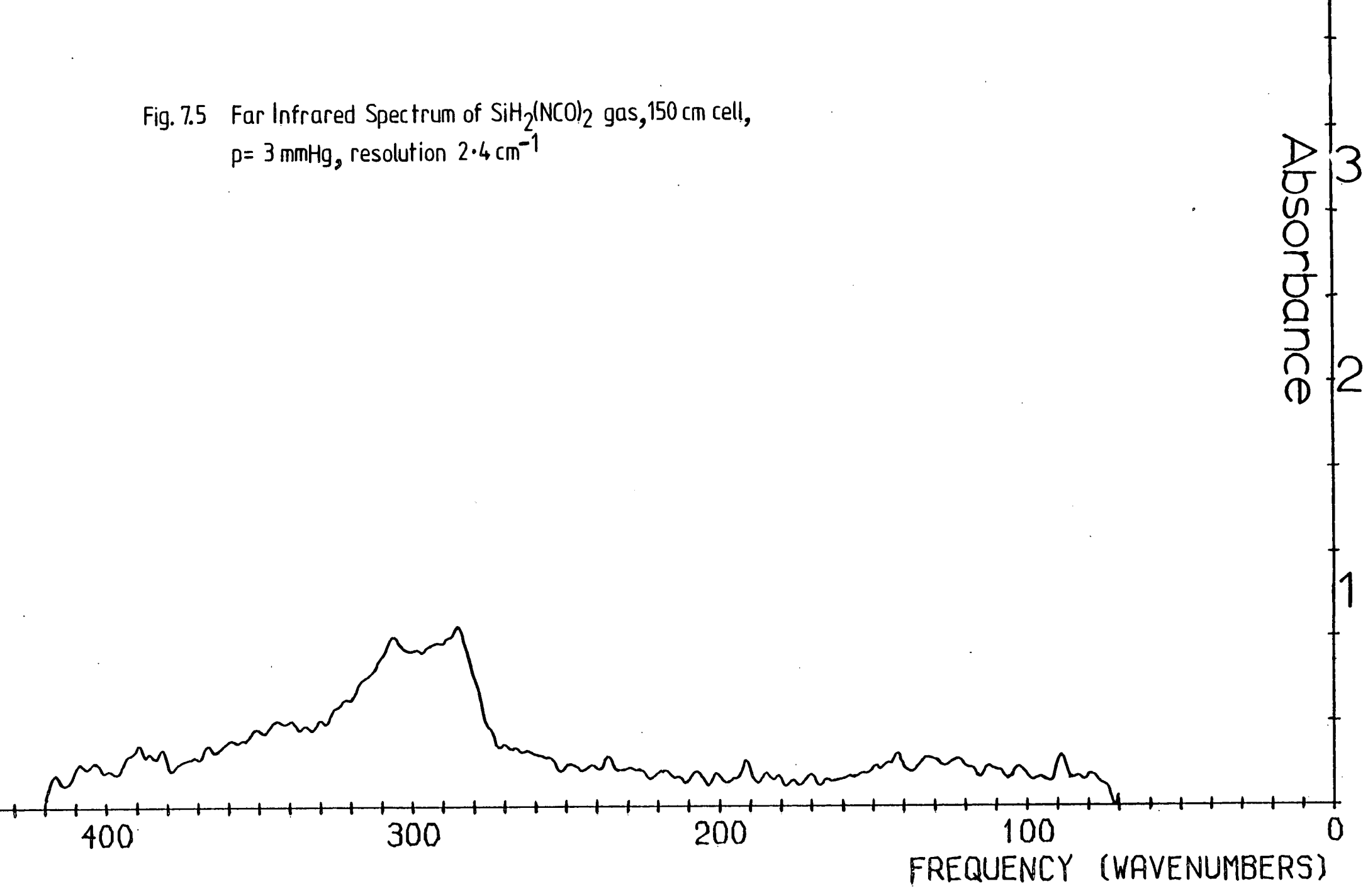

Fig. 7.6 Far Infrared Spectrum of $SiD_2(NCO)_2$ gas, 150 cm cell,
p = 7 mmHg, resolution 2·4 cm^{-1}

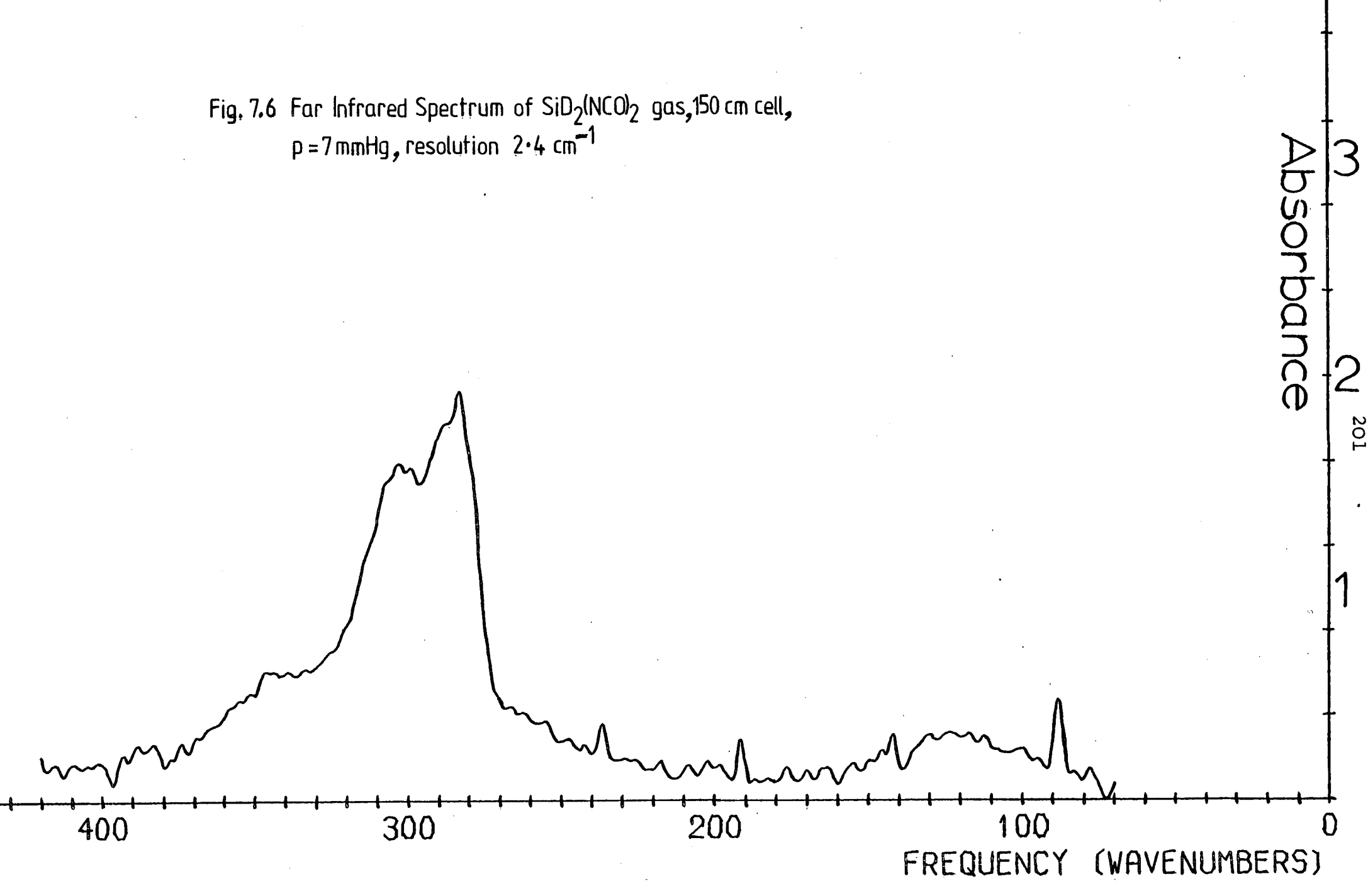

infrared active SiNC bends in similar positions. The series of sharp spikes in the spectra is due to the rotational spectrum of a small amount of HNCO impurity.

7.8 Normal Coordinate Analysis of $SiH_2(NCO)_2$

Although the assignment of the infrared spectrum of $SiH_2(NCO)_2$ is not complete, a normal coordinate analysis was carried out, making a very few reasonable assumptions. One assumption already made was that the molecule had C_{2v} symmetry with linear SiNCO chains. The vibrational modes which had not been observed directly were given reasonable frequencies on the basis of similar modes in the SiH_3NCO spectrum. The only vibrational modes not directly observed were the A_2 modes (NCO bend, SiH_2 twist and SiNC bend) and the three infrared active SiNC bends (A_1, B_1, B_2). Frequency values assumed for these modes were as follows:

NCO bend (A_2)	600 cm^{-1}	
SiH_2 twist (A_2)	900 cm^{-1}	
SiNC bends (A_1, A_2, B_1, B_2)	~65 cm^{-1}	(normal isotopic species)

7.8.1 Molecular structure, internal coordinates, symmetry coordinates

The molecular structure parameters used were the same as those used for SiH_3NCO. The atoms bound to

silicon were assumed to be in a tetrahedral arrangement. r(Si-H) 1.488 Å, r(Si-N) 1.703 Å, r(C-N) 1.216 Å, r(C-O) 1.164 Å.

Internal Coordinates

The internal coordinates were defined as follows:

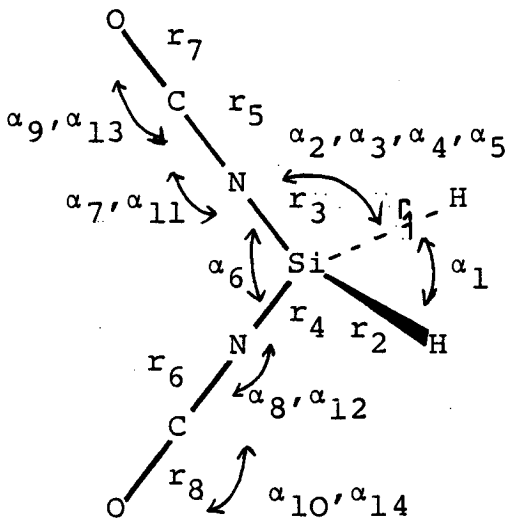

Symmetry Coordinates

The normal coordinate solution was refined in the following symmetry coordinate basis:

$\underline{A}_1$ $s_1 : \frac{1}{(2)^{\frac{1}{2}}}(\Delta r_7+\Delta r_8)$

$s_2 : \frac{1}{(2)^{\frac{1}{2}}}(\Delta r_1+\Delta r_2)$

$s_3 : \frac{1}{(2)^{\frac{1}{2}}}(\Delta r_5+\Delta r_6)$

$s_4 : (1+4\nu^2)^{-\frac{1}{2}}\{r_1\Delta\alpha_1+\nu(r_1r_3)^{\frac{1}{2}}(\Delta\alpha_2+\Delta\alpha_3+\Delta\alpha_4+\Delta\alpha_5)\}$

$$s_5 : \frac{(r_5 r_7)^{\frac{1}{2}}}{(2)^{\frac{1}{2}}}(\Delta\alpha_9+\Delta\alpha_{10})$$

$$s_6 : \frac{1}{(2)^{\frac{1}{2}}}(\Delta r_3+\Delta r_4)$$

$$s_7 : (1+4\nu^2)^{-\frac{1}{2}}\{r_3\Delta\alpha_6+\nu(r_1 r_3)^{\frac{1}{2}}(\Delta\alpha_2+\Delta\alpha_3+\Delta\alpha_4+\Delta\alpha_5)\}$$

$$s_8 : \frac{(r_3 r_5)^{\frac{1}{2}}}{(2)^{\frac{1}{2}}}(\Delta\alpha_7+\Delta\alpha_8)$$

$$\nu = \frac{-1/4\ \cos\frac{\alpha_6}{2}\sin\frac{\alpha_1}{2}}{\{1-\frac{1}{2}(1+\cos\frac{\alpha_1}{2}\cos\frac{\alpha_6}{2})\}^{\frac{1}{2}}\{\frac{1}{2}(1+\cos\frac{\alpha_1}{2}\cos\frac{\alpha_6}{2})\}^{\frac{1}{2}}} = -1/4 \text{ for}$$

α_1, α_6 tetrahedral angles.

$\underline{A}_2$ $s_1 : \frac{(r_1 r_3)^{\frac{1}{2}}}{(4)^{\frac{1}{2}}}(\Delta\alpha_2-\Delta\alpha_3-\Delta\alpha_4+\Delta\alpha_5)$

$$s_2 : \frac{(r_5 r_7)^{\frac{1}{2}}}{(2)^{\frac{1}{2}}}(\Delta\alpha_{13}+\Delta\alpha_{14})$$

$$s_3 : \frac{(r_3 r_5)^{\frac{1}{2}}}{(2)^{\frac{1}{2}}}(\Delta\alpha_{11}+\Delta\alpha_{12})$$

$\underline{B}_1$ $s_1 : \frac{1}{(2)^{\frac{1}{2}}}-(\Delta r_1-\Delta r_2)$

$$s_2 : \frac{(r_1 r_3)^{\frac{1}{2}}}{(4)^{\frac{1}{2}}}(\Delta\alpha_2+\Delta\alpha_3-\Delta\alpha_4-\Delta\alpha_5)$$

$$s_3 : \frac{(r_5 r_7)^{\frac{1}{2}}}{(2)^{\frac{1}{2}}}(\Delta\alpha_{13}-\Delta\alpha_{14})$$

$$s_4 : \frac{(r_3 r_5)^{\frac{1}{2}}}{(2)^{\frac{1}{2}}}(\Delta\alpha_{11}-\Delta\alpha_{12})$$

$\underline{B}_2$ $s_1 : \frac{1}{(2)^{\frac{1}{2}}}(\Delta r_7 - \Delta r_8)$

$s_2 : \frac{1}{(2)^{\frac{1}{2}}}(\Delta r_5 - \Delta r_6)$

$s_3 : \frac{(r_1 r_3)^{\frac{1}{2}}}{(4)^{\frac{1}{2}}}(\Delta\alpha_2 - \Delta\alpha_3 + \Delta\alpha_4 - \Delta\alpha_5)$

$s_4 : \frac{1}{(2)^{\frac{1}{2}}}(\Delta r_3 - \Delta r_4)$

$s_5 : \frac{(r_5 r_7)^{\frac{1}{2}}}{(2)^{\frac{1}{2}}}(\Delta\alpha_9 - \Delta\alpha_{10})$

$s_6 : \frac{(r_3 r_5)^{\frac{1}{2}}}{(2)^{\frac{1}{2}}}(\Delta\alpha_7 - \Delta\alpha_8)$

7.8.2 Normal coordinate solution for $SiH_2(NCO)_2$ - discussion

Tables 7.11-7.15 contain the normal coordinate solution for $SiH_2(NCO)_2$. The A_1 solution (Table 7.11) shows a fairly good fit for the frequency data apart from the SiH stretch on deuteration. Four off-diagonal elements were required to give the best fit. The potential energy distribution shows substantial mixing of symmetry coordinates - only the SiH stretch, the SiH deformation and the SiN stretch were fairly 'pure'. As expected there is mixing of the CO symmetric stretching coordinate and the NC symmetric stretching coordinate. The A_1 bending coordinates NCO, NSiN and SiNC are well mixed in the normal coordinates.

The A_2 solution (Table 7.12), in the absence of any frequency data, was refined only on the assumed values, with calculated frequencies for the deuterated species supplied.

In the B_1 solution (Table 7.13) the anharmonicities in the SiH mode are apparent, giving a less satisfactory fit. These shifts were given a reduced weighting in the refinement. It was noted that the NCO bend at 617.9 cm^{-1} (normal species) and at 618.9 cm^{-1} (deuterated species) fitted well with calculated values. All normal coordinates were fairly 'pure'.

Table 7.14 shows the solution for the B_2 modes. Here, the fit is good for all the frequencies. As expected the CO and CN asymmetric stretch mix considerably in the modes at 2324 cm^{-1} and 1466.0 cm^{-1}. The latter frequency also has a contribution from the SiN asymmetric stretch. The vibrational modes at 910.0 cm^{-1}, 604.4 cm^{-1} and 67.0 cm^{-1} are all predominantly the SiH_2 wag, NCO bend and SiNC bend respectively. The vibration assigned to 666.2 cm^{-1} is predominantly an SiN asymmetric stretch but with a small contribution from the CN asymmetric stretch.

The calculated parameters in Table 7.15 are quoted without comparison with experimental data, since none exist. They will, however, be useful in helping to refine a proposed electron diffraction structure for $SiH_2(NCO)_2$.

Table 7.11

NORMAL COORDINATE SOLUTION FOR SIH (NCO)
SYMMETRY SPECIES - A1 2 2
F MATRIX AND FREQUENCIES FOR 2 ISOTOPIC SPECIES
P. E. DISTRIBUTION AND L MATRIX FOR 1ST ISOTOPIC SPECIES

F MATRIX

16.71227							
0.00000	2.90952						
1.99835	0.00000	12.89076					
0.00000	0.00000	0.00000	0.19396				
0.00000	0.00000	0.00000	-0.01665	0.23942			
0.00000	0.00000	-0.93765	0.00000	0.00000	1.88293		
0.00000	0.00000	0.00000	0.00000	0.00000	0.34313	0.25629	
0.00000	0.00000	0.00000	0.00000	0.00000	0.00000	0.00000	0.20772

F.OBS	F.CALC	DIFF	
2284.00	2284.16	-0.16	
2241.00	2240.67	0.33	
1466.00	1466.48	-0.48	
964.00	964.15	-0.15	SIH (NCO)
575.40	575.24	0.16	2 2
310.60	310.15	0.45	
295.10	295.03	0.07	
67.00	67.59	-0.59*	

F.OBS	F.CALC	DIFF	
2283.00	2283.81	-0.81	
1617.00	1605.30	11.70	
1467.00	1465.45	1.55	
705.00	705.26	-0.26	SID (NCO)
568.70	566.84	1.86	2 2
307.30	305.15	2.15	
293.60	294.59	-0.99	
62.50	67.31	-4.81*	* GAS PHASE VALUE

P.E. DISTRIBUTION

2284.00	2241.00	1466.00	964.00	575.40	310.60	295.10	67.00	
0.632	0.006	0.376	0.001	0.000	0.002	0.002	0.000	C-O SYM. STR.
0.008	0.991	0.000	0.000	0.000	0.000	0.000	0.000	SI-H SYM. STR.
0.481	0.004	0.388	0.005	0.000	0.163	0.029	0.001	C-N SYM. STR.
0.000	0.000	0.001	0.914	0.041	0.004	0.018	0.027	SI-H SYM. DEF.
0.000	0.000	0.000	0.003	0.447	0.074	0.362	0.119	N-C-O BEND
0.007	0.000	0.068	0.001	0.008	1.172	0.055	0.080	SI-N SYM. STR.
0.000	0.000	0.000	0.059	0.122	0.303	0.332	0.524	N-SI-N BEND
0.000	0.000	0.000	0.002	0.432	0.033	0.068	0.464	SI-N-C BEND

L MATRIX

0.34090	0.03329	0.16876	0.00588	-0.00128	0.00284	0.00242	-0.00019
-0.09470	1.00351	-0.00687	0.00526	0.00241	0.00212	-0.00042	0.00006
-0.33862	-0.03075	0.19517	0.01460	-0.00060	0.02678	0.01072	0.00051
0.02035	-0.05143	-0.08377	1.60626	0.20375	-0.03521	-0.06968	0.01925
-0.00126	-0.00070	0.00833	-0.08024	0.60351	-0.13232	0.27854	0.03663
0.10559	-0.01578	-0.21425	0.01652	0.02808	0.18779	0.03870	0.01067
-0.00588	0.03996	-0.01008	0.35400	-0.30459	-0.25867	0.25773	-0.07415
-0.00403	0.02934	-0.00505	0.07800	-0.63686	-0.09547	0.12990	0.07749

Table 7.12

NORMAL COORDINATE SOLUTION FOR SIH (NCO)
SYMMETRY SPECIES - A2 2 2
F MATRIX AND FREQUENCIES FOR 2 ISOTOPIC SPECIES
P. E. DISTRIBUTION AND L MATRIX FOR 1ST ISOTOPIC SPECIES

F MATRIX

0.26363		
0.00000	0.45156	
0.00000	0.00000	0.01706

F.OBS	F.CALC	DIFF	
900.00	900.01	-0.01*	SIH (NCO)
600.00	600.00	0.00*	2 2
67.00	66.99	0.01*	

F.OBS	F.CALC	DIFF	
-	672.07	-	SID (NCO)
-	580.98	-	2 2
-	65.72	-	* ASSUMED VALUE

P.E. DISTRIBUTION

900.00	600.00	67.00	
0.988	0.012	0.000	SI-H2 TWIST
0.011	0.969	0.019	N-C-O BEND
0.001	0.019	0.980	SI-N-C BEND

L MATRIX

1.33692	0.09831	-0.00152
-0.10942	0.67459	0.01067
0.15999	-0.48275	0.38974

Table 7.13

NORMAL COORDINATE SOLUTION FOR SIH (NCO)
SYMMETRY SPECIES - B1 2 2
F MATRIX AND FREQUENCIES FOR 2 ISOTOPIC SPECIES
P. E. DISTRIBUTION AND L MATRIX FOR 1ST ISOTOPIC SPECIES

F MATRIX

2.81125			
0.00000	0.33252		
0.00000	0.04952	0.48161	
0.00000	0.00000	0.00000	0.01636

F.OBS	F.CALC	DIFF	
2230.00	2229.15	0.85	
681.20	681.44	-0.24	SIH (NCO)
617.90	617.88	0.02	2 2
67.00	66.97	0.03*	

F.OBS	F.CALC	DIFF	
1646.00	1614.85	31.15	
533.70	545.31	-11.61	SID (NCO)
618.90	619.97	-1.07	2 2
62.50	61.38	1.12*	* GAS PHASE VALUE

P.E. DISTRIBUTION

2230.00	681.20	617.90	67.00	
0.999	0.001	0.000	0.000	SI-H ASYM STR.
0.001	1.009	0.000	0.005	SI-H2 ROCK
0.000	0.014	0.983	0.018	N-C-O BEND
0.000	0.005	0.016	0.979	SI-N-C BEND

L MATRIX

1.01971	0.01049	0.00105	0.00006
-0.09990	0.91115	0.00364	-0.00629
0.00023	-0.09040	0.67741	0.01000
-0.05085	0.28590	-0.46814	0.39762

Table 7.14

NORMAL COORDINATE SOLUTION FOR SIH (NCO)
SYMMETRY SPECIES - B2 2 2
F MATRIX AND FREQUENCIES FOR 2 ISOTOPIC SPECIES
P. E. DISTRIBUTION AND L MATRIX FOR 1ST ISOTOPIC SPECIES

F MATRIX

18.83182					
1.87509	11.72274				
0.00000	0.00000	0.26956			
0.00000	0.52461	0.29842	4.67321		
0.00000	0.00000	0.00000	0.04994	0.45777	
0.00000	0.00000	0.00000	0.00000	0.00000	0.01620

F.OBS	F.CALC	DIFF	
2324.00	2324.03	-0.03	
1466.00	1466.24	-0.24	
910.00	910.07	-0.07	SIH (NCO)
666.20	666.45	-0.25	2 2
604.40	604.56	-0.16	
67.00	67.02	-0.02*	

F.OBS	F.CALC	DIFF	
2322.00	2323.98	-1.98	
1467.00	1463.71	3.29	
712.20	706.42	5.78	SIH (NCO)
639.10	638.63	0.47	2 2
590.70	590.94	-0.24	
62.50	66.34	-3.84*	

* GAS PHASE VALUE

P.E. DISTRIBUTION

2324.00	1466.00	910.00	666.20	604.40	67.00	
0.780	0.203	0.001	0.032	0.001	0.000	C-O ASYM. STR.
0.352	0.515	0.006	0.144	0.004	0.000	C-N ASYM. STR.
0.000	0.001	1.064	0.011	0.001	0.000	SI-H2 WAG
0.007	0.242	0.044	0.755	0.034	0.001	SI-N ASYM. STR.
0.000	0.000	0.003	0.032	0.948	0.019	N-C-O BEND
0.000	0.000	0.001	0.000	0.019	0.981	SI-N-C BEND

L MATRIX

0.36295	0.11686	0.00379	0.02099	-0.00336	-0.00004
-0.30910	0.23594	0.01552	0.05672	-0.00890	-0.00009
0.00909	-0.05553	1.38733	-0.10300	-0.02809	0.00186
0.07094	-0.25622	-0.06743	0.20562	-0.03955	-0.00069
0.00093	-0.00968	0.05640	0.13472	0.66756	0.01042
0.00019	-0.00897	-0.12323	-0.00839	-0.50211	0.40013

Table 7.15

CALCULATED PARAMETERS
1ST ISOTOPIC SPECIES

INTERATOMIC DISTANCES AND AMPLITUDES - 0.00K

ATOMS	DIST(RA).	U	P	L	K	RG	RALPHA
SI-H	1.4880	0.0880	0.1814	0.0052	0.0221	1.4932	1.4711
SI-N	1.7030	0.0482	0.1147	0.0014	0.0077	1.7044	1.6966
C-N	1.2160	0.0372	0.0957	0.0011	0.0075	1.2171	1.2096
C-O	1.1640	0.0340	0.1001	0.0010	0.0086	1.1650	1.1564
H..H	2.4299	0.1496	0.2677	0.0092	0.0295	2.4391	2.4096
H..N	2.6084	0.1188	0.2254	0.0054	0.0195	2.6138	2.5943
H..N'	2.6103	0.1187	0.2255	0.0054	0.0195	2.6157	2.5962
SI..C	2.9190	0.0520	0.0753	0.0009	0.0019	2.9199	2.9180
N..O	2.3800	0.0400	0.1569	0.0007	0.0103	2.3807	2.3703
N..N	2.7810	0.0650	0.1517	0.0015	0.0083	2.7825	2.7742
H..C	3.6919	0.1418	0.1870	0.0054	0.0095	3.6974	3.6879
H..C'	3.6933	0.1416	0.1871	0.0054	0.0095	3.6987	3.6892
SI..O	4.0830	0.0525	0.0861	0.0007	0.0018	4.0837	4.0819
N..C	3.8391	0.0857	0.1113	0.0019	0.0032	3.8410	3.8378
H..O	4.7891	0.1594	0.1687	0.0053	0.0059	4.7944	4.7884
H..O'	4.7901	0.1593	0.1689	0.0053	0.0060	4.7954	4.7895
N..O'	4.9208	0.1033	0.1053	0.0022	0.0023	4.9230	4.9207
C..C	4.7674	0.0869	0.0680	0.0016	0.0010	4.7690	4.7680
C..O	5.7576	0.1016	0.0707	0.0018	0.0009	5.7594	5.7586
O..O	6.6689	0.1198	0.0756	0.0022	0.0009	6.6711	6.6702

INTERATOMIC DISTANCES AND AMPLITUDES - 298.16K

ATOMS	DIST(RA).	U	P	L	K	RG	RALPHA
SI-H	1.4880	0.0880	0.3266	0.0052	0.0717	1.4932	1.4215
SI-N	1.7030	0.0550	0.2704	0.0018	0.0429	1.7048	1.6618
C-N	1.2160	0.0374	0.1970	0.0012	0.0319	1.2171	1.1852
C-O	1.1640	0.0341	0.2089	0.0010	0.0375	1.1650	1.1275
H..H	2.4299	0.1525	0.5214	0.0096	0.1119	2.4395	2.3276
H..N	2.6084	0.1235	0.4855	0.0058	0.0903	2.6142	2.5239
H..N'	2.6103	0.1233	0.4857	0.0058	0.0904	2.6161	2.5257
SI..C	2.9190	0.0603	0.1469	0.0012	0.0074	2.9202	2.9129
N..O	2.3800	0.0403	0.3854	0.0007	0.0624	2.3807	2.3183
N..N	2.7810	0.0840	0.3736	0.0025	0.0502	2.7835	2.7333
H..C	3.6919	0.2032	0.3663	0.0112	0.0363	3.7031	3.6668
H..C'	3.6933	0.2023	0.3666	0.0111	0.0364	3.7043	3.6680
SI..O	4.0830	0.0609	0.2068	0.0009	0.0105	4.0839	4.0734
N..C	3.8391	0.1643	0.2579	0.0070	0.0173	3.8462	3.8288
H..O	4.7891	0.2692	0.3188	0.0151	0.0212	4.8042	4.7830
H..O'	4.7901	0.2689	0.3196	0.0151	0.0213	4.8052	4.7839
N..O'	4.9208	0.2292	0.2516	0.0107	0.0129	4.9315	4.9186
C..C	4.7674	0.1621	0.1159	0.0055	0.0028	4.7729	4.7701
C..O	5.7576	0.2230	0.1436	0.0086	0.0036	5.7663	5.7627
O..O	6.6689	0.2821	0.1802	0.0119	0.0049	6.6809	6.6760

The interatomic mean parallel amplitudes are in close agreement with corresponding amplitudes for SiH_3NCO.

7.9 Conclusions

The detail shown in a nitrogen matrix infrared spectrum of $SiH_2(NCO)_2$ and $SiD_2(NCO)_2$ is explained adequately in terms of a C_{2v} molecular structure. A convincing assignment for the observed vibrational bands has been made, with some help from isotopic shift predictions from a normal coordinate analysis. Finally, the force field was refined from the best assignment. The refinement converged well indicating a correct assignment within the limits of an assumed C_{2v} structure.

7.10 Preliminary Work on $SiH(NCO)_3$

Small amounts of the normal isotopic species and the deuterated species were obtained as described in the experimental chapter. The gas phase infrared spectrum is very weak due to the extremely low vapour pressure at room temperature (~3 mmHg).

At 2260 cm^{-1} is a strong band associated with the NCO asymmetric stretches. There is no evidence for the appearance of the SiH stretch - it may lie 'under' the strong NCO band. However, the deuterated species shows a weak band at 1642 cm^{-1} (SiD stretch). Both the normal and deuterated species have a band at 1460 cm^{-1} associated

with the NCO symmetric stretches.

The normal isotopic species has a strong, narrow band at 845 cm^{-1} due to the SiH rock. This band proved invaluable in identifying $SiH(NCO)_3$ during the separation from $SiH_2(NCO)_2$. Between 550 and 750 cm^{-1} there is a very broad and relatively weak band with four slight intensity maxima at 690 cm^{-1}, 660 cm^{-1}, 610 cm^{-1} and 560 cm^{-1}. Here are all the NCO bending modes and SiN stretches. It is, however, impossible to assign any of the individual modes. The spectrum of the deuterated species in this region is dissimilar in appearance due to the SiD rock - a relatively strong band centred at 730 cm^{-1}.

The infrared spectrum of the normal species in a nitrogen matrix is shown in Figure 7.7. This spectrum was run after annealing the sample. In this case there was little improvement over the gas phase spectrum.

In the region 2200-2350 cm^{-1} there are bands which can be assigned to the NCO asymmetric stretches. A very weak band at 2235 cm^{-1} may be the SiH stretch. The SiD stretch in the deuterated species is at 1653 cm^{-1}. At 1468 cm^{-1} we have a broad band due to the NCO symmetric stretches, with the SiH rock showing as a very broad multiplet at about 850 cm^{-1}.

The remaining bands in the infrared spectrum of the normal species consist of a very broad band centred

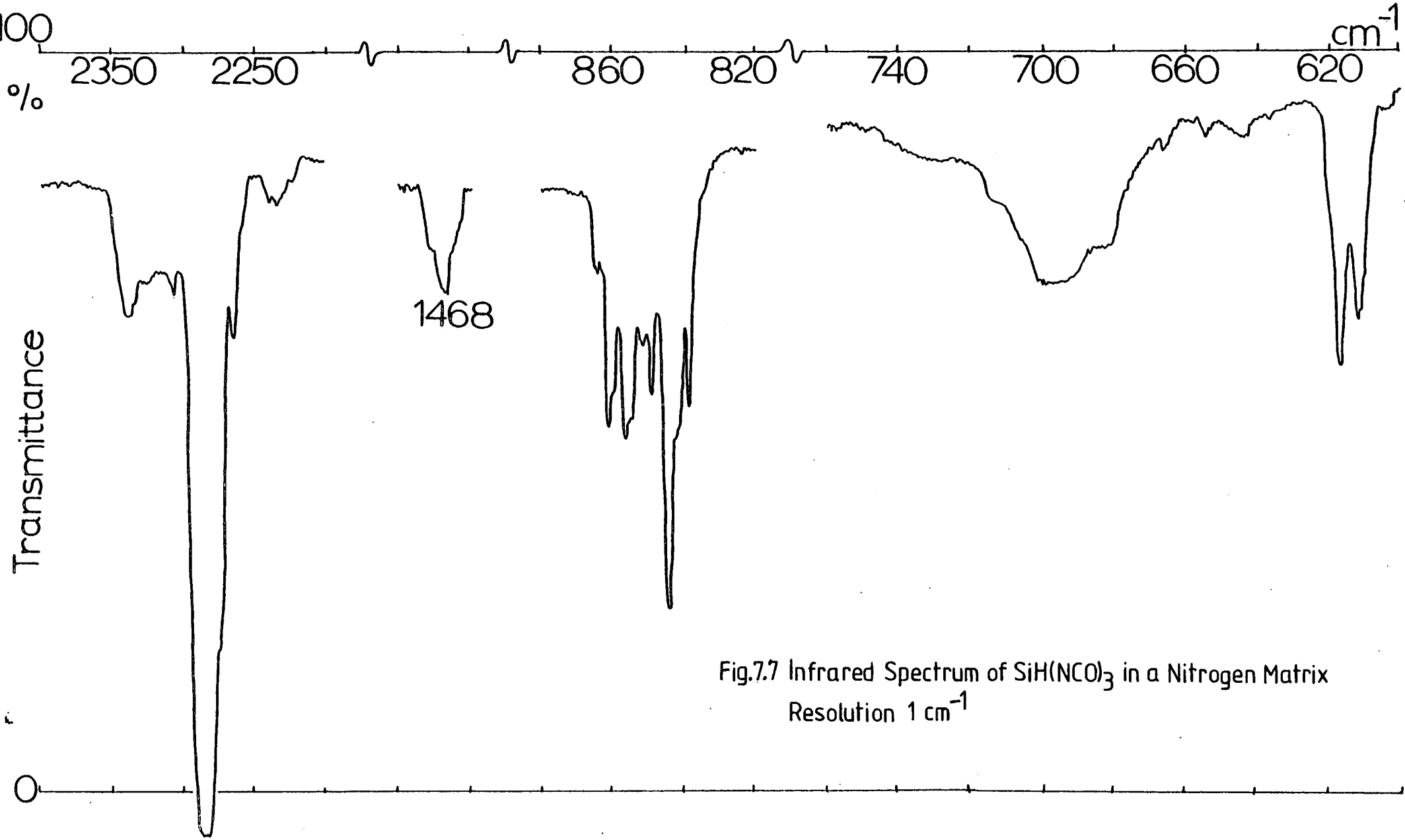

Fig.7.7 Infrared Spectrum of $SiH(NCO)_3$ in a Nitrogen Matrix
Resolution 1 cm^{-1}

at 697 cm^{-1} and a broad doublet with maxima at 617.2 cm^{-1} and 612.0 cm^{-1}. The deuterated species gives bands at 628.2 cm^{-1} and 617.3 cm^{-1}. There are also a few very weak bands in the spectra of both isotopic species near 550 cm^{-1}.

Assuming for the sake of argument that the $SiH(NCO)_3$ molecule has C_{3v} symmetry, the vibrational modes expected are $7A_1 + 2A_2 + 9E$. Examination of the matrix isolated infrared spectrum shows that such a number of fundamentals cannot be assigned from the bands observed. Thus the additional information gained from the matrix isolated spectrum is small. The spectrum can be seen to be unsatisfactory since even the SiH rock near 850 cm^{-1}, which is a very strong, sharp band in the gas phase spectrum, is a rather messy multiplet in the matrix spectrum. An assignment of the bands, apart from the very general one stated above, was not attempted.

CHAPTER 8 - N.M.R. STUDIES OF THE SILYL PSEUDOHALIDES

8.1 Introduction

In the course of the infrared studies a large number of substituted species were synthesised with ^{15}N and ^{13}C isotopes. ^{13}C has nuclear spin ½ and it is therefore possible to obtain its n.m.r. spectrum. ^{13}C nuclear magnetic resonance spectra are common in organic chemistry - here the spectrum is usually of the naturally occurring ^{13}C. However, with ^{13}C enriched samples the spectra obtained have better signal to noise, and consequently coupling constants are more easily determined.

Similarly, replacing the naturally occurring isotope ^{14}N with ^{15}N it is possible to obtain sharper spectral lines. In this case the line broadening effect of the ^{14}N (spin 1) nuclear quadrupole is removed by insertion of a ^{15}N (spin ½) nucleus.

Four molecules were studied using n.m.r. - SiH_3NCO, SiH_3NCS, SiH_3NCSe and SiH_3CN. Apart from ^{13}C and ^{15}N, these molecules also contain other nuclei with spin ½ - ^{1}H, ^{29}Si (4.7% natural abundance) and ^{77}Se (7.6% natural abundance) in the case of SiH_3NCSe. This chapter, then, describes the n.m.r. spectra obtained.

The majority of spectra were run on Fourier transform instruments. However, a few tickling experiments were carried out using a CW spectrometer to

yield chemical shifts and coupling constants which were otherwise not observable. Tickling experiments were done while observing protons.

N.m.r. tubes were 5 mm diameter and the solvent used was CD_2Cl_2 (unless otherwise stated). About 2.5 cm depth of solvent was used in each tube - about 0.4 cm^3 volume. The amount of sample used was 0.3 mmoles if possible, but in some cases such an amount was not available. The maximum concentration, then, was about 0.75 M. All spectra were run at -40°C unless otherwise stated.

The accuracy of the observed chemical shifts and coupling constants is determined by the number of Hz per data point (for a Fourier transform instrument) or the smallest measurable interval (for a CW instrument). Coupling constants are expressed in Hz and are quoted to plus or minus half of the Hz per data point (or smallest measurable interval). Chemical shifts are expressed in ppm and are quoted to the first decimal place (second decimal place for protons). Chemical shifts are often solvent, concentration and temperature dependent so a higher accuracy is unwarranted. However, where a real isotopic shift is observed, for samples with mixtures of isotopic species, more decimal places are quoted.

The following tables summarise the results obtained for each molecule studied. All chemical shifts are

(unless otherwise stated) with respect to the following:

^{1}H - T.M.S.

^{29}Si - T.M.S.

^{15}N - $Me_4{}^{15}N^+$

^{13}C - T.M.S.

^{77}Se - Me_2Se.

8.2 Additional N.M.R. Studies

As well as the data on the silyl pseudohalides, some data were obtained on the $NCSe^-$ anion. During the synthesis of this anion, the K^+ salt is extracted in acetone. It was possible to extract the salt with deuterated acetone and run the n.m.r. spectra.

Other n.m.r. spectra were run on a neat sample of SiD_3NCO in order to determine the % deuteration of the silyl group. This was done to aid the infrared studies.

8.3 Conclusions

The n.m.r. spectra indicate that there is no fast exchange of atoms, or groups of atoms, in any of the samples studied. The spectra and the parameters obtained are consistent with the proposed molecular structures. Any additional isotopic species present in the samples

have been easily detected. Indeed, a number of accurate isotopic shifts have been recorded. Those for the species containing ^{77}Se are especially striking.

It is interesting to make comparisons among the silyl pseudohalides (see Table 8.5). SiH_3CN, being of fundamentally different structure, can be seen as the 'odd one out'. However, the other three molecules, SiH_3NCO, SiH_3NCS and SiH_3NCSe are congeners and therefore comparisons are of special interest.

In the molecules SiH_3NCY, both δ^1H and $\delta^{29}Si$ are almost independent of Y. However, $\delta^{15}N$ is very sensitive to Y; J_{SiH} is (surprisingly) fairly sensitive. It is interesting that $\delta^{15}N$ is more sensitive to Y than is $\delta^{13}C$. The coupling constants J_{CN} and J_{SiC} decrease in magnitude as Y becomes more electropositive. J_{SiN} and J_{NH} do likewise, but not so markedly. J_{CH} stays fairly constant.

The parameters for $NCSe^-$ can be contrasted with the same parameters for the NCSe group in SiH_3NCSe. J_{CSe} is almost exactly the same, with $\delta^{13}C$ fairly similar. However, the parameters $\delta^{15}N$, J_{NSe} and J_{CN} are very much different in $NCSe^-$ as compared with SiH_3NCSe. The differences will result from the different bonding, and the fact that $NCSe^-$ is anionic, with the negative charge residing mostly on the nitrogen atom.

The ^2H spectrum of SiD_3NCO showed no evidence of ^1H

coupling which might indicate the presence of SiD_2HNCO. The coupling may not have been resolved in this spectrum. The ^1H spectrum of SiD_3NCO indicated a very small amount of SiD_2HNCO present plus a number of impurities, notably benzene. An estimate of the concentration of SiD_2HNCO was less than 1%.

Table 8.1

N.m.r. parameters for SiH_3NCO

The parameters were obtained from two samples - one $SiH_3{}^{15}NCO$, the other $SiH_3N{}^{13}CO$. Each sample contained a trace of SiH_3NCO.

	δ^1H[a]	$\delta^{29}Si$	$\delta^{15}N$	$\delta^{13}C$	$^1J_{SiH}$	$^1J_{SiN}$	$^1J_{CN}$	$^2J_{NH}$	$^2J_{SiC}$	$^3J_{CH}$
$SiH_3{}^{15}NCO$	4.40[b]	-58.1	-26.9[c]	123.8[d]	234.9[e]	18.6[f]	46.3[g]	5.1[e]	-	-
$SiH_3N{}^{13}CO$	4.40[h]	-58.1[i]	-	123.7[j]	235.0[k]	-	-	-	9.8[f]	2.6[k]

Notes: δ in ppm, J in Hz.

(a) ^1H n.m.r. spectrum shown in Fig. 8.1.

(b) SiH_3NCO resonance also observed at 4.40 ppm.

(c) Obtained from tickling experiment. Observing ^1H spectrum, ^{15}N coupling collapsed at 10,133,431.5 Hz. R.F. = 100,001,347 Hz, manual oscillator frequency 2102 Hz.

(d) From natural abundance ^{13}C.

(e) $\pm$0.06 Hz, from ^1H spectrum

(f) $\pm$0.1 Hz, from ^{29}Si spectrum

(g) $\pm$0.6 Hz, from ^{13}C spectrum

(h) ^1H resonance broad

(i) ^{29}Si resonance broad

(j) ^{13}C resonance broad

(k) $\pm$0.2 Hz, from ^1H spectrum

Fig. 8.1 ^{1}H n.m.r. spectrum of $SiH_3{}^{15}NCO$ in CD_2Cl_2

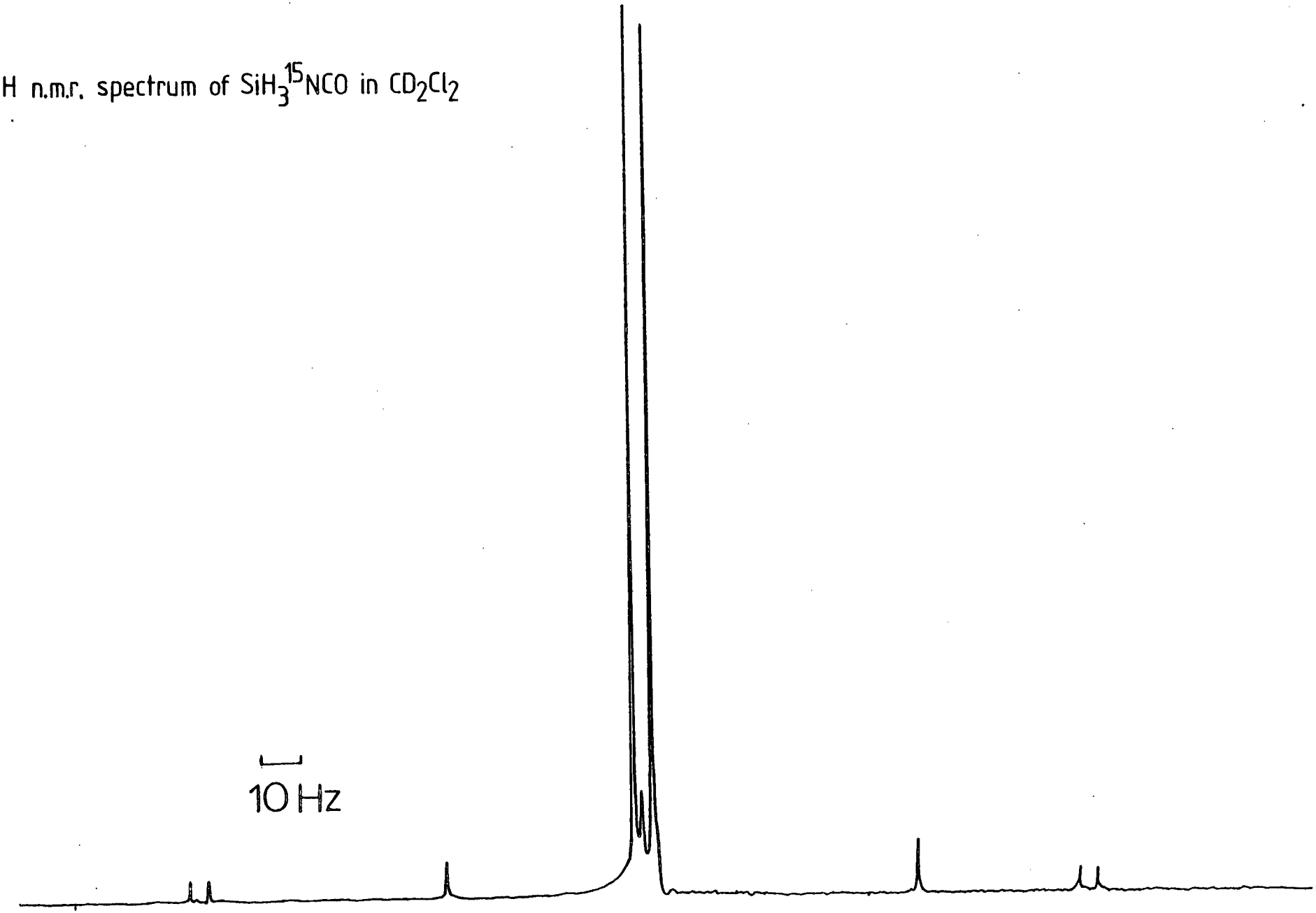

Table 8.2

N.m.r. parameters for SiH_3NCS

The parameters were obtained from a sample of $SiH_3{}^{15}N{}^{13}CS$. It contained a trace of $SiH_3{}^{15}NCS$.

δ^1H	$\delta^{29}Si$	$\delta^{15}N$	$\delta^{13}C$	$^1J_{SiH}$	$^1J_{SiN}$	$^1J_{CN}$	$^2J_{NH}$	$^2J_{SiC}$	$^3J_{CH}$
4.48	-59.7[a]	50.2[b]	143.6	240.2[c]	16.8[c]	39.4[d]	4.2[e]	7.1[c]	2.8[e]

Notes: δ in ppm, J in Hz.

(a) Isotopic shift: $\delta^{29}Si(SiH_3{}^{15}N{}^{13}CS) = -58.727$ ppm, $\delta^{29}Si(SiH_3{}^{15}NCS) = -58.721$ ppm.

(b) Obtained from a tickling experiment. Observing ^1H spectrum, ^{15}N coupling collapsed at 10,134,190 Hz and 10,134,229 Hz (neglecting ^1H coupling). RF = 100,001,347 Hz. Manual oscillator frequency 2102 Hz.
$sign(J_{CN}) = sign(J_{NH})$; $sign(J_{CN}) \neq sign(J_{CH})$ from ^{13}C tickling experiment.

(c) $\pm$0.1 Hz, from ^{29}Si spectrum.
Isotopic shift: $^1J_{SiN}(SiH_3{}^{15}N{}^{13}CS) = 16.8$ Hz, $^1J_{SiN}(SiH_3{}^{15}NCS) = 17.1$ Hz.

(d) $\pm$0.6 Hz, from ^{13}C spectrum.

(e) $\pm$0.05 Hz, from ^1H spectrum.

Table 8.3

N.m.r. parameters for SiH_3NCSe

In all, three samples were used to obtain the parameters - SiH_3NCSe, $SiH_3{}^{15}NCSe$ and $SiH_3{}^{15}N{}^{13}CSe$ (with traces of $SiH_3N{}^{13}CSe$ and $SiH_3{}^{15}NCSe$). The parameters quoted are from the $SiH_3{}^{15}N{}^{13}CSe$ sample unless otherwise stated.

δ^1H	$\delta^{29}Si$[a]	$\delta^{15}N$	$\delta^{13}C$[b]	$^1J_{SiH}$	$^1J_{SiN}$	$^1J_{CN}$	$^2J_{NH}$	$^2J_{SiC}$	$^3J_{CH}$	$\delta^{77}Se$[c]	$^1J_{CSe}$	$^2J_{NSe}$
4.49[d]	-59.5[e]	78.3[f]	142.2[g]	243.8[h]	15.1[i]	34.1[j]	4.0[k]	4.9[i]	2.8[j]	-347.2[l]	275.0[j]	3.7[m]

Notes: in ppm, J in Hz.

(a) ^{29}Si n.m.r. spectrum shown in Fig. 8.3.

(b) ^{13}C n.m.r. spectrum shown in Fig. 8.2.

(c) ^{77}Se n.m.r. spectrum shown in Fig. 8.4.

(d) SiH_3NCSe.

(e) Isotopic shift: $\delta^{29}Si(SiH_3{}^{15}N{}^{13}CSe) = -59.532$ ppm, $\delta^{29}Si(SiH_3{}^{15}NCSe) = -59.527$ ppm.

(f) Obtained from a tickling experiment. Observing ^1H spectrum, ^{15}N coupling collapsed at 10,134,511 Hz and 10,134,478 Hz (neglecting ^1H coupling). RF = 100,001,347 Hz, manual oscillator frequency 2102 Hz. $sign(J_{CN}) = sign(J_{NH})$; $sign(J_{CN}) \neq sign(J_{CH})$ from ^{13}C tickling experiment.

(g) Isotopic shift: $\delta^{13}C(SiH_3{}^{15}N{}^{13}CSe) = 142.168$ ppm, $\delta^{13}C(SiH_3{}^{15}NCSe) = 142.172$ ppm.

(h) $\pm$0.06 Hz, from ^1H spectrum of (d).

(i) $\pm$0.1 Hz, from ^{29}Si spectrum.

(j) $\pm$0.03 Hz, from ^{13}C spectrum.

(k) $\pm$0.2 Hz, from ^1H spectrum.

(l) Isotopic shift: $\delta^{77}Se(SiH_3{}^{15}N{}^{13}CSe) = -347.220$ ppm, $\delta^{77}Se(SiH_3{}^{15}NCSe) = -346.449$ ppm.

(m) $\pm$0.15 Hz, from ^{77}Se spectrum.

Fig. 8.2 ^{13}C n.m.r. spectrum of $SiH_3{}^{15}N{}^{13}CSe$ in CD_2Cl_2

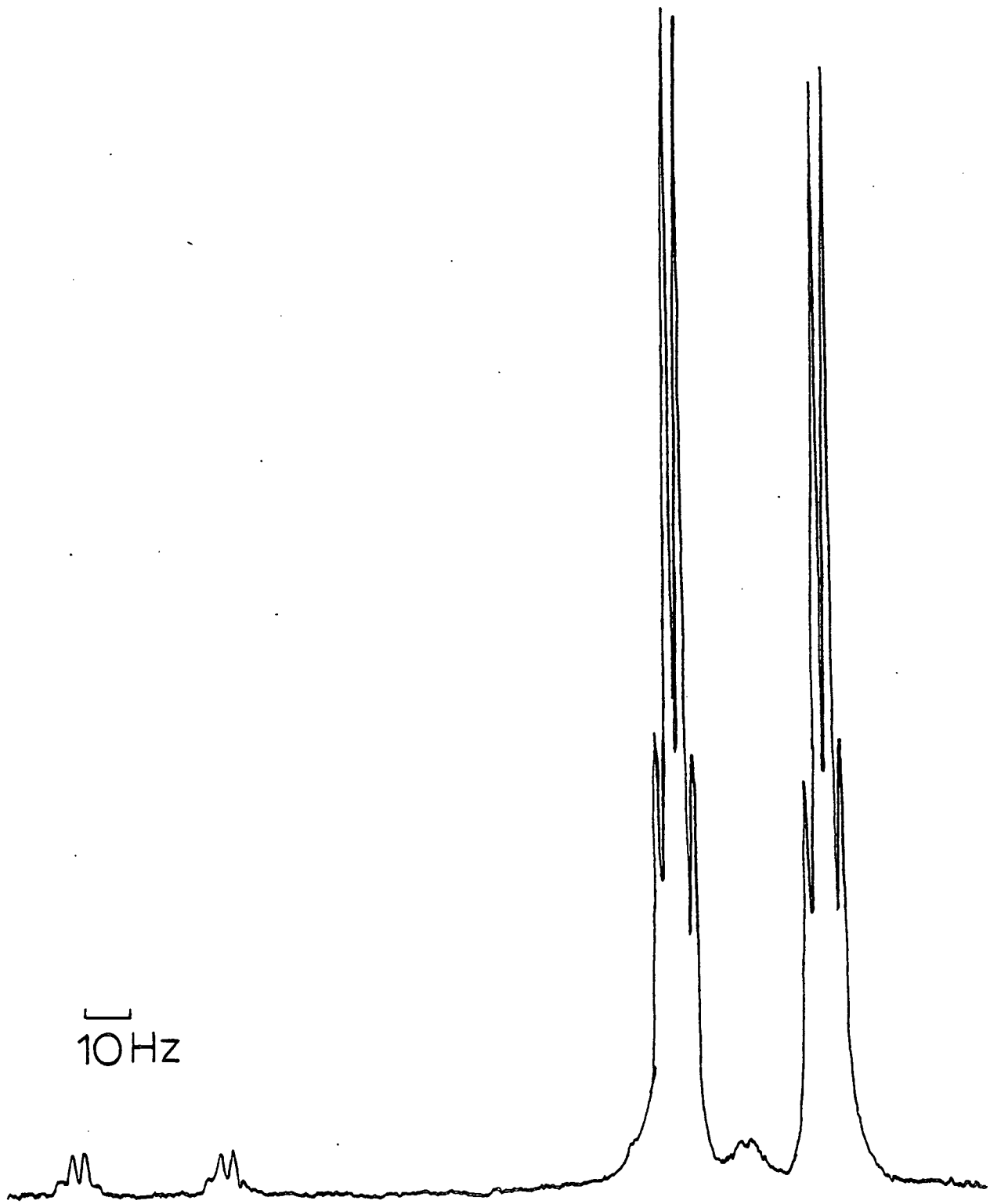

Fig. 8.3 ^{29}Si n.m.r. spectrum of $SiH_3{}^{15}N{}^{13}CSe$ in CD_2Cl_2

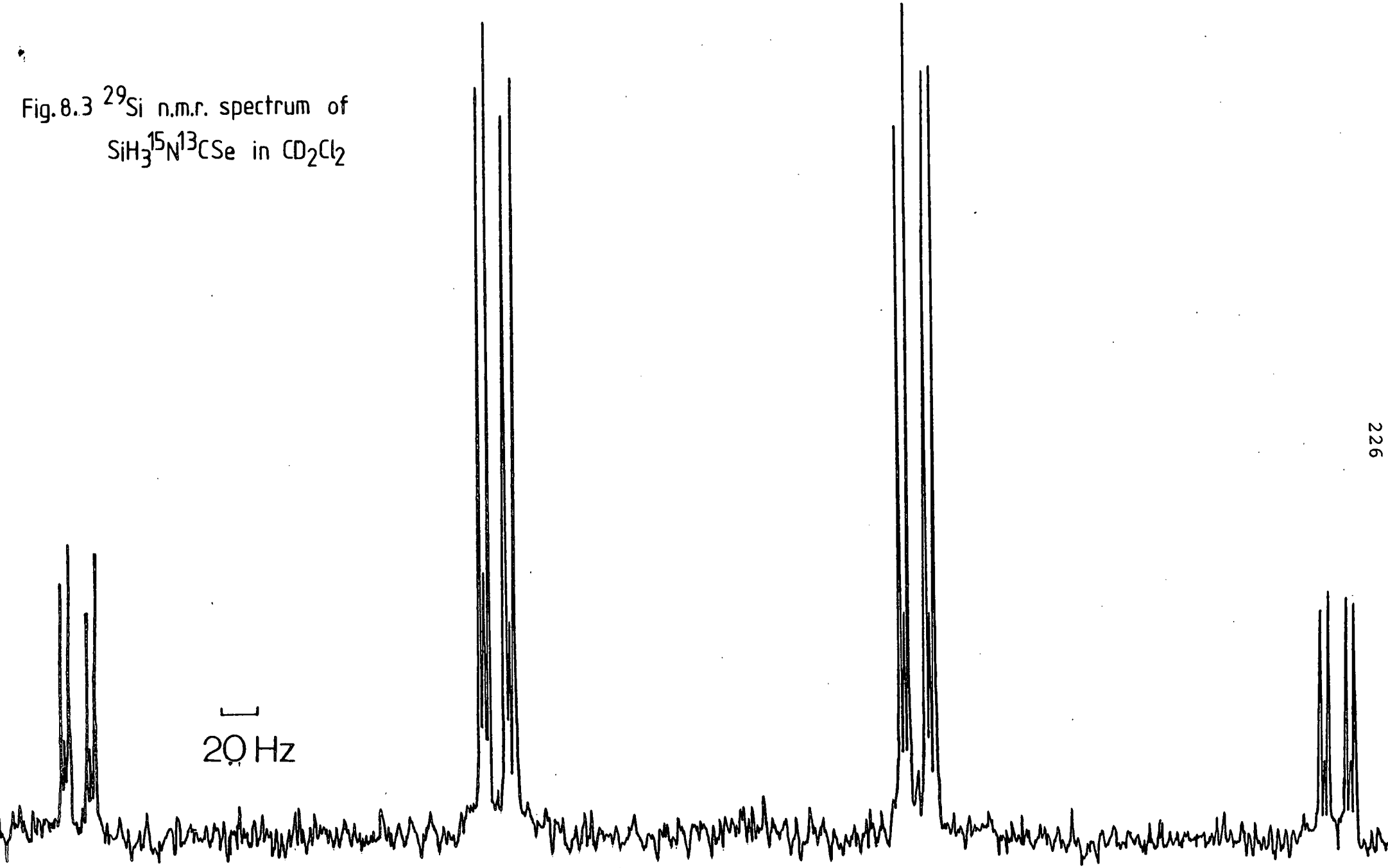

Fig. 8.4 ^{77}Se n.m.r. spectrum of $SiH_3{}^{15}N^{13}CSe$ in CD_2Cl_2

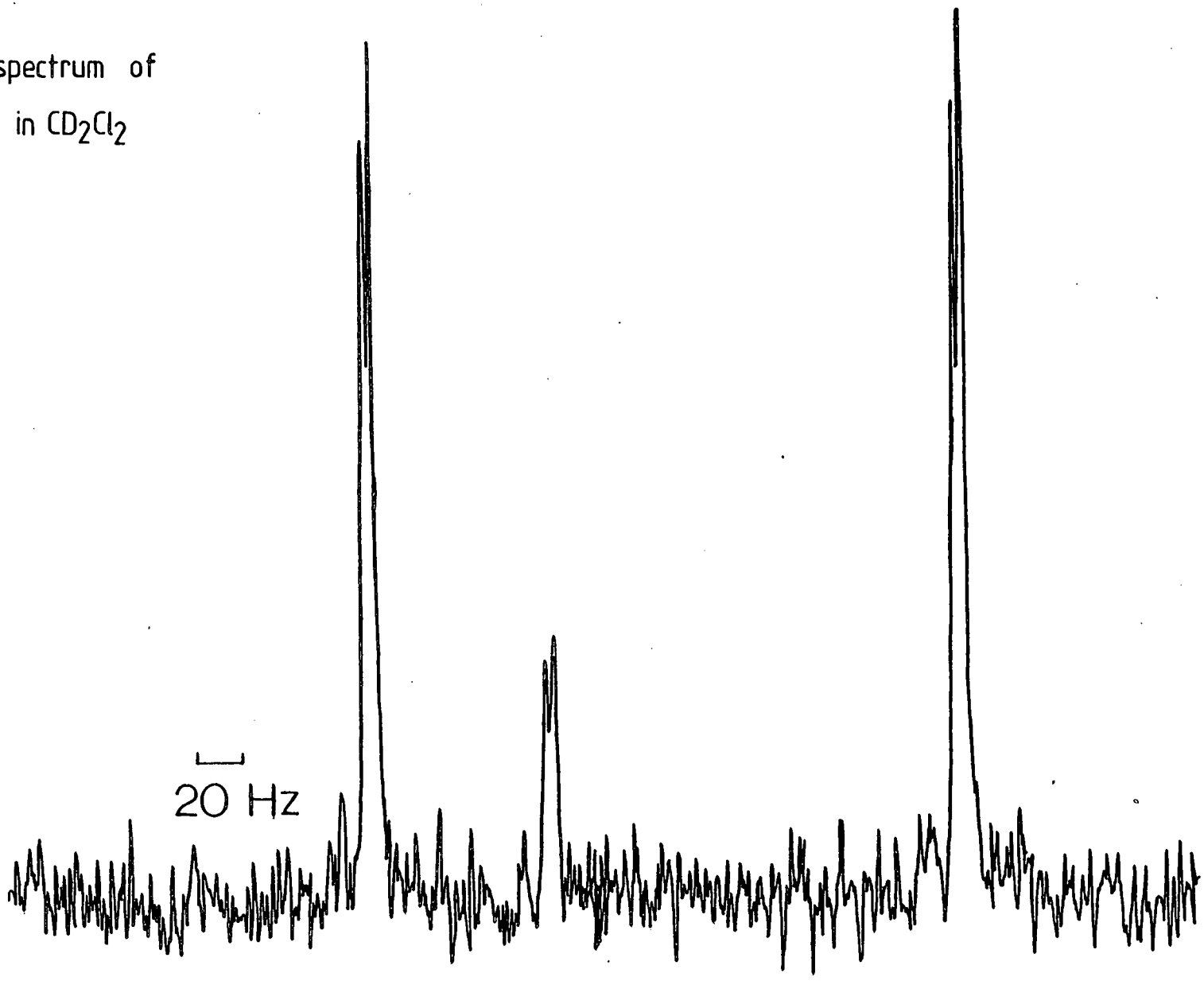

Table 8.4

N.m.r. parameters for SiH_3CN

All parameters for this molecule were obtained from a single sample of $SiH_3{}^{13}C^{15}N$. There was evidence for a trace of $SiH_3{}^{13}CN$.

δ^1H	$\delta^{29}Si$	$\delta^{13}C$	$\delta^{15}N$	$^1J_{SiH}$	$^1J_{SiC}$	$^1J_{CN}$	$^2J_{CH}$	$^2J_{SiN}$	$^3J_{NH}$
3.95	-87.4	118.3[a]	258.9[b]	238[c]	61.9[d]	12.8[d]	4.9[e]	<2[f]	1.1[e]

Notes: δ in ppm, J in Hz.

(a) Isotopic shift: $\delta^{13}C(SiH_3{}^{13}C^{15}N) = 118.347$ ppm; $\delta^{13}C(SiH_3{}^{13}CN) = 118.368$ ppm.

(b) Obtained from tickling experiment. Observing ^1H main resonance, ^{15}N coupling collapsed at 10,136,335 Hz and 10,136,322 Hz (neglecting ^1H coupling). RF = 100,001,347 Hz, manual oscillator frequency = 2102 Hz.
$sign(J_{NH}) = sign(J_{CN})$; $sign(J_{CH}) \neq sign(J_{CN})$ from ^{13}C tickling experiment. An example of a tickling experiment is shown in Figure 8.5.

(c) $\pm$0.5 Hz, from ^1H spectrum.

(d) $\pm$0.06 Hz, from ^{13}C spectrum.

(e) $\pm$0.05 Hz, from ^1H spectrum.

(f) Not resolved in ^{29}Si spectrum, estimated from line width.
From tickling experiment: $sign(J_{SiN}) = sign(J_{SiH})$.

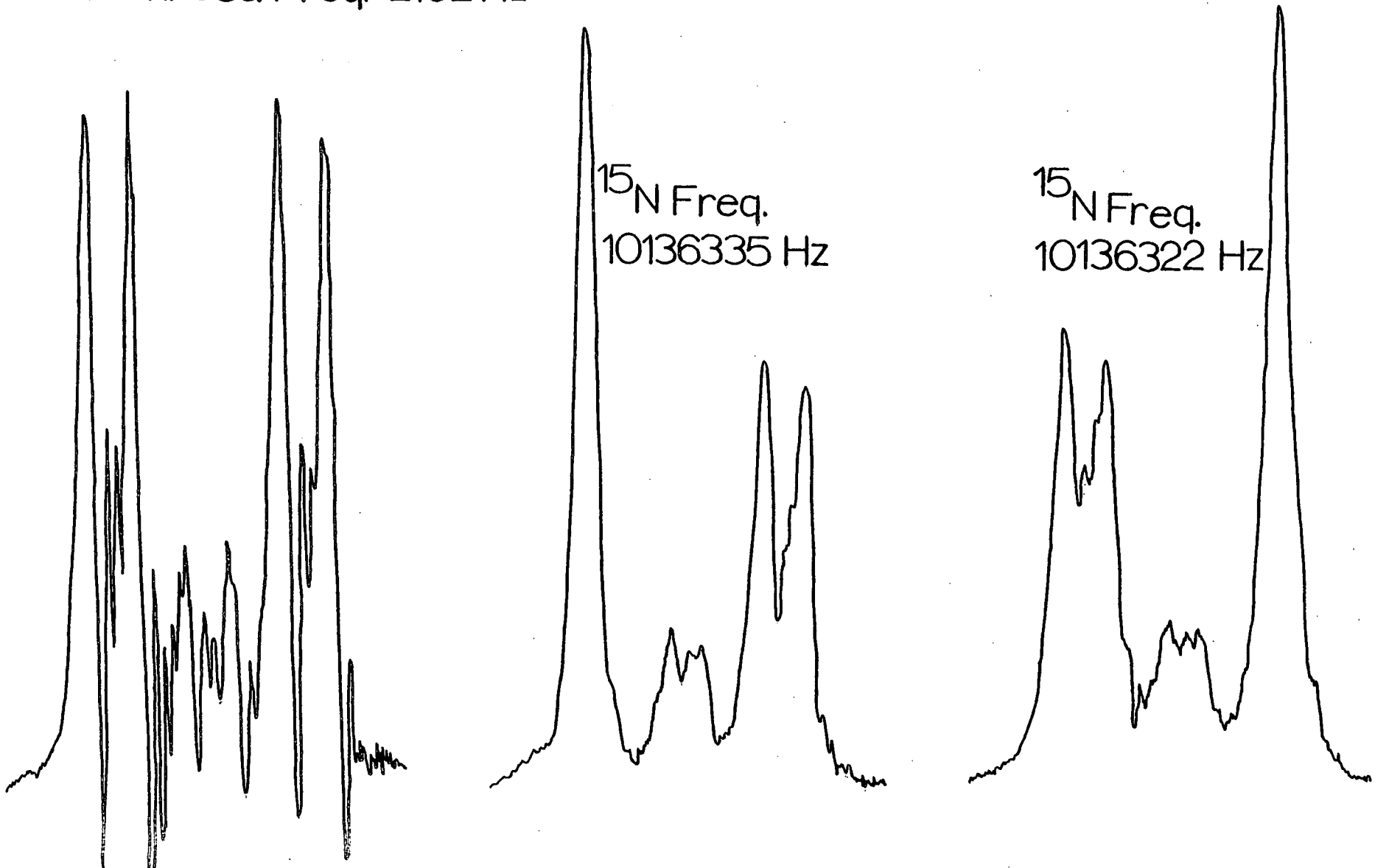

Fig. 8.5 ^{1}H n.m.r. spectrum of $SiH_3{}^{13}C{}^{15}N$ in CD_2Cl_2 with irradiation at ^{15}N frequency

Table 8.5

Summary of n.m.r. parameters for the silyl pseudohalides

	$\delta^{1}H$	$\delta^{29}Si$	$\delta^{15}N$	$\delta^{13}C$	J_{SiH}	J_{SiN}	J_{CN}	J_{NH}	J_{SiC}	J_{CH}
SiH_3NCO	4.40	-58.1	-26.9	123.8	234.9	18.6	46.3	5.1	9.8	2.6
SiH_3NCS	4.48	-59.7	50.2	143.6	240.2	16.8	39.4	4.2	7.1	2.8
SiH_3NCSe	4.49	-59.5	78.3	142.2	243.8	15.1	34.1	4.0	4.9	2.8
SiH_3CN	3.95	-87.4	118.3	258.9	238	<2	12.8	1.1	61.9	4.9

	$\delta^{77}Se$	J_{CSe}	J_{NSe}
SiH_3NCSe	-347.2	275.0	3.7

δ in ppm, J in Hz.

Table 8.6

N.m.r. parameters for K^+NCSe^-

The parameters were obtained from two samples - one $K^+N^{13}CSe^-$ (with some K^+NCSe^-) and $K^{+15}N^{13}CSe^-$ (with some $K^{+15}NCSe^-$ and $K^+N^{13}CSe^-$). All spectra were run at room temperature.

	$\delta^{15}N$	$\delta^{13}C$[a]	$\delta^{77}Se$[b]	$^1J_{CN}$	$^1J_{CSe}$	$^2J_{NSe}$
$K^{+15}N^{13}CSe^-$	-133.5[c]	118.3[d]	-316.3[e]	9.8[f]	274.0[g]	18.9[g]
$K^+N^{13}CSe^-$	-	118.4	-316.9[h]	-	274.0[g]	-

Notes: δ in ppm, J in Hz.

(a) ^{13}C spectrum of $K^{+15}N^{13}CSe^-$ shown in Figure 8.6.

(b) ^{77}Se spectrum of $K^{+15}N^{13}CSe^-$ shown in Figure 8.7.
^{77}Se chemical shifts are very sensitive to temperature.

(c) With respect to $^{15}NO_2^{\bullet}$.

(d) Isotopic shift: $\delta^{13}C(^{15}N^{13}CSe^-)$ = 118.291 ppm, $\delta^{13}C(N^{13}CSe^-)$ = 118.311 ppm.

(e) Isotopic shifts: $\delta^{77}Se(^{15}N^{13}CSe^-)$ = -316.321 ppm, $\delta^{77}Se(^{15}NCSe^-)$ = -315.588 ppm.
$\delta^{77}Se(N^{13}CSe^-)$ = -316.126 ppm.

(f) $\pm$0.25 Hz, from ^{15}N spectrum.

(g) $\pm$0.3 Hz, from ^{77}Se spectrum.

(h) Isotopic shifts: $\delta^{77}Se(N^{13}CSe^-)$ = -316.876 ppm, $\delta^{77}Se(NCSe^-)$ = -316.143 ppm.

Fig. 8.6 ^{13}C n.m.r. spectrum of $K^{+}\,^{15}N^{13}CSe^{-}$ in $(CD_3)_2CO$

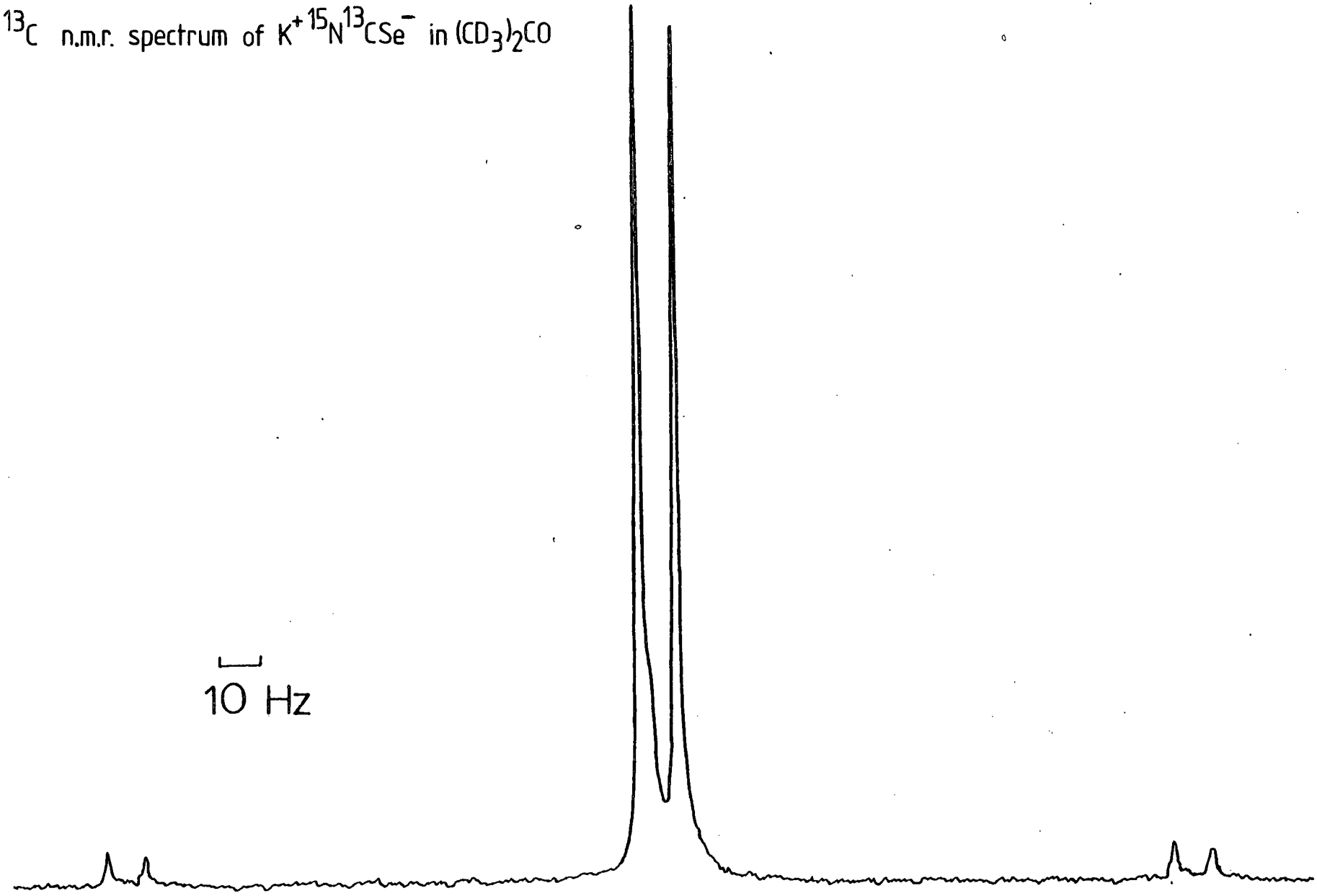

Fig. 8.7 ^{77}Se n.m.r. spectrum of $K^{+15}N^{13}CSe^{-}$ in $(CD_3)_2CO$

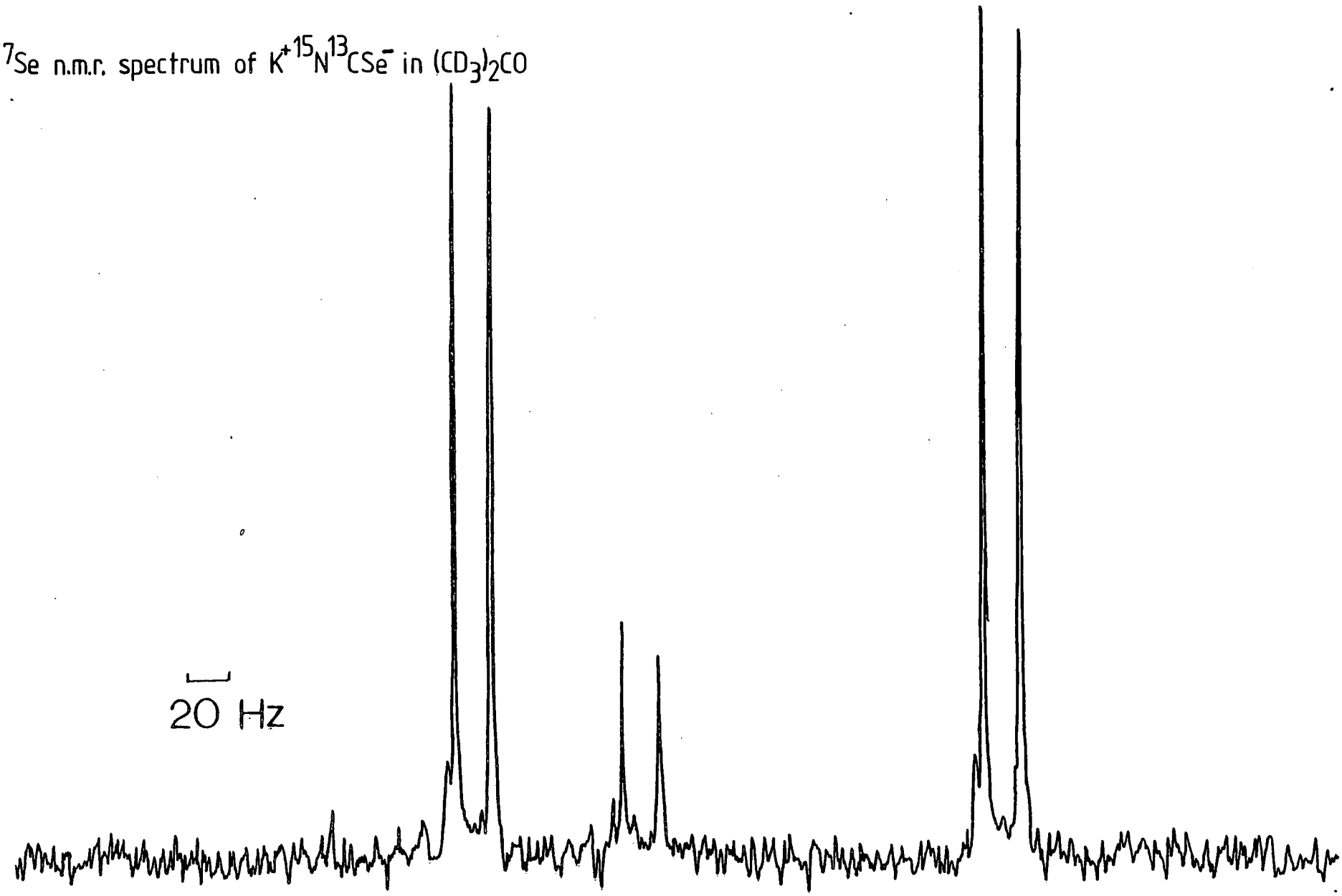

Table 8.7

N.m.r. parameters for SiD_3NCO

Both ^2H and ^1H spectra were run on a neat sample of SiD_3NCO (with a very small amount of SiD_2HNCO).

	δ^2H	δ^1H	$^1J_{SiD}$	$^2J_{HD}$
SiD_3NCO	4.33	4.57[a]	35.5[b]	1.6[c]

Notes: δ in ppm, J in Hz.

(a) Very small multiplet. For SiD_2HNCO we expect a 1:2:3:2:1 quintet due to coupling with two D atoms. This was only partly resolved.

(b) $\pm$0.05 Hz, from ^2H spectrum.

(c) $\pm$0.1 Hz, from ^1H spectrum.

CHAPTER 9 - GENERAL CONCLUSIONS

The study of stable molecules in matrix isolation by infrared spectroscopy provides much information about molecular symmetry and structure. The infrared bands produced are usually very sharp, giving accurate vibrational frequencies and isotopic shifts. However, the effects of the matrix on the sample molecules must be understood before any interpretation of a spectrum can begin.

Matrix isolation offers a means of studying isotopically substituted species, which are often expensive and in short supply, in the same detail as 'normal' isotopic species. The reason can be found in the extremely small amounts of sample required for matrix isolation. The technique can be used in both the mid and far infrared with the use of suitable window materials. Further experiments with matrix isolation could include the use of new matrix gases to produce different structural effects in the sample molecules.

Gas phase far infrared spectra provide more information than matrix isolated spectra in the same region, since there is a large number of hot-bands observed. Here, information about the potential governing a low frequency vibration can be obtained. A study at higher resolution of the gas phase far infrared spectra seen in this work would be a useful exercise. It might

yield detailed information about, for example, the variation of ζ with vibrational state for a low frequency degenerate mode.

Normal coordinate analysis provides a means of confirming vibrational assignments, if there is information on other isotopic species available. The analysis is subject to the approximations of harmonic and infinitesimal vibrations. Therefore care in interpretation of results must be exercised if these approximations are invalid. There are also errors introduced into a normal coordinate analysis through experimental uncertainties in observed frequencies, and the possibility of mathematically under-determined problems. However, normal coordinate analysis works well for a 'real' problem since there is good agreement with experimental results. Normal coordinate analysis also provides a number of useful calculated parameters which are not otherwise obtainable.

Specific areas of further study could include the assignment of the fundamental bands of GeH_3NCS. The vibrations not already assigned may be observed more easily in the Raman spectrum. Raman spectra would also be useful in the study of $SiH_2(NCO)_2$, as would the synthesis of more isotopically substituted species. In order to match the quality of the information obtained by matrix isolation, the Raman spectra should also be run using this technique, or using solid samples. Work on $SiH(NCO)_3$ has barely

started - there are infrared and Raman studies necessary in this area.

Before work on $SiH_2(NCO)_2$ and $SiH(NCO)_3$ can continue in detail, an effective synthetic route must be found. The method of synthesis described in Chapter 3 is useless for making ^{13}C and ^{15}N substituted species. These molecules are probably best prepared from the di- and tri-halosilanes. Work is progressing in this area at Edinburgh.

REFERENCES

1. R.G. Lett and W.H. Flygare, J. Chem. Phys., 47, 4730 (1967).

2. A.J. Careless, M.C. Green and H.W. Kroto, Chem. Phys. Lett., 16, 414 (1972).

3. J.R. Durig, J.F. Sullivan, A.W. Cox and B.J. Streusand, Spectrochim. Acta, 34A, 719 (1978).

4. J.R. Durig, K.S. Kalasinsky and V.F. Kalasinsky, J. Phys. Chem., 82, 438 (1978).

5. T.B. Freedman and E.R. Nixon, Spectrochim. Acta, 28A, 1375 (1972).

6. A. Bauer, M. Gordon and S. Maes, J. Mol. Spec., 59, 421 (1976).

7. D. Boucher et al, J. Mol. Spec., 64, 290 (1977).

8. M.R. Booth and S.G. Frankiss, Spectrochim. Acta, 26A, 859 (1970).

9. 'Molecular Quantum Mechanics', P.W. Atkins, Clarendon Press, Oxford (1970).

10. 'Vibrational States', S. Califano (J. Wiley & Sons).

11. 'Vibrating Molecules', P. Gans (Chapman & Hall, London).

12. 'Molecular Vibrations and Mean Square Amplitudes', S.J. Cyvin (Elsevier).

13. 'Molecular Structure by Diffraction Methods - Vol. 1', Specialist Periodical Reports (Chapter 4), A.G. Robiette (The Chemical Society).

14. Meal and Polo, J. Chem. Phys., 24, 1119 (1956).

15. 'Infrared and Raman Spectra', Herzberg (Van Nostrand).

16. 'Matrix Isolation', S. Cradock and A.J. Hinchcliffe (Cambridge University Press).

17. E.A.V. Ebsworth and M.J. Mays, J. Chem. Soc., 4844 (1962).

18. E.A.V. Ebsworth and J.C. Thompson, J. Chem. Soc. (A), 69 (1967).

19. G. Fritz and D. Kummer, Z. Anorg. Chem., 308, 105 (1961).

20. 'Organic Synthesis with Isotopes I', page 572, Murray, Williams (Interscience).

21. A. Stock and K. Somieski, Ber., 54, 740 (1921).

22. G.M. Sheldrick, Ph.D Thesis, Cambridge (1966).

23. E.A.V. Ebsworth and M.J. Mays, J. Chem. Soc., 3893 (1963).

24. 'Inorganic Syntheses II', page 186 (McGraw-Hill).

25. T.N. Srivastava, J.E. Griffiths and M. Onyszchuke, Can. J. Chem., 40, 739 (1962).

26. S. Cradock and E.A.V. Ebsworth, J. Chem. Soc. (A), 1226 (1967).

27. N.S. Hosmane, PhD Thesis, Edinburgh (1974).

28. W.L. Jolly, J. Amer. Chem. Soc., 83, 335 (1961).

29. H.J. Emeleus, A.G. Maddock and C. Reid, J. Chem. Soc., 353 (1941).

30. M.J. Mays, PhD Thesis, Cambridge (1963).

31. M.C.L. Gerry, J.C. Thompson and T.M. Sugden, Nature, 211, 846 (1966).

32. J.A. Duckett, A.G. Robiette and I.M. Mills, J. Mol. Spec., 62, 34 (1976).

33. C. Glidewell, A.G. Robiette and G.M. Sheldrick, Chem. Phys. Lett., 16, 526 (1972).

34. S. Cradock and D.C.J. Skea, J.C.S. Faraday II, 76, 860 (1980).

35. S.J. Cyvin, J. Brunvoll and A.G. Robiette, Chem. Phys. Lett., 11, 263 (1971).

36. J.R. Durig and K.S. Kalasinsky, J. Chem. Phys., 69, 2775 (1977).

37. J.R. Durig, M.J. Flanagan and V.F. Kalasinsky, J. Chem. Phys., 66, 2775 (1977).

38. A.G. MacDiarmid, J. Inorg. Nucl. Chem., 2, 88 (1956).

39. D.R. Jenkins, R. Kewley and T.M. Sugden, Trans. Farad. Soc., 58, 1284 (1962).

40. K.F. Dossel and A.G. Robiette, Z. Naturforch., 32A, 462 (1977).

41. E.A.V. Ebsworth et al, Trans. Farad. Soc., 58, 1069 (1961).

42. S. Cradock, J.C.S. Faraday II, 76, 496 (1980).

43. B. Krakow, R.C. Lord and G.O. Neely, J. Mol. Spec., 27, 148 (1968).

44. M. Born and R. Oppenheimer, Ann. Physik., 84, 457, (1927).

45. J. Blanc, C. Brecher and R.S. Halford, J. Chem. Phys., 36, 2654 (1962).

46. S.H. Walmsley and J.A. Pople, Mol. Phys., 8, 345 (1964).

47. J.E. Griffiths, J. Chem. Phys., 48, 278 (1968).

48. K.M. Mackay and S.R. Stobart, Spectrochim. Acta, 26A, 373 (1970).

49. J.R. Durig and J.F. Sullivan, J. Mol. Struct., 56, 41 (1979).

50. K.R. Ramaprasad and R. Nelson, J. Am. Chem. Soc., 90, 6247 (1969).

51. Rankin and Beagley, J. Mol. Struct., 31, 291 (1976).

52. J.R. Durig, Y.S. Li and J.F. Sullivan, J. Chem. Phys., 71, 1041 (1979).

53. G. Davidson and L.A. Woodward, Spectrochim. Acta, 23A, 2383 (1967).

54. Linton and Nixon, Spectrochim. Acta, 10, 299 (1958).

55. N. Muller and R.C. Bracken, J. Chem. Phys., 32, 1577 (1960).

56. J. Sheridan and A.C. Turner, Proc. Chem. Soc., 21 (1960).

57. H. Burger and G. Schirawski, Spectrochim. Acta, 27, 159 (1969).

58. Careless and Kroto, J. Mol. Spec., 57(2), 198 (1975).

59. R. Westwater, 4th year Honours project (1979).

60. J.W. Cooley, Math. Computation XV, 363 (1961).

LIST OF COURSES ATTENDED

1. Molecular Vibrations (Chemical Physics 4).

2. Molecular Structure (Chemical Physics 4).

3. Nuclear Magnetic Double Resonance.

4. Colourful Chemistry.

5. Mass Spectrometry.

6. Neutron Scattering.

7. Crystallographic Data Base.

8. Inorganic Chemistry Group Seminars (for 3 years).

APPENDIX I

Observed frequencies (cm^{-1}) and assignments for various 'impurities'

Control spectra were run on possible impurities in order to clarify certain sample spectra. The following were the species studied:

I.1 SiH_3Br - N_2 matrix

(assignment assumes a C_{3v} configuration)

2233	s	ν_1, ν_4, SiH stretches
2224	s	
2210	m.s.	
948.5	w	ν_5, SiH asymmetric deformations
943.9	s	
939.5	s	
922.0	v.s.	ν_2, SiH symmetric deformation
642.0	w	ν_6, SiH rock
638.3	w	
633.1	w	
631.1	w	
421.4	s	ν_3, SiBr stretch

I.2 $(SiH_3)_2O$ - N_2 matrix

2202	v.s.	SiH stretches
2192	v.s.	
2183	m.s.	
1105.5	v.s.	SiOSi asymmetric stretch
961.4(sh)	v.s.	SiH deformations
959.0	v.s.	
948.6	v.s.	
763.4	s	SiH_3 rocks
746.2	s	

I.3 HNCO, $HN^{13}CO$, DNCO - Ar matrix

HNCO	$HN^{13}CO$	DNCO		
3516	3515	2616	w	NH stretch
2258.7	2198	2228	v.s.	NCO asymmetric stretch
769.0	758.5	456.5s		HNC bend?
573.0	565.6	572.5s		NCO bend?

I.4 $HN^{13}CO$ - N_2 matrix

3487	s	NH stretch
2208	v.s.	NCO asymmetric stretch
760.0(br)	w	HNC bend?
569.4	s	NCO bend?

I.5 $GeH_3Br - N_2$ matrix

2153	s	GeH stretches
2147	s	
2132	s	
868.3	s	GeH asymmetric deformations
865.7	s	
827.3	v.s.	GeH symmetric deformation
592.5	m.s.	GeH_3 rocks
580.6	m.s.	
297.2	s	GeBr stretch

I.6 CO_2 - solid

3710	v.s.	combination bands
3600	v.s.	
2455	v.s.	OCO asymmetric stretch
2350(br)	v.s.	
2280	v.s.	OCO asymmetric stretch, ^{13}C natural abundance
1382	w	Fermi interaction of 2 x OCO bend with OCO symmetric stretch
1275	w	
760(br)	w	?
662	v.s.	OCO bend
638	v.s.	OCO bend, ^{13}C natural abundance

I.7 Allene - solid

3200(br)	w	CH stretches
3060	m.s.	
3008	m.s.	
2982	m.s.	
1947	v.s.	CCC asymmetric stretch
1902	w	CCC asymmetric stretch, ^{13}C natural abundance
1700(br)	s	overtone 2x848 cm^{-1} = 1696 cm^{-1}
1434	s	?
1382	v.s.	CH deformations
1353(sh)	w	
1069	w	?
1000	s	?
848	v.s.	CH rocks
358	v.s.	CCC bend

APPENDIX II

Computer Programming Work

II.1 Programme for Calculating Eigenvalues for a 2-D Oscillator

The eigenvalue programme was developed from a method used to calculate eigenvalues for a 1-dimensional problem[60]. The one dimensional problem in dimensionless coordinates is a Schroedinger equation of the form:

$$-\frac{d^2\psi}{dr^2} + V(r)\psi = E\psi.$$

The procedure for solving this equation employs integration to give values of the wavefunction at a particular point using the second order difference equation,

$$Y(r+h) + Y(r-h) - 2Y(r) = h^2(V(r)-E)\psi(r),$$

where $Y(r) = \{1 - \frac{h^2}{12}(V(r)-E)\}\psi(r)$. h is the interval between each integration point, V(r) is the potential at r, E is a trial energy value.

Integration begins at a suitably large value of r by setting $\psi(r+h)$ to a small arbitrary value and letting

$$\psi(r) = \psi(r+h)\ \exp\{(r+h)(V(r+h)-E)^{\frac{1}{2}} - r(V(r)-E)^{\frac{1}{2}}\}.$$

This expression is derived from the exponential decay

expected for a wavefunction within a potential barrier. After fixing the first two points, inward integration proceeds by the difference equation until ψ reaches a maximum. Outward integration is begun by setting $\psi(0) = 0$ and letting $\psi(h)$ have a small arbitrary value, and thereafter is continued until reaching the limit of the backward integration. The values of ψ are normalised at this point.

If the trial value, E, is not an eigenvalue, the slopes of the wavefunction, ψ, will not match at the meeting of the backward and forward integrations. A correction, D(E), is applied to the value, E, according to

$$D(E) = \frac{\{(-Y(r-h)+2Y(r)-Y(r+h))h^{-2}+(V(r)-E)\psi(r)\}}{\sum_r \psi(r)^2}$$

$$E' = E+D(E)$$

The whole process is then repeated with the new value, E', until D(E) becomes smaller than a specified value. Modifications to this procedure for a 2-dimensional problem were as follows:

Instead of the equation above, the 2-D radial equation is,

$$-\frac{1}{r}\frac{d}{dr}\left(r\frac{d\psi}{dr}\right) + V(l,r) = E\psi$$

where $V(l,r) = V(r) + \frac{l^2}{r^2}$, $r^2 = x^2+y^2$.

Making the substitution $\psi = r^{-\frac{1}{2}}P$ we obtained:

$$-\frac{d^2P}{dr^2} + \{V(l,r) - \frac{1}{4r^2}\}P = EP$$

$$\rightarrow \quad -\frac{d^2P}{dr^2} + V_{eff}(l,r)P = EP$$

where $V_{eff}(l,r) = V(r) + \frac{l^2-0.25}{r^2}$

This is now in the correct form for use with the above method. The 2-dimensional form has been programmed to give eigenvalues for a given l (angular momentum quantum number) and V(r). At r = 0, V_{eff} becomes infinite and this is approximated in the programme by a very large real number. In any case, $\psi_0 = 0$ is set at the beginning of the integration - physically reasonable since at r = 0, V = ∞.

In calculating the eigenvalue the function P(r) is also calculated. By counting the number of nodes, m, in this radial wavefunction, the vibrational quantum number, v, can be assigned according to v = l + m. With the function P(r) it is also possible to calculate

quantities like $\langle r^2 \rangle$ and $\langle r^4 \rangle$ which are useful in, for example, calculating B rotational constants in a particular quantum state using empirical equations of the form $B_{v,l} = \alpha\langle r^2 \rangle + \gamma\langle r^4 \rangle + const.$

A listing of the eigenvalue programme, SUBROUTINE VALUE, is given in the following pages. Initially the parameters defining the potential are supplied together with a specified l quantum number. The programme then goes through a loop where trial energies are supplied and eigenvalues are output. It is possible after each eigenvalue output to change the l quantum number if desired or to end the computation.

Separate subroutines (also listed) are called to perform the backward and forward integrations and to apply the corrections to the trial energy values. After the eigenvalue has been calculated, the number of nodes is found and the quantum state output. Such values as $\langle r^2 \rangle$ and $\langle r^4 \rangle$ are then also calculated.

II.2 Programme to Calculate Coriolis Coupling Constants

(Refer to theory of coriolis coupling constant calculations - Chapter 2).

SUBROUTINE CORIOLIS was called by the normal coordinate refinement programme after the force field had been defined. The following page shows a listing of the

```
      SUBROUTINE VALUE
C     CALCULATES EIGEN ENERGIES FOR GIVEN 2-D POTENTIAL
      IMPLICIT REAL*8(A-H,O-Z)
      DIMENSION P(501),R(501),U(501)
      DATA NOTRY,NO,DELTA,EPSIL,TOL/50,501,2*1.0D-70,1.0D-06/
      CALL EMASFC('DEFINE',6,'8,OUT',5)
      CALL FPRMPT('V2 :',4)
      READ(5,101)V2
      CALL FPRMPT('VH :',4)
      READ(5,101)VH
      CALL FPRMPT('VW :',4)
      READ(5,101)VW
      CALL FPRMPT('RATIO:',6)
      READ(5,101)RATIO
      CALL FPRMPT('SCALE:',6)
      READ(5,101)SCALE
      WRITE(8,100)V2,VH,VW,RATIO,SCALE
100   FORMAT(' HARMONIC + LORENTZIAN + ANG. MOM. PARAMETERS-V2,VH,
     XVW,RATIO,SCALE',5F12.4)
      UMIN=VW*(2.0*DSQRT(V2*VH)-V2*VW)
      HUMP=VH-UMIN
      RMIN=VW*DSQRT(DSQRT(VH/(V2*VW**2))-1)
      V2=V2/RATIO
      VH=VH/RATIO
      UMIN=UMIN/RATIO
      WRITE(6,105)RMIN,HUMP
      WRITE(8,105)RMIN,HUMP
105   FORMAT(' MINIMUM AT',F10.3,6X,'HUMP =',F10.3)
      WRITE(8,108)
108   FORMAT('  V',3X,'L',3X,'EIGENVALUE',3X,'<R**2>',3X,'<R**4>'
     X,3X,'THETA',4X,'B/MHZ')
4     CALL FPRMPT('L QUANTUM NO. :',15)
      READ(5,102)L
      CALL DIST(U,R,V2,VH,VW,NO,L,H,UMIN)
1     CALL FPRMPT('TRIAL ENERGY  :',15)
      READ(5,101)E
      IF(E.EQ.0)GO TO 2
      IF(E.EQ.999)GO TO 4
      E=E/RATIO
C
C     FIND EIGENVALUE
C
      DO 14 I=1,NOTRY
      IFAIL=0
      CALL BACKINT(P,R,U,E,H,EPSIL,NO,IFAIL,LIMIT,BPM)
C
C     INDICATE FAILURE TO FIND MAXIMUM
C
      IF(IFAIL.EQ.0)GO TO 15
      WRITE(6,1005)
1005  FORMAT('0','FAILS TO FIND MAXIMUM IN WAVE FUNCTION')
      GO TO 1
15    CALL FORWINT(P,R,U,NO,DELTA,H,E,LIMIT,FPM,L)
      CALL NORMA(P,NO,FPM,BPM,LIMIT)
      CALL CORRE(P,R,U,NO,LIMIT,E,H,CORR)
C
C     PRINT OUT ENERGY VALUE AND CHECK FOR CONVERGENCE
C
      IF(DABS(CORR).LT.TOL)GO TO 13
14    CONTINUE
      WRITE(6,1003)NOTRY
1003  FORMAT('0','FAILS TO REACH ACCURACY AFTER',I4,'ATTEMPTS')
      GO TO 1
13    CALL NODES(P,M,NO)
      E=E*RATIO
      M1=M+L
      CALL EXPEC(P,R,NO,R2,R4)
      THETA=57.29577951*DSQRT(R2)
      R2=R2*SCALE**2
      R4=R4*SCALE**4
      BV=2457.3+67.0*R2-2.0*R4
      WRITE(8,1009)M1,L,E,R2,R4,THETA,BV
1009  FORMAT(I3,I4,F13.7,2F9.4,F8.2,F10.2)
      WRITE(6,1004)E,M,M1,L
1004  FORMAT(' EIGENVALUE IS ',F13.6,'  NO. OF NODES =',I3
     X,4X,'V =',I3,4X,'L =',I3)
      GO TO 1
2     RETURN
101   FORMAT(F8.2)
102   FORMAT(I2)
      END
```

```
      SUBROUTINE BACKINT(P,R,U,E,H,EPSIL,NO,IFAIL,LIMIT,BPM)
      IMPLICIT REAL*8(A-H,O-Z)
      DIMENSION P(NO),U(NO),R(NO)
C
C     ROUTINE USES TWO GIVEN VALUES OF PSI AND
C     INTEGRATES BACK TOWARDS THE ORIGIN UNTIL PSI
C     REACHES A MAXIMUM
C
C     SET INITIAL VALUES
C
      P(NO)=EPSIL
      P(NO-1)=EPSIL*DEXP(R(NO)*DSQRT(U(NO)-E)
     C           -R(NO-1)*DSQRT(U(NO-1)-E))
C
C     ESTIMATE OTHER POINTS
C
      DO 30 I=3,NO
      J=NO-I+2
      P(J-1)=(P(J)*(5.0*H**2*(U(J)-E)/6.0+2.0)+P(J+1)*
     X(H**2*(U(J+1)-E)/12.0-1.0))/(1.0-H**2*(U(J-1)-E)/12.0)
C
C     FIND MAXIMUM
C
      IF(P(J-1).LT.P(J)) GO TO 31
30    CONTINUE
C
C     CHECKFOR FAILURE TO PEAK
C
      IF(I.EQ.NO) IFAIL=1
      GO TO 32
C
C
C     INDICATE MAXIMUM
C
31    LIMIT=J
      BPM=P(J)
32    RETURN
      END

      SUBROUTINE FORWINT(P,R,U,NO,DELTA,H,E,LIMIT,FPM,L)
C
C       ROUTINE CARRIES FOWARD INTEGRATION FROM ORIGIN
C     USING SOME INITIAL ESTIMATE FOR FIRST TWO  POINTS
C
      IMPLICIT REAL*8(A-H,O-Z)
      DIMENSION P(NO),U(NO),R(NO)
      P(1)=0.0
      P(2)=DELTA
      P(3)=DELTA*2.0**(DFLOAT(L)+0.5)
      N=LIMIT-1
      DO 40 I=3,N
      P(I+1)=(P(I-1)*(1.0-H**2*(U(I-1)-E)/12.0)-P(I)*
     X(5.0*H**2*(U(I)-E)/6.0+2.0))/(H**2*(U(I+1)-E)/12.0-1.0)
40    CONTINUE
      FPM=P(LIMIT)
      RETURN
      END


      SUBROUTINE NORMA(P,NO,FPM,BPM,LIMIT)
C
C     ROUTINE NORMALISES RESULTS OF
C     FORWARD AND BACKWARD INTEGRATIONS BY
C     SETTING VALUES OF BOTH AT MAXIMUM TO 1.0
C
      IMPLICIT REAL*8(A-H,O-Z)
      DIMENSION P(NO)
      DO 50 I=1,LIMIT
50    P(I)=P(I)/FPM
      K=LIMIT+1
      DO 51 I=K,NO
51    P(I)=P(I)/BPM
      RETURN
      END
```

```
      SUBROUTINE CORRE(P,R,U,NO,LIMIT,E,H,CORR)
C
C     ROUTINE FINDS THE CORRECTION TO BE MADE TO
C     VALUE OF E BEFORE REPEATING PROCESS.
C
      IMPLICIT REAL*8(A-H,O-Z)
      DIMENSION P(NO),U(NO),R(NO),Y(3)
      Y(1)=(1.0-H**2*(U(LIMIT-1)-E)/12.0)*P(LIMIT-1)
      Y(2)=(1.0-H**2*(U(LIMIT)-E)/12.0)*P(LIMIT)
      Y(3)=(1.0-H**2*(U(LIMIT+1)-E)/12.0)*P(LIMIT+1)
      SUM=0.0
      DO 60 I=1,NO
60    SUM=SUM+P(I)**2
      CORR=((-Y(1)+2.0*Y(2)-Y(3))/H**2+(U(LIMIT)-E)
     X*P(LIMIT))/SUM
      E=E+CORR
      RETURN
      END


      SUBROUTINE NODES(P,M,NO)
      IMPLICITREAL*8(A-H,O-Z)
      DIMENSION P(NO)
      K=NO-1
      M=0
      DO 1 J=2,K
      P1=P(J)*P(J+1)
      IF(P1.LT.0.0D 00)M=M+1
1     CONTINUE
      M=2*M
      RETURN
      END
      SUBROUTINE DIST(U,R,V2,VH,VW,NO,L,H,UMIN)
      IMPLICITREAL*8(A-H,O-Z)
      DIMENSION U(NO),R(NO)
      H=3.0/DFLOAT(NO-1)
      DO 1 I=1,NO
      R(I)=(I-1)*H
      IF(R(I).EQ.0.0)U(I)=1.0D70
      IF(R(I).EQ.0.0)GO TO 1
      U(I)=V2*R(I)**2+VH/(1.0+R(I)**2/VW**2)-UMIN
     X+(L**2-0.25)/R(I)**2
1     CONTINUE
      RETURN
      END
      SUBROUTINE EXPEC(P,R,NO,R2,R4)
      IMPLICITREAL*8(A-H,O-Z)
      DIMENSION P(NO),R(NO)
      SUM1=0.0
      SUM2=0.0
      SUM3=0.0
      DO 1 I=1,NO
      SUM1=SUM1+P(I)**2
      SUM2=SUM2+R(I)**2*P(I)**2
      SUM3=SUM3+R(I)**4*P(I)**2
1     CONTINUE
      R2=SUM2/SUM1
      R4=SUM3/SUM1
      RETURN
      END
      SUBROUTINE CHECK(M1,L,E,*)
      IMPLICITREAL*8(A-H,O-Z)
      M2=M1+L
      S1=DFLOAT(M2)/2.0+0.000001
      M3=2*IDINT(S1)
      IF(M2.NE.M3)GO TO 2
      RETURN
2     WRITE(6,100)E
100   FORMAT(' INVALID EIGENVALUE',2X,F13.7)
      RETURN 1
      END
```

programme.

The input parameters to the routine are:

N the number of atoms in the molecule under study.

NP the number of vibrational modes. This, of course, can be calculated from N. However, NP was used in the main programme to construct the $\underline{L}$ and $\underline{B}$ matrices to input to the subroutine. The final value after all symmetry species have been refined is 3N-6 (or 3N-5 for linear molecules).

AW array containing the atomic masses for all isotopic species.

BY array containing the $\underline{B}$ matrix transpose, constructed in columns after each symmetry species.

WLH array containing the $\underline{L}$ matrix transpose. It has block diagonal structure, each block added after refinement of each symmetry species.

The subroutine sets up the three $\underline{I}_\mu$ matrices corresponding to the three orthogonal directions. Each then undergoes the matrix multiplications as described in Chapter 2 (routines GMPRD and GTPRD) with zeta matrices output as TX, TY, TZ for the three directions. SUBROUTINE CORIOLIS is a general routine (as is the normal coordinate refinement programme) which calculates

```
      SUBROUTINE CORIOLIS(N,NP,AW,BY,WLH)
      DIMENSION AW(10,20),BY(30,30),WLH(30,30),V1(30),V2(30)
     #,TX(30,30),TY(30,30),TZ(30,30),A(900),B(900),C(900),D(900),E(900)
      DATA TX,TY,TZ/2700*0.0/
      DO 5 I=1,N
      K=1+3*(I-1)
      J=K+1
      TX(K,J)=1/AW(1,I)
      TX(J,K)=-1/AW(1,I)
      J=J+1
      TY(K,J)=1/AW(1,I)
      TY(J,K)=-1/AW(1,I)
      K=K+1
      TZ(K,J)=1/AW(1,I)
      TZ(J,K)=-1/AW(1,I)
5     CONTINUE
      M=3*N
      CALL ARRAY(2,M,NP,30,30,A,BY)
      CALL ARRAY(2,M,M,30,30,B,TX)
      CALL ARRAY(2,M,M,30,30,C,TY)
      CALL ARRAY(2,M,M,30,30,D,TZ)
      CALL GMPRD(B,A,E,M,M,NP)
      CALL GMPRD(C,A,B,M,M,NP)
      CALL GMPRD(D,A,C,M,M,NP)
      CALL GTPRD(A,E,D,M,NP,NP)
      CALL GTPRD(A,B,E,M,NP,NP)
      CALL GTPRD(A,C,B,M,NP,NP)
      CALL ARRAY(2,NP,NP,30,30,A,WLH)
      CALL MINV(A,NP,DET,V1,V2)
      CALL GMPRD(D,A,C,NP,NP,NP)
      CALL GMPRD(E,A,D,NP,NP,NP)
      CALL GMPRD(B,A,E,NP,NP,NP)
      CALL GTPRD(A,C,B,NP,NP,NP)
      CALL GTPRD(A,D,C,NP,NP,NP)
      CALL GTPRD(A,E,D,NP,NP,NP)
      CALL ARRAY(1,NP,NP,30,30,B,TX)
      CALL ARRAY(1,NP,NP,30,30,C,TY)
      CALL ARRAY(1,NP,NP,30,30,D,TZ)
      WRITE(1,104)
      WRITE(6,104)
104   FORMAT(1HO,'ZETA MATRIX X-DIRECTION')
      DO 18 I=1,NP
      WRITE(1,105)(TX(I,K),K=1,NP)
      WRITE(6,105)(TX(I,K),K=1,NP)
18    CONTINUE
      WRITE(1,106)
      WRITE(6,106)
106   FORMAT(1HO,'ZETA MATRIX Y-DIRECTION')
      DO 19 I=1,NP
      WRITE(1,105)(TY(I,K),K=1,NP)
      WRITE(6,105)(TY(I,K),K=1,NP)
19    CONTINUE
      WRITE(1,108)
      WRITE(6,108)
108   FORMAT(1HO,'ZETA MATRIX Z-DIRECTION')
      DO 20 I=1,NP
      WRITE(1,105)(TZ(I,K),K=1,NP)
      WRITE(6,105)(TZ(I,K),K=1,NP)
20    CONTINUE
105   FORMAT(1H,30F7.3)
      RETURN
      END
```

zeta constants for any molecule studied up to a limit of N = 10.

II.3 Data Averaging for Far Infrared Spectra

As described in the experimental chapter (Chapter 3), the far infrared spectra were stored as data points on a disc linked to the Edinburgh computer system. The file containing the Fourier transformed spectrum has two storage areas, one holding the background array, the other the background + sample array. In order to obtain better spectra, a number of separately scanned spectra, held in different files, were averaged digitally by SUBROUTINE AVERAG (see next page).

The files holding the spectra are direct access files, each having the first three letters DAF. Much of the subroutine is employed in defining the input and output streams to the programme. The programme firstly prompts the user to indicate whether he wishes to average the background or sample + background array, and then calls for the number of spectra, N, to be averaged. The programme then asks for N different four digit codes which name the files holding the spectra and assigns each a different input stream. For example if the code of the first file is "ABCD" then the file "DAFABCD" is defined as the first input stream.

After the input files have been defined, a code is

```
      SUBROUTINE AVERAG
C     AVERAGES SPECTRA
      DIMENSION IN(3),IF(6),A(6000),P(5,6000)
      DATA IB,IN(2),IF/'S   ',',DAF','FT21','FT22','FT23','FT24'
     #,'FT25','FT20'/
      IK=202
      CALL FPRMPT('AVERAGE S OR B?',15)
      READ(5,101)IA
      IF(IA.NE.IB)IK=2
      CALL FPRMPT('NO. OF FILES:',13)
      READ(5,105)N
      IF(N.GT.5)GO TO 5
      WRITE(6,102)
      DO 1 I=1,N
      CALL FPRMPT('CODE:',5)
      READ(5,101)IN(3)
      IN(1)=IF(I)
      CALL EMASFC('DEFINE',6,IN,12)
1     CONTINUE
      IF(N.EQ.5)GO TO 4
      K=N+1
      DO 3 I=K,5
      IN(1)=IF(I)
      CALL EMASFC('DEFINE',6,IN,12)
3     CONTINUE
4     WRITE(6,103)
      CALL FPRMPT('CODE:',5)
      READ(5,101)IN(3)
      IN(1)=IF(6)
      CALL EMASFC('DEFINE',6,IN,12)
      DEFINE FILE 20(401,30,U,IJ)
      DEFINE FILE 21(401,30,U,IJ)
      DEFINE FILE 22(401,30,U,IJ)
      DEFINE FILE 23(401,30,U,IJ)
      DEFINE FILE 24(401,30,U,IJ)
      DEFINE FILE 25(401,30,U,IJ)
      DO 7 I=1,N
      M=20+I
      READ(M'IK)A
      DO 8 J=1,1024
      P(I,J)=A(J)
8     CONTINUE
7     CONTINUE
      DO 9 J=1,1024
      SUM=0.0
      DO 10 I=1,N
      SUM=SUM+P(I,J)
10    CONTINUE
      A(J)=SUM/FLOAT(N)
9     CONTINUE
      WRITE(20'IK)A
      IF(IK.EQ.202)WRITE(6,100)
      IF(IK.EQ.2)WRITE(6,110)
      GO TO 6
5     WRITE(6,104)
6     RETURN
100   FORMAT(1HO,' SPECTRAL AVERAGE COMPLETED')
101   FORMAT(A4)
102   FORMAT(1HO,'SUPPLY FILE CODES')
103   FORMAT(1HO,'SUPPLY OUTPUT FILE CODE')
104   FORMAT(1HO,' MAXIMUM N IS 5!')
105   FORMAT(I1)
110   FORMAT(1HO,' BACKGROUND AVERAGE COMPLETED')
      END
```

prompted for the name of the output file in which the averaged spectrum is to be stored. The programme then reads the required arrays from each input file, calculates an average for each point, and writes the result into the specified file. The resulting file can then be used to output the averaged sample spectrum.

II.4 3-Dimensional Least Squares Fit

A computer programme was written to perform a least squares fit of the form $Z = a + bx + cy$ on a set of observed data. Let the observed values of Z be z for known values of x and y - the parameters a, b, c are calculated to give the least squares fit on the observed data z.

The squared deviation of calculated and observed values at a given x,y is:

$$s = (z-a-bx-cy)^2.$$

The sum over all x and y is $T = \sum_n s$

$$= \sum_n (z-a-bx-cy)^2.$$

Least squares solution for a, b, c requires that $\frac{\partial T}{\partial a} = \frac{\partial T}{\partial b} = \frac{\partial T}{\partial c} = 0$. This results in the equations:

$$\sum_n (z-a-bx-cy) = 0$$

$$\sum_n (z-a-bx-cy)x = 0$$

$$\sum_n (z-a-bx-cy)y = 0.$$

Multiplying out and dividing by the number of data points we obtain the three equations:

$$\bar{z}-a-b\bar{x}-c\bar{y} = 0$$

$$\overline{xz}-a\bar{x}-b\overline{x^2}-c\overline{xy} = 0$$

$$\overline{yz}-a\bar{y}-b\overline{xy}-c\overline{y^2} = 0$$

There are three equations in three unknowns, a, b, c:

$$a = \frac{\overline{x^2}.\bar{y}.\bar{z}.\overline{y^2}-\overline{x^2}.\bar{y}^2.\overline{yz}+\bar{x}.\overline{xy}.\bar{y}.\overline{zy}-\bar{z}.\overline{xy}^2.\bar{y}+\bar{y}^2.\overline{xz}.\overline{xy}-\bar{x}.\overline{y^2}.\bar{y}.\overline{xz}}{2\bar{x}.\bar{y}^2.\overline{xy}-\overline{xy}^2.\bar{y}-\bar{x}^2.\bar{y}.\overline{y^2}-\overline{x^2}.\bar{y}^3+\overline{x^2}.\bar{y}.\overline{y^2}}$$

$$b = \frac{\bar{y}.\overline{xz}-\bar{z}.\overline{xy}-a(\bar{x}.\bar{y}-\overline{xy})}{\overline{x^2}.\bar{y}-\bar{x}.\overline{xy}}$$

$$c = \frac{\bar{z}-a-b\bar{x}}{\bar{y}}$$

The programme shown on the next page uses the above formulae in the case of a least squares fit of the Q branch positions of symmetric top perpendicular infrared bands (see Chapter 2). Here, x ≡ K quantum number and y ≡ K^2. In this case the parameters a, b, c are the values:

$$\nu_0+\{A'(1-2\zeta_i)-B'\},\ 2\{A'(1-\zeta_i)-B'\},\ (A'-B')-(A''-B'').$$

SUBROUTINE LSQS first calls for the number of data points, N, to be input. This includes any unobserved

```
      SUBROUTINE LSQS
C     LEAST SQUARES SURFACE FIT
      IMPLICITREAL*8(A-H,O-Z)
      DIMENSION X(100),Y(100),Z(100),ZC(100),ZS(100),SUM(9)
      DATA SUM/9*0.0/
      CALL FPRMPT('NO. OF POINTS:',14)
      READ(5,106)N
      CALL FPRMPT('-VE K VALUES :',14)
      READ(5,106)N1
      CALL FPRMPT('OBS. FREQ.   :',14)
      M=0
      DO 1 I=1,N
      M=M+1
      READ(5,107)Z(M)
      ZS(I)=Z(M)
      K=I-N1-1
      X(M)=DFLOAT(K)
      Y(M)=X(M)**2
      IF(Z(M).EQ.0.0)GO TO 4
      GO TO 1
4     M=M-1
1     CONTINUE
      DO 2 I=1,M
      SUM(1)=SUM(1)+X(I)
      SUM(2)=SUM(2)+Y(I)
      SUM(3)=SUM(3)+Z(I)
      SUM(4)=SUM(4)+X(I)*Z(I)
      SUM(5)=SUM(5)+X(I)*Y(I)
      SUM(6)=SUM(6)+Y(I)*Z(I)
      SUM(7)=SUM(7)+X(I)**2
      SUM(8)=SUM(8)+Y(I)**2
2     CONTINUE
      D=DFLOAT(M)
      XB=SUM(1)/D
      YB=SUM(2)/D
      ZB=SUM(3)/D
      XZB=SUM(4)/D
      XYB=SUM(5)/D
      YZB=SUM(6)/D
      X2B=SUM(7)/D
      Y2B=SUM(8)/D
      P1=X2B*YB*ZB*Y2B
      P2=X2B*YB**2*YZB
      P3=XB*XYB*YB*YZB
      P4=ZB*XYB**2*YB
      P5=YB**2*XZB*XYB
      P6=XB*Y2B*YB*XZB
      P7=XB*YB**2*XYB
      P8=XYB**2*YB
      P9=XB**2*YB*Y2B
      P10=X2B*YB**3
      P11=X2B*YB*Y2B
      A=(P1-P2+P3-P4+P5-P6)/(2.0*P7-P8-P9-P10+P11)
      B=(YB*XZB-ZB*XYB-A*(XB*YB-XYB))/(X2B*YB-XB*XYB)
      C=(ZB-A-B*XB)/YB
      WRITE(14,103)
      WRITE(14,104)A,B,C
      WRITE(14,105)
      DO 3 I=1,N
      K=I-N1-1
      X(I)=DFLOAT(K)
      Y(I)=X(I)**2
      ZC(I)=A+X(I)*B+Y(I)*C
      Z(I)=ZS(I)-ZC(I)
      IF(ZS(I).EQ.0.0)Z(I)=0.0
      WRITE(14,107)ZS(I),ZC(I),Z(I)
      SUM(9)=SUM(9)+Z(I)**2
3     CONTINUE
      RMS=DSQRT(SUM(9)/D)
      WRITE(14,110)RMS
      RETURN
103   FORMAT(' DERIVED PARAMETERS')
104   FORMAT(3F15.5)
105   FORMAT('      FREQ.OBS.      FREQ.CALC.      OBS.-CALC.')
106   FORMAT(I3)
107   FORMAT(3F15.2)
110   FORMAT(' RMS DEVIATION = ',F7.3)
      END
```

values for a particular K. The programme then calls for the number of negative K values. The N observed frequencies are then input in sequence, lowest frequency first. An unobserved value is entered as 0.0. After all the frequencies have been stored, the programme calculates the average values for use in the above formulae and then evaluates a, b and c. Using the calculated a, b, c a list of observed and calculated frequencies is output together with the 'observed-calculated' values and the root mean square deviation.

II.5 Symmetric Top Perpendicular Band Contour

A programme was written to calculate the band contour for the v = 0 → v = 1 transition of SiH_3CN, ν_8. This was done in order to compare the observed and calculated band shapes and therefore deduce whether a hot band transition is observed.

Theory[15]

The intensity, I, of an infrared transition is proportional to the frequency of the transition, ν.

$$I \propto A_{KJ} \nu g_{KJ} e^{-\frac{F(K,J)hc}{KT}}$$

For the v = 0 state of a symmetric top the rotational levels are:

$$F_{[v]}(J,K) = B_{[v]}J(J+1)+(A_{[v]}-B_{[v]})K^2-D_J^{[v]}J^2(J+1)^2$$
$$- D_{JK}^{[v]}J(J+1)K^2-D_K^{[v]}K^4.$$

For the v = 1 state of a symmetric top (degenerate level) the rotational levels are:

$$F'_{[v]}(J,K) = B_{[v]}J(J+1)+(A_{[v]}-B_{[v]})K^2\mp 2A_{[v]}\zeta_i K$$
$$- D_J^{[v]}J^2(J+1)^2-D_{JK}^{[v]}J(J+1)K^2-D_K^{[v]}K^4.$$

$\nu = F'-F+\nu_O$ where ν_O is the band origin, g_{kJ} is the multiplicity of the rotational level concerned and is equal to 2J+1 for K = 0 and 2(2J+1) for K ≠ 0. A_{kJ} is an intensity factor related to J and K for the lower state.

The selection rules for a perpendicular band are $\Delta J=0, \pm 1; \Delta K=\pm 1$.

$$A_{kJ} = \frac{(J+2\pm K)(J+1\pm K)}{(J+1)(2J+1)} \qquad \Delta J = +1$$

$$= \frac{(J+1\pm K)(J\mp K)}{J(J+1)} \qquad \Delta J = 0$$

$$= \frac{J-1\mp K)(J\mp K)}{J(2J+1)} \qquad \Delta J = -1.$$

The upper sign refers to $\Delta K = +1$, lower to $\Delta K = -1$.

For K = 0 and $\Delta K = +1$ this factor is twice the magnitude stated. Also, taking account of the nuclear spin statistics for SiH_3CN (3 off-axis atoms with spin ½) A_{KJ} has twice the magnitude for K, a multiple of 3.

The programme listed on the following page calculates the band contour of a symmetric top perpendicular band - specifically that of SiH_3CN, ν_8. Initially the rotational constants A', A", B', B", D'_J, D''_J, D'_{JK} and D''_{JK} are set, together with the zeta constant for the upper state. There are then a series of loops which calculate the frequencies and intensities for each rotational transition.

The outer loop deals with firstly the $\Delta K = +1$ transitions and then the $\Delta K = -1$ transitions. Within this loop transition frequencies and intensities are calculated for K up to 40. The inner loop deals with the $\Delta J = +1$, $\Delta J = 0$ and $\Delta J = -1$ transitions in turn, up to a value of J = 100.

At each stage g_{KJ} and A_{KJ} are set according to the J and K values. The intensity is calculated, using the above equation for each individual rotational transition. This intensity is then added to a storage array according to the frequency of the transition. The summed data in the store is normalised and output to a graph plotting routine giving a band contour.

```
C     IR PERP. BAND CONTOUR - C3V WITH I=1/2 OFF AXIS ATOMS
      IMPLICITREAL*8(A-H,0-Z)
      DIMENSION FREQ(100),ABS(100)
      DATA ABS/100*0.0/
      ZETA=0.890
      AD=2.7667
      ADD=2.7667
      BD=0.1665
      BDD=0.1658
      DJD=5.7D-08
      DJDD=4.9667D-08
      DJKD=2.2067D-06
      DJKDD=2.1133D-06
      CENTRE=235.0
      DO 7 I=1,100
      FREQ(I)=CENTRE+1.2207*I-50*1.2207
7     CONTINUE
      DO 3 I=1,2
      DO 1 K2=1,40
      WRITE(6,110)K2
      K=K2-1
      IF(I.EQ.2.AND.K.EQ.0)GO TO 1
      IF(I.EQ.1)K1=K+1
      IF(I.EQ.2)K1=K-1
      IF(I.EQ.1)F=1.0
      IF(I.EQ.2)F=-1.0
      DO 4 M=1,3
      DO 2 J2=K2,100
      J=J2-1
      IF(M.EQ.3.AND.J.EQ.0.OR.M.EQ.2.AND.J.EQ.0)GO TO 2
      IF(M.EQ.1)J1=J+1
      IF(M.EQ.2)J1=J
      IF(M.EQ.3)J1=J-1
      E1=BDD*J*(J+1)+(ADD-BDD)*K**2-DJDD*J**2*(J+1)**2
     #-DJKDD*J*(J+1)*K**2
      E2=BD*J1*(J1+1)+(AD-BD)*K1**2-2.0*AD*ZETA*K1*F
     #-DJD*J1**2*(J1+1)**2-DJKD*J1*(J1+1)*K1**2
      DIFF=E2-E1
      DIFF=DIFF+CENTRE
      IF(I.EQ.1.AND.M.EQ.1)AKJ=DFLOAT((J+2+K)*(J+1+K))/DFLOAT((J+1)
     #*(2*J+1))
      IF(I.EQ.1.AND.M.EQ.2)AKJ=DFLOAT((J+1+K)*(J-K))/DFLOAT(J*(J+1))
      IF(I.EQ.1.AND.M.EQ.3)AKJ=DFLOAT((J-1-K)*(J-K))/DFLOAT(J*(2*J+1))
      IF(I.EQ.2.AND.M.EQ.1)AKJ=DFLOAT((J+2-K)*(J+1-K))/DFLOAT((J+1)
     #*(2*J+1))
      IF(I.EQ.2.AND.M.EQ.2)AKJ=DFLOAT((J+1-K)*(J+K))/DFLOAT(J*(J+1))
      IF(I.EQ.2.AND.M.EQ.3)AKJ=DFLOAT((J-1+K)*(J+K))/DFLOAT(J*(2*J+1))
      IF(K.EQ.0.AND.I.EQ.1)AKJ=2*AKJ
      Q=DFLOAT(K)/3.0+0.1
      N1=3*IDINT(Q)
      IF(          N1.EQ.K)AKJ=2*AKJ
      GKJ=2*J+1
      IF(K.GT.0)GKJ=2*GKJ
      Y=AKJ*DIFF*GKJ*DEXP(-E1/206.505)
      Z=(DIFF-FREQ(1)+1.2207)/1.2207
      N=IDINT(Z)
      IF(N.GT.100.OR.N.LT.1)GO TO 4
C      ABS(N-2)=ABS(N-2)+Y
C      ABS(N-1)=ABS(N-1)+Y
      ABS(N)=ABS(N)+Y
C      ABS(N+1)=ABS(N+1)+Y
C      ABS(N+2)=ABS(N+2)+Y
2     CONTINUE
4     CONTINUE
1     CONTINUE
3     CONTINUE
      AMAX=ABS(1)
      DO 15 N=2,100
      IF(ABS(N).GT.AMAX)AMAX=ABS(N)
15    CONTINUE
      DO 16 N=1,100
      ABS(N)=ABS(N)/AMAX
16    CONTINUE
      CALL GRAPH(FREQ,ABS,N)
      STOP
110   FORMAT(1H,I8)
      END
```

J.C.S. Faraday II, 1980, **76**, 860–871

Low-frequency Bending Motions of the Silyl Pseudohalides SiH_3NCY (Y = O, S, Se)

An Experimental and Theoretical Study

BY STEPHEN CRADOCK* AND DONALD C. J. SKEA

Department of Chemistry, University of Edinburgh, West Mains Road, Edinburgh EN9 3JJ, Scotland

Received 26th September, 1979

We report the observation of far-infrared bands assigned to fundamental and overtone transitions involving the low-frequency bending motions of the title compounds and the simulation of the spectrum of silyl isocyanate using energy levels deduced from a potential function involving a pure quadratic well with a central hump of Lorentzian form. The observed spectra enable this potential to be specified to a higher level of precision than earlier indirect measurements.

Silyl isocyanate has been investigated repeatedly since its vibrational spectrum was first reported;[1] interest has particularly focused on the low-frequency bending motion, which is of extremely low energy and gives rise to extensive and complex structure in the microwave spectrum because of a very high population of excited-state molecules with effective geometries very different from that of the ground state.[2, 3] On the basis of a detailed study of the microwave spectrum [3] and a careful analysis of the electron diffraction pattern [4] it has been concluded that the molecule is best described as pseudolinear at nitrogen, with a hump at the linear configuration of $\approx 30\ cm^{-1}$ and an average bond angle (room temperature expectation value) of 151.7°. The Raman spectrum of the vapour contains a band peaking near $140\ cm^{-1}$ assigned [5] to the overtone of the bend ($\Delta v = 2$, $\Delta l = 0$ transitions) and apparent fine-structure on the low-frequency side of this band has been analysed in terms of a " quartic–quadratic " potential of the form:

$$V = Aq^4 + Bq^2$$

where q represents a radial coordinate related to the bond angle at nitrogen, characterising a cylindrically-symmetric 2-dimensional potential well. Such potentials have been found to describe the puckering motions of small ring systems;[6] however, there are good reasons for postulating a basically quartic potential for such systems, whereas there seems to be no physically-reasonable basis for such a potential in the bending of a heavy-atom chain.

Recently it has been shown [7] that the microwave data can be explained more precisely in terms of a 3-parameter potential that is basically quadratic with a Gaussian or Lorentzian hump:

$$V = V_2q^2 + V_h \exp(-q^2/V_w^2) \qquad \text{Gaussian hump}$$

or

$$V = V_2q^2 + V_h/(1 + q^2/V_w^2) \qquad \text{Lorentzian hump.}$$

While it is not easy to see what might be the physical origin of either form of hump the basic quadratic well is more familiar than a quartic.

It is also relevant to note that the crystal structure of solid silyl isocyanate,[8] nvestigated at −135°C, shows the molecule to be bent at nitrogen by some 20° from inear.

In all previous spectroscopic investigations no direct observation of the " fundamental " ($\Delta v = 1, \Delta l = 1$) transition has been reported; we have investigated the ar-infrared spectra of SiH_3NCO and SiD_3NCO and used the observations to define a 3-parameter potential that reproduces the bands we observe and some of the microwave observations of Duckett *et al.*[3, 7] It is also possible to suggest a reassignment of some of the apparent fine-structre in the Raman spectrum reported by Durig *et al.*[5] in terms of our potential. We also report, for comparison, the far-nfrared spectra of SiH_3NCS, SiH_3NCSe and SiD_3NCSe; only the isothiocyanate has been studied previously in this region.[9]

EXPERIMENTAL

Far-infrared spectra were obtained using a Beckman-RIIC IR720 interferometer; up to 10 scans were recorded digitally on paper tape and processed using a fast Fourier transform programme. Final spectra were obtained by averaging those spectra that appeared to be free from spurious features such as those due to large noise spikes in the interferogram. In this way we were able to obtain spectra with noise levels of 1 % or less, rather than 2-3 % as with a single scan.

Samples were studied in a 150 cm glass cell with high-density polythene windows; for the isocyanate sample pressures of 70 Torr were used to obtain the best spectra. Sample purity was critical, as the spectrum of HNCO, a usual contaminant, hydrolysis product and decomposition product, is strong and complex in the region of interest (20-220 cm^{-1}). Samples free of HNCO could best be made by reaction [10] of a slight excess of trisilylamine with HNCO; careful fractionation of the product to remove excess $(SiH_3)_3N$ gave a sample of pure SiH_3NCO. This was liable to hydrolysis, giving HNCO and $(SiH_3)_2O$, so all glass to be used for transfer to the cell and the cell itself were dried exhaustively with SiH_3Br. With these precautions we are confident that our final spectra contain no features due to HNCO; spectra containing small peaks due to HNCO were obtained during the purification and drying procedure for comparison.

Spectra of silyl isothiocyanate were obtained using the same instrument and cell; sample purity was less critical here as the spectrum of SiH_3NCS is much stronger than that of the socyanate. For SiH_3NCSe the low vapour pressure (8 Torr) made it easier to prepare a pure sample by fractionation but meant that the observed spectra were relatively weak.

The resolution used in all our spectra to date was 1.2 cm^{-1}; we intend to obtain spectra at higher resolution in the future.

RESULTS

EXPERIMENTAL SPECTRA

These are illustrated in fig. 1. It is noticeable that in all cases there are two bands in the range 20-200 cm^{-1}, one at about twice the frequency of the other, and it seems clear that these must represent the fundamental ($\Delta v = 1$) and overtone ($\Delta v = 2$) transitions. The intensities are comparable, which is not the usual pattern; this seems to be a feature of this particular type of motion rather than due to any special feature of the mechanical potential, as it is common to all three cases, some of which are much closer to harmonic than the isocyanate. On a crude basis, the dipole changes for a bend θ from linear are expected to be $\approx \mu \sin\theta$ perpendicular to the axis and $\mu(1-\cos\theta)$ parallel to the axis, representing the intrinsic intensities of the fundamental and overtone bands, respectively. If, as here, the average bending angle θ is large ($\approx 40°$ on average) these terms are of comparable magnitude, whereas if θ is small the $(1-\cos\theta)$ term rises more slowly with θ than the $\sin\theta$ term.

It is also noticeable that the bands of the isocyanate are both weaker and broade than those of the heavier congeners; this broadness is associated, as we show below with the very anharmonic potential of the isocyanate. There is definite fine-structur in the 80-120 cm^{-1} region in the spectrum of the isocyanate; the peak positions ar listed in table 1, with suggested band designations based on the detailed analysi presented below.

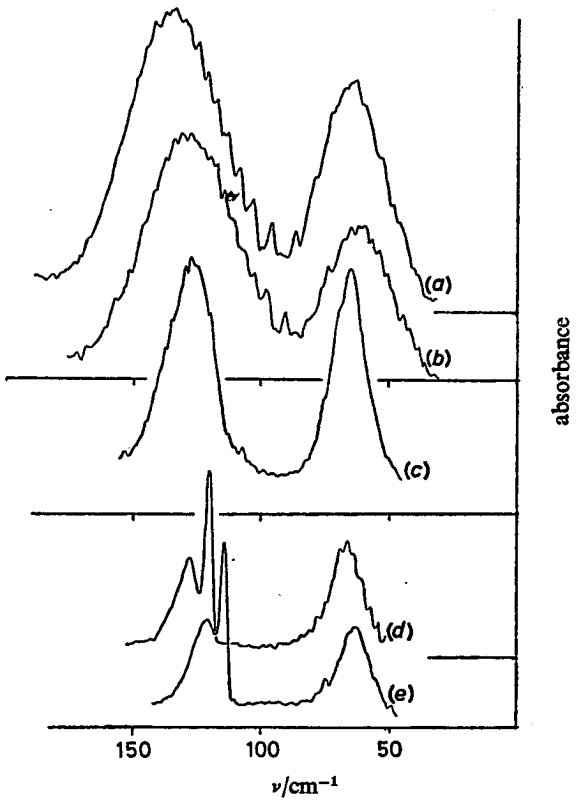

FIG. 1.—Far-infrared spectra of: (*a*) SiH_3NCO; (*b*) SiD_3NCO; (*c*) SiH_3NCS; (*d*) SiH_3NCS and (*e*) SiD_3NCSe.

SIMULATION

The theory of the anharmonic 2-dimensional oscillator has been developed by others [5, 7] and a programme designed to calculate its eigenvalues is available.[11] This uses a variational approach with harmonic oscillator wavefunctions as a basis set. We have adopted an orthogonal approach to the eigenvalue problem, developing a programme based on numerical integration as outlined by Cooley.[12] Details are given in Appendix 1.

Given the eigenvalues for a particular potential, it is necessary to compare the predicted transitions with the observed infrared bands; we have also calculated the expectation values of the coordinate functions $\langle q^2 \rangle$ and $\langle q^4 \rangle$ so as to compare the calculated and observed anomalous variation of the B rotation constant with v and l, the vibrational quantum number and the vibrational angular momentum quantum number.

For a doubly degenerate motion of a symmetric top the relevant selection rules are:

fundamental	$\Delta v = 1, \Delta l = \pm 1$;
overtone	$\Delta v = 2, \Delta l = 0$ or 2.

We have succeeded in simulating the observed spectra using $\Delta v = 1$, $\Delta l = \pm 1$ and $\Delta v = 2$, $\Delta l = 0$ transitions only; the fundamental gives rise to perpendicular bands with rotational selection rules $\Delta l = \pm 1$, $\Delta L = 0, \pm 1$ and the overtone ($\Delta v = 2$, $\Delta l = 0$) gives rise to parallel bands with $\Delta l = 0$, $\Delta J = 0, \pm 1$ rotational selection rules.

It might have been necessary to include transitions with $\Delta l = 2$; in this case the selection rule for k is $\Delta k = \pm 2$, so that $\Delta(k-l) = 0$ and the sub-bands of each vibrational band are about twice as far apart as for the fundamental. The $\Delta l = 2$ band should thus be spread over twice as wide a region, from ≈ 20 to nearly 200 cm^{-1}, and will underlie both observed bands. If results at higher resolution become available it may be possible to pick out lines due to this type of transition. Our present results do not appear to us to be capable of providing information about the relative intensity of the $\Delta l = 2$ band and we have simply omitted it from our preliminary simulations.

TABLE 1.—OBSERVED AND CALCULATED P-HEAD POSITIONS FOR OVERTONE BANDS

SiH_3NCO		SiD_3NCO	
observed/cm^{-1}	calculated/cm^{-1}	assignment	observed/cm^{-1}
—	64.0	0,0–2,0	—
78.7	81.0	1,1–3,1	81.5
86.6	87.2	2,0–4,0	86.7
	95.0	2,2–4,2	94.0
95.5	96.5	3,1–5,1	97.0
	102.0	4,0–6,0	
102.8	103.5	3.3–5,3	103.2
105.0	105.5	4,2–6,2	106.8
107.6	108.5	5,1–7,1	
109.5	111.7	4,4–6,4	111s
	112.0	5,3–7,3	
113.0[a]	112.5	6,0–8,0	
114.0[a]	114.0	6,2–8,2	115[a]
	116.7	7,1–9,1	
	117.5	6,4–8,4	
118.0[a]	117.5	5,5–7,5	118[a]
	118.5	7,3–9,3	
	119.5	8,0–10,0	120[a]
	121.0	8,2–10,2	
122.0[a]	122.2	6,6–8,6	
	122.5	7,5–9,5	
	123.0	8,4–10,4	
	123.2	9,1–11,1	
125[a]	125.2	9,3–11,3	124.5[a]
	125.5	10,2–12,2	
at least 7 more between 126 and 130 cm^{-1}			

[a] Broad feature.

Because the vibrational interval is so small many levels have high populations and many transitions contribute to the bands; we have calculated all eigenvalues up to $\approx 1200\,cm^{-1}$ above the potential minimum, some 120 levels in all. To be able to combine the various transitions in each band it is necessary to know the matrix elements governing the transition moments; for instance, for the fundamental, the harmonic oscillator has a matrix element $\langle v+1, l+1|q_+|v, l\rangle$ of $\frac{1}{2}[2(v+l+2)]^{\frac{1}{2}}$. For the anharmonic oscillator such simple functions do not apply and it is necessary to calculate the matrix elements for each pair of levels required. We have used the values calculated by Robiette [13] using the variation programme, which gives such quantities in matrix form. Although we have used a different potential it is not expected that the values will be very different. (We have calculated the expectation values for q_+, which is directly related to the transition moment for both types of transition, both for our final potential and for Duckett's potential; the values we obtain using Duckett's potential are identical to those derived by Robiette using the variation programme and the values using our final potential differ by ≈ 2 % and in such a fashion that relative intensity calculations will be almost unaffected by the use of values from the other potential.)

At first we attempted to use a standard band shape for each transition; thus the fundamental was simulated using 70 vibrational transitions, each K sub-band being given a standard envelope. Apart from the potential, which governed the vibrational transition energies, the major variable was then the familiar term $2[A(1-\zeta)-B]$, giving the separation of K sub-band origins in a perpendicular band. It soon became clear that although the results were not unreasonable it would be easier to define the potential if the effect of ζ, the Coriolis coupling constant, could be neglected and attention was switched to the overtone band, for which $\Delta k = 0$ and ζ has little effect on the transition energies.

An immediate complication arises from the fact that for parallel bands the Q branch intensity is much less than that of the P or R branch, in contrast with the situation in the perpendicular bands where P, Q and R branches have comparable overall intensity and the narrowness of the Q branch results in its dominating the band shape. This relative weakness of the Q branch implied that the sharp features on the infrared band were in fact P-heads rather than Q branches, arising because of the pronounced change in B with vibrational state. It therefore became necessary to calculate the J fine-structure of each k sub-band of each vibrational transition separately. The final programme used for the simulation of the overtone band took $100\,\Delta v = 2$, $\Delta l = 0$ transitions, with k up to 30 and J up to 102. For every third value of J the P, Q and R branch transition energies and line intensities were obtained by calculating energy levels F and exponential factors E as:

$$F(v, l, k, J) = G(v, l)+(A-B)k^2-2A\zeta kl+A\zeta^2l^2+BJ(J+1)- D_{JK}J(J+1)k^2-D_JJ^2(J+1)^2$$

$$E(v, l, k, J) = \exp[-F(v, l, k, J)/209].$$

For each transition the energy is the difference between the relevant F values and the Boltzmann intensity factor is the difference between the relevant E values (thus taking account of stimulated emission as well as stimulated adsorption).

The statistical factors for P, Q and R branch transitions were taken from Herzberg.[14] Each pair of calculated frequency/intensity data was then added into an array of $0.5\,cm^{-1}$ intervals to generate a band shape for a particular vibrational transition; this was then modified by multiplying each intensity by the corresponding frequency and by the transition moment factor for the particular transition. The

final simulation involved adding all 100 bands and scaling to an arbitrary maximum intensity of 256, chosen to fit a computer graphics package available in our Department, and comparing, both visually and using the root mean square difference, with a similarly digitised and scaled version of the observed (experimental) spectrum from 80 to 180 cm^{-1}.

The full simulation thus required the calculation of $100 \times 30 \times 102 = 306\,000$ pairs of frequency and intensity data, taking a little over 4 min c.p.u. time on an ICL 4-75 computer using the EMAS multi-access system. The parameters required for the calculations were obtained either from our eigenvalue routine [$G(v, l)$ and B] or from the experimental observations of Duckett [7] (D_{JK}, D_J) (as these last were only available for the lowest 20 levels we had to extrapolate for higher levels; asymptotic convergence on values of 2.5×10^{-6} and 2.5×10^{-8} cm^{-1}, respectively, was assumed from the behaviour of those values reported by Duckett). The large rotation constant A was set at 2.91 cm^{-1}, as representing an average over all levels involved, and ζ was set at 0.95 for the initial simulations; the overall band shape is not very sensitive to these parameters.

TABLE 2.—OBSERVED AND CALCULATED B ROTATION CONSTANTS

level v	level l	$B_{observed}$ [a] /MHz	$B^*_{calculated}$ /MHz	Δ(observed−calculated)
0	0	2517.93	2518.23	−0.30
2	0	2543.07	2543.06	0.01
4	0	2577.1	2577.06	0.03
1	1	2542.35	2542.22	0.13
3	1	2565.17	2565.38	0.21
2	2	2562.76	2562.46	0.30
3	3	2581.13	2580.81	0.32

$B^*_{calculated} = B^*_0 + \alpha\langle q^2\rangle + \gamma\langle q^4\rangle$; with $B^*_0 = 2458.7(3)$, $\alpha = 63.5(3)$ and $\gamma = -1.33(5)$ MHz.

[a] Ref. (3).

Trial simulations with potentials similar to those suggested by Duckett [7] showed that the overall band shape of the overtone could be simulated quite well with a potential of this type, but not with potentials of the quartic–quadratic type as suggested by Durig;[5] the fine-structure was not reproduced well, but it appeared that a relatively small change in the potential might markedly improve the fit.

After some further trials it was decided to concentrate on potentials that put the main P-heads for the 4,0 ← 2,0 transition at 86.5 cm^{-1}; the vibrational origin then lay at 92.8 cm^{-1}. As a further constraint, only potentials that reproduced the remarkably small difference [7] in B rotation constant between the levels 2, 0 and 1, 1 (0.716 MHz) with the correct sign ($B_{1,1} < B_{2,0}$) within 0.1 MHz were investigated. The precision of this microwave observation is of the order of 0.01 MHz or better, but the 18 observed B values had to be fitted empirically to a function of $\langle q^2\rangle$ and $\langle q^4\rangle$; the r.m.s. deviation between observed and calculated values was ≈ 0.24 MHz.

These two constraints enabled us to reduce the three-parameter quadratic plus Lorentzian potential to one degree of freedom, which was investigated using the overall fit between observed and simulated overtone band shapes, expressed as r.m.s.

difference between intensities, as the criterion. A clear minimum appeared in the curve of r.m.s. difference against this degree of freedom and a potential was thereby found giving a minimum conventional R factor of 9.7 %.

It was then possible to return to the fundamental. P-heading was not important here, both because of the relative weakness of the P branches relative to the Q branches and because the change of B is only about half as great as for the overtone; however, it was decided to use a level of simulation comparable with that employed on the overtone. Accordingly, $94\,\Delta v = 1, \Delta l = +1$ and $74\,\Delta v = 1, \Delta l = -1$ vibrational transitions were included, with k up to 30 and J up to 60 (taking only every third value). Both $\Delta K = +1$ and $\Delta K = -1$ transitions had to be considered and many more levels had to be calculated than for the overtone; for each value of k, 120 different J transition energy/intensity pairs were involved, making $168 \times 30 \times 120 = 604\,800$ pairs of data in all.

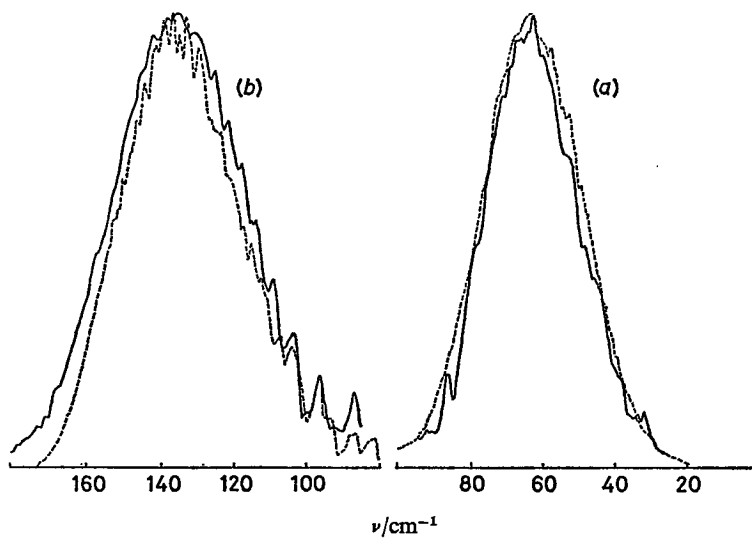

FIG. 2.—Observed (——) and simulated (- - -) band contours for SiH_3NCO; (*a*) fundamental, (*b*) overtone.

The band shape proved to be significantly dependent on the Coriolis coupling constant, ζ, as expected; a value between 0.90 and 0.95 was anticipated for a bending motion of a heavy atom chain, but it became clear that a much lower value would be needed to give a satisfactory fit. The best fit was obtained, by a process based on r.m.s. differences between observed and calculated intensities, with an " effective " ζ of 0.687 ± 0.008 (99 % confidence limits); this clearly represents an average over all relevant vibrational levels and it is hoped to be able to define the variation of ζ with v and l by more detailed analysis (see Appendix III).

Repeating the simulation of the overtone band with $\zeta = 0.69$ gave an improved fit, the conventional R factor decreasing by 0.2, or 2 % of its value, which is significant at the 99 % level. The final best fit was achieved by slightly modifying the potential using a Coriolis constant of 0.69; the final R factor was 9.4 %.

The final potential has the form:

$$V = 1445(5)\theta^2 + 1740(15)/\{1 + [\theta/0.950(3)]^2\}\ \text{cm}^{-1}\ (\theta \text{ in rad})$$

with a hump of 31.37 cm^{-1}; the potential minimum lies at 21.2±0.1° from linear. The uncertainties in the parameters are strongly correlated and the potential is very closely defined. The aptness of the constraint selected to represent the microwave B values ($B_{1,1}-B_{2,0} = -0.716\pm0.100$ MHz) is shown by the excellent agreement between the observed and calculated B values for which measurements are available (table 2).

TABLE 3.—Q BRANCH ORIGINS EXPECTED BELOW 130 cm^{-1}, WITH REPORTED RAMAN FEATURES[a]

transition l	v'	v''	$\Delta G_{calc}/cm^{-1}$	Q_{obs}/cm^{-1}
0	2	0	68.97	—
1	3	1	88.62	—
0	4	2	92.96	—
2	4	2	101.25	99.9
1	5	3	103.40	102.8
0	6	4	108.68	109.6
3	5	3	110.45	
2	6	4	111.79	111.5
1	7	5	114.85	115.1
4	6	4	117.68	—
3	7	5	118.58	118.8
0	8	6	118.98	
2	8	6	120.53	120.8
1	9	7	123.30	—
5	7	5	123.56	—
4	8	6	124.19	124.4
3	9	7	125.51	126.0
0	10	8	126.52	
2	10	8	127.43	—
6	8	6	128.47	—
5	9	7	128.92	129.3
4	10	8	129.84	
1	11	9	129.77	

[a] Ref. (5).

Although the overall fit between observed and calculated band shapes is satisfactory (fig. 2), some of the detail, particularly the distinct P-heads on the overtone band, is not perfectly reproduced; it is possible that further refinements to the potential (such as, for instance, the inclusion of a small quartic term) might improve the fit, but we regard the potential proposed here to be that defined by our spectra as a whole, taken together with the microwave B values. It is clear that the recently reported [15] calculated potential, with a hump of 70 cm^{-1}, is not an adequate basis for interpretation of the infrared and microwave spectra.

It is possible, as mentioned above, to use our levels to deduce the $\Delta v = 2$, $\Delta l = 0$ vibrational origins directly and hence the positions of the Q branches expected to be prominent in the Raman spectrum of the vapour. A list of those expected below 130 cm^{-1} is compared (table 3) with the features reported by Durig;[5] it is clear that the observed features are reasonably consistent with our potentiall Our spectra, on the other hand, are not compatible with any quartic–quadratic potential of the type proposed by Durig.

SPECTRUM OF SiD_3NCO

This is very similar to that of SiH_3NCO, both in its general form and in the appearance of P-heads on the low-frequency side of the overtone peak. It is not perfectly straightforward to calculate the expected positions of these; the P-head position depends on both the band origin (and thus the reduced mass of the system) and on the B rotation constant, which governs the position of the P-head relative to the band origin. The change in B rotation constant can be calculated to be ≈ -7 % of the value for the light isotopic species; the P-head position is then ≈ 0.45 cm^{-1} nearer the band centre for the heavy species. If we assume that the low-frequency bend is not significantly mixed with any other vibrations the reduced mass can be calculated to be ≈ 0.7 % greater for the SiD_3 species; applying appropriate corrections to the coordinate and energy scaling factors [7] then gives a set of band origins ≈ 0.4-0.5 cm^{-1} lower than for the SiH_3 species. The two effects should thus cancel out; any changes in P-head positions greater than ≈ 0.1 cm^{-1} must therefore be attributed to the effects of coupling of the low-frequency bend with other vibrations, particularly the Si(H, D)$_3$ rocking mode. As can be seen from table 1 there are indeed changes in P-head positions, though it has not yet been possible to make specific assignments correlating the two sets; it does not, however, appear possible to specify a single " shift " for the vibration that could be used in defining the interaction between the bend and the rock.

SPECTRA OF SiH_3NCS AND SiH_3NCSe

The far-infrared spectrum of silyl isothiocyanate has been published before; our observations confirm those of Durig *et al.*[9] We have made no attempt to simulate the observed bands, though it is clear that, as deduced by Durig [9] and by Dossel and Robiette [16] from the microwave spectrum, the potential must be close to harmonic. It is, however, puzzling that the overtone band shows no sign of P-heads, either as a sequence as for SiH_3NCO or superimposed as for SiH_3NCSe (see below); the variation of B with v is such [16] that P-heads are expected only 4 cm^{-1} from the band origins, dominating the parallel band contours. This suggests that the overall band shape near 130 cm^{-1} may be due to a set of closely overlapping P-heads, implying a significant degree of harmonicity.

The spectrum of SiH_3NCSe in this region has not been reported previously; the fundamental band is distinctly narrower than that of the isocyanate and we have attempted to simulate the spectrum using a classical anharmonic oscillator expression for energy levels:

$$G(v, l) = \omega(v+1)+x(v+1)^2+gl^2.$$

The overtone band shows a clear P-head structure, implying that x is very small. Unfortunately, we have been unable to adequately simulate the overtone band without experimental data on the variation of B with vibrational state. Nevertheless, we have simulated the fundamental band shape with $\omega = 60$ cm^{-1}, $x = 0$ and $g = 0.45(10)$ cm^{-1} (chosen to reproduce the two-band centres) and obtained a best fit with an " effective " ζ (see above) of 0.82(1). This is much closer to the expected 0.9-0.95 than that found for the isocyanate, as might be expected for a more harmonic oscillator.

Finally, it seems clear that for SiH_3NCS, as for SiH_3NCSe, the " harmonic " vibration frequency must be close to the fundamental band maximum; we thus have the intriguing coincidence that all three of these molecules have apparent vibration frequencies (corresponding to this band maximum) very close to 60 cm^{-1}. We

intend to carry our analysis further using experimental spectra of higher resolution for all these molecules; it seems clear that much more detailed information about the potential and the above interactions between rotation and vibration is potentially available for such spectra.

APPENDIX I

NUMERICAL INTEGRATION EIGENVALUE ROUTINE FOR THE 2-DIMENSIONAL ANHARMONIC OSCILLATOR

The 2-dimensional potential surface for the bending motion of SiH_3NCO is not cylindrically symmetric, but has 3 minima and 3 maxima per revolution because of the 3-fold symmetry of the SiH_3 group. However, Duckett [7] has shown that these maxima are low ($< 3\ cm^{-1}$) compared with the central hump ($\approx 30\ cm^{-1}$) and our analysis ignores their influence on the vibrational energy levels (see Appendix II for an estimate of the effect of this perturbation).

We can then use the operator equation for a cylindrically symmetric 2-dimensional oscillator:

$$\frac{1}{r}\frac{\partial}{\partial r}\left(r\frac{\partial\psi}{\partial r}\right)-V(l,r)\psi+E\psi=0 \tag{I.1}$$

where $V(l,r) = V(r)+l^2/r^2$. Making the substitution

$$\psi = r^{-\frac{1}{2}}P$$

we find

$$\frac{\partial\psi}{\partial r} = \frac{-r^{-\frac{1}{2}}}{2}P+r^{-\frac{1}{2}}\frac{\partial P}{\partial r}$$

so

$$\frac{\partial}{\partial r}\left(r\frac{\partial\psi}{\partial r}\right) = \frac{r^{-\frac{1}{2}}}{4}P-\frac{r^{-\frac{1}{2}}}{2}\frac{\partial P}{\partial r}+\frac{r^{-\frac{1}{2}}}{2}\frac{\partial P}{\partial r}+\frac{r^{\frac{1}{2}}\partial^2 P}{\partial r^2}.$$

Thus eqn (I.1) becomes:

$$\frac{r^{-\frac{1}{2}}\partial^2 P}{\partial r^2}-\left[r^{-\frac{1}{2}}V(l,r)-\frac{r^{-\frac{1}{2}}}{4}\right]P+Er^{-\frac{1}{2}}P=0$$

or

$$\frac{\partial^2 P}{\partial r^2}-\left[V(l,r)-\frac{1}{4r^2}\right]P+EP=0. \tag{I.2}$$

Defining an " effective potential "

$$V_{\text{eff}} = V(r)+\frac{l^2-0.25}{r^2} \tag{I.3}$$

we obtain

$$\frac{\partial^2 P}{\partial r^2}+(E-V_{\text{eff}})P=0. \tag{I.4}$$

This is the correct form for the use of Cooley's numerical method,[12] employing an eigenvalue predictor–corrector formula correct to second order; this gives speedy convergence and the eigenvalues derived are independent of the initial trial values. Our routine calculates the effective potential at 1001 points, including the origin, which is a singularity; V_{eff} tends to $+\infty$ as $r\to 0$ if $l>0$, but to $-\infty$ if $l=0$.

These infinities are approximated by very large real numbers [r^2 is put equal to 1×10^{-20} in eqn (I.3)]. The only other consequence of the central singularity is that for $l = 0$, $(\partial P/\partial r)_{r=0}$ is infinite and the Numerov integration fails unless started using points 2 and 3, rather than points 1 and 2 as is usual.

Each solution found for a given value of l is assigned its quantum number v by counting the number of nodes in the radial wavefunction P, m; then

$$v = l+m.$$

The expectation values of r^2 and r^4, functions of the dimensionless coordinate r used in the routine, are calculated as sums over all 1001 points, rather than integrals, and scaled to give $\langle q^2\rangle$, $\langle q^4\rangle$ and $\langle\theta^2\rangle^{\frac{1}{2}}$, the expectation value of the bending angle. Energies are also expressed in a dimensionless form within the routine, but are input and output in cm^{-1} using a single factor such that our method gives eigenvalues identical to Robiette's [13] for the same potential; the coordinate scale factor relating r and q is similarly chosen to give values of $\langle q^2\rangle$ and $\langle q^4\rangle$ in agreement with Duckett's.[7] Finally, the B rotation constant for each state is calculated using a relationship employed by Duckett:[7]

$$B_{v,l} = {}^*B_0+\alpha\langle q^2\rangle+\gamma\langle q^4\rangle$$

where ${}^*B_0$, α and γ are found empirically to give the best agreement between calculated and observed B values for the first 20 levels.

The complete calculation for each level takes 2 s c.p.u. time on the ICL 4-75; the required 120 levels thus need $\approx$ 4 min c.p.u. time.

APPENDIX II

EFFECT OF 3-FOLD SYMMETRY OF THE SiH_3 GROUP

As mentioned above, this will have the effect of a 3-fold perturbation to the cylindrical potential; it is possible to express this perturbation as:

$$V_{\text{pert}} = V_3 \cos 3\phi. \qquad \text{(II.1)}$$

Second-order perturbation theory then shows that the perturbation only connects levels with l quantum numbers differing by 3; the magnitude of the perturbation for two such levels depends on the overlap integral of the radial parts of their wavefunctions and on the separation between them, ΔE. The maximum shift to be expected is of the order of $(V_3)^2/\Delta E$. Duckett [7] has shown, by an analysis of $\Delta l = 3$ perturbations among the pure rotational transitions, that V_3 is ≈ 1.33 cm^{-1}, so for the levels 0,0 and 3,3, with $\Delta E = 90$ cm^{-1}, the shifts are expected to be ≈ 0.02 cm^{-1} at most. For levels with different numbers of nodes in their radial wavefunctions (*e.g.*, 2,0 and 3,3) the overlap integral will be much smaller, so that even with $\Delta E = 20$ cm^{-1} the shifts expected will also be small. We therefore conclude that the 3-fold perturbation will not give rise to observable effects in our spectra at the resolution used (≈ 1 cm^{-1}).

APPENDIX III

VIBRATIONAL DEPENDENCE OF A AND ζ

As mentioned in the main text, we have not included the vibrational dependence of A and ζ in our analysis, but have used " average " or " effective " values of each in calculation of the term values. This is clearly a gross oversimplification. It does not seem to be possible to separate the vibrational dependences of A and ζ from each

other and it has been suggested [7] that the values of A and $A\zeta$ which occur independently should be represented as

$$A_v = A_0 + \langle q^2 \rangle \alpha^A : \quad (A\zeta)_v = (A\zeta)_0 + \langle q^2 \rangle \alpha^{A\xi}.$$

It seems logically necessary then to include the vibrational dependence of the coefficient of l^2, $(A\zeta^2)$ as $(A\zeta^2)_v = (A\zeta^2)_0 + \langle q^2 \rangle \alpha^{A\zeta^2}$; we then have three unknown coefficients of variation, as well as the three unknown zero-point parameters A_0, $(A\zeta)_0$ and $(A\zeta^2)_0$. Values of $[A_v - (A\zeta)_v]$ have been measured in the microwave for a number of states with $l = 1$,[7] but the associated uncertainties are too high for any conclusions about the αs to be drawn. Again it seems that further progress with defining these factors must await the availability of spectra at higher resolution. Note that inclusion of the variation of B with vibrational state is logically necessary in the treatment of the overtone band, as the P-heading behaviour is strongly dependent upon the difference in B between the upper and lower state; the effect of variations in A and the like is to alter the P-heading as k and l vary and is thus of secondary significance.

It is a great pleasure to acknowledge the assistance of Dr. A. G. Robiette of the University of Reading; he has been generous with advice, the provision of unpublished data and the loan of an unpublished thesis, without all of which we could not have interpreted our experimental results. Dr. K. Lawley of our own Department provided invaluable assistance in the implementation of Cooley's method in this particular system; the analysis presented in the first two Appendices derives almost entirely from his advice.

[1] E. A. V. Ebsworth and M. J. Mays, *J. Chem. Soc.*, 1962, 4844.
[2] M. C. L. Gerry, T. M. Sugden and J. C. Thomson, *Nature*, 1966, **211**, 846.
[3] J. A. Duckett, A. G. Robiette and I. M. Mills, *J. Mol. Spectroscopy*, 1976, **62**, 34.
[4] C. Glidewell, A. G. Robiette and G. M. Sheldrick, *Chem. Phys. Letters*, 1972, **16**, 526.
[5] J. R. Durig, K. S. Kalasinsky and V. F. Kalasinsky, *J. Chem. Phys.*, 1978, **69**, 918.
[6] S. I. Chan, J. Zinn and W. D. Gwinn, *J. Chem. Phys.*, 1961, **34**, 1319.
[7] J. A. Duckett, *Ph.D. Thesis* (Reading University, 1976).
[8] M. J. Barrow, S. Cradock, E. A. V. Ebsworth and M. M. Harding, *J.C.S. Chem. Comm.*, 1976, 744.
[9] J. R. Durig, K. S. Kalasinsky and V. F. Kalasinsky, *J. Phys. Chem.*, 1978, **82**, 438.
[10] E. A. V. Ebsworth and J. C. Thomson, *J. Chem. Soc. A*, 1967, 69.
[11] L. A. Carreira, I. M. Mills and W. B. Person, *J. Chem. Phys.*, 1972, **56**, 1444.
[12] J. W. Cooley, *Math. Comp.*, 1961, XV, 363.
[13] A. G. Robiette, personal communication.
[14] G. Herzberg, *Infrared and Raman Spectra of Polyatomic Molecules* (Van Nostrand, Princeton, N.J., 1945), pp. 422 and 426.
[15] R. E. Wasylishen, M. R. Graham and W. Danchura, *J. Mol. Structure*, 1979, **51**, 145.
[16] K. F. Dössel and A. G. Robiette, *Z. Naturforsch.*, 1977, **32a**, 462.

(PAPER 9/1543)